

Department of Transport Technology,
University of Technology,
Loughborough,
England.

Von-Karman Institute for Fluid
Dynamics,
Rhode St. Genese,
Brussels.

"On the Response and Interaction with the Flow of Structures
Immersed in Turbulent Flow Fields."

By:

GEORGE P. SKORDILIS

B.Tech. - Loughborough University.

Postgr. Dipl. V.K.I. - Von-Karman Institute.

Master of Science Thesis

Thesis submitted in fulfillment of the requirements for the award of
"Master of Science" of the Loughborough University of Technology.

APRIL 1976

Supervisors:

University of Technology
Loughborough.

1) Professor D. Johns,
Head of Department of
Transport Technology.

2) Mr. F.G. Maccabee,
Lecturer,
Department of Transport
Technology.

Von-Karman Institute,
Brussels.

1) Professor J.J. Ginoux,
Associate Director.

2) Mr. D. Olivari,
Lecturer,
Low Speed Aerodynamics
Department.

(VOLUMES I AND II)

© by George P. Skordilis, 1976

VOLUME II

CERTIFICATE OF ORIGINALITY.....	I
FLYLEAF	II
TABLE OF CONTENTS	III

PART II

ON THE RESPONSE OF BLUFF BODIES IMMERSED
IN TURBULENT FLOW FIELDS

10. INTRODUCTION.....	84
11. A REVIEW OF THE GENERAL PROBLEMS PRESENT IN THE INVESTIGATION OF THE RESPONSE OF STRUCTURES TO TURBULENT FLOW FIELDS.....	87
12. THEORETICAL CONSIDERATIONS	
12.1 General Concepts.....	90
12.2 Mechanical Admittance.....	91
12.3 Linearized Theory.....	92
13. DESCRIPTION OF APPARATUS	
13.1 Model Mounting.....	96
13.2 Model-Load Balance Assembly Calibration.....	96
13.3 Extraneous Inputs.....	97
14. INSTRUMENTATION	
14.1 Strain Gauges.....	99
14.2 General Arrangement.....	99
14.3 Comments on the Performance of the Balance.....	100
14.4 Accuracy of Measurements.....	101
15. RESULTS AND DISCUSSION	
15.1 Discussion of the General Experimental Procedure.....	104
15.2 Effect of Frontal Area on Aerodynamic Admittance.....	106

IV

15.3	Effect of Aspect Ratio on Aerodynamic Admittance.....	107
15.4	Effect of Turbulence Level on Aerodynamic Admittance.....	107
15.5	Effect of Scale of Turbulence on Aerodynamic Admittance.....	108
15.6	Mean and Fluctuating Drag.....	109
16.	CONCLUSIONS.....	112
17.	RECOMMENDATIONS.....	113

PART III

A MATHEMATICAL MODEL OF THE FLOW SITUATION

IN FRONT OF THE MODEL

18.	INTRODUCTION	118
19.	FORMULATION.....	123
20.	MODEL PREDICTION.....	127
21.	DISCUSSION OF THE MATHEMATICAL MODEL.....	128
22.	CONCLUSIONS DRAWN ON THE MATHEMATICAL MODEL.....	128
23.	GENERAL CONCLUSIONS.....	130
24.	REFERENCES.....	131

APPENDICES

Appendix A.	Joint Probability Density Distribution of the Velocity Fluctuations.....	140
Appendix B.	Hot-Wire Instrumentation	
B.1	Linearization and Longitudinal Velocity Component Measurements.....	143
B.2	Frequency Response Considerations.....	144
Appendix C.	Measurement of Frequency-Dependent Correlation.....	146

Appendix D. Measurements of the Turbulence Kinetic Energy Using a Single Hot-Wire	148
Appendix E. Calculation of the Mechanical Admittance.....	151
Appendix F. Statistical Reliability of Power-Spectrum Measurements.....	152

PARTS II AND III

(References are on pp 131 - 139)

PART II

PART II

ON THE RESPONSE OF BLUFF BODIES IMMERSED IN TURBULENT
FLOW FIELDS

10. INTRODUCTION.

This part deals with the question of relating the atmospheric turbulence inputs to pressures and forces on the body which theoretically is, in most cases, unsolved. Theories of aircraft and structural response to turbulence, (Ref. 12 and 54), usually are restricted in application by the inability at present to describe adequately general relations between the forces induced on the body and the turbulence inputs. The resulting linearizations and simplifications used to model these relations are successful in predicting the body response in some regimes - notably the response of aircraft to turbulence at high altitudes (Ref. 55 or "line-like" structural response (Ref. 56, 57 and 58) - where the input energy is concentrated at wavelengths large with respect to the characteristic body dimensions. However, for low altitude flight, and for structures which do not fulfill the "line-like" assumptions, the atmospheric boundary layer presents turbulence inputs with energy concentration at wavelengths of the same order of magnitude as the characteristic body dimensions. (The longitudinal scale of atmospheric turbulence, L_x , in the ground boundary layer is of the order of 60m to 600m). In this case, the simplifications in the usual assumptions of the force-velocity relations become suspect.

In particular, for structures (such as buildings, rockets on the launch pad, VTOL aircraft while near the ground e.t.c.), the aerodynamics of the body response become extremely complex. Stru-

ctures in non-turbulent flow would in any case be subjected to unsteady forces. These are caused by large wakes and vortex shedding phenomena which are sensitive to the particular body geometry and its flexibility, as well as, to the flow variables themselves. Hence the addition of turbulence produces a situation which in many cases yields only to direct experimental investigation.

Much work has already been carried out to determine the effects of winds on buildings and structures (Ref. 22, 59, 60, 61, and 62). However, much remains to be done, in particular for the problems introduced by severe turbulence.

Most of the work done to date in this field is characterized by measurement of the overall structural response using simplified force-turbulence relations, or directly to measure the response of complex structures to design purposes. This part of the report describes an experimental study of the loading of simple bluff structures by turbulent flow fields with a L_x/b or L_y/b of $O(1)$.

In general the response to any random excitation is also random and so must be treated in a statistical manner. This response can be described in terms of either a spectral density function (in the frequency domain) or a correlation function (in the time domain). Following usual practice, the response analysis is expressed in the frequency domain. It is clear that as the flow field consists of a static and a dynamic component so the response of the model in the drag direction has a mean and a time dependent component. This fluctuating drag component is of primary interest.

In relating the fluctuating force to the fluctuating velocity Davenport's suggestion of a frequency-dependent transfer function was adopted. The effect of the frontal area, aspect ratio,

and the turbulence level on the aerodynamic admittance was looked at.

An attempt has been made to correlate the aerodynamic admittance when plotted against a reduced frequency which is a function of the frontal area and the scale of turbulence. Measurements of the mean and fluctuating drag for the different models were carried out and the effect of turbulence level was investigated.

11. A REVIEW OF THE GENERAL PROBLEM PRESENT IN THE INVESTIGATION OF THE RESPONSE OF STRUCTURES TO TURBULENT FLOW FIELDS.

The general bluff body problem involves the response to time-dependent forces induced both by the free stream turbulence and by the wake formation. Other important problems in aeroelasticity (response of panels to turbulent boundary layers and the response of aircraft wings to large scale turbulence) allow considerable simplification in the theoretical and experimental investigations.

In addition to the structural properties, three principal parameters are required to define a particular dynamic system:

- a) Degree of streamlining of the structure,
- b) Reynolds' No., — *inc turbulence intensity effect?*
- c) Relative magnitude of the scale of turbulence to a typical dimension of the structure.

The importance of the above parameters is illustrated by reference to two simple shapes of structure, a flat plate, and a circular cylinder. The flat plate at zero incidence represents a bluff body exhibiting a negligible Reynolds's no. effect. The cylinder is a bluff body whose response characteristics in a steady flow are strongly influenced by Reynolds' No. || ?

If D denotes a typical dimension of the structure, in this case either plate (or square section cylinder) width or cylinder diameter, and L_x the longitudinal integral scale of turbulence, then the practical problems could be subdivided into three groups:

1. Circular cylinder

- a) $L_x \gg D$ and with the wind stream normal to the cylinder axis. In this group we have the calculation of the response of a) slender stacks, b) rocket shells, c) electrical conductors, d) structural elements.

- b) $L_x < D$ and with the wind stream parallel to the cylinder axis.

The calculation of the response of rocket shells to noise generated in the wake is a representative example of this group.

2. Flat plates at zero incidence.

- a) $L_x > D$

In this group belong the usual calculations of the response of aircraft wings to buffeting by random downwash and similarly for sections of suspension bridges with flat plate aerodynamic properties.

- b) $L_x < D$

The calculation of the effects of wind pressure fluctuations on the sides of large buildings, and of the response of panels to random excitation belong to this category.

3. Flat plate at 90° incidence including square - section cylinder with the wind normal to one face.

- a) $L_x > D$

In this section belongs the calculation of the response of structures to buffeting by gusts

- b) $L_x < D$

Finally in this category belong the calculation of the effects of wind pressure fluctuations on the sides of large buildings and of the response of panels.

The investigation of any of the problems indicated above must necessarily take the form of determining the relationships in non-steady flows between a) velocity, b) force, and c) displacement.

The difficulty in the above lies in the relationship between

velocity and force. Any relationship between the two will be non-linear and obviously this introduces complex theoretical problems when the independent variable is given random properties.

On the other hand to calculate the displacements of the body on knowing the forces is a structural mechanical problem. If a linear relationship between force and displacement exists, then knowing the statistical properties of the forcing function, it is a simple matter to determine the statistical properties of the displacements. If a non-linear relationship is involved, then the same difficulties arise as in the fluid mechanical case referred to above.

12. THEORETICAL CONSIDERATIONS

12.1 General Concepts.

The nearly random nature of the turbulence allows application of the ideas of stationary stochastic processes. The statistical quantities measured are the turbulence spectrum and the load spectrum while the mechanical admittance is calculated. From these measurements and calculations, the aerodynamic admittance may be found. It is this aerodynamic admittance which is of the utmost importance in considering the dynamic response of bluff bodies to turbulent flow fields. Past work has shown that the aerodynamic admittance, *ref?*

Not in installation should be?
 C_N $|A|^2$ depends on the ratio L_x/D . The response of a bluff structure involves further difficulties, as the force coefficients C_D and C_M cannot be regarded as constants and the change in the flow pattern due to the presence of the structure complicates the relationship between the velocity correlations in the free stream and the pressure correlations on the structure. While $|A|^2$ cannot, usually be calculated theoretically the determination by model experiment still allows the use of a distorted scale of turbulence provided it is assumed that there is a linear relationship between $S_{u'}(f)$ and $S_n(f)$.

For a linear system under stochastic forcing the ratio of the response spectrum to the input spectrum is equal to the absolute square of the overall admittance. For the case of a bluff body immersed in a turbulent flow field the load may be regarded as the response and the velocity field as the input.

The relation is given by:

$$\frac{f S_n(f)}{\bar{N}^2} = |\phi|^2 \frac{f S_{u'}(f)}{\bar{u}^2}$$

where $|\phi|^2 = |\psi|^2 / A|^2$

Therefore

$$\frac{\int S_n(f)}{\bar{N}^2} = |\psi|^2 |A|^2 \frac{\int S_{u'}(f)}{\bar{u}^2}$$

and

$$\frac{\frac{\int S_n(f)}{\bar{N}^2} \times \frac{1}{|\psi|^2}}{\frac{4 \int S_{u'}(f)}{\bar{u}^2}} = |A|^2$$

12.2 Mechanical Admittance.

The measured quantities are the mechanical admittance (the mechanical admittance is calculated by measuring other parameters discussed below), the load spectrum and the turbulence spectrum

In calculating the mechanical admittance for each case of balance-model assembly it was assumed, as a first approximation, that the assembly acted as a one-degree-of-freedom damped oscillator.

The motion could then be described by the equation:

$$m\ddot{x} + c\dot{x} + K_s x = P(t)$$

$$\ddot{x} + \frac{c}{m}\dot{x} + \frac{K_s}{m}x = \frac{1}{m}P(t)$$

with $\frac{K_s}{m} = \omega^2$ and $\frac{c}{m} = 2h\omega_0$ the above equation becomes:

$$\ddot{x} + 2h\omega_0\dot{x} + \omega_0^2 x = \frac{1}{m}P(t)$$

h not
in
notation

and the transfer function is given by:

$$\frac{x(\omega)}{P(\omega)} = 1 / \{m(\omega_0^2 - \omega^2 + 2hi\omega_0\omega)\}$$

Consequently the square of the mechanical admittance is given by the modulus of the transfer function, i.e.

$$|\psi|^2 = 1 / \{m^2(\omega_0^2 - \omega^2)^2 + c^2\omega^2\}$$

Therefore to calculate the mechanical admittance we only need to measure m , w_0 , w , and c . An example of the calculation of the mechanical admittance is given in appendix E, while calculated constants for the assemblies are shown in fig. 144 and 145.

12.3 Linearized Theory.

As no theoretical development exists today to fully account for the response of a structure in a turbulent field the linearized approach used by Davenport (Ref. 22), is utilized. It is obvious that a linear theory would generally be valid for only very small displacements.

In considering the problem a simplified physical situation is assumed where there are no spatial variations in velocity, so that the velocity fluctuations are a function of time only. In steady flow the force per unit area on an object immersed in the flow field can be expressed in the usual form:

$$P = \frac{1}{2} \rho u^2 C_D$$

Understatement

There is considerable evidence (Ref. 63), that suggests that in the flow is unsteady, the numerical value of the drag coefficient is questionable. As a first approximation, however, it could be assumed that in unsteady flow the drag per unit area is related to the velocity by the relations:

$$t \quad \bar{P} = \frac{1}{2} \rho \bar{u}^2 C_D$$

$$\text{and} \quad p(t) = \frac{1}{2} \rho \bar{u}^2(t) C_D$$

$$\text{where} \quad p = p(t) = \bar{p} + p' \quad \text{and} \quad u = u(t) = \bar{u} + u'$$

Therefore $\bar{p} + p' = \frac{1}{2} \rho (\bar{u} + u')^2 C_D$

ignoring high order terms we obtain:

$$\bar{p} + p' = \frac{1}{2} \rho \bar{u}^2 C_D + \rho \bar{u} u' C_D$$

therefore $p' = \rho \bar{u} u' C_D$

and

$$\frac{p'^2}{\bar{p}^2} = \frac{(\rho \bar{u} C_D)^2 u'^2}{(\frac{1}{2} \rho \bar{u}^2 C_D)^2} = 4 \frac{u'^2}{\bar{u}^2} \dots (1)$$

Since we postulated a linear relation, it follows that the normalized power spectra are related by:

$$\frac{f S_n(f)}{\bar{N}^2} = 4 \frac{f S_{u'}(f)}{\bar{u}^2} \dots (2)$$

However it has been shown by experiments in a water tank (Ref.63) that there is a variation of the drag coefficient associated with the frequency of the flow fluctuation, and that the coefficient is only equal to the steady value or C_D when the wavelength of the fluctuation $\frac{\bar{u}}{f}$ is large compared with the size of the model. At shorter wavelengths the drag coefficient increases appreciably.

Therefore, since \bar{p}^2 in equation (2) is based on the steady flow value of C_D , it would be reasonable to modify eqn.(2) to:

$$\frac{f S_n(f)}{\bar{N}^2} = 4 \frac{C_D^2(f)}{C_D^2} \cdot \frac{f S_{u'}(f)}{\bar{u}^2} \dots (3)$$

Characteristically, a turbulent flow will have spatial variations, that can be correlated over local areas only. Clearly, the resistance of an object of finite size, placed in the flow, will be dependent on the size of the object relative to the size of the area where there is a positive correlation. Furthermore, if the resistance is being looked at frequency by frequency, it will depend on the spatial correlation of the velocity for each particular frequency.

Consequently assuming that $R_n(f)$ is a frequency dependent function taking into account the spatial correlation of the velocity the force spectrum can be thought of, as a function of the type:

$$\frac{\int S_n(f)}{\bar{N}^2} = 4 R_n(f) \frac{C_0^2(f)}{C_D^2} \frac{\int S_{u'}(f)}{\bar{u}^2} \dots (4)$$

The magnitude of $R_n(f)$ is clearly such that, for low-frequency fluctuations (large wavelengths compared with the body itself), the correlation of the velocity will be effectively unity through the region of flow affecting the body. At very high frequencies, i.e. very small wavelengths compared with the body typical dimensions, the value of $R_n(f)$ must approach zero, since these very small eddies cannot be expected to affect the resistance. Transition must occur over some intermediate range of eddy size.

As it is not possible, in practice, to separate all the various quantities contributing to the overall drag coefficient, in the present work, the purpose basically was to measure the overall quantity $R_n(f) \left\{ \frac{C_0(f)}{C_D} \right\}^2$ by measuring the force spectrum and the velocity spectrum and determining the ratio of the two after noise and mechanical admittance were accounted for.

Therefore

$$\frac{\int S_n(f)}{\bar{N}^2} / 4 = \frac{\int S_n(f)}{\bar{u}^2} = R_n(f) \left\{ \frac{C_0(f)}{C_D} \right\}^2 \dots (5)$$

Following electrical nomenclature the ratio of the output to input power spectral densities gives the square of the absolute value of the admittance. It is assumed that the admittance includes all the unknown factors which in this case are presented by the expression $R_n(f) \left\{ \frac{C_0(f)}{C_D} \right\}^2$

Therefore

$$\frac{f S_n(f)}{\bar{N}^2} / 4 \frac{f S_{u'}(f)}{\bar{u}^2} = R_n(f) \left\{ \frac{C_D(f)}{C_D} \right\}^2 = |A|^2 \dots (6)$$

The normalization of the load and velocity spectra is not expected to affect the above relation.

13. DESCRIPTION OF APPARATUS.

13.1 Model Mounting.

The method of mounting the model was described in section 6.2.2. Care was required in the manner of supporting the model so that extraneous inputs and vibrations in the frequency band of interest could be eliminated. The mount was thus isolated from the wind tunnel by being supported directly from the concrete floor beneath the tunnel. The mounting provided four degrees of freedom used to align the model accurately with the airflow. Once aligned, the mount with the model, could be held at position with the use of set screws. The natural frequency of the model - (modified) balance assembly varied with the mass of the model from about 36Hz for the smaller plates to about 24Hz for the larger plates. The circular cylinders and orthogonal parallelepipeds natural frequencies are found between these two limits. Any acceleration present at the top of the mount was not accounted for. It is thought that any acceleration present would have been negligible so that the equivalent force, if any, would have been small compared with the wind forces.

13.2 Model - Load Balance Assembly Calibration.

In calibrating the load balance a zero null reading was taken, for each model - modified load balance configuration, with the balance and model assembly in its normal horizontal position; the balance was then mounted in the wind tunnel in the position to be used and calibrated weights were applied on the surface where the wind loads were to be experienced and in the drag direction through a low friction pulley system. The calibrations were accurately repeatable and little hysteresis was noted. The calibration

was carried out on a number of occasions during the experiments and no variations were detected. The output remained proportional to the applied load over a range exceeding that required in the experiments. A typical calibration curve is shown in Fig. 143.

It was found that there was a small error associated with changing the point of application of the load, shifted in a spanwise direction. This error was anti-symmetric, with reference to the vertical - z-direction - centreline along the plate. The errors when the load was applied entirely at the edge of the $AR=2$ plate were about 10%; however this is an extreme situation which is thought could not occur in practice; the maximum shifts of the centre of pressure could be expected to be a small fraction of the plate width. Therefore, the effect of the total fluctuating load will be small. In general, it could be said that all the implications of a balance of this sort are not immediately clear. In the case of a normal flat plate there can be no side force or if such a force does exist it must be very small. If there were a centre of pressure oscillation of this sort, the interaction discussed above would cause it to appear, incorrectly, as an oscillating force occurring at the frequency of eddy shedding from one side of the plate (Strouhal frequency). Genuine force fluctuations due to shedding would occur at twice the Strouhal frequency, since the force would be affected by shedding from either side of the model.

13.3 Extraneous inputs.

Extraneous inputs into the system could be introduced from:

- a) Flow non-homogeneities outside the primary influenced zone.
- b) Electronic noise of the instruments used. This is not

expected to affect the measurements significantly as the noise level measured directly on a Bruel & Kjaer Noise Metre did not exceed 0.2% of the typical r.m.s. signal.

14. INSTRUMENTATION.

14.1 Strain Gauges.

In the load balance the transducers used were strain gauges with the following characteristics:

Micro-Measurements,

Romulus, Michigan,

Resistance $120 \pm 0.1\%$ and a gauge factor of $2.00 \pm 0.5\%$
at 75°F .

Strain limits = 5000 microstrains.

Temperature variations are thought to be negligible as all measurements and calibrations were carried out within a temperature range of $17^{\circ} - 19^{\circ}\text{C}$.

Power to the strain gauges was supplied through a D.C. power unit. The output, through an amplifier was fed into the frequency analyser.

14.2 General Arrangement.

The balance output through the strain gauges was fed into a D.C. Power Unit constructed at V.K.I. and then the signal was fed into:

- a) a r.m.s. metre,
- b) digital voltmeter,
- c) frequency analyser.

A schematic diagram of the arrangement is shown in Fig.

276.

From the r.m.s. meter the r.m.s. value of the fluctuating drag was obtained, while from the digital voltmeter - which was suitably adjusted during the calibration procedure - the mean drag was

given.

By feeding the signal into the frequency analyser the load spectrum was obtained.

14.3 Comments on the Performance of the Balance.

The initial balance used, shown in Pl. VI, was found inadequate for use with the three-dimensional bluff bodies. The reason was the vortex excited oscillations which provided additional unwanted inputs to the balance. In the case of the flat plates the initial balance performed satisfactorily as the cause of the above oscillations was, to a great extent, suppressed by chamfering the edges of the plates, Pl. II and Pl. III.

In order to eliminate the above difficulties a new balance was designed which responded, mainly, to inputs in the drag direction only. This was achieved by using a linkage mechanism as the main arm of the balance. The modified balance is shown in Pl. IX. This arrangement proved adequate. The balance was checked for additional inputs when transverse displacements of the models were taken place, by placing weights on the models (the weight acting in the z-direction). A maximum displacement of 3mm was achieved in the z-direction without any appreciable output from the balance. A second aspect of the previous arrangement which was improved by modifying the balance was a certain instability of the mechanical admittance. This instability was noticed with the original system. The instability was presumably caused by the flexure links being connected to a comparatively small aluminium base which was fixed to the main supports by screws. This caused, occasionally, some slippage to occur during vibration, at the interface of the two different metal pieces. As a result end-fixity conditions were changed and a shift occurred in the natural frequencies of the model-balance

systems. With the modified balance a much larger base is provided and this helped in attaching the balance to the main frame more easily and rigidly. Measurement of the parameters required for the calculation of the mechanical admittance before and after the experiments showed no variation.

Although the balance was shielded from the airstream by placing it inside a zero camber aerofoil section a hole was necessary on the top part of the section to allow the exit of the sting supporting the model. In order to investigate any adverse effects present on the balance output by the air entering the section, the wind tunnel was run with the shielded balance in place (no model) and the balance output was noted. This output was found to be negligible, being not more than 1% - 2% from the value of the mean drag noted with the smaller circular disc attached to it. The same was true for the effect on the fluctuating drag.

14.4 Accuracy of Measurements.

The errors in the present investigation could be divided into the following categories:

1. Measurement errors arising from changes in the equipment response, inaccuracies in calibration, reading errors, and so forth. It is difficult to estimate the total probable error of a system as complicated as the one used here. The accuracy of voltmeters and other instruments used in calibrations is generally within ± 1 to ± 3 percent. Repeatability of the strain-gauges calibrations is about of the same order as inevitable changes occur in the electronic circuits because of tube aging, line voltage fluctuation, and so forth. Therefore a total error of several percent has to be considered.

2. Statistical errors, arising from the fact that the power spectral densities are measured as finite time average. Since the power spectral density can be considered an infinite time average of the filtered signal, a measurement over a finite time has to suffer in accuracy. Fortunately, it is possible to estimate this error on the basis of results presented by Rice (Ref. 50). Such an analysis applicable to the present measurements is presented in appendix F.

The calculated r.m.s. error curves in Fig. 31 were used in choosing averaging times at each selected frequency. In general a 3% r.m.s. error was planned for the power spectrum measurements. The experimental value of the transfer function, computed as the ratio of two such spectrum measurements, could then be expected to have a statistical r.m.s. error of the order of 5%. One has to realize however, that these numbers refer to the r.m.s. error of an infinite ensemble of measurements performed under identical conditions. All that can be said regarding an individual measurement is to state its probability of being within specified limits of error. For instance, if the probability density distribution of the transfer function is assumed to be Gaussian (approximate analysis indicates that this may not be an unreasonable assumption), a 5% error implies that a single measurement would have an approximately 90% probability of being within $\pm 10\%$ of the correct value.

A series of individual measurements at different frequencies would show scatter of the order of the r.m.s. error. In the present case, it is not possible to say definitely whether the few points at low frequencies reflect an unduly large scatter or an anomalous behaviour of the transfer function. At higher frequencies, where the computed averaging times were also generally exceeded for practical reasons, the scatter is of acceptable magnitude.

The best way to increase the reliability of the present results would be to obtain a large number of power spectrum measurements at each selected frequency. The average of such measurements would be essentially equivalent to a result obtained by using a longer, otherwise impractical, averaging time. The statistical accuracy would be correspondingly improved and some measurement errors of random nature would be minimized.

15. RESULTS AND DISCUSSION.

15.1 Discussion of the General Experimental Procedure.

The present investigation being basic in its nature the construction of complicated models was thought to be unnecessary. Attention has been paid to the instrumentation used especially after the poor results obtained with the use of the initial balance. The modified balance gave considerably better results. It should be noted that the instrumentation used was the best available at the time.

For the large models blockage corrections were used.

Detailed description and specification of all apparatus and instrumentation were dealt with in previous sections.

The objectives of the work were to consider the following aspects of the problem:

- 1) A general determination of the aerodynamic admittance.
- 2) The aerodynamic admittance, including the unknown factors in the velocity - force spectra relation, is thought to be of primary importance. By considering the aerodynamic admittance of a number of bodies it is hoped to consider the effect the following parameters have on it:
 - a) frontal area of model,
 - b) aspect ratio of model,
 - c) turbulence level, and
 - d) scale of turbulence.
- 3) The variation of the mean and fluctuating drag.

The relation between the load spectrum and the velocity spectrum together with the derived aerodynamic admittance are shown in Fig. 147 to Fig. 236. The aerodynamic admittance is given as the

geometric difference between the respective points on the two log-log curves. According to the linearized theory this difference is equal to $4|A|^2$. Therefore the variation of the aerodynamic admittance with a reduced frequency is presented as $4 \times (\text{aerodynamic admittance}) \sim \text{frequency}$.

It is a general characteristic of all curves that at higher frequencies, the force spectra fall off faster than the velocity spectra, which indicates a reduced high frequency response.

The linearized theory ~~presented in the text~~ ^{4x} implies that at low frequencies the ^{where?} aerodynamic admittance should approach the value of 4. Although there seems to be such a tendency we could not be emphatic about it. In few cases the values of the aerodynamic admittance go above this limiting value; this could be attributed to wrong readings taken from the analyser. It is thought that the accuracy of the results at lower frequencies is rather limited. This is expected if we consider the inherent difficulty of measuring spectra at low frequencies. Even at higher frequencies the accuracy of the force measurements is questionable up to a certain extent, as the load spectrum determination required the lowest range in the frequency analyser, i.e. while the velocity spectrum was read in mV, the load spectrum was measured in μV . A d.c. current supply unit was used to eliminate the effect of the 50Hz - 60Hz mains, but this was not proved very succesful. In the load spectrum curves the 50Hz reading is omitted. In general the measured values of the aerodynamic admittance have considerable variation around the value of 4, having greater values for the smaller models.

The load spectra did not show any peaks. This is rather suspect as at double the Strouhal frequency a certain amplification

was expected. All the same turbulence would have attenuated such peaks. It is thought that even if the peaks do exist, they should be very narrow (otherwise they would have been observed) and consequently are expected to make an insignificant contribution to the integral of the power spectral density function and therefore have a negligible effect on the mean square value of the drag component.

The results for the prisms tested are expected to suffer from greater inaccuracies because of the transverse fluctuations induced by the shedding of vortices. The same applies for the circular cylinders. The effect of any reattachment of the flow on the sides of the prisms is not exactly known.

15.2 Effect of Frontal Area on Aerodynamic Admittance.

One of the parameters which is expected to affect the response of the model is the model frontal area.

Fig. 238, 242 and 246 present the results of $4|A|^2$ plotted against a reduced frequency $\frac{fA}{u_z}$ for the slotted, 30mm holes and 50mm holes baffles produced turbulent fields, respectively. Within the experimental accuracy achieved there seems to be a tendency for the results to collapse on a single line. This could be taken as an indication that there is a certain dependence of the aerodynamic admittance on the frontal area of the model. For the same reduced frequency, the larger frontal area models have a smaller aerodynamic admittance, compared to a model of smaller frontal area. As the used reduced frequency has the corresponding ratio of frontal area to integral scale of turbulence as a factor, it could be concluded that the lateral scale of turbulence in conjunction with the frontal area play a role on the aerodynamic admittance

of the models.

15.3 Effect of Aspect Ratio on Aerodynamic Admittance.

A second parameter which is expected to have a certain influence on the aerodynamic admittance is the aspect ratio of the model.

Fig. 237, 241 and 245 present the data for the AR =1, 2 and 4 flat plates in the slotted, 30mm holes and 50mm holes baffles produced turbulent fields respectively.

Fig. 239, 243 and 247 present the respective results for the square section cylinders while Fig. 240, 244 and 248 present the respective data for the circular section cylinders.

For all configurations used the trend for a decrease in aerodynamic admittance as the aspect ratio increases is evident. This could be explained if it is considered that the correlation of the forces on the model - when the AR increases - is reduced with a consequent reduction on the ratio of the force spectrum to the velocity spectrum, i.e. to the aerodynamic admittance.

One might expect that the aerodynamic admittance of the square section cylinders should be lower to those of the flat plates due to the possible reattachment of the flow with a consequent reduction in the drag. This is not obvious from the present results.

15.4 Effect of Turbulence Level on Aerodynamic Admittance.

The way the degree of turbulence level affected the aerodynamic admittance, was looked at by considering the aerodynamic admittance of the same model for the three turbulent fields used. The aerodynamic admittance for each model for the three turbulent fields is plotted in Fig. 253 to Fig. 263.

The general trend observed is that as the turbulent level

decreases the aerodynamic admittance increases. Theoretically this is expected because as the turbulence level tends to zero, i.e. the flow tends to become laminar, the aerodynamic admittance versus frequency plot should approach a single point, of $4|A|^2=4$ at zero frequency.

Fig.264 to Fig.266 present the results for all models when the aerodynamic admittance is plotted against a reduced frequency for each turbulent field. Because of the relatively great spread of the data a contour presentation is used. All the same the contours for all turbulent fields seem to correlate.

15.5. Effect of Scale of Turbulence on Aerodynamic Admittance.

The last important parameter considered in connection with its effect on the aerodynamic admittance is the integral scale of turbulence.

It has a direct bearing on the correlation of the forces exerted by the flow upon the whole frontal area of the model. This correlation of the forces on the model is expected to be primarily affected by L_y instead of L_x . Consequently in the graphs the L_y scale is used. (The L_x could be thought of as giving an indication of the time the model's frontal area is subjected to a continuous longitudinal force). It is interesting to note that the aerodynamic admittance for the 50mm holes baffle produced turbulent field, having an integral scale (L_y) about 3 times larger than the other two fields, for almost all the models tested, is higher than the aerodynamic admittance obtained for the other fields. This, in a certain way, is suspect as in all cases the aerodynamic admittance is plotted against a reduced frequency based on the ratio of the frontal area to the integral scale of turbulence. Theoretically, if the

aerodynamic admittance was only related to the model's frontal area and the lateral integral scale of turbulence, this way of plotting the data should result in their collapse on to one curve. Therefore it is suggested that the variation in the aerodynamic admittance mentioned above is the result of the aerodynamic admittance being dependent on other parameters as well, e.g. turbulence level, integral scale of turbulence in the z-direction and the integral scale of turbulence in the x-direction.

The conclusions reached by Vickery (Ref. 6) for isotropic turbulence, i.e. that for long wavelengths the aerodynamic admittance is a function of the integral scale where as for short wavelengths it is a function of the wavelength, could, up to a certain extent, be deduced from the graphs.

15.6 Mean and Fluctuating Drag.

The mean and fluctuating drag in relation to the AR of the models were investigated for the plates, square and circular section cylinders. In addition, the effect of the frontal area on drag is examined in the case of the flat plates. The data are plotted in Fig. 267 to Fig. 275.

Fig. 267 shows the mean drag coefficient plotted against the aspect ratio of flat plates for the three turbulent fields. The tendency for the mean drag coefficient to decrease as the AR increases is obvious. At the same time it is shown, in the above mentioned figure, that the higher turbulence level fields produce slightly higher mean drag coefficients. This result could also be demonstrated in a theoretical way as follow:

If the local velocity u is not constant we may express it as the sum of the mean component, \bar{u} , together with a fluctuating

component u' .

Therefore $u = \bar{u} + u'$

Squaring this expression and then averaging with respect to time, we obtain:

$$\overline{u^2} = \bar{u}^2 + \overline{u'^2}$$

A form of the local drag force in terms of the local drag coefficient, $C_D(y)$ or $C_D(x)$ - depending on the direction chosen - could be expressed as

$$N(y) = C_D(y) \cdot \frac{1}{2} \rho \bar{u}^2 \left(1 + \frac{\overline{u'^2}}{\bar{u}^2}\right) l dy$$

where the quantity $\left(\frac{\overline{u'^2}}{\bar{u}^2}\right)^{1/2}$ is defined as the intensity of turbulence.

From the above equation it could be seen that for an increase of, say, 10% in the turbulent intensity the drag coefficient would be increased by 1%.

Fig. 268 presents the results of the fluctuating/mean drag of plates for the three turbulent fields. The same reduction in $\left\{\frac{\overline{u'^2}}{\bar{u}^2}\right\}^{1/2}$ is observed as the AR increases.

The effect of the frontal area of plates is looked at in Fig. 270 and Fig. 271 where the mean and the (fluctuating/mean) drag is plotted against the frontal area. The same reduction of $C_D(\text{mean})$ and of the (fluctuating/mean) drag, as with the case of increasing AR, is apparent.

For non-turbulent flow, Hoerner (Ref. 64) has a value of drag coefficient of 1.17 for plates with AR up to 5, where the coefficient begins to rise and extrapolates to a value of 1.97 for the infinite aspect ratio case. The values of the drag coefficient of plates in the present case are about 10 to 20 percent higher than Hoerner's steady value.

From the linearized theory of aerodynamic admittance considered in previous section one would expect, for (say) the slotted baffle produced turbulent field (intensity about 11%) that:

$$\frac{(r.m.s.)^2}{(\overline{u})^2} = \frac{\overline{u'^2}}{\overline{u}^2} = 4 \frac{\overline{u'^2}}{\overline{u}^2} = 4 \times (0.11)^2$$

$$\text{i.e.} \quad \frac{\overline{u'^2}}{\overline{u}^2} = 4 \times 0.0121 = 0.0484$$

$$\text{or} \quad \sqrt{\frac{\overline{u'^2}}{\overline{u}^2}} = 0.22$$

This value seems to be rather low if we assume an exponential decay law, Fig. 268, and extrapolate the data to zero AR where the theory is most likely to hold. The best-fit relation for the slotted baffle could be given as $\sqrt{\frac{\overline{u'^2}}{\overline{u}^2}} = 0.2875e^{-0.14AR}$

In general the linearized theory meets with limited success.

The values of the mean drag coefficient for the circular and square section cylinders are lower than those of the flat plates. This may be the result of flow reattachment. Considerable reduction is also observed in the values of the (fluctuating/mean) drag of the circular and square section cylinders compared with those of flat plates.

16. CONCLUSIONS.

The conclusions reached are:

- 1) The aerodynamic admittance seems to have a high frequency fall off at about a reduced frequency, based on the model frontal area and the scale of turbulence, of about 0.1.
- 2) Increase in the AR of the models results in a decrease in the aerodynamic admittance.
- 3) Increase in the frontal area of the models is followed by a general decrease in the aerodynamic admittance.
- 4) A decrease in the aerodynamic admittance is the result of an increase in the turbulence level.
- 5) For the same frontal area an increase in the integral scale of turbulence is followed by an increase in the aerodynamic admittance.
- 6) The linearized theory between force and velocity achieves only a limited success.
- 7) Mean drag coefficient values at low AR values tend to values higher than the corresponding steady flow values by 10 to 20 percent.
- 8) The load intensity (fluctuating/mean) drag could be assumed to follow an exponential decay curve when plotted against the AR.
- 9) Fluctuating and mean drag for circular and square section cylinders have values much lower than those of flat plates.

17. RECOMMENDATIONS

The experiments reported herein have been basic in nature but have established that the wind tunnel can provide useful information and research data for further study of the fluctuating loads on structures in the atmospheric turbulence of the earth's boundary layer.

Improvements could be made in the design of the model and the support system thus eliminating possible sources of extraneous inputs to the measuring system, i.e.

The model sting support aerodynamically represents an "afterbody" that might have an important effect, particularly for small plates.

There might be small errors due to the sensitivity of the balance to the point of application of the resultant load.

These factors should be carefully considered in designing further experiments using a similar approach.

There are several useful extensions of these experiments that could be conducted, using the same techniques as those described in this report. At the same time there are many other experiments, requiring different approaches, that could also help expand the knowledge in this field. Some possibilities are listed below:

1. The effect of turbulence intensity, as a parameter, on aerodynamic response, especially turbulence levels of the order of magnitude met with in the atmospheric boundary layer near the earth's surface, 20% - 40%.
2. The forces and moments on the wings of VTOL and STOL aircraft flying at low speeds near the ground will be affected by atmospheric turbulence. It becomes important in this case to measure the response at angles

of incidence to the wind throughout a range from 0° to 90° .

3. Duplication of the present experiments at much larger scale to investigate scale effects. This could be an extension of the experiments already reported by Davenport that were done in natural turbulence in an open field. An alternative would be to use a large free jet as it is available downstream of any non-return circuit wind tunnel.
4. Increase the variety of cross-sections of the cylinders, 3-D bodies being the ones usually met with in practice.
5. Direct measurement of two-point space and time correlation of the pressures on the face of a flat plate, including flat plates, at several angles of incidence.
6. A new approach to the problem could be tried by measuring the power spectrum of the input (velocity or pressure) together with the cross-power spectra between the input and output i.e. between velocity, or pressure and load. In this case according to Bendat (Ref. 40) the complete frequency response function is related to the input spectral density $S_{u'}(f)$ and the cross-power spectral density $S_{u'n}(f)$ (between the input and output).

This simple (complex valued) formula is

$$S_{u'n}(f) = \mathcal{H}(f) S_{u'}(f) \dots \dots \dots A$$

where $\mathcal{H}(f)$ = frequency response function

Rewriting in the complex notation

$$|S_{u'n}(f)|/e^{j\theta(f)} = S_{u'}(f)/\mathcal{H}(f)/e^{j\phi(f)} \dots \dots B$$

which implies that

$$|S_{u'n}(f)| = S_{u'}(f)/|\mathcal{H}(f)| \dots \dots \dots C$$

and

$$\Theta(f) = \phi(f) \dots \dots \dots D$$

where $\Theta(f)$ and $\phi(f)$ are defined in B, above.

Therefore, with knowledge of the input power spectra and the cross-power spectra, the frequency response function is completely determined both as to amplitude magnification and phase shift. At the same time one must always bear in mind the assumptions being made when applying any of the other formulas to the present problem. It must always be remembered that the above results assume;

1. a constant parameter linear system,
2. an input which is a stationary random process.

A MATHEMATICAL MODEL OF THE FLOW SITUATION

IN FRONT OF THE MODEL

NOTATION.

(Used in the Mathematical Model)

$\text{Coh}(\vec{r}, k_1)$	-non-dimensional coherence function
$d\vec{z}(\vec{k}, \omega)$	-complex vector amplitude of an elementary spectral component
$E()$	-expectation operator
$E(k)$	-scalar energy spectrum function
J_0, j	-Bessel function of the first kind
k_1	-wavenumber in the u direction = $2\pi\ell/\lambda$
\vec{k}	-wavenumber vector
$S(\vec{r}, \omega)$	-cross-spectral density function
$S(k_1)$	-measurable one-dimensional spectrum
t	-time
$u(x, t)$	-random vector velocity field in space and time
\bar{u}	-mean velocity
u_1'	-fluctuating velocity component in the x_1 direction
$Cr(r, k)$	-cross-correlation function
\vec{x}_i	-space coordinate vector for position i
x_1	-space coordinate in the \bar{u} direction
x_0	-virtual origin of turbulence behind the baffle
$\phi(\vec{k}, \omega)$	-spectrum tensor
ω	-circular frequency

PART III

A MATHEMATICAL MODEL18. INTRODUCTION.

In understanding the effect turbulence has on a body an examination of the effect the body (especially when the body is oscillating) has on turbulence is required. A theory has been developed by Hunt (Ref.24), based on the rapid distortion theory of turbulence, in order to analyse the turbulence in a flow sweeping past a body. The rapid distortion theory itself, developed by Batchelor and Proudman (Ref.25), requires the following assumptions:

- a) the mean flow should be irrotational, which limits the analysis to that region of the flow outside the boundary layers and wake;
- b) $\sqrt{u'^2} \ll \bar{u}$ so that the only contribution to vortex line stretching and twisting comes from changes in the mean flow;
- c) in the time it takes for a fluid element to be swept past the body the turbulent energy dissipated by viscous stresses is small; this leads to the condition $\frac{L_x}{D} \gg \frac{\sqrt{u'^2}}{\bar{u}}$.

Hunt shows that with these assumptions the problem reduces to the solution of a number of linear equations.

In the present work $L_x/D = O(1)$ so that the conditions in the free stream are met as $\frac{\sqrt{u'^2}}{\bar{u}} \ll 1$ and consequently

$$\frac{L_x}{D} \gg \frac{\sqrt{u'^2}}{\bar{u}}.$$

Qualitatively it is expected that as $\frac{L_x}{D} \rightarrow \infty$, the effect of the body on the turbulence will be similar to its ef-

Spectrum of the Longitudinal
Velocity Component in the Energy
Containing Region

Slotted Baffle

Experimentally Determined
Free Stream at Test Section

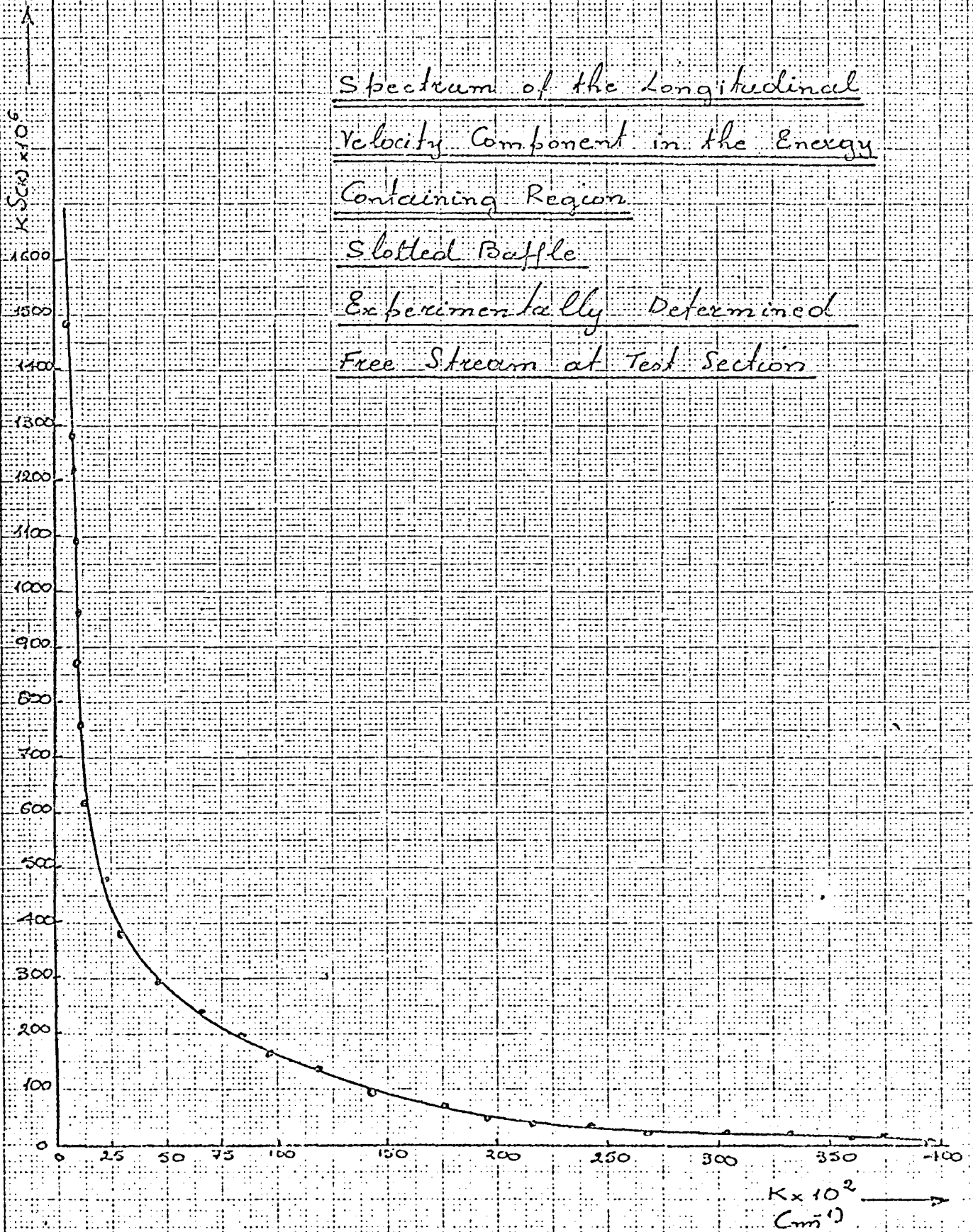


FIG: A

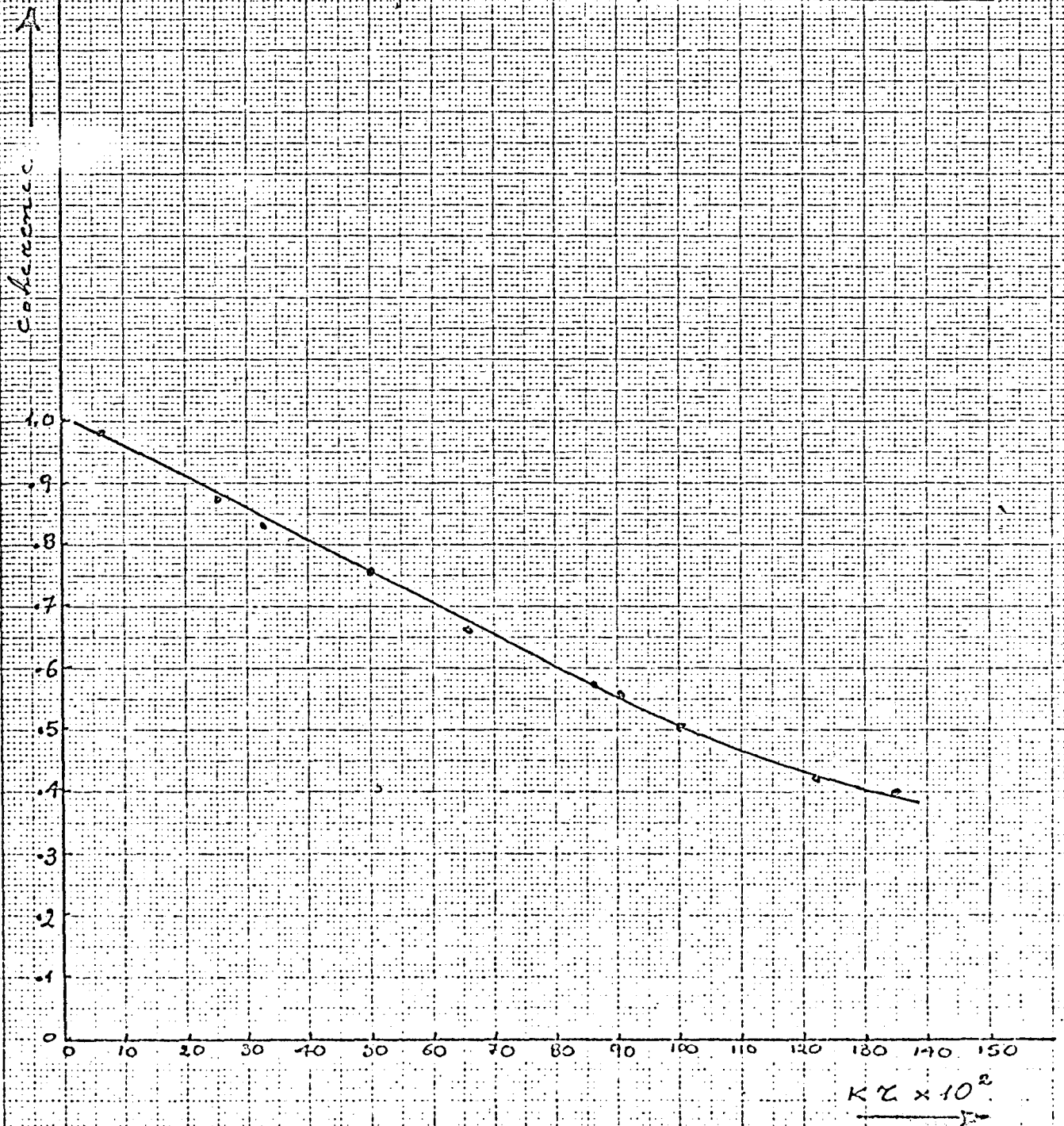
Variation of Derived Coherenceversus $K\lambda$. $\lambda = 0.5 \text{ mm}$ Slotted Baffle - Test Section

FIG: B

The Function $G(\theta)$

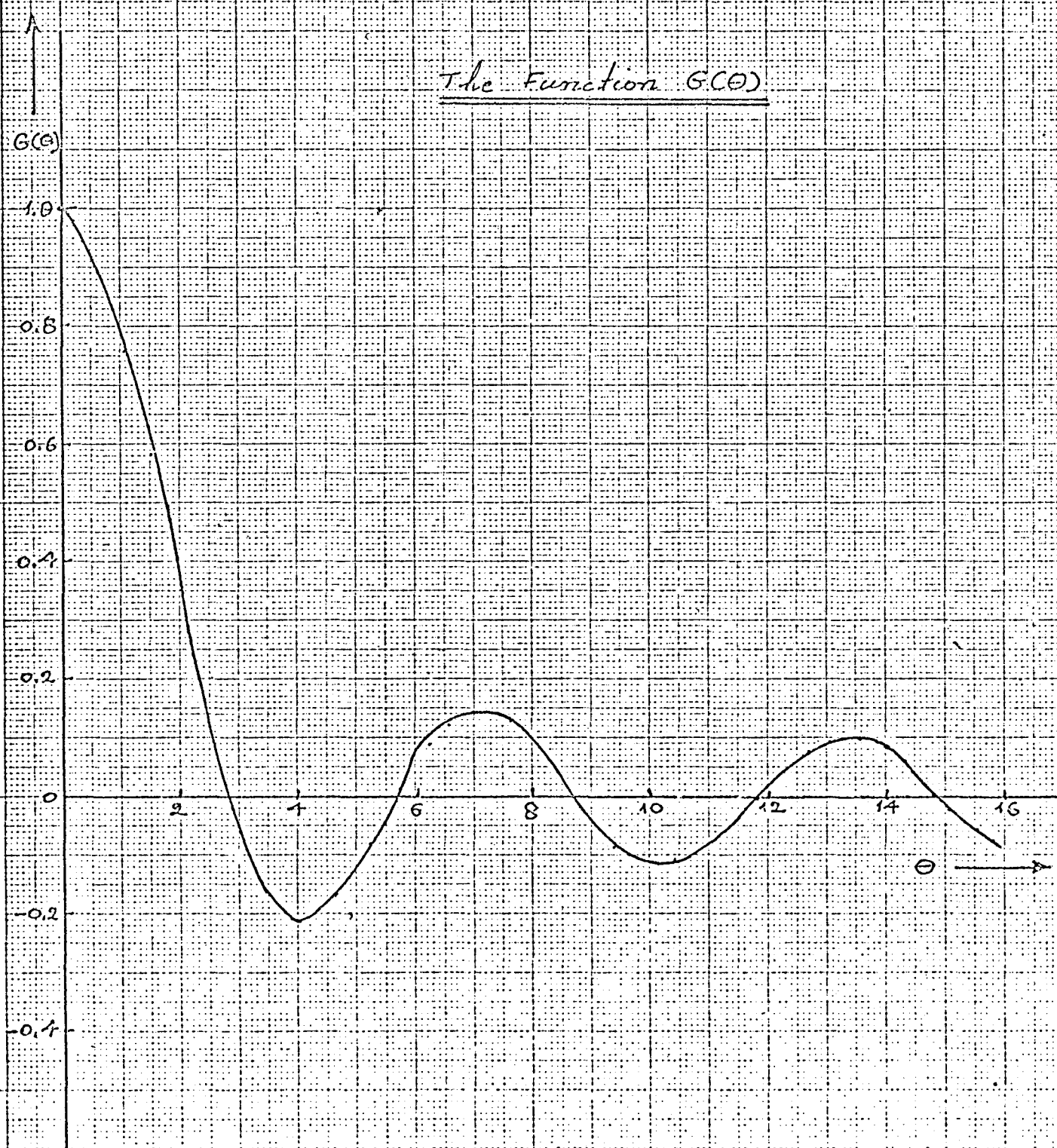


FIG: C.

fect on the mean flow. On the other hand as the sizes of the eddies become very small compared to the size of the body $\frac{L}{D} \rightarrow 0$ the dominant effect will be the stretching of the vortex lines by the mean flow. When $\frac{L}{D} = 0 < 1$, as in the present case it is expected that some combination of these two effects will be present.

Considering the above, the theoretical analysis of the flow field in front of the models in terms of the turbulence level is complicated.

It is the author's opinion that the situation could be analysed in a comparatively easier manner if the coherence of the turbulence field in front of the models is examined.

As mentioned earlier it has been shown by Davenport (Ref.10), by Etkin (Ref.11) and Harris (Ref.12) that the statistical description of the turbulent wind properties can be fulfilled by specifying the general two-point cross-spectrum. This could be followed - according to the author's opinion - by a consideration on how the coherence function changes as the model is approached from upstream.

Therefore, as a first step, a primitive attempt is being made in finding an analytical model by which the coherence function may be calculated from the velocity power spectrum. This implies that once the spectrum variation in front of the model is known the respective variation of the coherence function could be deduced and consequently the statistical properties of the varying turbulent field as it approaches the model could - up to a certain extent - be estimated.

In the analytical work which follows the turbulence field in front of the model is assumed homogeneous and isotropic. This is a simplification which could be justified by the fact that

as there are only a few measurements of the coherence function in the atmospheric boundary layer, it seems advisable to work with the simple isotropic model as a first step. At the same time, such a model could be served as a base for subsequent refinements.

Previous work on the coherence of isotropic turbulence has been restricted to simple spectral models, and experimental data have not yet conclusively demonstrated the suitability of such models. In the present work it is shown that the coherence function can be calculated from the respective velocity power spectrum.

19. MODEL FORMULATION.

The random velocity field in a flow stream could be represented by:

$$\vec{u}(\vec{x}, t) = \vec{u} + \vec{u}'(x, t) \dots \dots \dots (1)$$

The coordinate axes system could be chosen in such a way so that x and u' lie in the direction of \vec{u} . The fluctuating velocity field $u'(x, t)$ has zero mean and can be presented by the Fourier Stieltjes integral:

$$\vec{u}'(\vec{x}, t) = \int e^{i(\vec{k}\vec{x} - \omega t)} d\vec{z}(\vec{k}, \omega) \dots (2)$$

The integration is over all \vec{k}, ω space.

The cross-correlation function for the u' velocity components at two positions in the flow, \vec{x}_1 and \vec{x}_2 , in a plane perpendicular to \vec{x}_1 , may be defined as:

$$C_r(\vec{x}_1, \vec{x}_2, t_1, t_2) = E\{u'(\vec{x}_1, t_1) u'(\vec{x}_2, t_2)\} \dots (3)$$

where $E\{ \}$ is the expectation operator.

For homogeneous, stationary turbulence this function depends on:

$$\left. \begin{aligned} \vec{x}_2 - \vec{x}_1 &= \vec{r} \\ \text{and } t_2 - t_1 &= \tau \end{aligned} \right\} \dots \dots \dots (4)$$

In this case, it is readily shown, by considering eqns (2) and (3) that:

$$C_r(\vec{r}, \tau) = \int e^{i\vec{r} \cdot \vec{k} - i\omega\tau} \phi(\vec{k}, \omega) d\vec{k} d\omega \dots (5)$$

$$\text{where } \phi(\vec{k}, \omega) d\vec{k} d\omega = E \{ dz_1^*(\vec{k}_1, \omega) dz_2(\vec{k}_2, \omega) \} \dots (6)$$

$$\text{and } \omega = \kappa, \bar{a}$$

for overlapping pairs $(d\vec{k}_1, d\vec{k}_2)$ and $(d\omega_1, d\omega_2)$.

If now we assume that Taylor's hypothesis is valid it follows that:

$$\phi(\vec{k}, \omega) = \phi(\vec{k}) \delta\left(\kappa - \frac{\omega}{|\bar{a}|}\right) \dots \dots \dots (7)$$

and that the cross-spectral density function, defined as:

$$S_{1,2}(\vec{r}, \omega) = \frac{1}{2\pi} \int_{-\infty}^{\infty} C_r(\vec{r}, \tau) e^{i\omega\tau} d\tau \dots \dots (8)$$

is given, referring to equation (5):

$$S_{1,2}(\vec{r}, \omega) = \int_{-\infty}^{\infty} \int_{-\infty}^{\infty} e^{i\vec{k} \cdot \vec{r}} \phi(\vec{k}) d\vec{k}_2 d\vec{k}_3 \dots \dots (9)$$

The non-dimensional coherence function is simply:

$$\begin{aligned} \text{coh}(\vec{r}, \kappa) &= \frac{S(\vec{r}, \omega)}{S(0, \omega)} \\ &= \frac{1}{S(\kappa)} \int_{-\infty}^{\infty} \int_{-\infty}^{\infty} e^{i\vec{k} \cdot \vec{r}} \phi(\vec{k}) d\kappa_2 d\kappa_3 \dots (10) \end{aligned}$$

$$\text{where } S(\kappa) = \int_{-\infty}^{\infty} \int_{-\infty}^{\infty} \phi(\vec{k}) d\kappa_2 d\kappa_3 \dots \dots \dots (11)$$

is the measured, one-dimensional spectrum.

It is reasonable to suppose that the turbulence generated by a grid will tend to be axially symmetric, about the mean flow direction.

Further it could be assumed that for axially symmetric turbulence about the direction x_1 , Rao and Swamy's theory (Ref. 65) could apply. Assuming this theory the wavenumber spectrum has the form:

$$\phi(\vec{k}) = \Theta_1 C(k, k_1) \left(1 - \frac{k_1^2}{k^2}\right) + \Theta_2 C(k, k_1) \left(1 - \frac{k_1^2}{k^2}\right)^2 \dots (12)$$

where $k = |\vec{k}|$ and Θ_1, Θ_2 are arbitrary functions of k and k_1 .

Substituting the value of $\phi(\vec{k})$ given by eqn. (12) into eqn. (10) we obtain:

$$C_{01}(k, k_1) = \frac{2\pi}{S C(k_1)} \int_{k_1}^{\infty} \left(\Theta_1 C(k, k_1) + \Theta_2 C(k, k_1) \left(1 - \frac{k_1^2}{k^2}\right) \right) \cdot (k^2 - k_1^2) J_0(\epsilon \sqrt{k^2 - k_1^2}) d k \dots (13)$$

$$\text{where } \epsilon = |\vec{r}| = \epsilon_1^2 + \epsilon_2^2 \dots (14)$$

The functions Θ_1 and Θ_2 are difficult to estimate by direct measurement. In order to be able to introduce some experimental value some further simplification of the above theoretical model is required. Such a simplification could be introduced by assuming that the turbulence is isotropic (i.e. spherically symmetric).

In such a case considering eqn. (12) we have:

$$\Theta_2 = 0 \dots (15)$$

and Θ_1 is a function of k only.

If we let:

$$\Theta_1 C(k, k_1) = \Theta_1 C(k) = \frac{E C(k)}{4\pi k^2} \dots (16)$$

then for an isotropic field, we have:

$$\phi(\vec{k}) = \frac{E(k)}{4\pi k^2} (k^2 - k_1^2) \dots \dots \dots (17)$$

Now $E(k) dk$ is the contribution to the total energy of the flow from that part of the wavenumber space between spheres of radii k and $k+dk$.

From equations (13), (15) and (16) it follows that, for an isotropic field,

$$\text{Coh}(r, k) = \frac{1}{2S(k_1)} \int_{k_1}^{\infty} \frac{E(k)}{k^3} (k^2 - k_1^2) J_0(k\sqrt{k^2 - k_1^2}) dk \dots (18)$$

Batchelor (Ref. 29) in his theory showed that:

$$\frac{E(k)}{k^3} = \frac{d}{dk} \left(\frac{1}{k} \frac{d}{dk} S(k) \right) \dots \dots \dots (19)$$

Therefore it can be seen that a direct relationship exists between $\text{Coh}(r, k)$ and the measured spectrum $S(k_1)$.

By substitution of equation (19) into eqn. (18) and integrating by parts, twice, we find that if $S(k_1)$ and its derivative with respect to k_1 approach zero sufficiently rapidly as $k_1 \rightarrow \infty$, we have:

$$\text{Coh}(r, k) = 1 - \frac{r^2}{S(k_1)} \int_{k_1}^{\infty} k S(k) G(k\sqrt{k^2 - k_1^2}) dk \dots (20)$$

$$\text{where } G(\theta) = \frac{J_0(\theta)}{2} + \frac{J_1(\theta)}{\theta} \dots \dots \dots (21)$$

In Fig. C the behaviour of the function $G(\theta)$ is shown.

From the curve it is seen that

$$G(\theta) \rightarrow 1 \text{ as } \theta \rightarrow 0 \dots \dots \dots (22)$$

and that

$$G(\theta) \rightarrow \frac{1}{\sqrt{2\pi\theta}} \cos(\theta - \pi/4) + o(|\theta|^{-1}) \dots (23)$$

as

$$\theta \rightarrow \infty$$

Therefore if the form of $S(k_1)$ or $E(k)$ is known, we can evaluate $Co_h(r, k_1)$ from either eqns (20) or (18), by a single integration.

A further simplification could be achieved if we consider a small spacing between the two measuring points. In such a case eqn (20) reduces to:

$$Co_h(r, k_1) = 1 - \frac{r^2}{S(k_1)} \int_{k_1}^{\infty} k S(k) dk \dots \dots \dots (24)$$

This is solely a function of the spectrum $S(k_1)$.

If now we consider the spectra obtained in the previous experimental investigation it could be seen that the one-dimensional spectrum could be measured with a satisfactory degree of accuracy in the region from the energy containing wavenumbers to higher wavenumbers.

To try to obtain the coherence function from the experimentally obtained low frequency spectrum could not be advisable as the spectrum itself is not measured within a satisfactory accuracy range. Therefore in this work it was thought advisable to consider the relation (as far as the actual practice was concerned) between the coherence and the respective part of the energy spectrum in the higher wavenumber range.

20. MODEL PREDICTION.

The experimentally determined velocity power spectrum for the slotted baffle produced turbulent flow field at the test section is shown in Fig.A. The part of the velocity power spectrum shown in Fig.A represents the portion of the experimentally determined spectrum from the energy containing region to the inertial subrange. The derived coherence function, from this spectrum, for a small separation distance r is shown in Fig.B. The derivation

of the coherence function is based on eqn (24) which is true for only small values of r . In this case r was taken as $r = 0.5\text{mm}$. It is obvious that for larger values of r eqn (24) does not hold.

21. DISCUSSION OF THE MATHEMATICAL MODEL.

The mathematical model arrived at, eqn (24), for the determination of the coherence of the turbulent field, from the respective velocity power spectrum, seems to give a satisfactory result. It should be noted that the actual mathematical model is represented by eqn (20), eqn (24) being a simplification of this. A second fact that should be considered is that the derivation of the model assumed an isotropic field. Although this could be acceptable for any first attempt in deriving a mathematical model it is far from being true in actual fact. The resulted plot of the coherence function against kr , ^{Fig. B,} does not seem to have the exponential form usually associated with it; examples of experimentally determined coherence functions are shown in Fig. 26 to Fig. 28. The simplified form of the equation assumed could be the reason for it. On the other hand it should be noted that: a) the wavenumber range considered is rather limited, and b) only the higher wavenumber range of the velocity power spectrum was considered. Nevertheless it could be said that with further refinement the present mathematical model could attain a more realistic nature.

22. CONCLUSIONS DRAWN ON THE MATHEMATICAL MODEL.

The main conclusion reached in trying to find a mathematical model for the calculation of the coherence function from the spectrum function was that a certain success was achieved as far as the primitive mathematical model was concerned.

The use of a faster calculating technique (computerized

method), it is obvious that, it would make possible the utilization of the complete equation representing the mathematical model. If this is taken further perhaps it would be possible to estimate the coherence function from any spectrum resulting from a turbulence field the nature of which would not be restrained (as far as numerical calculations are concerned) by non-isotropic or non-axisymmetric properties. In such a case the mere measurement of the spectrum in front of a model could possibly give us the whole picture of the situation.

23. GENERAL CONCLUSIONS.

a) The examination of the interaction of the flow with the model has shown that the mere presence of the model distorts the flow in such a way that the correlation of the forces on the frontal surface of it decreases. This decrease is more pronounced in the case of the rigidly held model compared with the case of the freely oscillating model. Consideration of the harmonic content of the oscillations of the model (model externally excited) has shown that the integral scale of turbulence decreases as the frequency or/and amplitude of oscillations increase.

b) The variation of the energy level of the different eddies as the model is approached from upstream seems to follow a power law decay curve.

c) For the regions of low frequencies the pressure spectra at the stagnation point on the model coincide with the velocity spectra, the latter measured just in front of the stagnation point; at higher frequencies the pressure spectra fall below the respective velocity spectra.

d) Increase in: 1) AR of the models, 2) their frontal area, and 3) the turbulence level, is followed by a decrease in aerodynamic admittance. At the same time it should be noted that the linearized theory used between force and velocity seems to achieve only a limited success.

e) The load intensity, when considered as a function of AR shows an exponential decay law.

f) The mathematical model, arrived at, for the calculation of the coherence function from the spectrum function seems to have achieved a certain success.

24. REFERENCES.

1. el Baroudi, M.Y.

Measurement of two-point Correlations of Velocity near a Circular Cylinder Shedding a Karman Vortex Street.

U.T.I.A. Technical Note No.31,
January 1960

2. Mattingly, G.E.

An Experimental Study of the Three-Dimensionality of the Flow Around a Circular Cylinder.

University of Maryland,
T.N. BN-295, June 1962.

3. Roshko, A.

On the Drag and Shedding Frequency of Two-dimensional Bluff Bodies.
NACA TN 3169, July 1954.

4. Surry, J.
&
Surry, D.

The Effect of Inclination on the Strouhal Number and other Wake Properties of Circular Cylinders at Subcritical Reynold's Numbers.
U.T.A.S. Tech. Note No. 116,
August 1967.

5. Bearman, P.W.

An Investigation of the Forces on Flat Plates in Turbulent Flow.
N.P.L. Aero Report 1296, April 1969.

6. Vickery, B.J.

On the Flow Behind a Coarse Grid and its Use as a Model of Atmospheric Turbulence in Studies Related to Wind Loads on Buildings. N.P.L. Aero Report 1143, March 1965.

7. Lappe, U.O.

8. Etkin, B.

9. Lumpley, J.L.
&
Panofsky, H.A.

10. Davenport, A.G.

11. Etkin, B.

12. Harris, R.I.

13. Schuber, G.B.
&
Dryden, H.L.

14. Willmarth
&
Woodridge, C.E.

15. Corcos, G.M.

A Low Altitude Turbulence Model for
Estimating Gust Loads on Aircraft.
AIAA Paper 65 - 14. January 1965.

Dynamics of Aerospace Vehicles,
A Quarter Century of Change and two
Current Problems.

Canadian Aeronautics and Space Jour-
nal, Vol.11, No. 8, October 1965.

The Structure of Atmospheric Turbu-
lence. Interscience Publishers,
John Wiley and Sons, Inc. 1964.

J.Inst. Civ. Eng. 23, p.389, 1962.

Proc. Meeting on Ground Wind Load
Problems in Relation to Launch Ve-
hicles.

NASA Langley Research Centre, 1966.

Wind Effects on Buildings and
Structures. H.M.S.O. London 1965.

The Effect of Turbulence on the Drag
of Flat Plates.

NACA Report No. 546 (1935)

Measurement of the Fluctuating Pres-
sure at the Wall Beneath a Thick
Turbulent Boundary Layer.

The University of Michigan College of
Engineering, Tech. Report, April, 1962.

Pressure Fluctuations in Shear Flows,
University of California,

Inst. of Eng. Research, Series No. 183

Issue No. 12. July 1962.

16. McGregor, D.M.

An Experimental Investigation of the Oscillating Pressures on a Circular Cylinder in a Fluid Stream.

U.T.I.A. Technical Note No. 14,
June 1957.

17. Pasquill, F.

Atmospheric Diffusion,

Van Nostrand, New York, 1962.

18. Best, A.G.

Transfer of Heat and Momentum in the Lower Layers of the Atmosphere,
Geophys. Memoirs, No. 65, pp. 40-66,
1935.

19. Cramer, H.E.

Preliminary Results of a Program for Measuring the Structure of Turbulent Near the Ground.

Geophys. Res. Paper AFGR, No. 19 Pt. 2
pp. 187 - 205, 1952.

20. Sutton, O.G.

Micrometeorology,

McGraw-Hill, New York, 1953.

21. Huss, P.O.
&
Portman, D.J.

The Study of the Natural Wind and Computation of the Austausch Turbulence Constant. Daniel Cuggenheim Airship Inst. Report No. 156, The University of Akron, Akron, Ohio, Feb. 1949.

22. -----

Proceedings of the Conference Held at N.P.L., Wind Effects on Buildings and Structures, Teddington, Middlesex.
June 26 - 28, 1963.

H.M.S.O. London.

23. Petty, D.G.

The Distortion of Turbulence by a Cir

24. Hunt, J.C.R.

25. Batchelor, G.K.
&
Proudman, I.

26. Heisenberg, W.Z.

27. Obukhoff, A.M.

28. Batchelor, G.K.

29. Batchelor, G.K.

30. Uberoi, M.S.

31. Kobashi, Y.

32. Doak, P.E.

cular Cylinder. Symposium on External Flows, University of Bristol, July 1972.
Some Theories for the Mean and Turbulent Velocity Distributions in Flows Around Bluff Bodies. Symposium on External Flows, University of Bristol, July 1972

Quart. J. Mech. App. Math. 7, 83 (1954)

Zur Statistischen Theorie der Turbulenz, Z. Phys. 124, 628 (1948).

Pressure Fluctuations in a Turbulent Flow, Doklady Akad. Naut. S.S.S.R. 66, 17, 1949.

Pressure Fluctuations in Isotropic Turbulence.

Proc. Camb. Phil. Soc. 47, 359 (1951).

The Theory of Homogeneous Turbulence, Cambridge University Press 1959.

Correlations Involving Pressure Fluctuations in Homogeneous Turbulence NACA TN 3116, 1954.

Measurements of Pressure Fluctuations in the Wake of a Cylinder, Journal of the Physical Society of Japan 12, 533, 1957.

Acoustic Radiation from a Turbulent Fluid Containing Foreign Bodies.

Proc. Roy. Soc. A254 129, 1960.

33. Marshall, R.D.
&
Cermak, J.E.

34. Lamb, L.

35. Roshko, A.

36. Thom, A.

37. Fromm, J.E.
&
Harlow, F.H.

38. Sarpkaya, T.
&
Garrison, G.W.

39. Robson, J.D.

40. Bendat, J.S.

41. Van der Hegge Zijnen,
B.G.

42. Corrsin S.
&
Uberoi, M.S.

Wind Studies of Bank of America World Headquarters Building - Part II, Wind Tunnel Study. Report CE R66-67RDM-JEC19, Fluid Dynamics and Diffusion Laboratory, Colorado State University Fort Collins, Colorado, 1966.

Hydrodynamics, Cambridge, 1932, p.99.
On the Wake and Drag of Bluff Bodies. Journal of Aerospace Sciences, February, 1955.

Proc. Roy. Soc. A141, 1933.

Numerical Solutions of the Problem Vortex Street Development. Physics of Fluids 6, July, 1963.

Vortex Formation and Resistance in Unsteady Flow. Journal of Applied Mechanics, March 1963.

An Introduction to Random Vibration, Chapter 3, Edinburgh University Press 1963

Principles and Applications of Random Noise Theory. John Wiley and Sons, Inc. New York, 1958.

Measurement of Turbulence in a Plane Jet of Air by the Diffusion Method and by the Hot-wire Method. App. Sci. Res. Section A, Vol. I, Oct. 1957.

Spectra and Diffusion in a Round Turbulent Jet. NACA Report 1040, 1951.

43. Whitelaw, J.H.

Laser Anemometry in Liquids and Gases
V.K.I. Lecture Series 64. Laser Applications in Single and Two-phase Flows, 1974.

44. Skordilis, G.

Measurement of the Fluctuating Loads on Bodies of Simple Shape Placed in a Highly Turbulent Stream,
V.K.I. Report 74-12, June 1974.

45. Disa Manual

C.T. Anemometer Type 55D01

46. Disa Manual

C.T. Anemometer Type 55A01

47. Bruel & Kjaer

Instructions and Applications of the Frequency Analyser, Type 2120, February, 1973.

48. Laurence, J.C.
&
Landes, L.G.

Auxilliary Equipment and Techniques for Adapting the Constant-Temperature Hot-wire Anemometer to Specific Problems in Air-flow Measurements.

49. Sandborn, V.A.

NACA TN 2843 1952.
Experimental Evaluation of Momentum Terms in Turbulent Pipe Flows.

49. Sandborn, V.A.

NACA TN 3266, 1955

50. Rice, S.O.

Mathematical Analysis of Random Noise
The Bell Systems Techn. Journal,
Vol.23, No.3, July 1944.

51. Allen H.J.

Wall Interference in a Two-dimensional Flow Wind Tunnel with Considerations of the Effect of Compressibility
Nat. Adv. Comm. Aero., Wash.,
Rep. 782, 1944.

52. Singer, I.A.

53. Taylor, G.I.

54. Diederich, F.N.

55. -----

56. Cooper, K.

57. Campbell, A.C.
&
Etkin, B.

58. Skordilis, G.

59. -----

Wind Gust Spectra, Annals of the New York Academic of Sciences, Vol. 116 Article 1, pp. 116-133, June 26, 1964

Turbulence in a Contracting Stream. Z. Angew. Math. Mech. 15, 91 (1935).

The Response of Airplane to Random Atmospheric Disturbances.

NACA Rep. No. 1345, 1958.

Compilation of Papers Presented at the NASA Langley Research Centre Meeting on Aircraft Response to Turbulence.

September 24 - 25, 1968.

Bending Response of a Cantilever Cylinder to Turbulent Shear Flow. U.T.I.A.S. Tech. Note No. 139.

August 1969.

The REsponse of a Cylindrical Structure to a Turbulent Flow Field at Subcritical Reynolds No.

U.T.I.A.S. Tech. Note No. 115, July 1967.

Wind Excited Oscillations of Simply Supported Circular Beams.

Final Year Undergraduate Project, Dpt. of Transport Technology, Loughborough University, 1973

Proceedings of the International Research Seminar, Held at the N.R.C. Ottawa, Canada, On Wind Effects on

60. -----
Buildings and Structures. September 11 - 15, 1967. University of Toronto Press, Canada, 1968.
Proceedings of a Symposium on Wind Effects on Buildings and Structures. April 2 - 4, 1968. Loughborough University of Technology, England.
61. -----
Proceedings of the Third International Conference on Wind Effects on Buildings and Structures. September 6 - 9, 1971, Tokyo, Japan.
62. -----
Wind Effects on Buildings and Structures, Lecture Series 45, February 21 - 25, 1972, Von-Karman Institute, Belgium.
63. McNown, J.S.
Drag in Unsteady Flow. The University of Michigan and the Sandia Corporation. IX^e Congrès International de Mécanique Appliquées. Tome III, Université de Bruxelles. *Date?*
64. Hoerner, S.F.
Fluid Dynamic Drag. Midland Park, 1958.
65. Rao N.S.G.
and
Swamy, N.V.C.
J. Eng. Mech. Div., ASCE, EM2, (1), 88, 1962.
66. Hinze, J.O.
Turbulence: An Introduction to its Mechanism and Theory. McGraw-Hill Book Co. Inc. 1959
67. Portforos, E.A.
Isotropy in Strained and Unstrained Grid Turbulence.

68. Uberoi, M.S.
&
Kavaszny, L.S.G.

69. Davenport, A.G.

70. Tukey, J.W.

71. Davenport, W.B.
Johnson, R.A.
&
Middleton, D.

Ph.D. Thesis, Dpt. of Mechanical Engineering, University of Toronto, 1969.

On Mapping and Measurement of Random Fields. Quarterly Applied Mathematics, Vol. X, No.4, pp 375 - 393, 1953.

The Buffeting of Large Superficial Structures by Atmospheric Turbulence. Reprinted from the Annals of the New York Academy of Sciences, Vol. 116, Article 2, pages 135 - 159, June 26, 1964.

The Sampling Theory of Power Spectrum Estimates.

Symposium on Applications of Autocorrelation Analysis to Physical Problems. Office Naval Res. May 1950.

Statistical Errors in Measurements on Random Time Functions.

Jour. Appl. Phys. Vol. 23, No.4, pp 377 - 380, April 1952.

APPENDICES

APPENDICESAppendix A.Joint Probability Density Distribution of the Velocity Fluctuations

It could be assumed that - approximately - we have two normal distributions of the fluctuating velocity given by:

$$\left. \begin{aligned} N_1 p_1(u') &= \frac{N_1}{\sigma_1 \sqrt{2\pi}} e^{-\frac{1}{2} \left(\frac{u'}{\sigma_1} \right)^2} \\ \text{and} \\ N_2 p_2(u') &= \frac{N_2}{\sigma_2 \sqrt{2\pi}} e^{-\frac{1}{2} \left(\frac{u'}{\sigma_2} \right)^2} \end{aligned} \right\} \dots\dots A.1$$

where

$p_1(u'), p_2(u') \dots$ respective probability density functions

$N_1, N_2 \dots$ respective number of observations for each distribution

$\sigma_1, \sigma_2 \dots$ standard deviations of respective distributions

The combined distribution is defined by:

$$N p(u') = N_1 p_1(u') + N_2 p_2(u') \dots\dots\dots A.2$$

where $N_1 + N_2 = N$

The question is to examine this distribution for normality.

Since the two frequency distributions $N_1 p_1(u')$ and $N_2 p_2(u')$ are each normal with mean zero, (assumed), the combined distribution $N p(u')$ is also symmetrical about zero. The mean zero assumption is valid as far as the experimental data are concerned as the probability density function displayer could be adjusted accordingly. Consequently, for the moments of the frequency distribution, μ_m , defined by:

$$\mu_m = \int_{-\infty}^{\infty} (u')^m p(u') du \dots\dots\dots A.3$$

where m is a positive number and designates the moment order, the following relations apply:

$$\left. \begin{array}{l} \mu_m = 0 \quad (m \text{ odd}) \\ \mu_m \neq 0 \quad (m \text{ even}) \end{array} \right\} \dots \dots \dots A4$$

For a normal distribution, the coefficient of kurtosis α_4 is defined by:

$$\alpha_4 = \frac{\mu_4}{\mu_2^2} = \frac{\mu_4}{\sigma^4} \dots \dots \dots A5$$

and has a fixed value of:

$$\alpha_4 = 3 \dots \dots \dots A6$$

In order to examine the normality of the distribution defined by equation A.2 consider only the value of α_4 , the coefficient of kurtosis, for that frequency distribution.

By definition the coefficient of kurtosis α_4 for the distribution of the equation A.2 is given by:

$$\alpha_4 = \frac{\frac{1}{N_1 + N_2} \left\{ \int_{-\infty}^{\infty} (u')^4 N_1 P_1(u') du' + \int_{-\infty}^{\infty} (u')^4 N_2 P_2(u') du' \right\}}{\left\{ \frac{\int_{-\infty}^{\infty} (u')^2 \{ N_1 P_1(u') + N_2 P_2(u') \} du'}{N_1 + N_2} \right\}^2} \dots \dots \dots A7$$

which when simplified yields:

$$\alpha_4 = \frac{\frac{3}{N_1 + N_2} (N_1 \sigma_1^4 + N_2 \sigma_2^4)}{\left\{ \frac{N_1 \sigma_1^2 + N_2 \sigma_2^2}{N_1 + N_2} \right\}^2} \dots \dots \dots A8$$

From equation A.6 a necessary condition for the distribution

on $Np(u)$ to be normal is that α_4 be equal to 3. From equation A.8 this condition is obviously true only when

$$N_1 \sigma_1^4 + N_2 \sigma_2^4 = \frac{1}{N_1 + N_2} (N_1 \sigma_1^2 + N_2 \sigma_2^2)^2 \dots\dots\dots A.9$$

Expanding the term on the right and simplifying yields:

$$\sigma_1^4 + \sigma_2^4 = 2 \sigma_1^2 \sigma_2^2 \dots\dots\dots A.10$$

Equation A.10 is thus a necessary condition for the distribution defined by A.2 to be normal. However, from the inequality

$$a^2 + b^2 > 2ab \quad (a \neq b) \dots\dots\dots A.11$$

the only case for which equation A.10 holds is when $\sigma_1 = \sigma_2$. Therefore the distribution $p(u)$ has a normal distribution only for the trivial case $\sigma_1 = \sigma_2$. If $\sigma_1 \neq \sigma_2$ it also follows from equation A.10 that the coefficient of kurtosis α_4 for $Np(u)$ given by equation A.8 is greater than 3. The combined distribution consequently has an excess of kurtosis.

Appendix B.

Hot-wire Instrumentation.

B.1 Linearization and Longitudinal Velocity Component Measurements.

Each hot-wire was calibrated by mounting it alongside the reference pitot-static tube in a constant flow velocity region, i.e. the wind tunnel test section when empty and with the turbulence generating baffle removed.

The initial voltage V_0 at zero flow velocity was noted. The wind tunnel was then run at different speeds starting above the maximum flow velocity expected. The flow velocity was then reduced in steps and for each speed the voltage output of the wire V_B was noted.

By plotting the expression $\left\{ \left(\frac{V_B}{V_0} \right)^2 - 1 \right\}$ against V (m/s), the flow velocity, in a log-log plot a linear relationship was obtained and the coefficient that has to be fed into the linearizer was given as:

$$K = \Delta V / \left\{ \Delta \left(\left(\frac{V_B}{V_0} \right)^2 - 1 \right) \right\}$$

The voltmeter gain adjustment was then set to a convenient value at will.

A typical linearization curve is shown in Fig.12.

The linearization of the system was verified by plotting volts against flow velocity as in Fig. 13.

The linearization procedure used above is not applicable for low velocities i.e. 0 - 1 m/s say, and consequently the relation of volts against flow velocity below 1m/s is not quite linear. This is expected to have no effect in the present work as the velocities used are well above this limit even for cases for which the flow is

retarded.

Calibrations were repeatable, except for residual temperature effects drifts that were normally less than 2%. Attention has also been paid to cleanliness, i.e. the experiments were interrupted when the laboratory atmosphere was not clean e.g. use of smoke in the neighbouring wind tunnel.

B.2 Frequency Response Considerations.

The frequency response of a hot-wire system can be viewed as made up of two separate parts:

1. The response of the system to a coherent two dimensional sinusoidal gust.
2. The attenuation of the real three-dimensional turbulence due to the finite length of the hot-wire.

The basic response of a constant temperature hot-wire anemometer has been treated widely both as to the thermal lag effects of the wire and to the electronic characteristics of the anemometer networks. Square wave tests have shown that the upper frequency limit for the different anemometers was between 25 - 30kHz.

The second aspect of the anemometer's response arises because of the three dimensional nature of the turbulent flow. The wire then responds to the integrated average velocity fluctuations along the wire if a locally two-dimensional cooling relation is assumed. An error is then introduced in the mean square measurements.

Ref. 66 discusses the form of these corrections in detail. They are usually small because the correction is an attenuation of the higher frequency components which usually contain only a small fraction of the energy. Generally it is difficult to infer the effect of the finite wire length on the spectral density measurements at high frequency.

cy.

Some experimental evidence exists as to the effects of finite wire length on measured spectral results, but the data are somewhat contradictory. Portforos (Ref.67) made measurements of the same turbulent field with three wire lengths and for two different turbulent regimes. In both cases his results show less effect than that predicted by Uberoi's and Kovazsnay's approach (Ref.68). Furthermore, the results show different effects for the same frequency in the two different cases. However, a similar but brief experiment by Teunissen of U.T.I.A.S., using the DISA 55A01 hot-wire anemometer with two different probe lengths for one turbulent case showed a difference in spectral results agreeing well with the results predicted by Davenport (Ref.69). In both experimental cases, however, the wire parameters were necessarily changed and hence the basic system response to coherent gust was altered. This should not be severe at the frequencies of interest. However, it is obvious that clarification of the situation is required both by exploring the applicability of Davenport's results and by hot-wire measurements which included system response measurements to a coherent input. Because of the weight of hot-wire investigations which have previously neglected a length correction, and because of the lack of concrete experimental verification, the above corrections were not made to the data presented herein.

Appendix C.Measurement of the Frequency - Dependent Correlation.

Let e_1' and e_2' be the voltage signals from two parallel hot-wires separated by a distance y in an air stream where the velocity fluctuations are u_1' and u_2' . If these voltage signals are combined by addition and subtraction to obtain $(e_1' + e_2')$ and $(e_1' - e_2')$ and these results are fed into two average-square circuits, the results are given by: $\overline{(e_1' + e_2')^2}$ and $\overline{(e_1' - e_2')^2}$. These processes are all carried out by feeding the initial signals into a DISA correlator.

If these readings are now added and subtracted, the result is:

$$\overline{(e_1' + e_2')^2} + \overline{(e_1' - e_2')^2} = 2\overline{e_1'^2} + 2\overline{e_2'^2} \text{----- (1)}$$

$$\text{and } \overline{(e_1' + e_2')^2} - \overline{(e_1' - e_2')^2} = 4\overline{e_1' e_2'} \text{----- (2)}$$

Dividing (2) by (1) yields:

$$\frac{\overline{(e_1' + e_2')^2} - \overline{(e_1' - e_2')^2}}{\overline{(e_1' + e_2')^2} + \overline{(e_1' - e_2')^2}} = \frac{4\overline{e_1' e_2'}}{2\overline{e_1'^2} + 2\overline{e_2'^2}} \text{----- (3)}$$

If the turbulence field is uniform and isotropic (or nearly isotropic) so that the average square of the fluctuations is the same and if the hot-wires are carefully matched as to the output, then eqn. (3) becomes:

$$\frac{\overline{(e_1' + e_2')^2} - \overline{(e_1' - e_2')^2}}{\overline{(e_1' + e_2')^2} + \overline{(e_1' - e_2')^2}} = \frac{4\overline{e_1' e_2'}}{4\overline{e_1'^2}} = \frac{\overline{e_1' e_2'}}{\overline{e_1'^2}} = \frac{\overline{u_1' u_2'}}{\overline{u_1'^2}} = R_{11}(0, r_2, 0) \text{--- (4)}$$

The averaging procedures considered in eqn. (4) take account of all frequencies. If now the averaging procedure is looked at from frequency to frequency the variation of the lateral correlation coefficient $R_{11}(0, r_2, 0)$ with frequency could be given by:

$$R_{11}(0, \alpha_2, 0)(f) = \frac{\text{Spectrum of sum} - \text{Spectrum of difference}}{\text{Spectrum of sum} + \text{Spectrum of difference}}$$

Appendix D.

C.1 Measurement of the Turbulence Kinetic Energy Using a Single Hot-wire.

In measuring the turbulence kinetic energy per unit mass at a point (theoretically) in a flow stream with a single hot-wire, the wire is rotated about itself as described below, noting its output at each position. At each position the wire is calibrated. With the hot-wire calibrated so that the true 45° angle relative to the flow is known, as shown in Fig. 275, the following outputs are noted:

First arrangement.

Wire normal to the flow and with the probe axis perpendicular to the x-y plane:

Output: $A_1 = \sqrt{u'^2}$ (1)

At $+45^\circ$ from this position: Output $A_2 = \sqrt{(u' + v')^2}$ (2)

At -45° from the same position: Output $A_3 = \sqrt{(u' - v')^2}$ (3)

Second arrangement.

Wire normal to the flow and with the probe axis perpendicular to the x-y plane:

Output: $A_4 = \sqrt{u'^2}$ (4)

(Theoretically the mid-point of the wire -considering the longitudinal axis of the wire- must be in the same position in space as in the first arrangement. Output (4) must be the same as output (1)). In this case the adjustment achieved was up to $\pm 0.02\text{mm}$.

At $+45^\circ$ from this position: Output: $A_5 = \sqrt{(u' + w')^2}$ (5)

Note: Clockwise rotation is assumed +ve, anticlockwise rotation is taken as -ve.

At -45° from the same position: Output: $A_6 = \sqrt{(\overline{u'}^2 + \overline{w'}^2)} \dots \dots \dots (6)$

Squaring and expanding relations 2,3,4 and 5 we get:

$$(A_2)^2 = \overline{u'^2} + \overline{v'^2} + 2\overline{u'v'} \dots \dots \dots (7)$$

$$(A_5)^2 = \overline{u'^2} + \overline{w'^2} + 2\overline{u'w'} \dots \dots \dots (8)$$

$$(A_3)^2 = \overline{u'^2} + \overline{v'^2} - 2\overline{u'v'} \dots \dots \dots (9)$$

$$(A_6)^2 = \overline{u'^2} + \overline{w'^2} - 2\overline{u'w'} \dots \dots \dots (10)$$

Adding relations (7) and (9) as well (8) and (10) respectively we get:

$$(A_2)^2 + (A_3)^2 = 2(\overline{u'^2} + \overline{v'^2}) \dots \dots \dots (11)$$

$$(A_5)^2 + (A_6)^2 = 2(\overline{u'^2} + \overline{w'^2}) \dots \dots \dots (12)$$

Squaring outputs (1) and (4).

$$(A_1)^2 = \overline{u'^2} = (A_4)^2 \dots \dots \dots (13)$$

Subtracting $2 \times A_1^2$ from relations (11) and (12) and dividing the result by 2 we get:

$$\frac{(A_2)^2 + (A_3)^2 - 2(A_1)^2}{2} = \overline{v'^2} \dots \dots \dots (14)$$

$$\frac{(A_5)^2 + (A_6)^2 - 2(A_1)^2}{2} = \overline{w'^2} \dots \dots \dots (15)$$

Therefore from (13), (14) and (15) the values of $\overline{u'^2}$, $\overline{v'^2}$ and $\overline{w'^2}$ obtained.

The turbulence kinetic energy per unit mass is given by:

$$K.E. = \frac{1}{2} \rho (\overline{u'^2} + \overline{v'^2} + \overline{w'^2})$$

C.2 Results of Turbulence Kinetic Energy measurements.

(Slotted baffle - $30 \times 120 \text{ mm}^2$ plate)

Model free to oscillate

$$\text{at } \frac{x}{D} = -1/10$$

$$\overline{u'^2} = 1.68 \text{ m}^2/\text{s}^2$$

$$\overline{v'^2} = 0.16 \text{ m}^2/\text{s}^2$$

$$\overline{w'^2} = 0.13 \text{ m}^2/\text{s}^2$$

$$\begin{aligned} \therefore E_{-1/10} &= \frac{1}{2} \rho (\overline{u'^2} + \overline{v'^2} + \overline{w'^2}) \\ &= \frac{1}{2} \times 1.97 = 0.985 \text{ J/unit mass} \end{aligned}$$

{ where $m = \text{unit mass}$ }

$$\text{at } \frac{x}{D} = -1$$

$$\overline{u'^2} = 1.60 \text{ m}^2/\text{s}^2$$

$$\overline{v'^2} = 0.14 \text{ m}^2/\text{s}^2$$

$$\overline{w'^2} = 0.13 \text{ m}^2/\text{s}^2$$

$$\therefore E_{-1} = \frac{1}{2} m (\overline{u'^2} + \overline{v'^2} + \overline{w'^2})$$

$$= \frac{1}{2} \times 1.87$$

$$= 0.935 \text{ J/unit}_{\text{mass}}$$

Model held rigidly.

$$\text{at } \frac{x}{D} = -1/10$$

$$\overline{u'^2} = 1.92 \text{ m}^2/\text{s}^2$$

$$\overline{v'^2} = 0.17 \text{ m}^2/\text{s}^2$$

$$\overline{w'^2} = 0.11 \text{ m}^2/\text{s}^2$$

$$E_{-1/10} = \frac{1}{2} m (\overline{u'^2} + \overline{v'^2} + \overline{w'^2})$$

$$= \frac{1}{2} \times 2.2 = 1.1 \text{ J/unit}_{\text{mass}}$$

$$\text{at } \frac{x}{D} = -1$$

$$\overline{u'^2} = 1.86 \text{ m}^2/\text{s}^2$$

$$\overline{v'^2} = 0.15 \text{ m}^2/\text{s}^2$$

$$\overline{w'^2} = 0.12 \text{ m}^2/\text{s}^2$$

$$E_{-1} = \frac{1}{2} m (\overline{u'^2} + \overline{v'^2} + \overline{w'^2})$$

$$= \frac{1}{2} \times 2.13 = 1.065 \text{ J/unit}_{\text{mass}}$$

Appendix E.Calculation of Mechanical Admittance.

An example of the calculation of the mechanical admittance is presented below.

The calculation of the mechanical admittance for the "30 x 120" mm² plate balance assembly was carried out through the examination of the free damped oscillations trace shown in Fig. 140

From section 12.2 the square of the mechanical admittance is given by:

$$|\Psi|^2 = \frac{1}{m^2(\omega_0^2 - \omega^2)^2 + c^2\omega^2}$$

From the free damped oscillations trace:

$$\delta = \frac{1}{N} \ln \frac{x_0}{x_N} = 2.303 \frac{1}{N} \log_{10} \frac{x_0}{x_N} = 0.0475$$

where N=number of cycles

and $\omega_d = 2\pi f_d = 185 \text{ rad/s}$

Then $\frac{2\pi h}{\sqrt{1-h^2}} = 0.0475$ for $h < 1$

i.e. $h = 0.0075 =$ damping ratio

and $\frac{\omega_d}{\omega_0} = \sqrt{1-h^2}$, i.e. $\omega_0 = 186 \text{ rad/s}$

By direct measurement $K_s = 1965 \text{ N/m}$

Therefore $m = \frac{K_s}{\omega_0^2} = 5.68 \times 10^{-2} \text{ kg}$

and $c = 2h\omega_0 m = 0.1568 \text{ Ns/m}$

Consequently the expression for the mechanical admittance is given by:

$$|\Psi|^2 = \frac{1}{\{32.4 \times 10^{-4} (3.46 \times 10^4 - 39.4 f^2)^2 + 1.05 f^2\}}$$

Appendix F.Statistical Reliability of Power - Spectrum Measurements.

A random signal analysis used in the present work is presented in section 7.3. A more general approach is presented below.

Since it is impossible to measure, in practice, the infinite time average implied by the use of generalized harmonic analysis, determination of sufficient observation time to obtain values of power spectral density with a specified statistical reliability poses an important problem. In general, the observation time has to be large compared with any characteristic times of the random process. However, since these quantities are themselves objects of measurement, being involved as parameters in the power spectrum or correlation functions, one has to resort to assumptions regarding the probable shape of the power spectrum.

Tukey (Ref. 70) considered the accuracy of power spectra computed from a discrete set of sample points of the random function, including different spectrum shapes. The present analysis deals with the reliability of continuous mean-square measurements of the output of a narrow-band-pass filter subjected to the random input and it is based on the line of thought presented by Rice (Ref. 50). Davenport, Johnson and Middleton (Ref. 71) discuss the same problem employing assumptions, somewhat different from those of the present investigation.

It is assumed that:

- 1) the power spectral density to be measured is constant over the filter range;
- 2) the random process, on the whole, is Gaussian;
- 3) the band-pass filter is approximately a single tuned circuit with response

$$|a(\omega, \omega_0)|^2 = 1 / \left\{ 1 + 4Q^2 \left(\frac{\omega - \omega_0}{\omega_0} \right)^2 \right\}$$

ω - circular frequency, rad/sec,

ω_0 - central circular frequency, rad/sec.

$a(\omega, \omega_0)$ - filter response curve.

Q - filter-band-width parameter in $|a(\omega, \omega_0)|^2 = \frac{1}{1 + 4Q^2 \left(\frac{\omega - \omega_0}{\omega_0}\right)^2}$

4) the averaging is done by direct integration of the squared signal;

5) the squaring device has a time lag.

Let $f(t)$ represent the filter output; then the squaring device output is:

$$s(t) = \frac{1}{T} \int_{-\infty}^t e^{-\frac{t-t'}{T_c}} f^2(t') dt'$$

where T_c is the time constant of the squaring device. The infinite time average of s is $\bar{s} = \overline{f^2}$ (Ref.50), while measurement over time T yields:

$$\tilde{s} = \frac{1}{T} \int_0^T s(t) dt = \frac{1}{T} \int_0^T \frac{1}{T_c} \left\{ \int_{-\infty}^t e^{-\frac{t-t'}{T_c}} f^2(t') dt' \right\} dt$$

It is desired to determine the variance of \tilde{s} that is, the quantity

$$\sigma^2 = \left(\frac{\tilde{s} - \bar{s}}{\bar{s}} \right)^2 = \frac{\overline{\tilde{s}^2}}{\bar{s}^2} - 1$$

Now,

$$\overline{\tilde{s}^2} = \frac{1}{T^2} \iint_0^T \overline{s(t_1) s(t_2)} dt_1 dt_2 = \frac{2\bar{s}^2}{T^2} \int_0^T (T-\tau) \varphi_{ss}(\tau) d\tau$$

where φ_{ss} is the normalized correlation function of $s(t)$. The product $\bar{s}^2 \varphi_{ss}(\tau)$ can be derived from the filter response; by Fourier transform one finds that the normalized correlation function of the filter output is:

$$\varphi_{ff}(\tau) = e^{-\frac{|\omega_0 \tau|}{2Q}} \cos \omega_0 \tau$$

and according to Rice (Ref.50),

$$\bar{s}^2 \varphi_{ss}(\tau) = \bar{s}^2 \left\{ 1 + \frac{1}{T_c} \int_0^\infty e^{-\frac{t}{T_c}} \left\{ \varphi_{ff}^2(t+\tau) + \varphi_{ff}^2(t-\tau) \right\} dt \right\}$$

The resulting mathematical expressions become rather

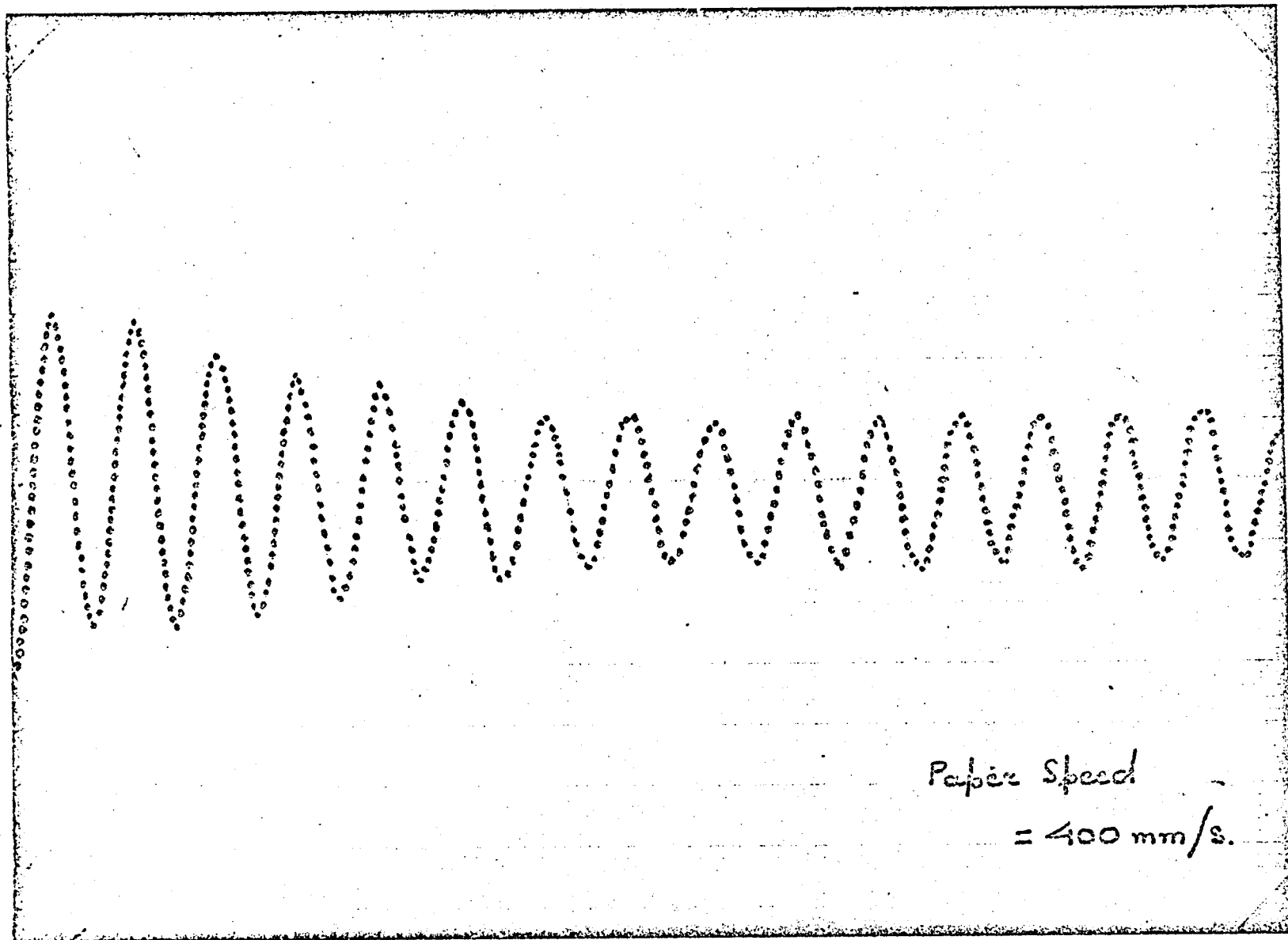
lengthly; however, a convenient simplification can be made by assuming that $Q^2 \gg 1$ and $(\omega_c T_c)^2 \gg 1$ (which is true in many practical cases). By carrying out the detailed computation and successive substitutions one finally obtains (denoting $\frac{\omega_c T_c}{Q} = \rho$ and $\frac{\omega_c T_c}{Q} = \gamma$)

$$\sigma = \frac{1}{\rho} \left\{ \frac{2\gamma (1 - \gamma + \gamma e^{-\rho/\gamma} - e^{-\rho})}{1 - \gamma^2} \right\}^{1/2}$$

γ - dimensionless device time const., ρ - dimensionless integration time.

The values of Q , T_c , and ω_c will depend on the investigation and consequently the value of γ could be defined.

For $Q = 80$, $T_c = 5$ secs and $3 < \frac{\omega_c}{2\pi} < 150$ for which approximately $1 < \gamma < 50$ the curves of $\sigma \sim \rho$ are plotted for $\gamma = 1, 10$, and 50 in Fig. 31, of Vol. I.

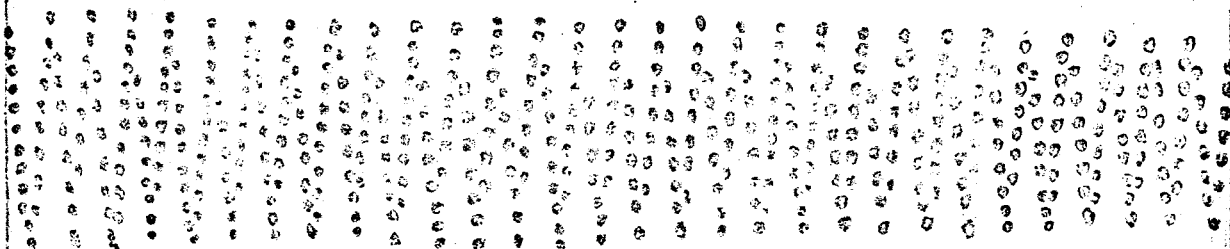


Free Damped Oscillations
Balance + 30 x 120 (mm²) Plate

FIG: 140

Paper Speed = 250 mm/s
Timer at 0.1 s.

Natural (in-line) frequency of
vibration = 50 cycles/s



In-line, Oscillations of Balance @ Circular
Section Cylinder AR = 2

FIG; 141

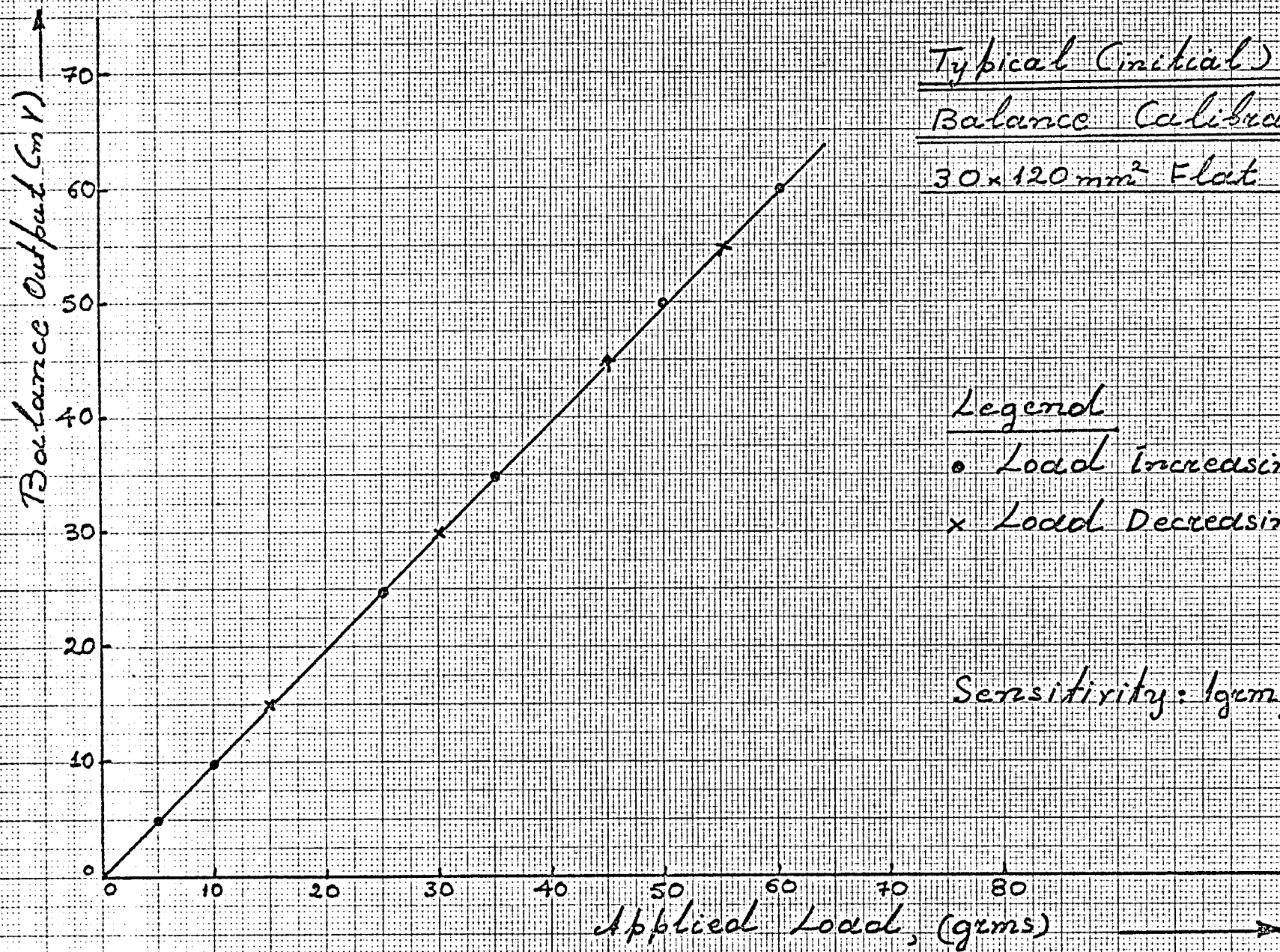


FIG: 142

Typical Modified Force Balance
Calibration
Circular Section Cylinder $R=2$

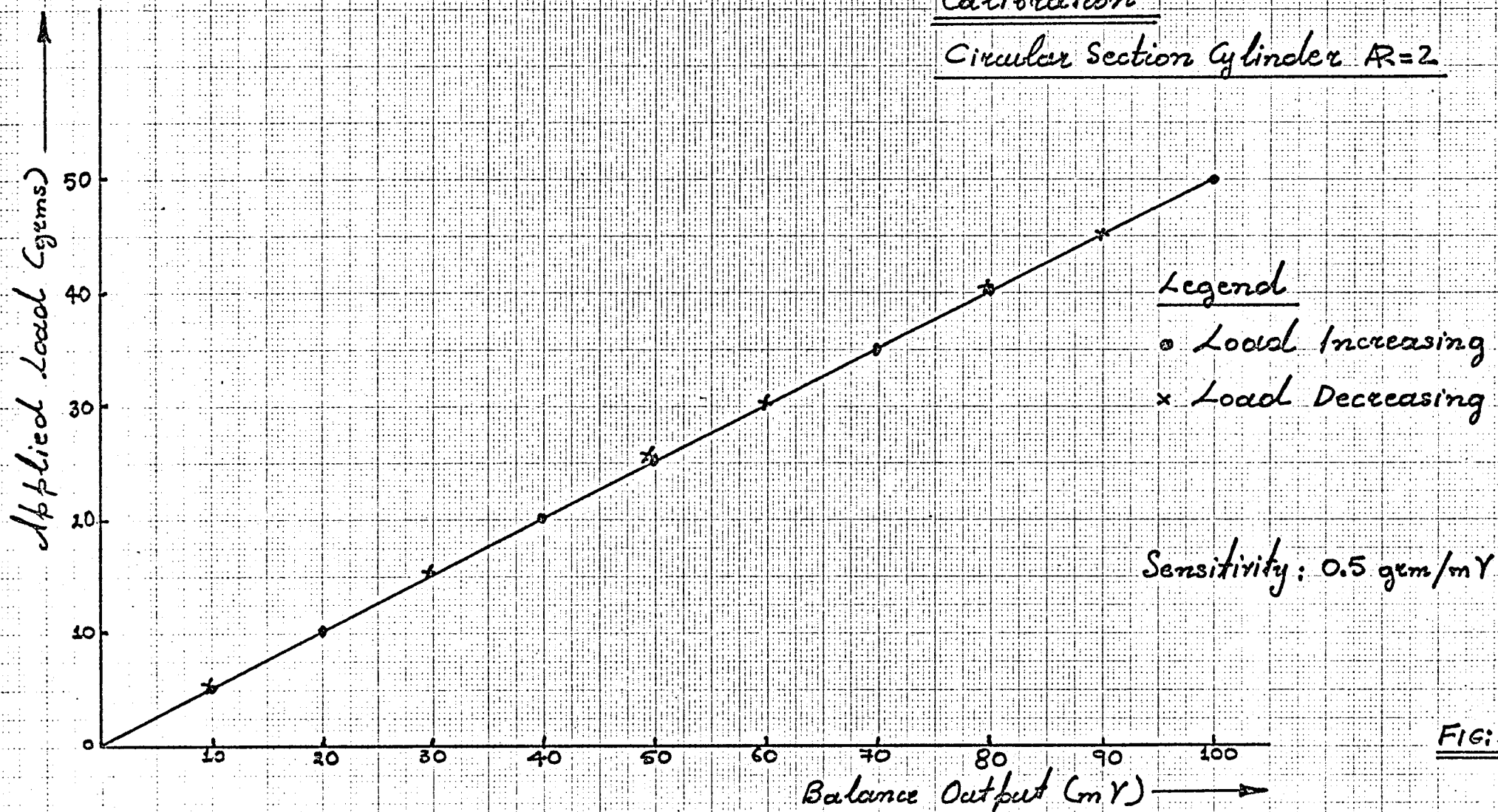


FIG:143

Assembly (Balance Plus)	Damping Decrement δ	Damped Natural Frequency ω_d (s)	Damping Ratio h	Undamped Natural Frequency ω_n (s)	Constant K_s (N/m)	Oscillating Mass m (kg $\times 10^2$)	Constant c (Ns/m)
Disc 20mm Dia.	0.0659	219	0.0104	220	2113	4.35	0.195
Disc 40mm Dia.	0.0602	207	0.0096	209	2113	4.85	0.194
Plate AR = 1	0.0638	211	0.0102	213	2113	4.65	0.198
Plate AR = 2	0.0605	201	0.0097	202	2113	5.2	0.204
Plate AR = 4	0.0475	185	0.0075	186	2113	6.1	0.17
Plate 42.5x42.5mm ²	0.0466	179	0.0074	180	2113	6.5	0.174
Plate 60x60mm ²	0.0457	175	0.0071	176	2113	6.8	0.17
Plate 85x85mm ²	0.0451	171	0.0070	172	2113	7.18	0.172
Plate 120x120mm ²	0.0441	164	0.0069	165	2113	7.75	0.177
Parallelepiped AR = 1	0.0510	185	0.0081	186	2113	6.5	0.196
Parallelepiped AR = 2	0.0356	164	0.0056	165	2113	7.75	0.144
Parallelepiped AR = 4	0.0330	127	0.0052	128	2113	12.6	0.168

should read Details of Systems Used, Utilized in Calculating the Mechanical Joint
 "Continued on
 Fig. 145"

FIG. 144 (continued)

Where is it started?

Assembly (Balance Plus ↓)	Logarithmic Decrement δ	Damped Natural Frequency $\omega_d (s^{-1})$	Damping Ratio h	Undamped Natural Frequency $\omega_0 (s^{-1})$	Stiffness Constant $k_s (N/m)$	Total Oscillating Mass $m (kg \times 10^2)$	Damping Constant $c (Ns/m)$
Circular Cylinder AR = 1	0.0923	314	0.0146	316	2113	2.11	0.196
Circular Cylinder AR = 2	0.0821	294	0.0131	295	2113	2.4	0.186
Circular Cylinder AR = 4	0.0767	205	0.0122	207	2113	4.9	0.024

1. Systems Used, Utilized in Calculating the Mechanical Admitt.

FIG:145

511.4 f
(mP)

Load and Noise

$|\psi|^2$
(Mechanical admittance)

Comparison Magnitude of
Mechanical Admittance, Load
and Overall Noise Spectra

Legend

• Overall Noise Spectrum of
balance and instrumentation

x Load Spectrum

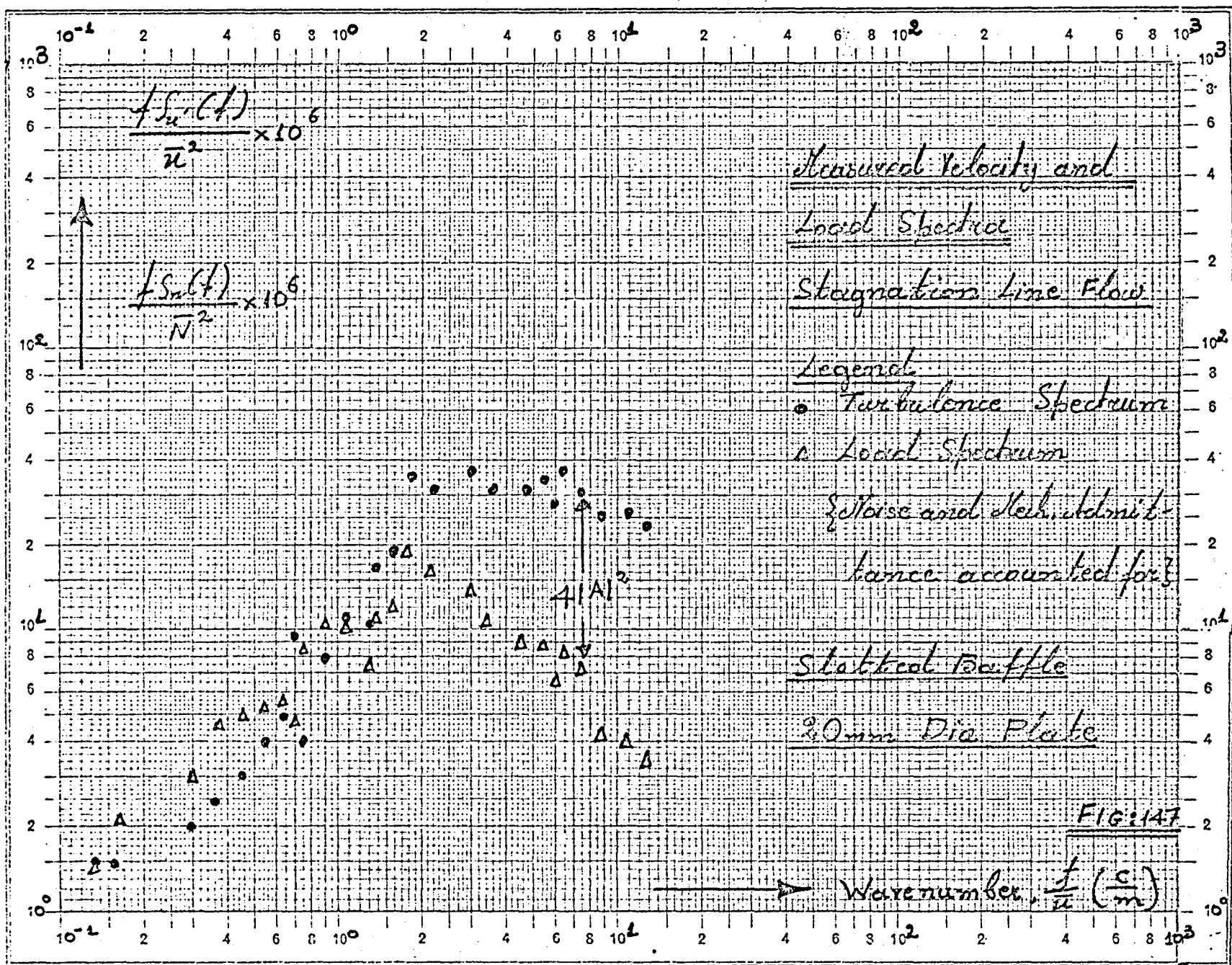
Plate: $n=4$

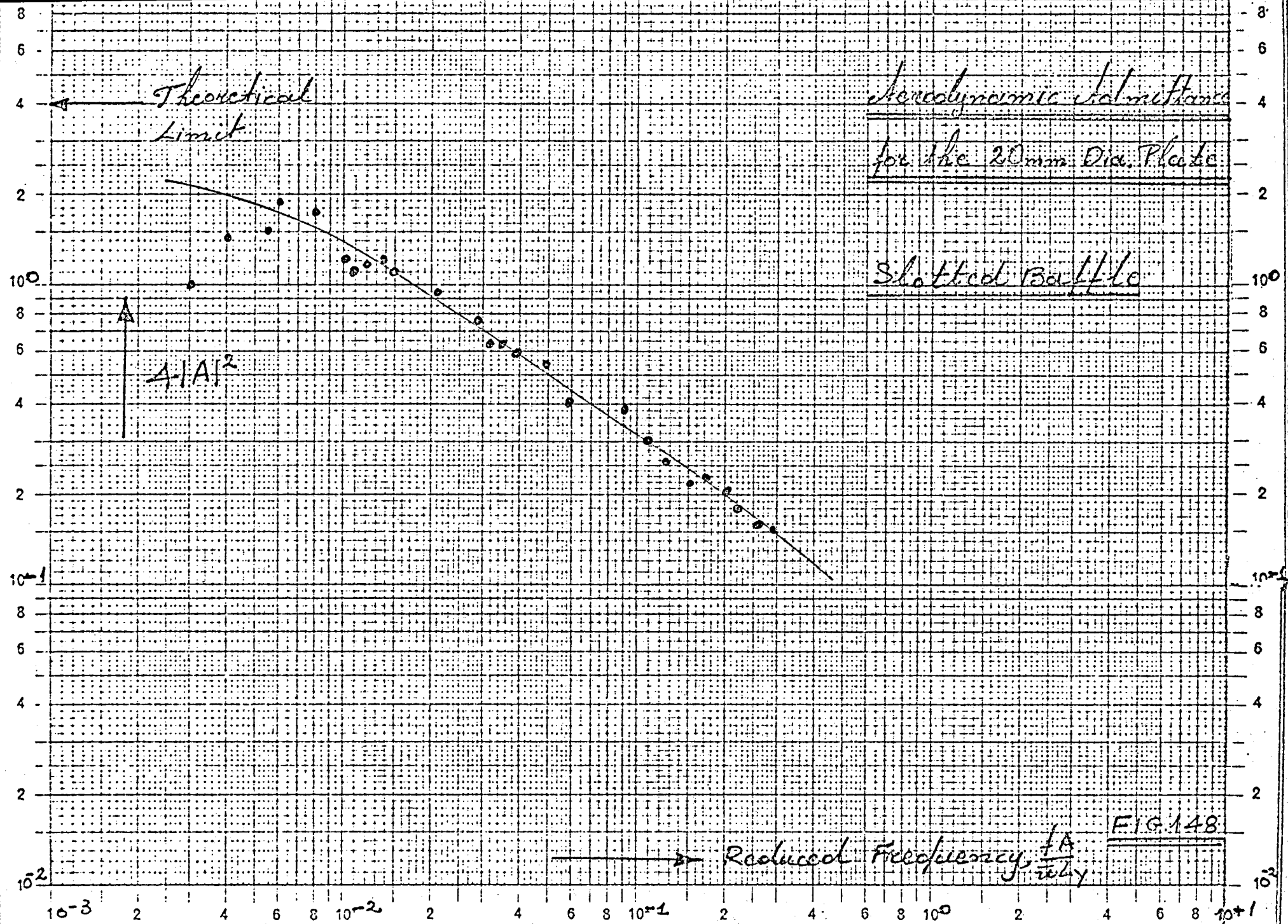
20 mm Holes Raffle

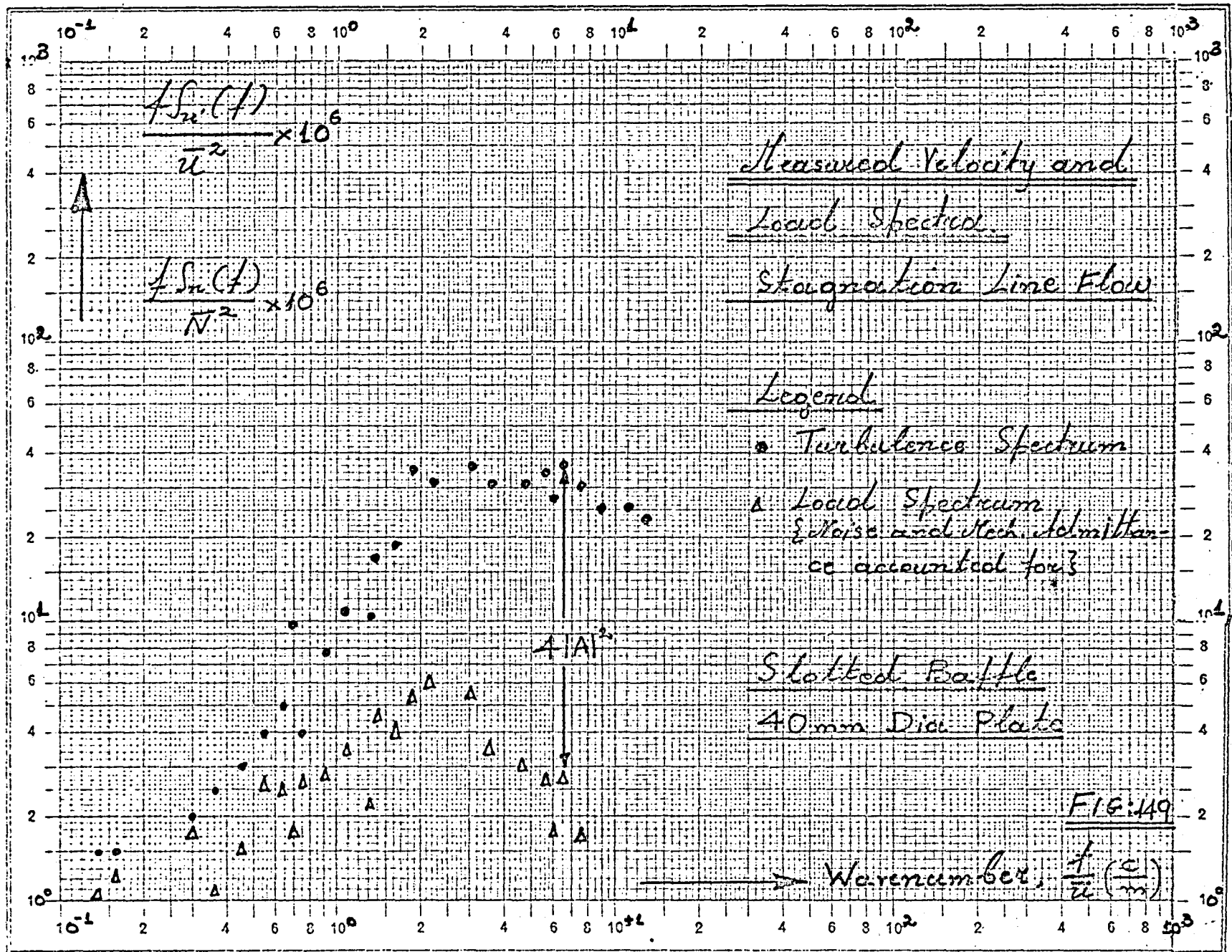
o Mechanical Admittance

Fig 146

Frequency (Hz)







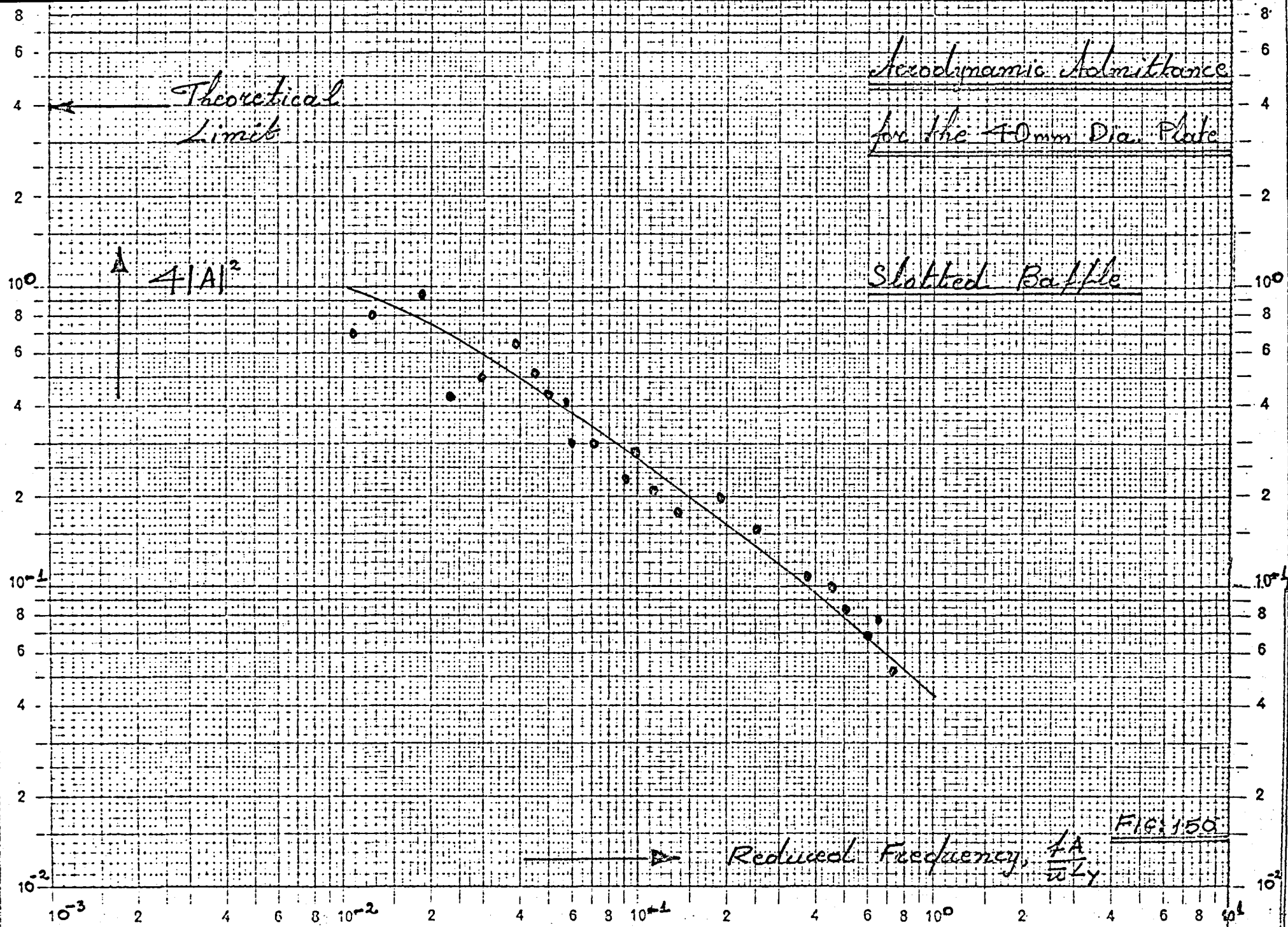
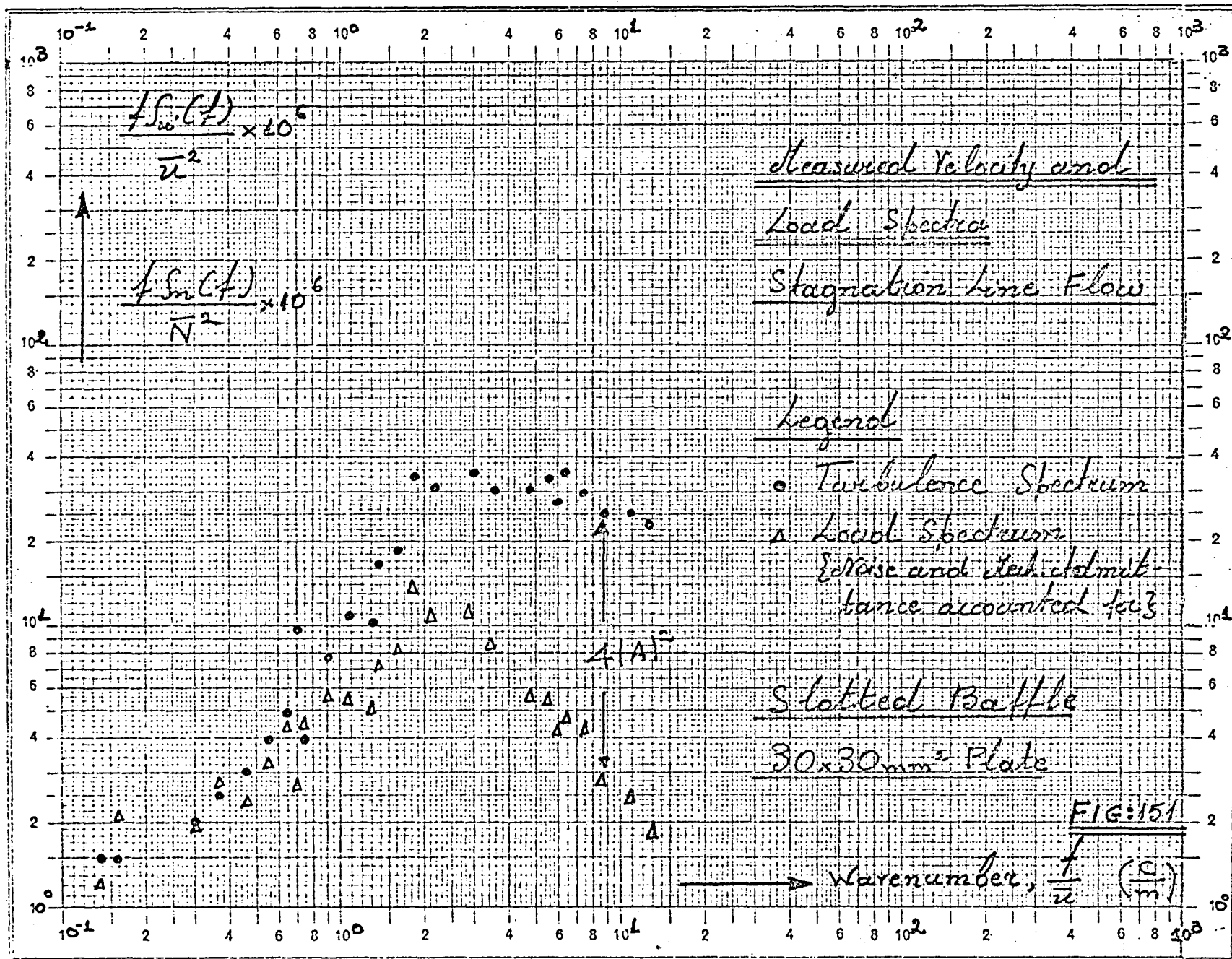
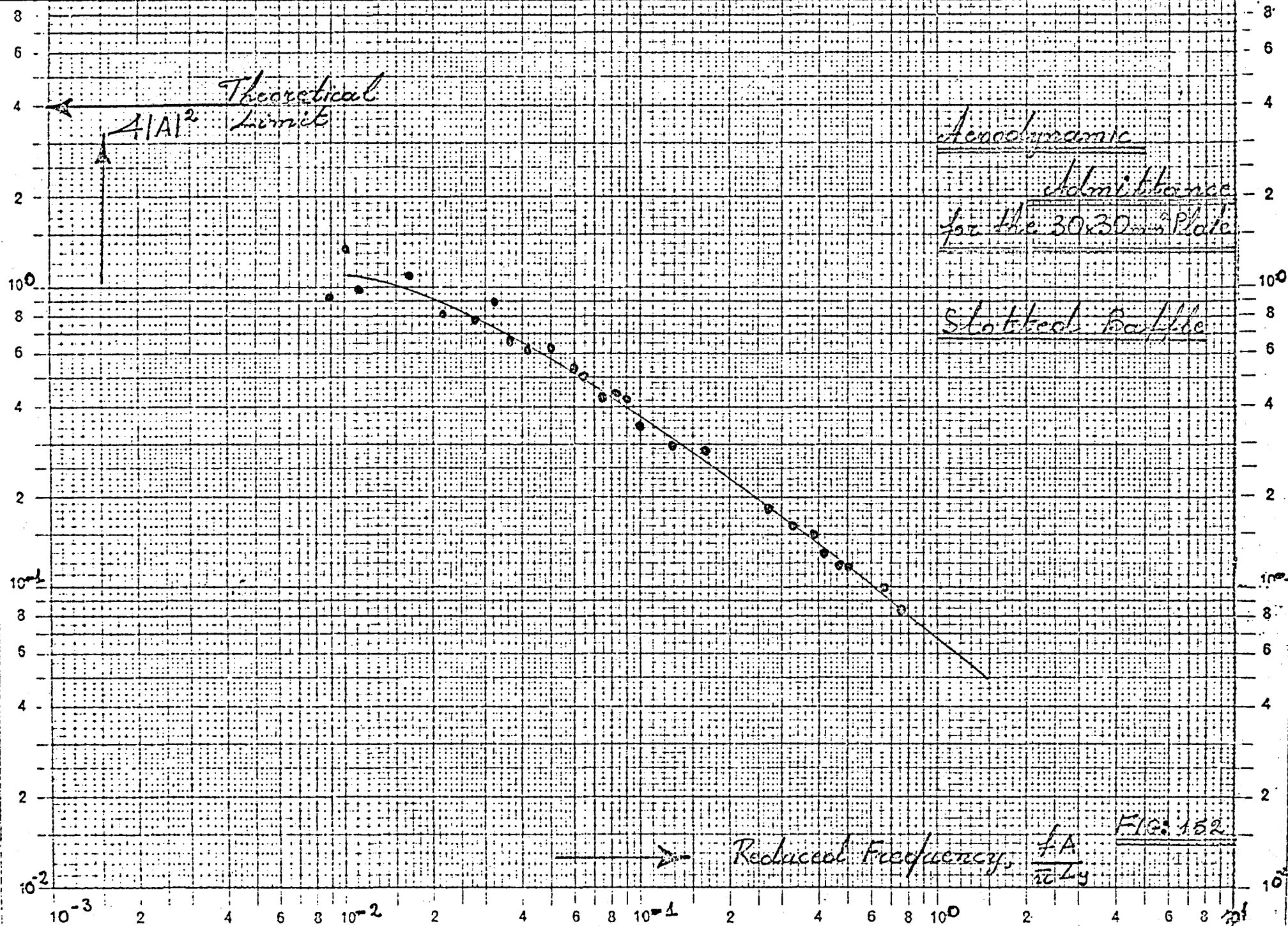
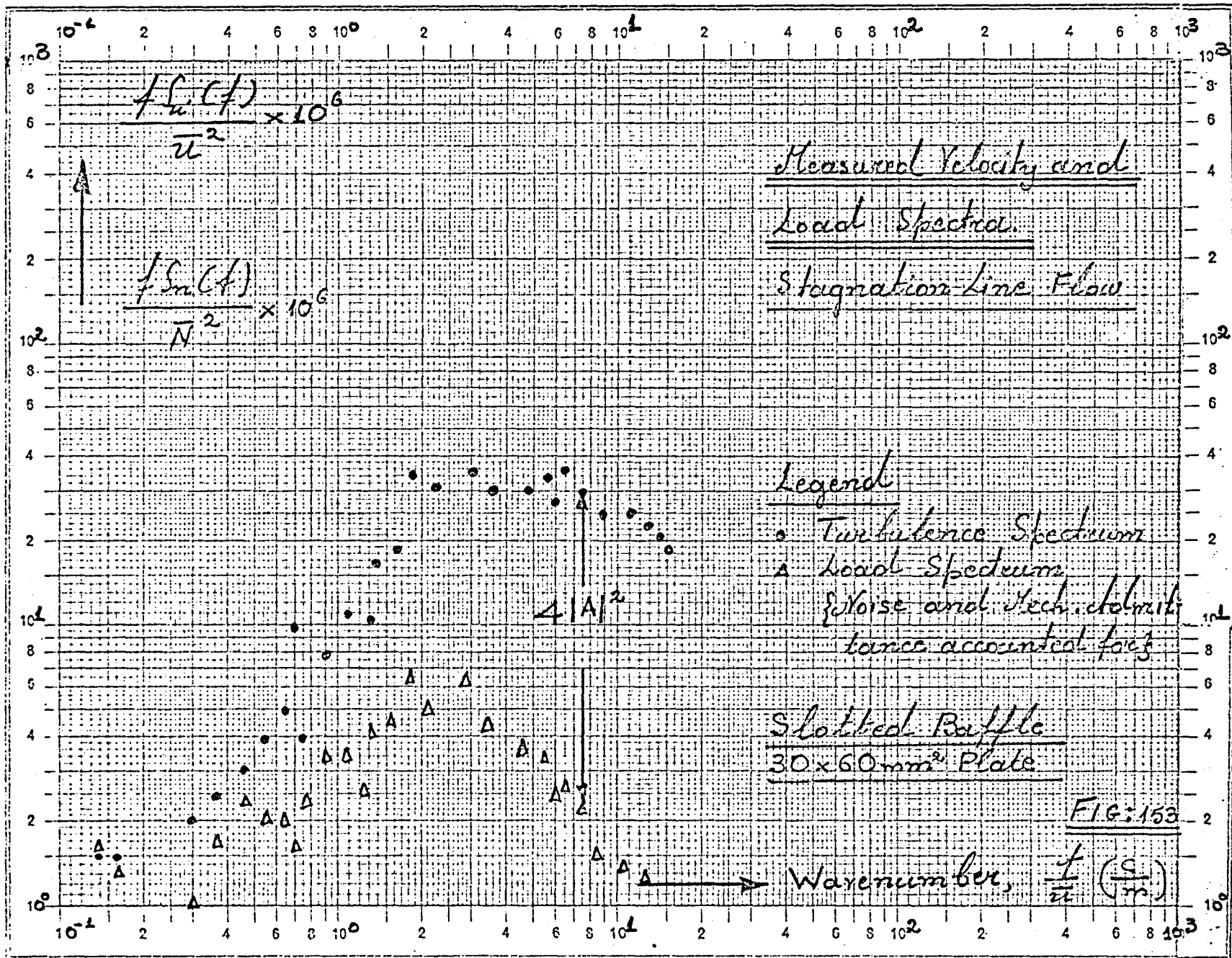
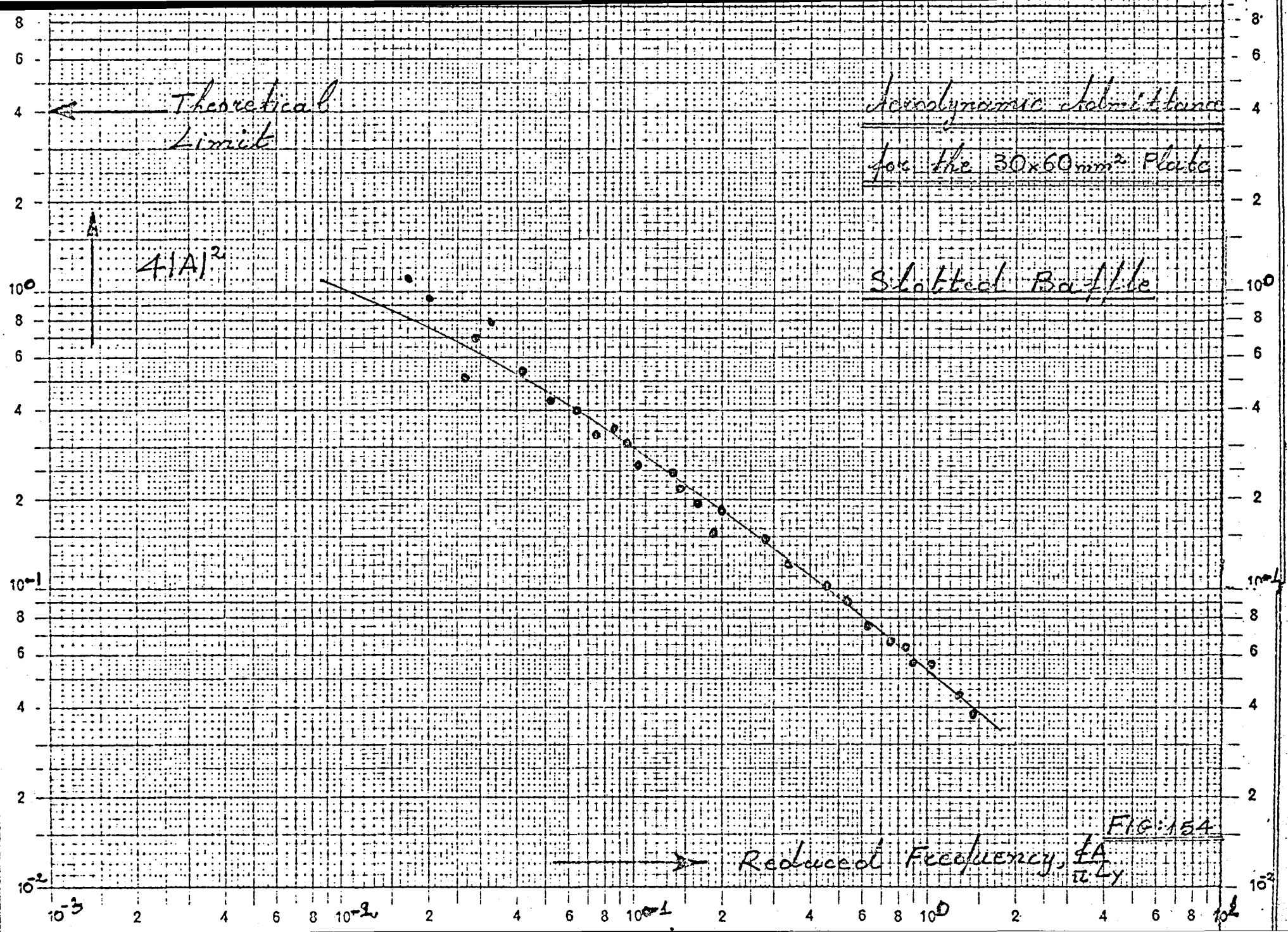


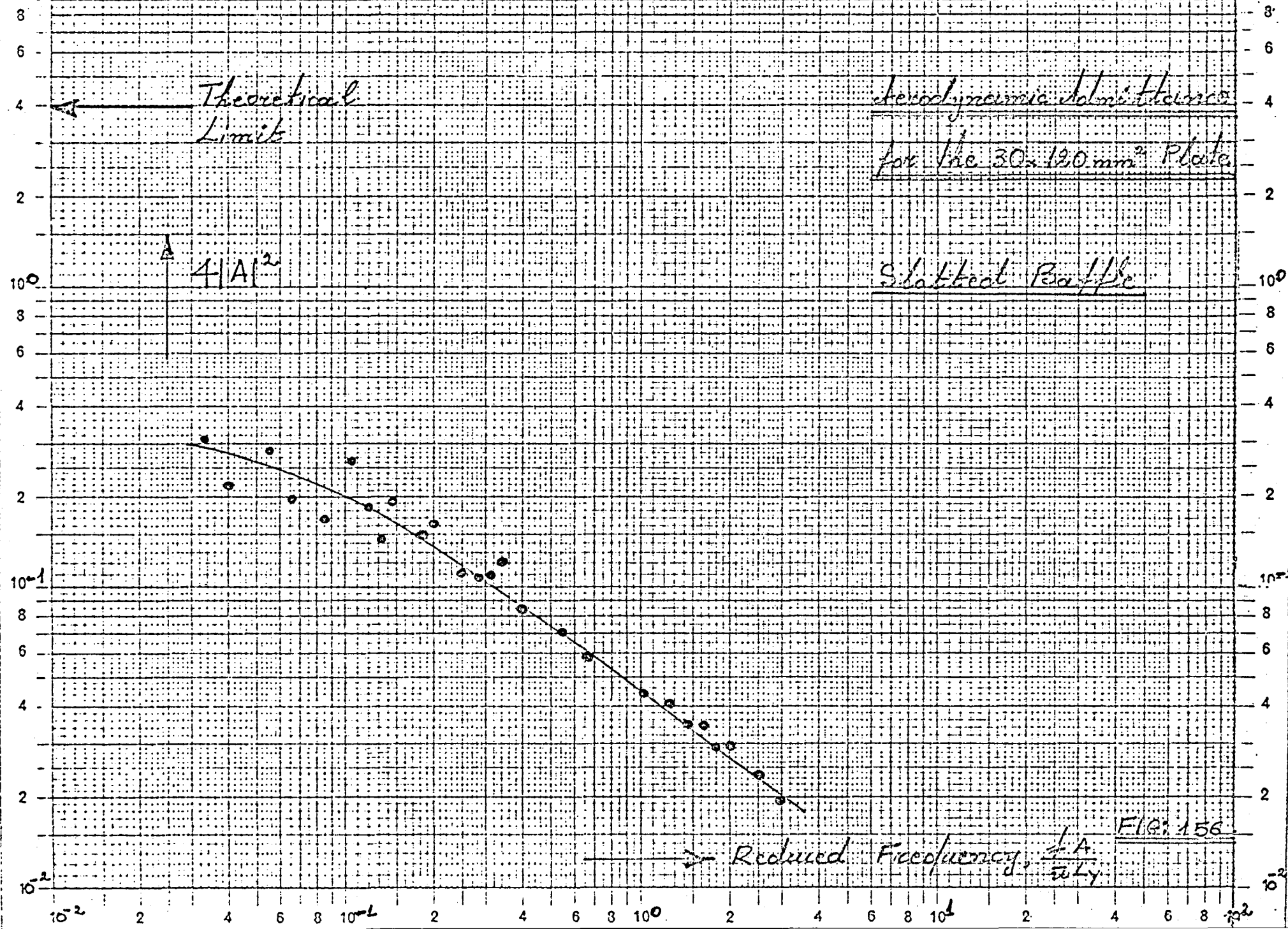
FIG. 150

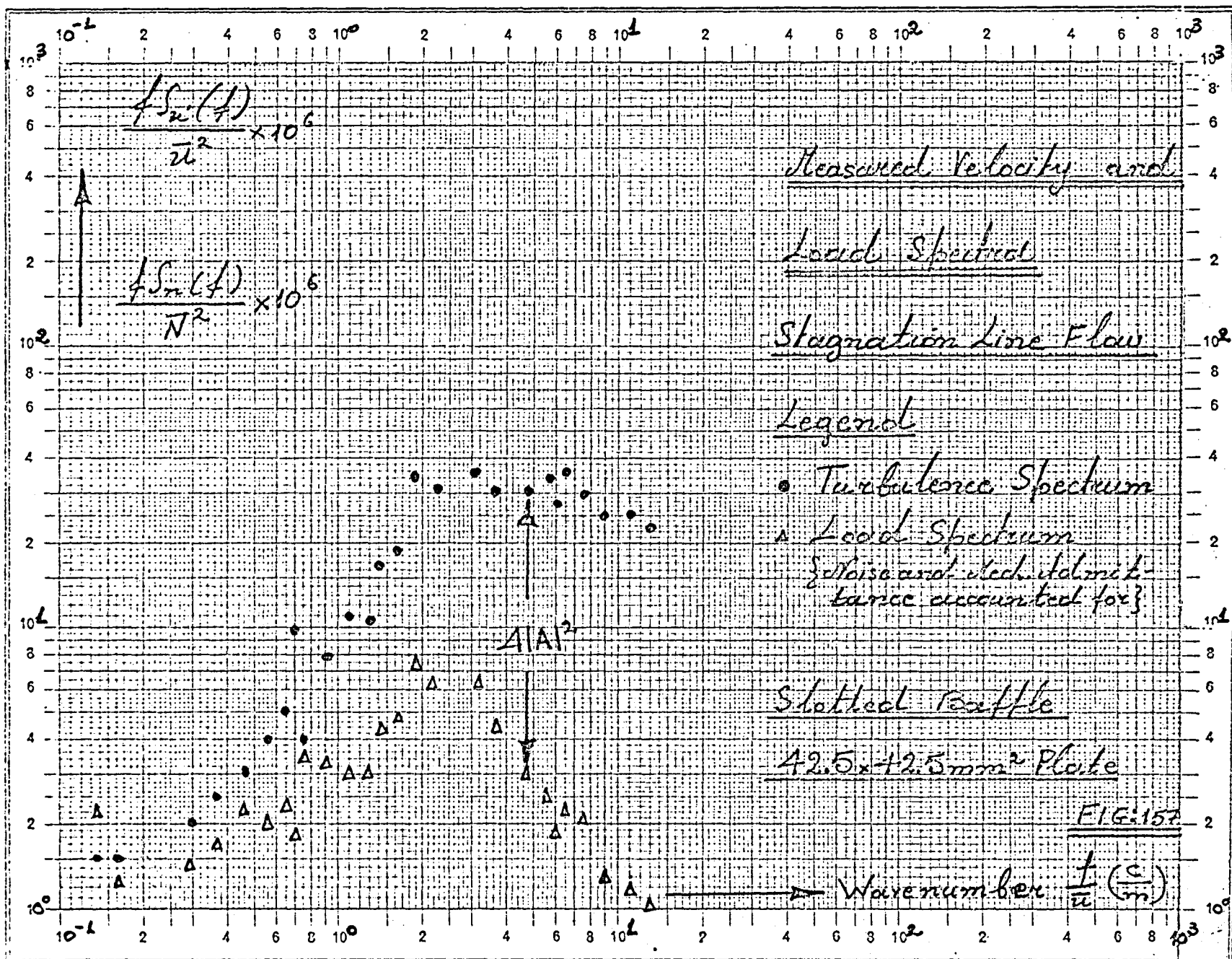


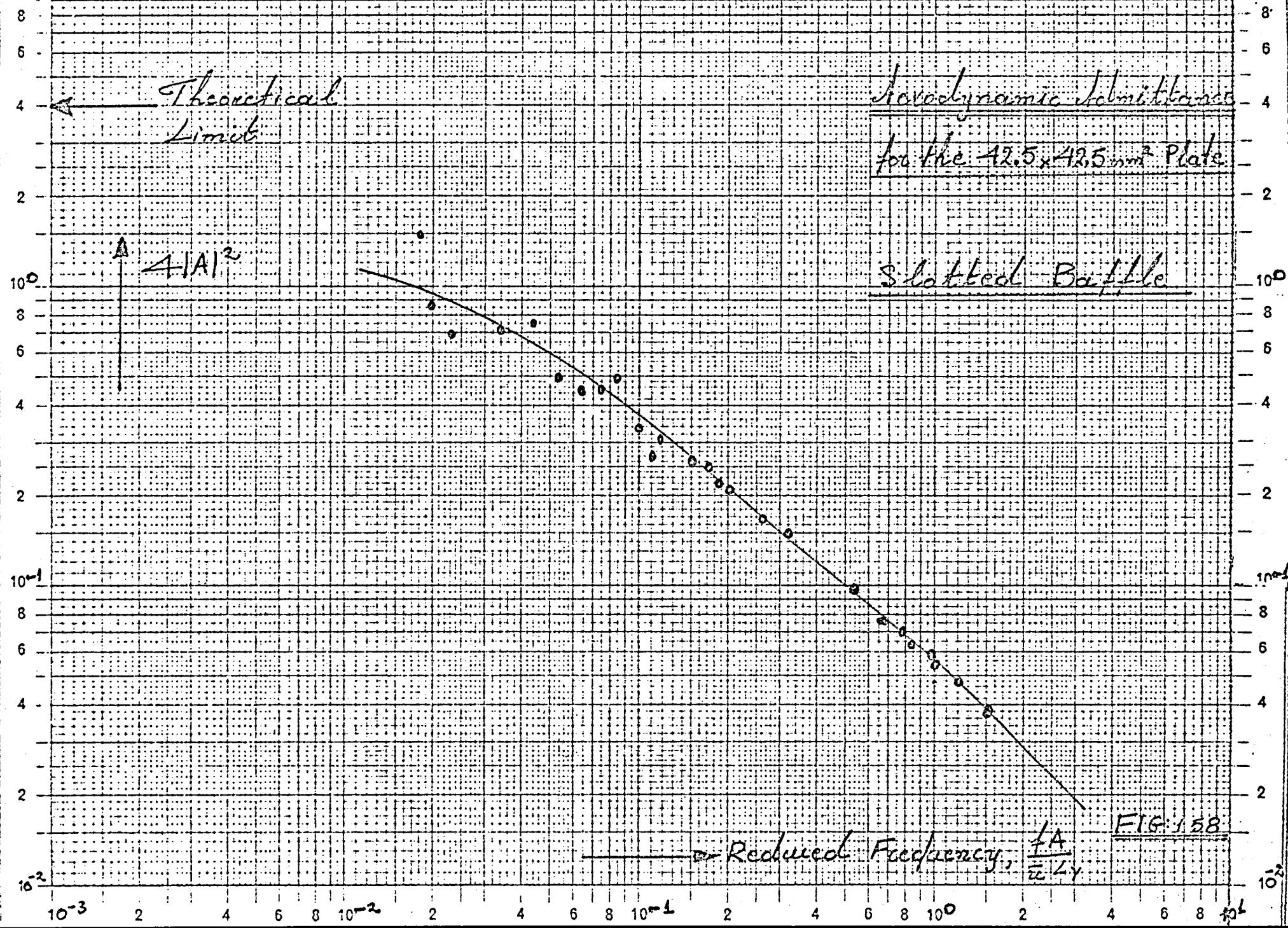


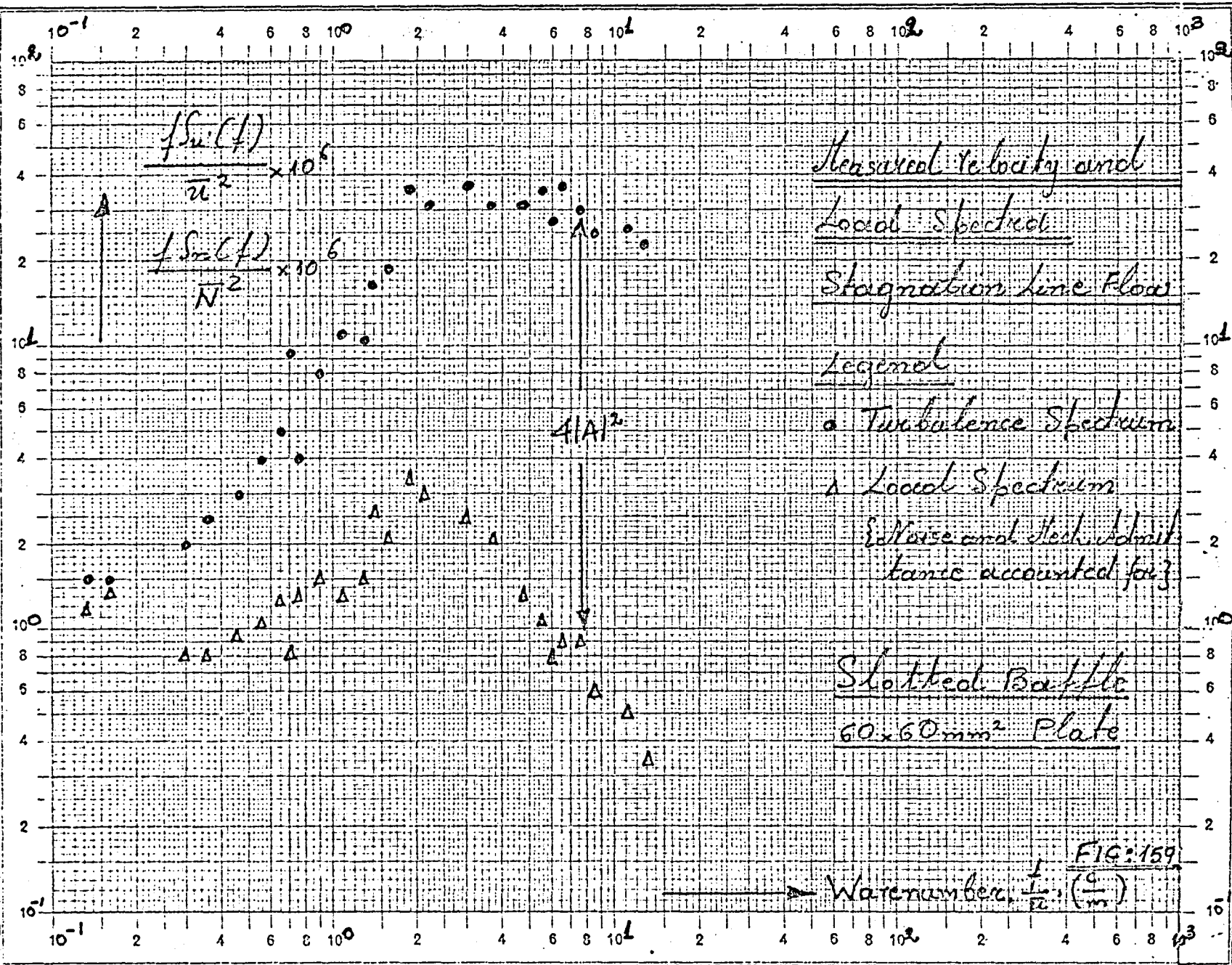


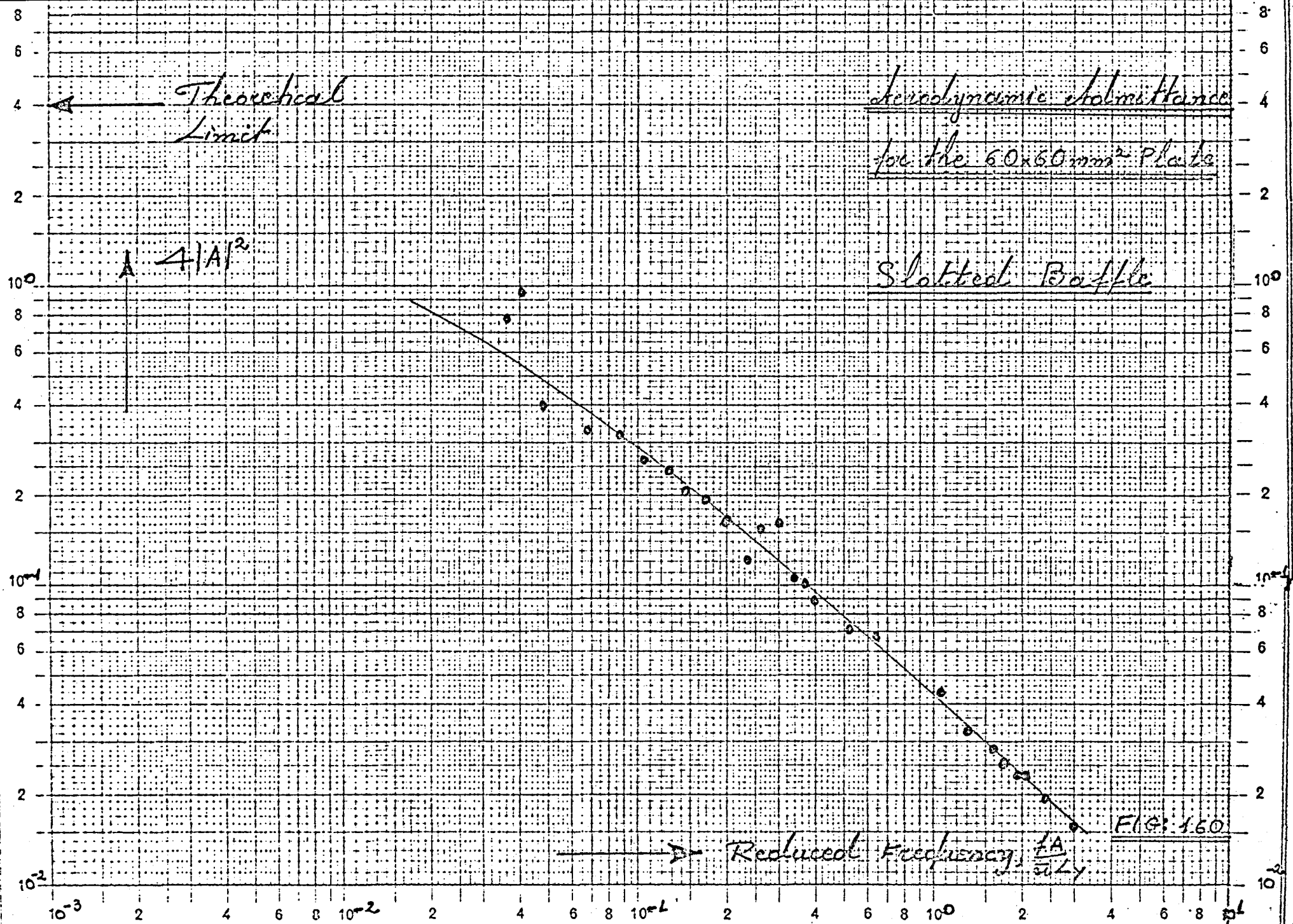


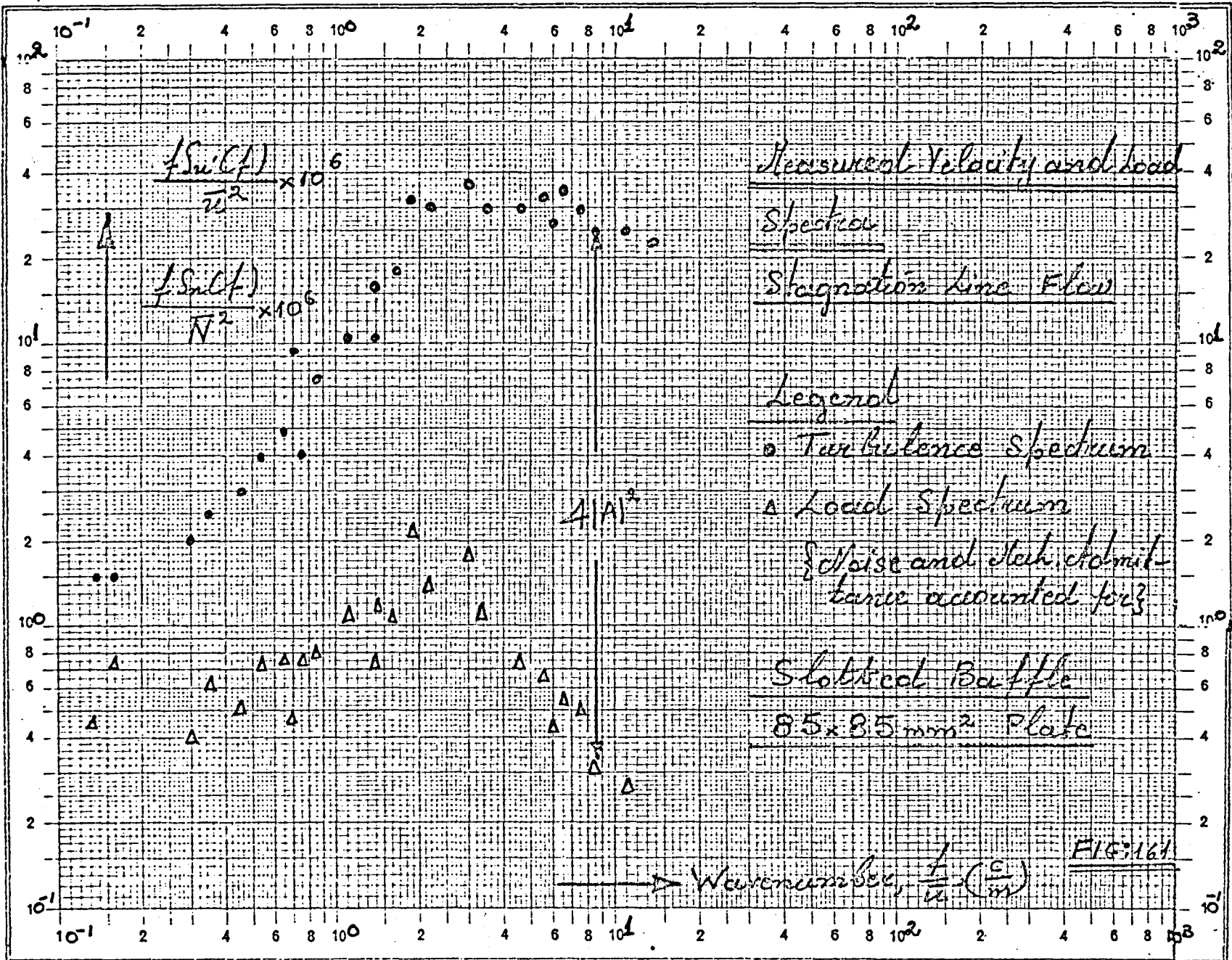


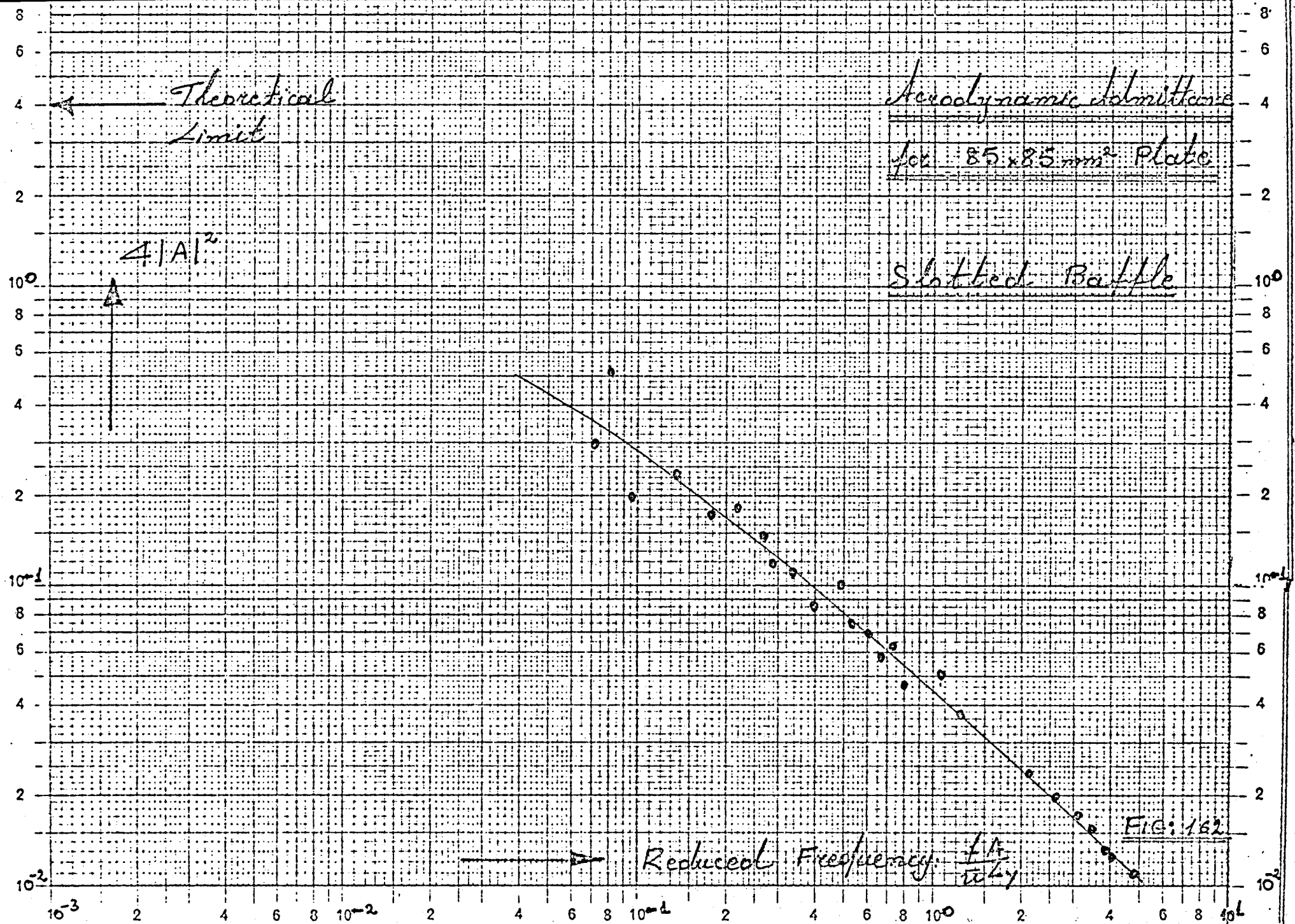


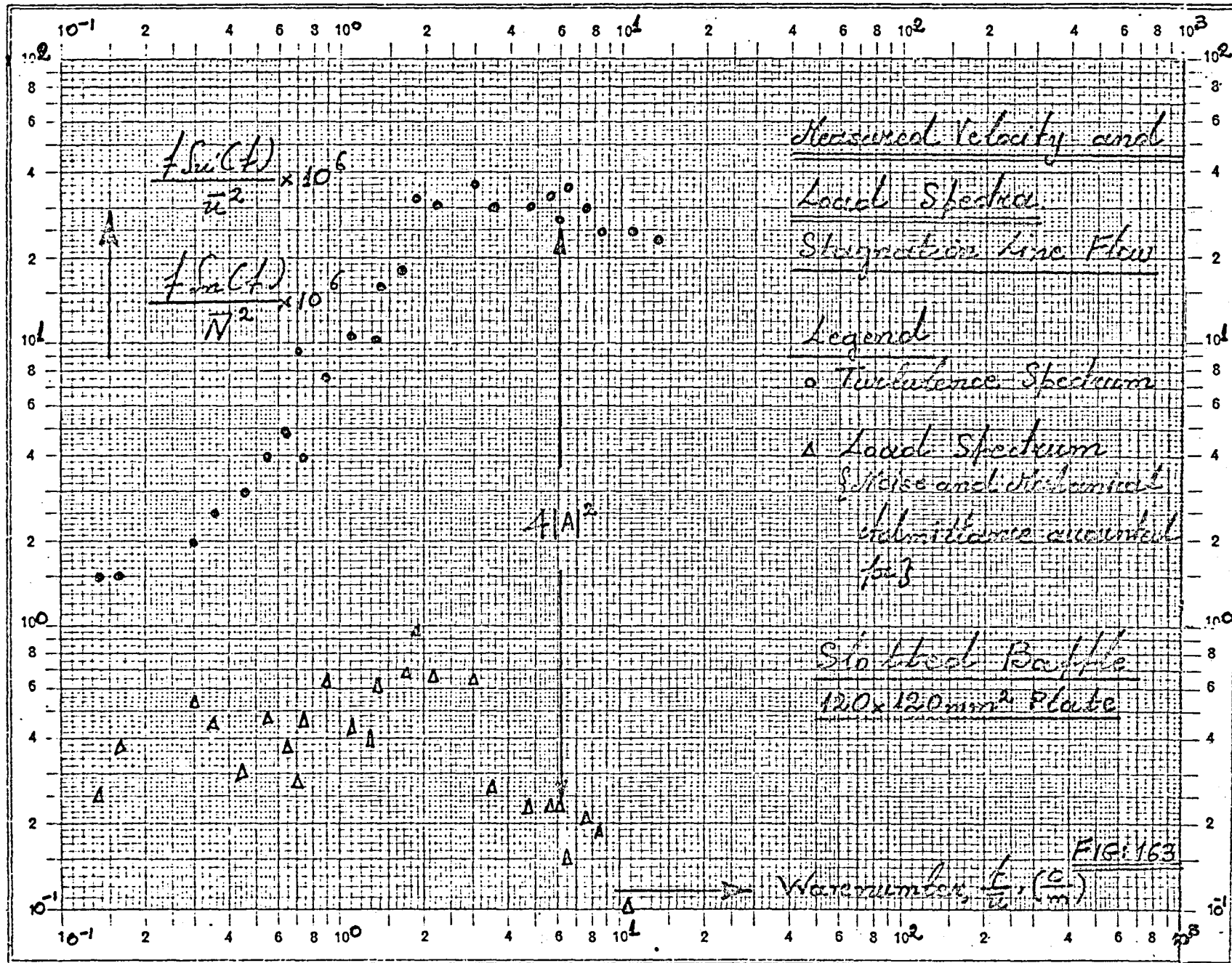










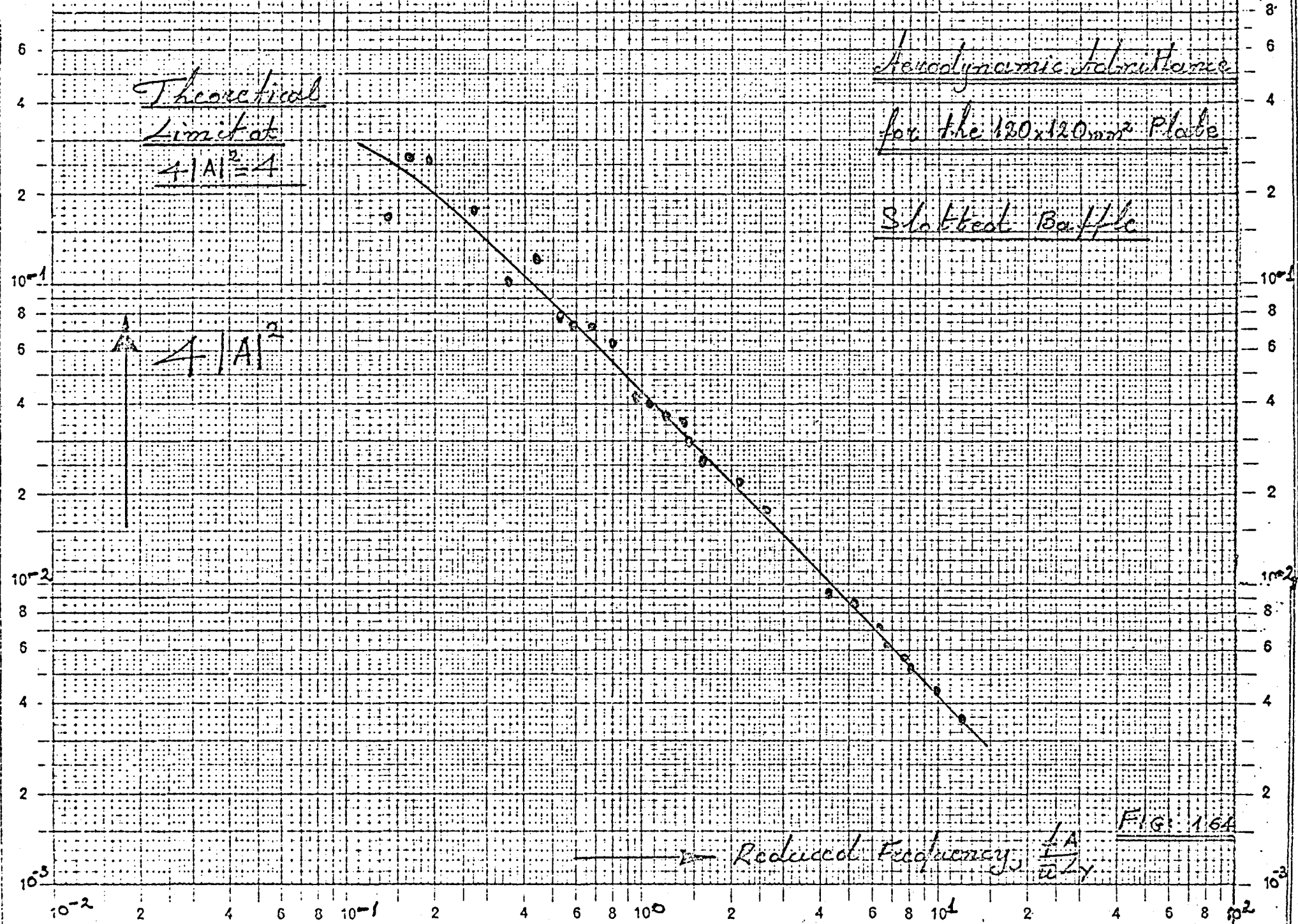


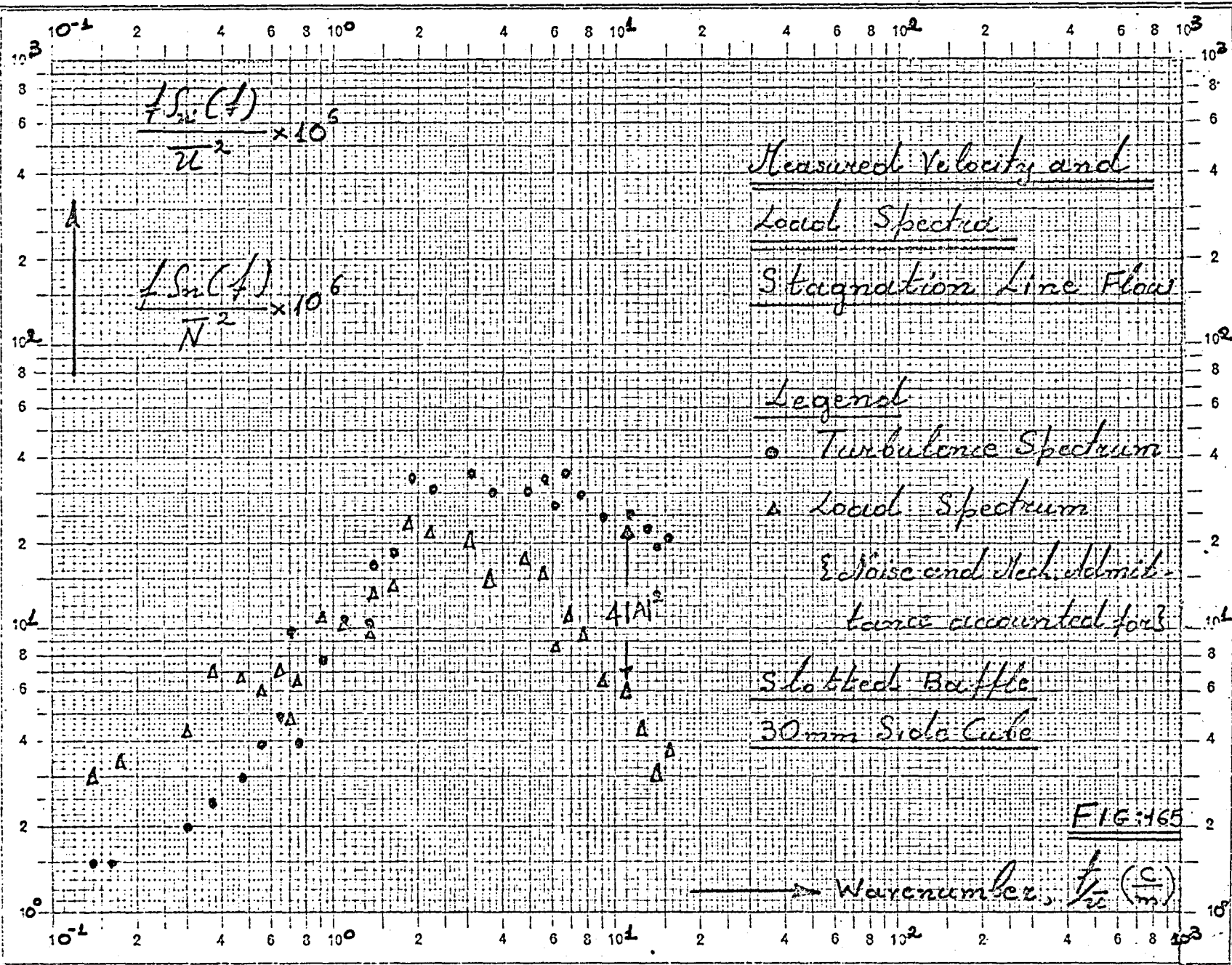
Theoretical
Limit at
 $4|A|^2=4$

Aerodynamic Interference
for the 120x120mm² Plate

Slotted Baffle

$4|A|^2$





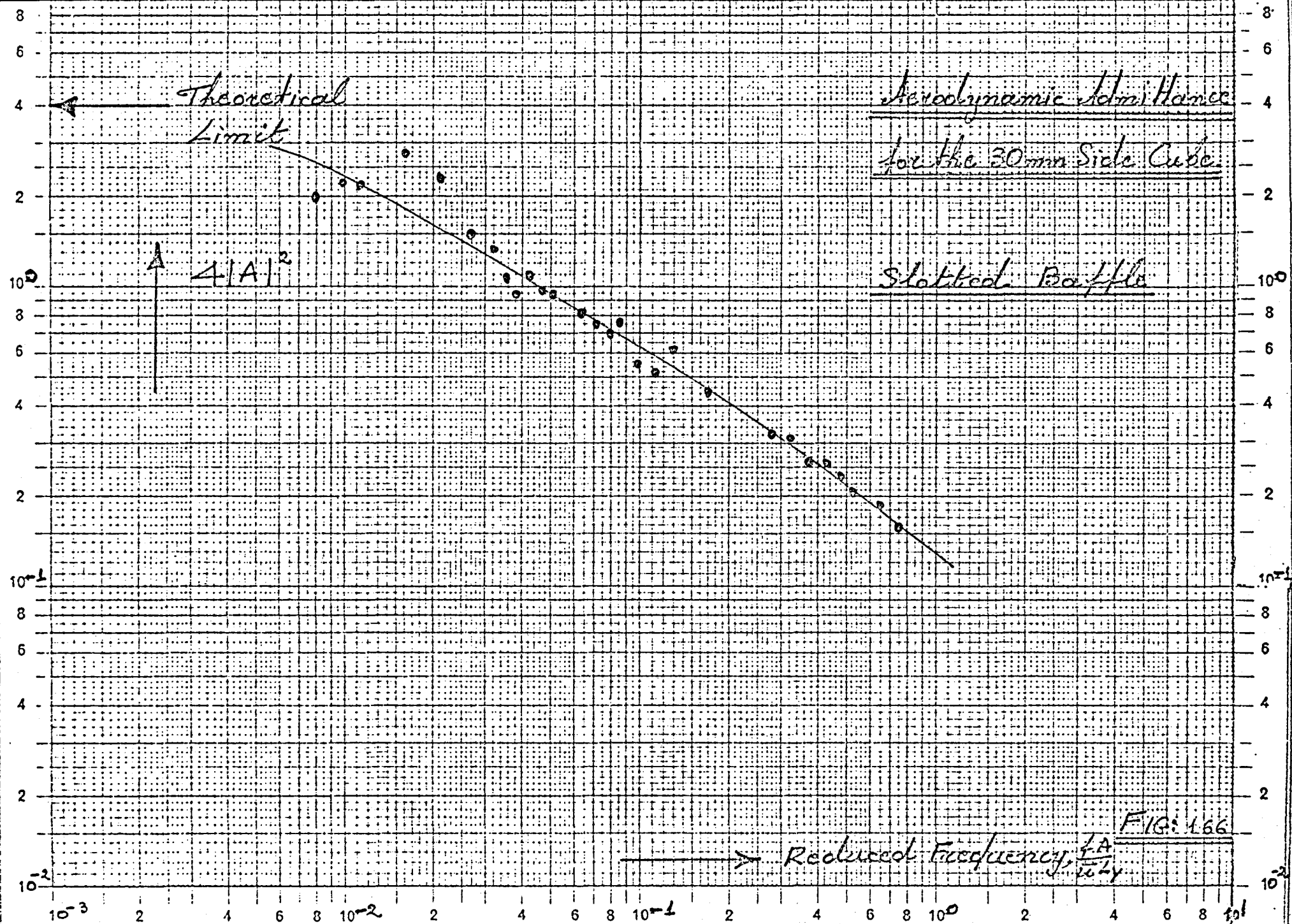
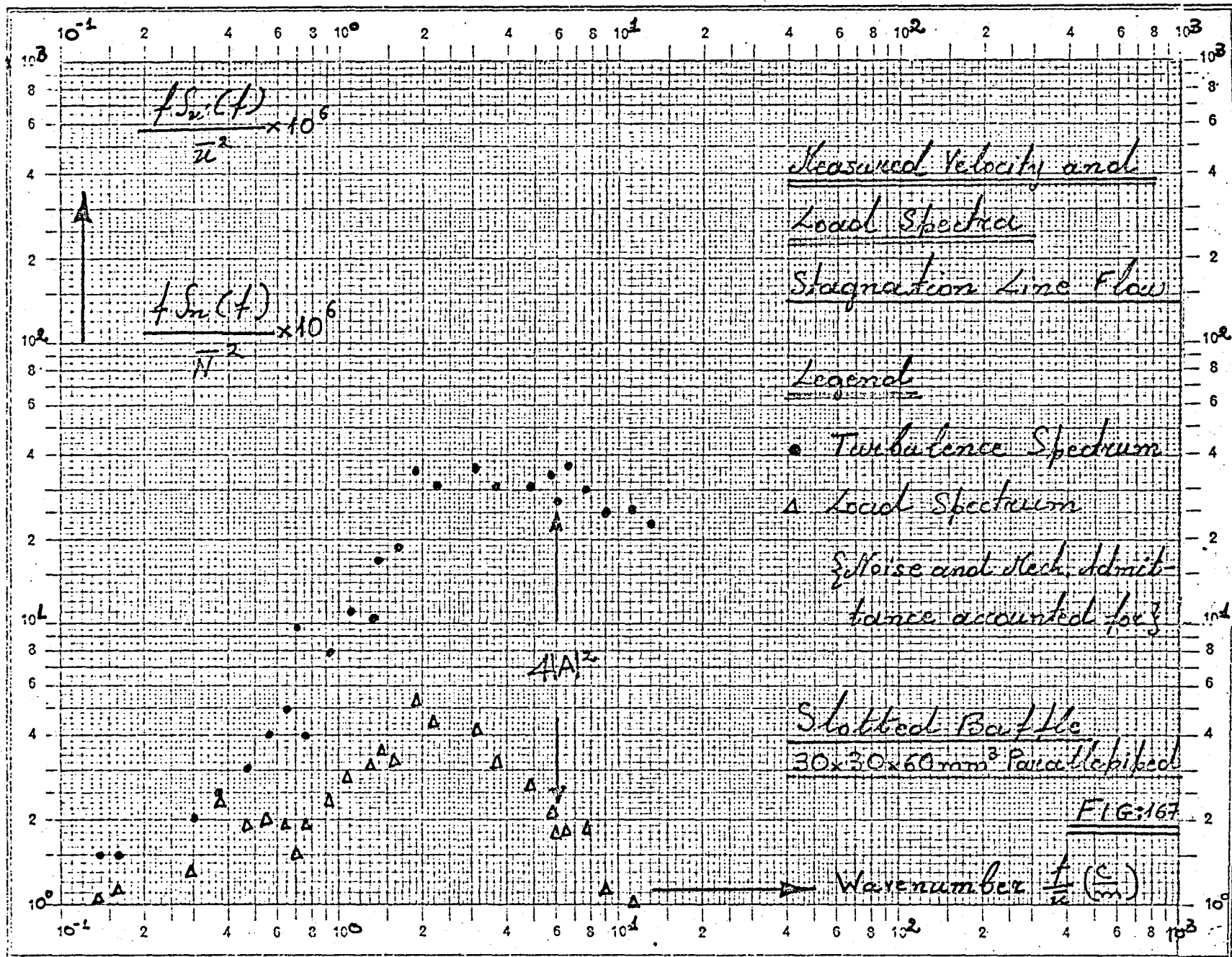
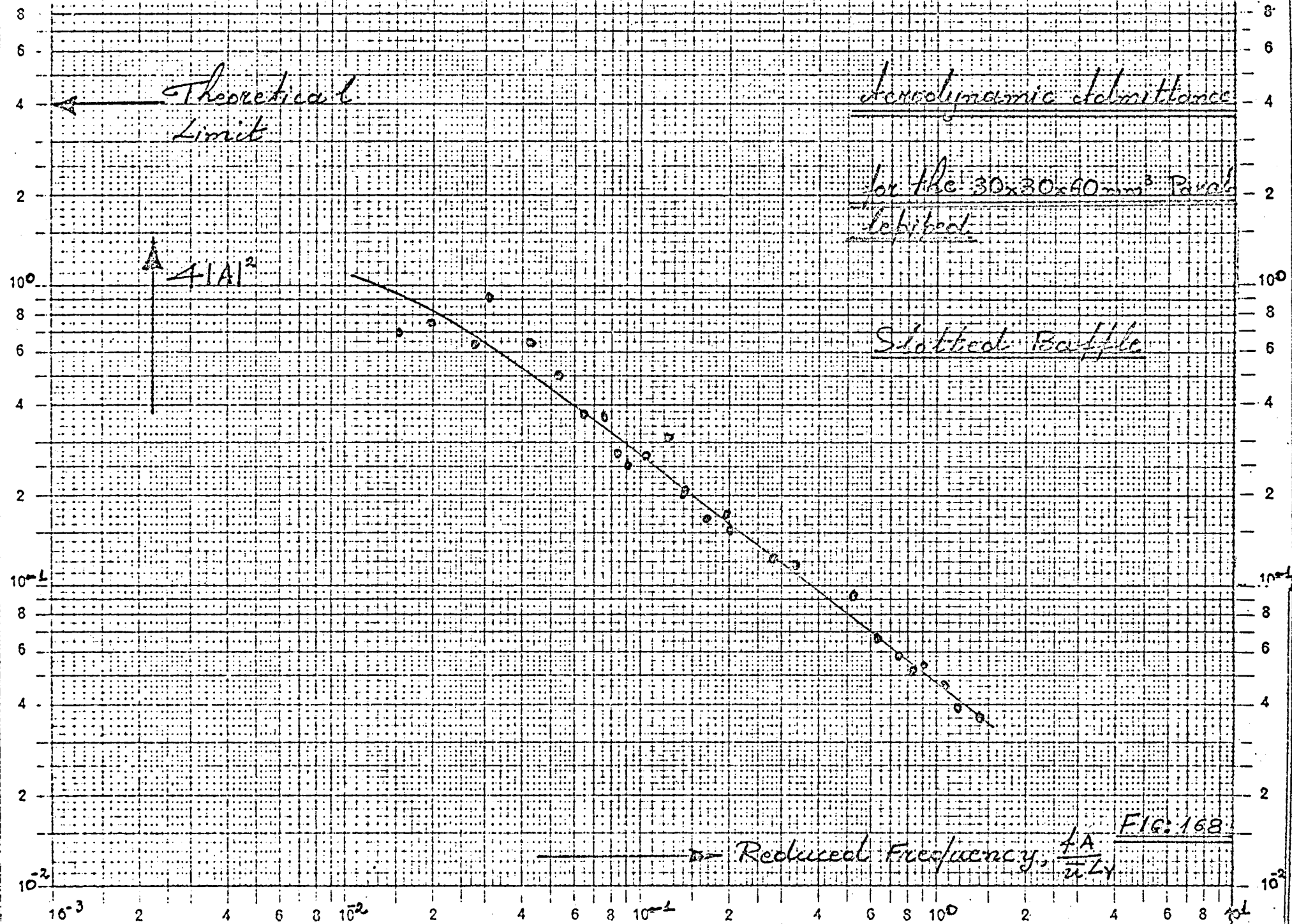
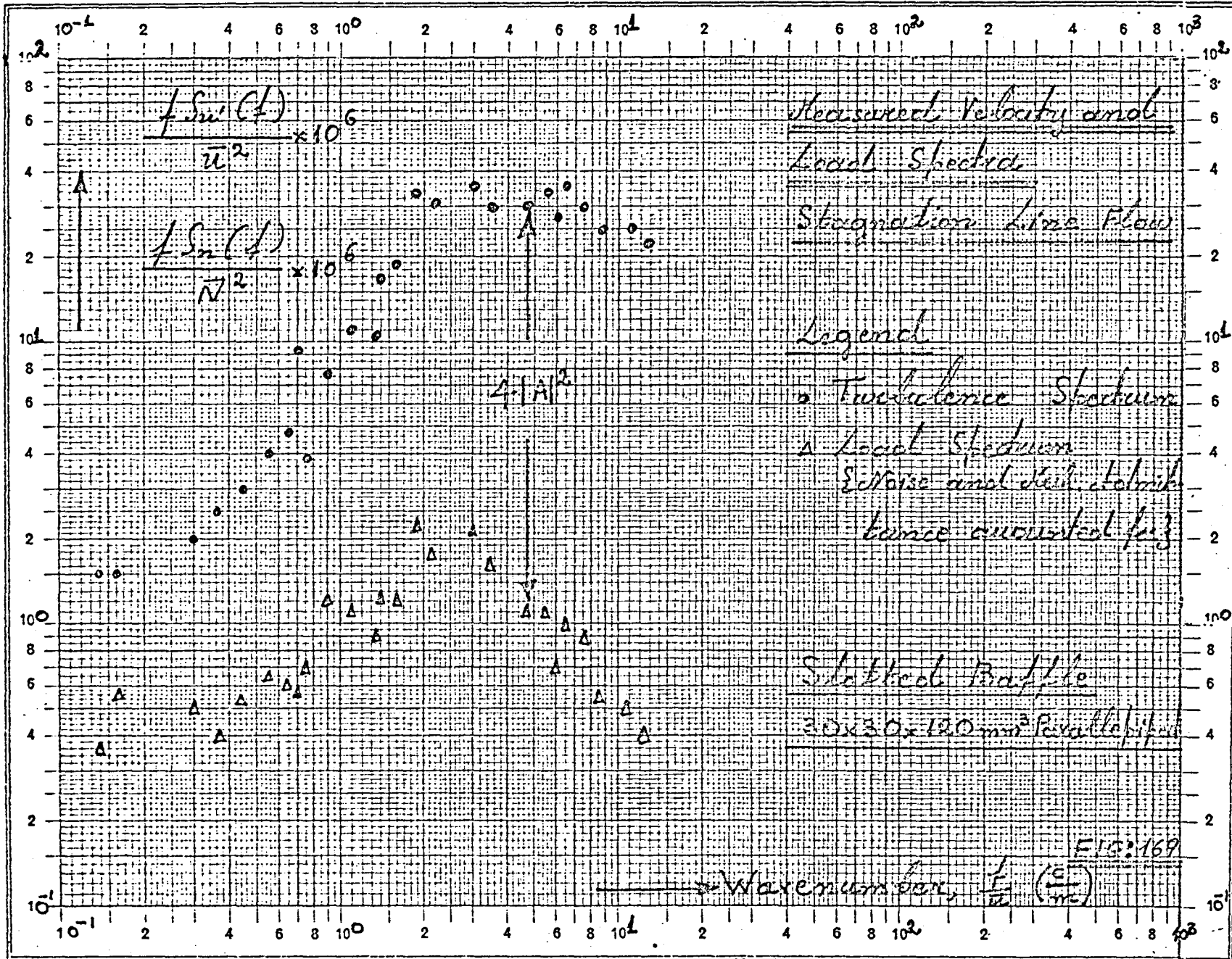
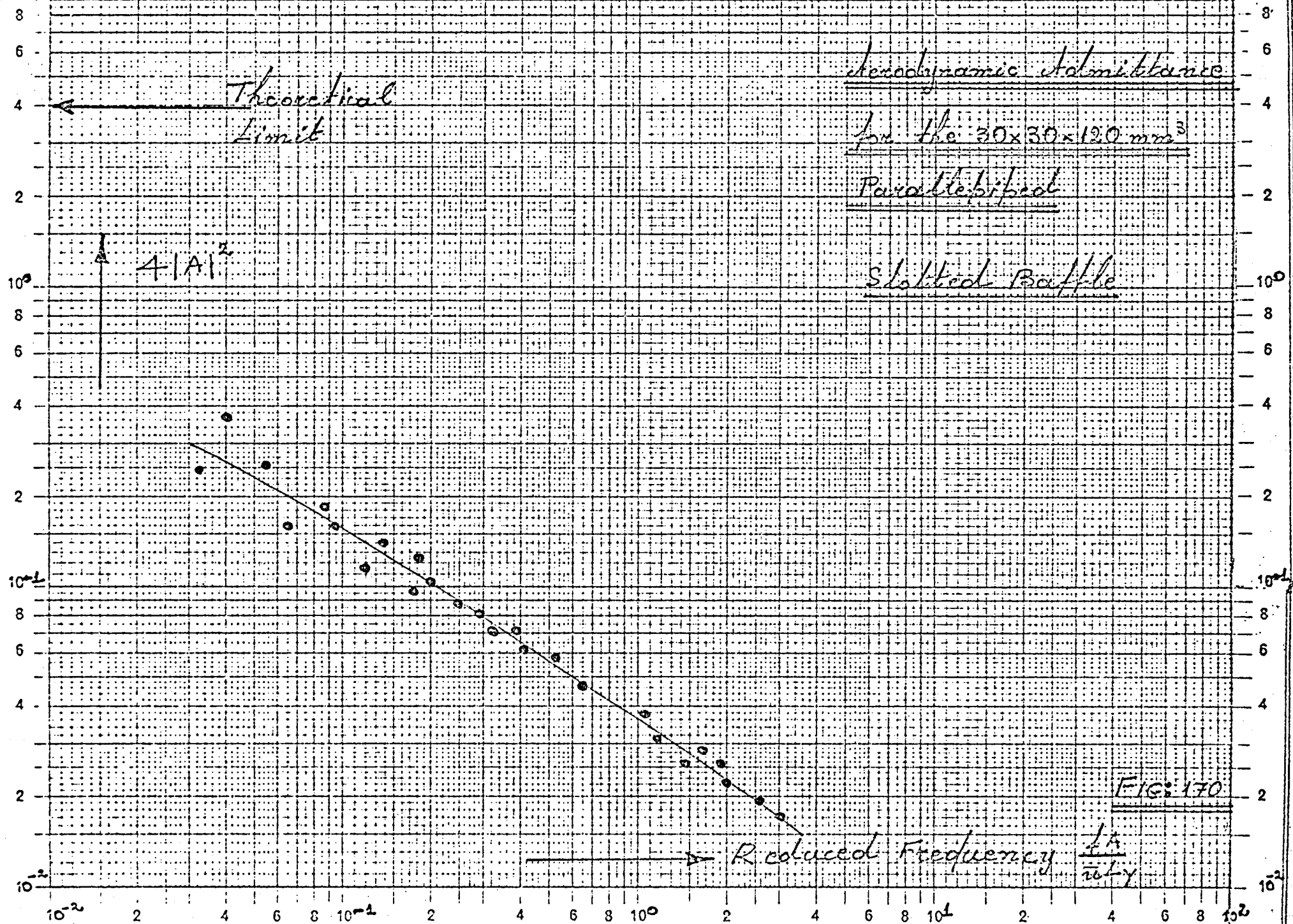


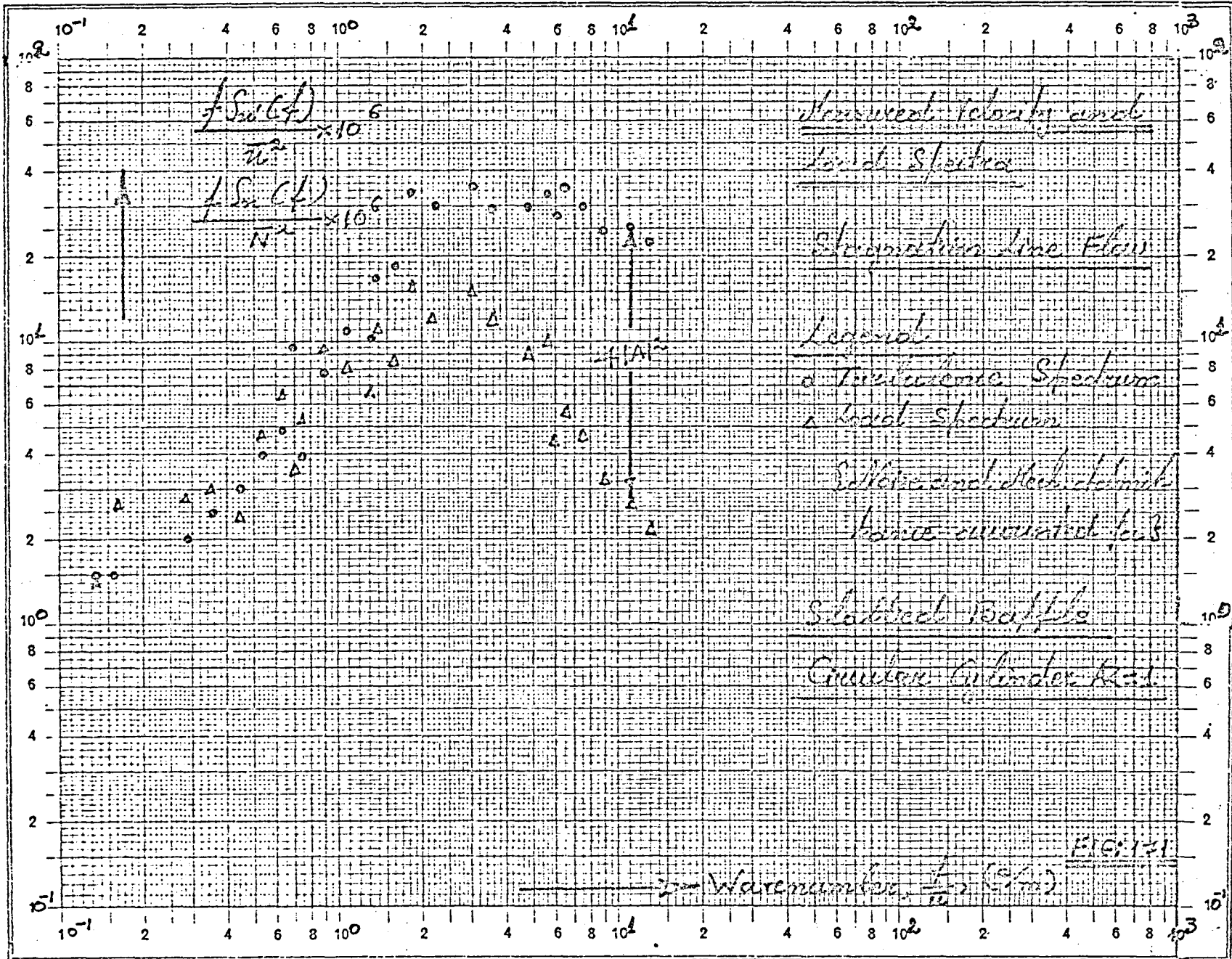
FIG. 166

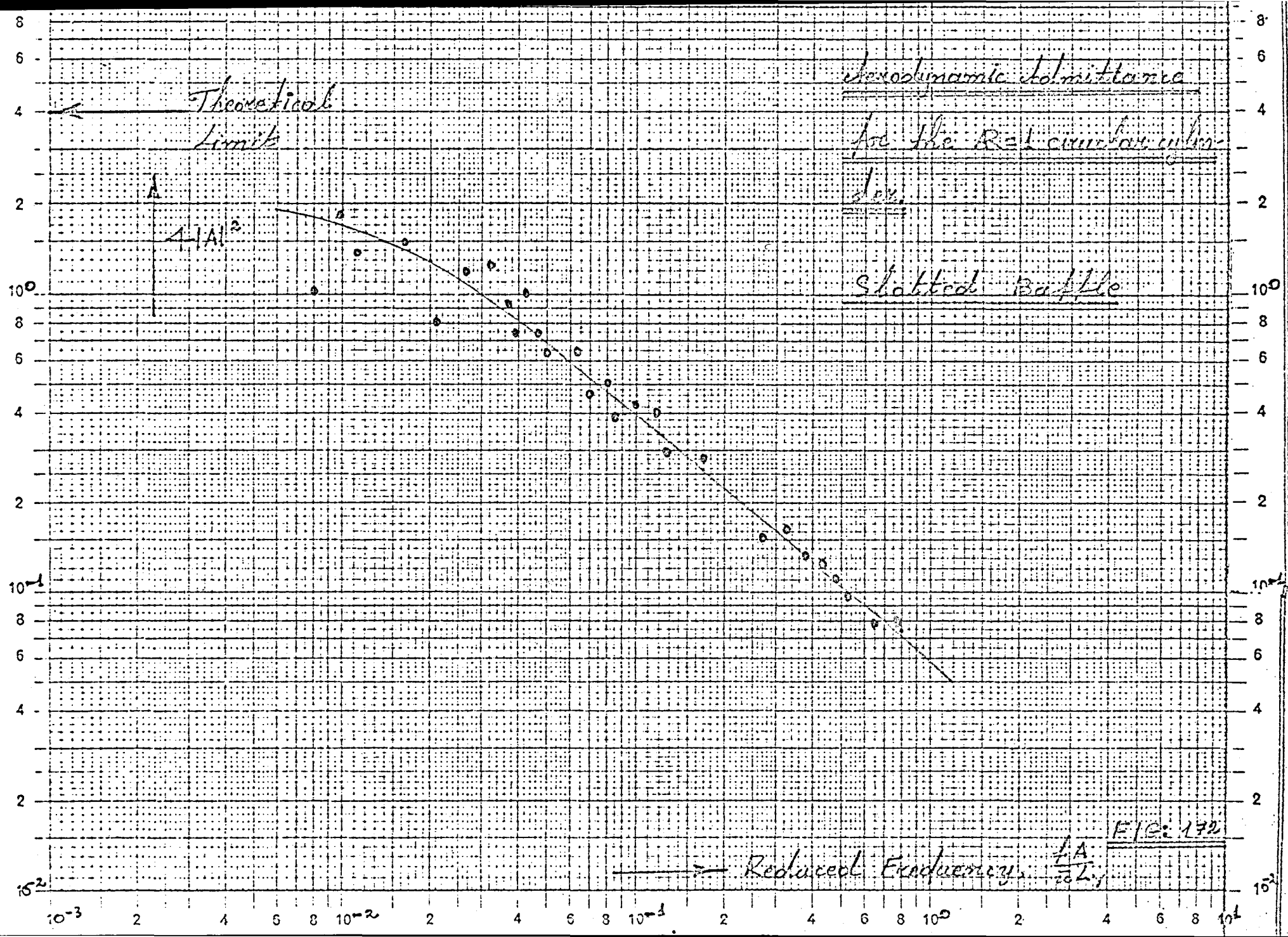


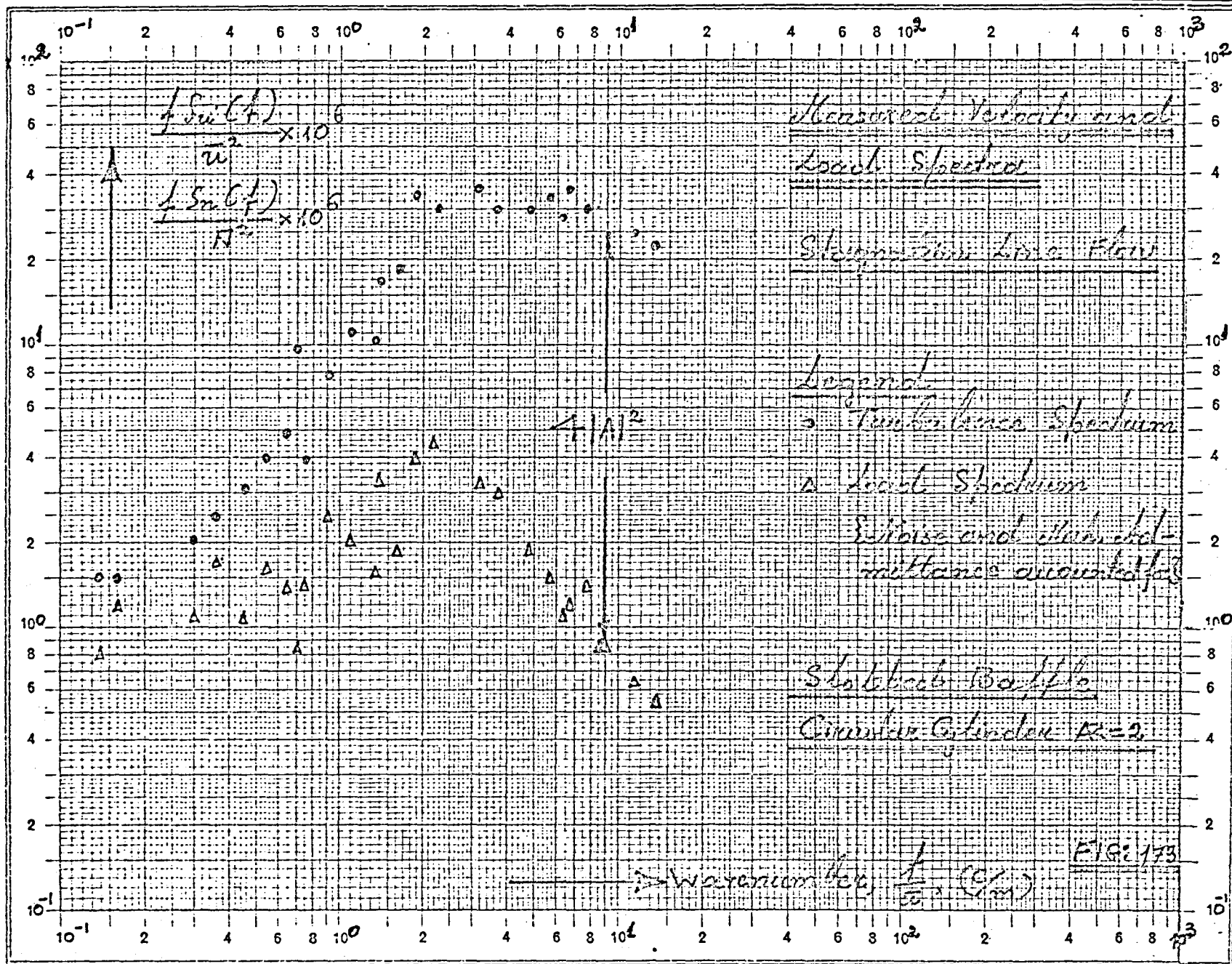


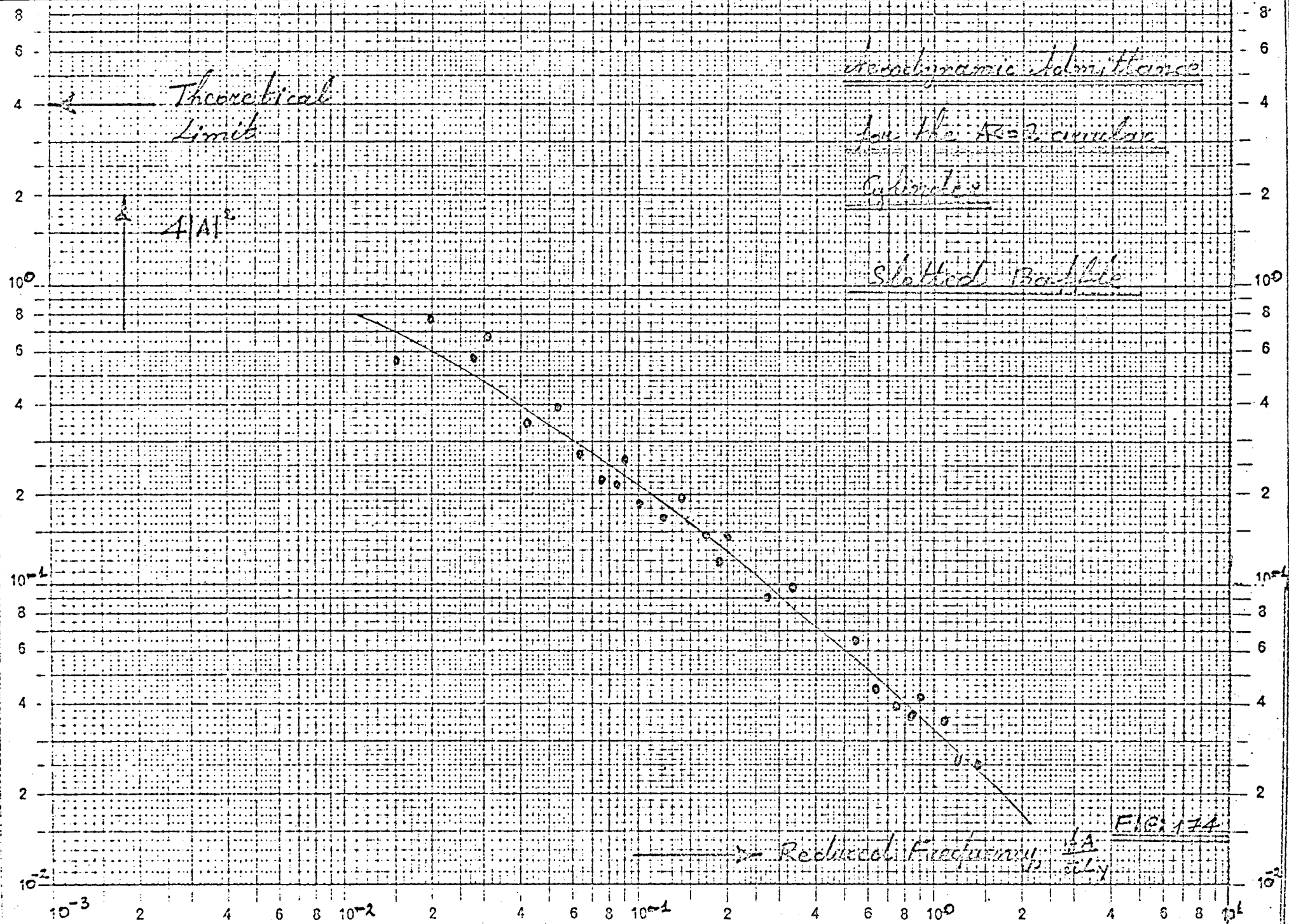


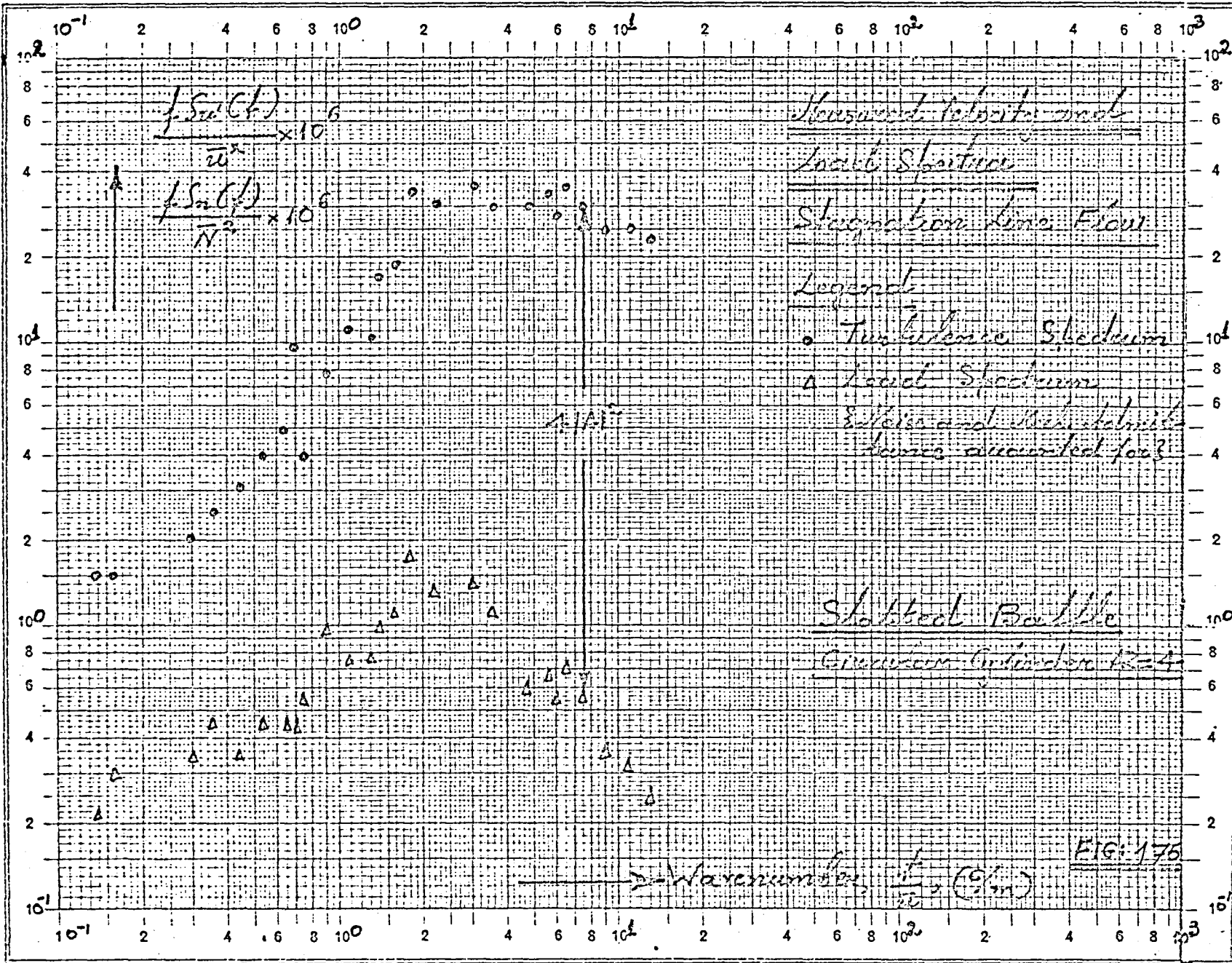


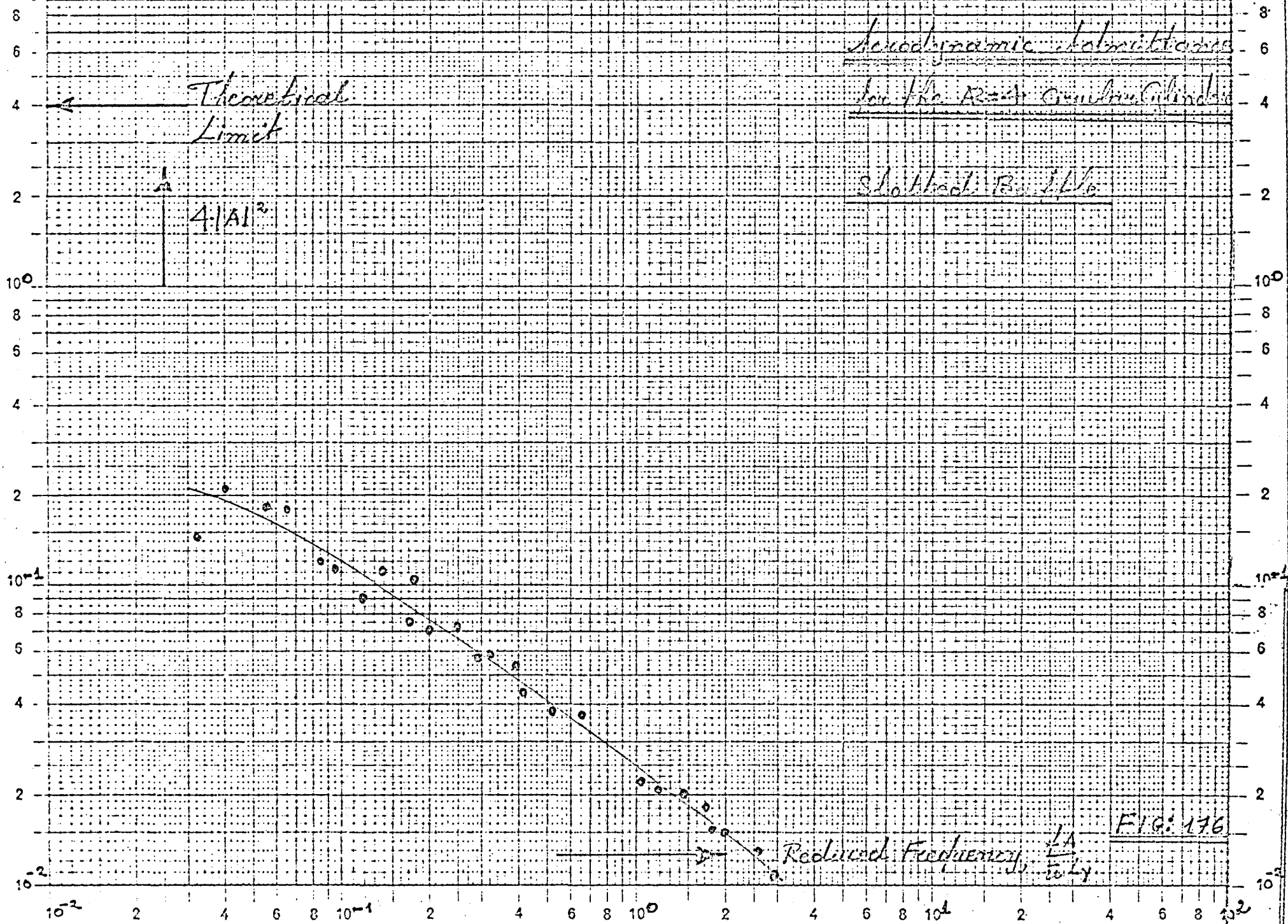


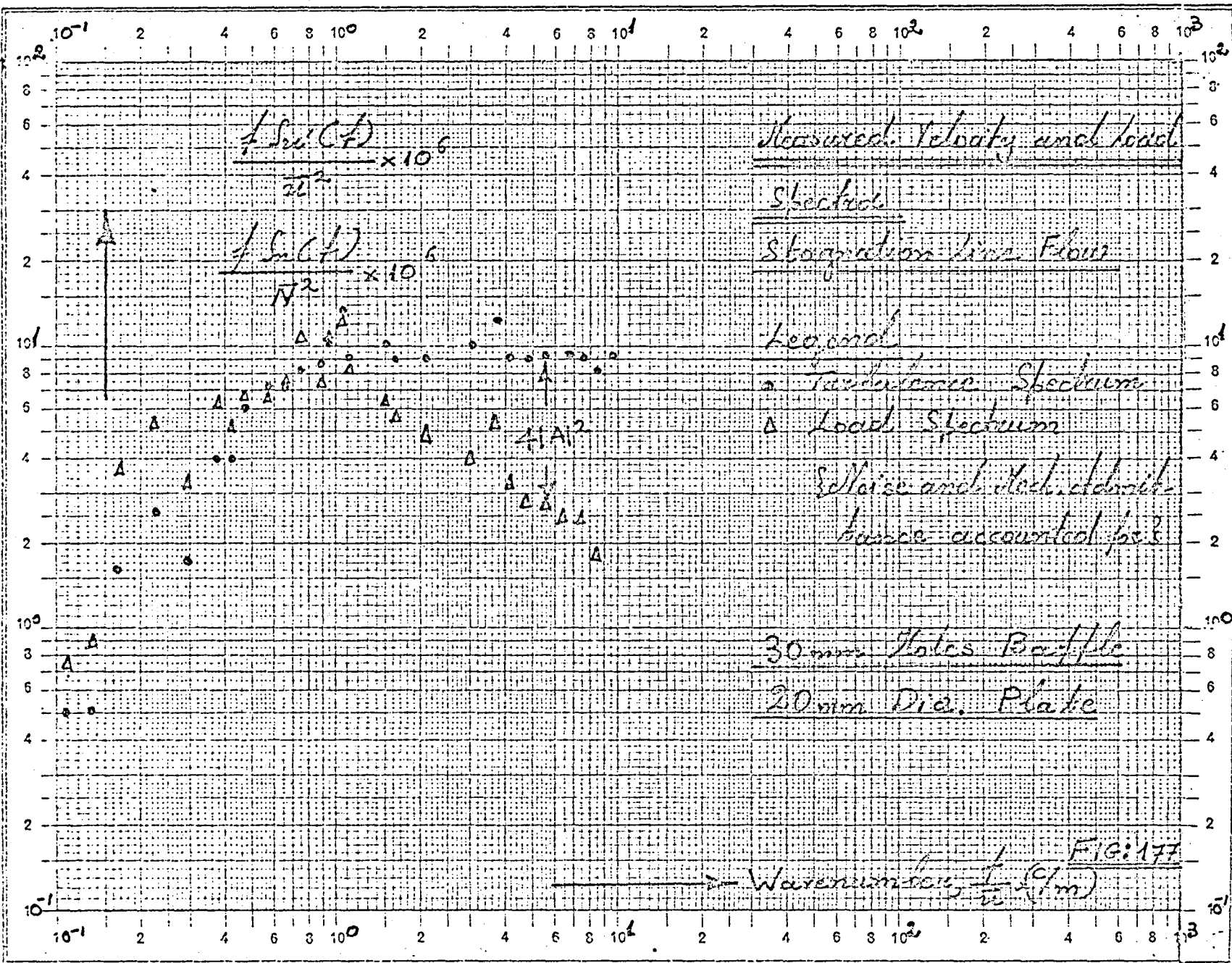


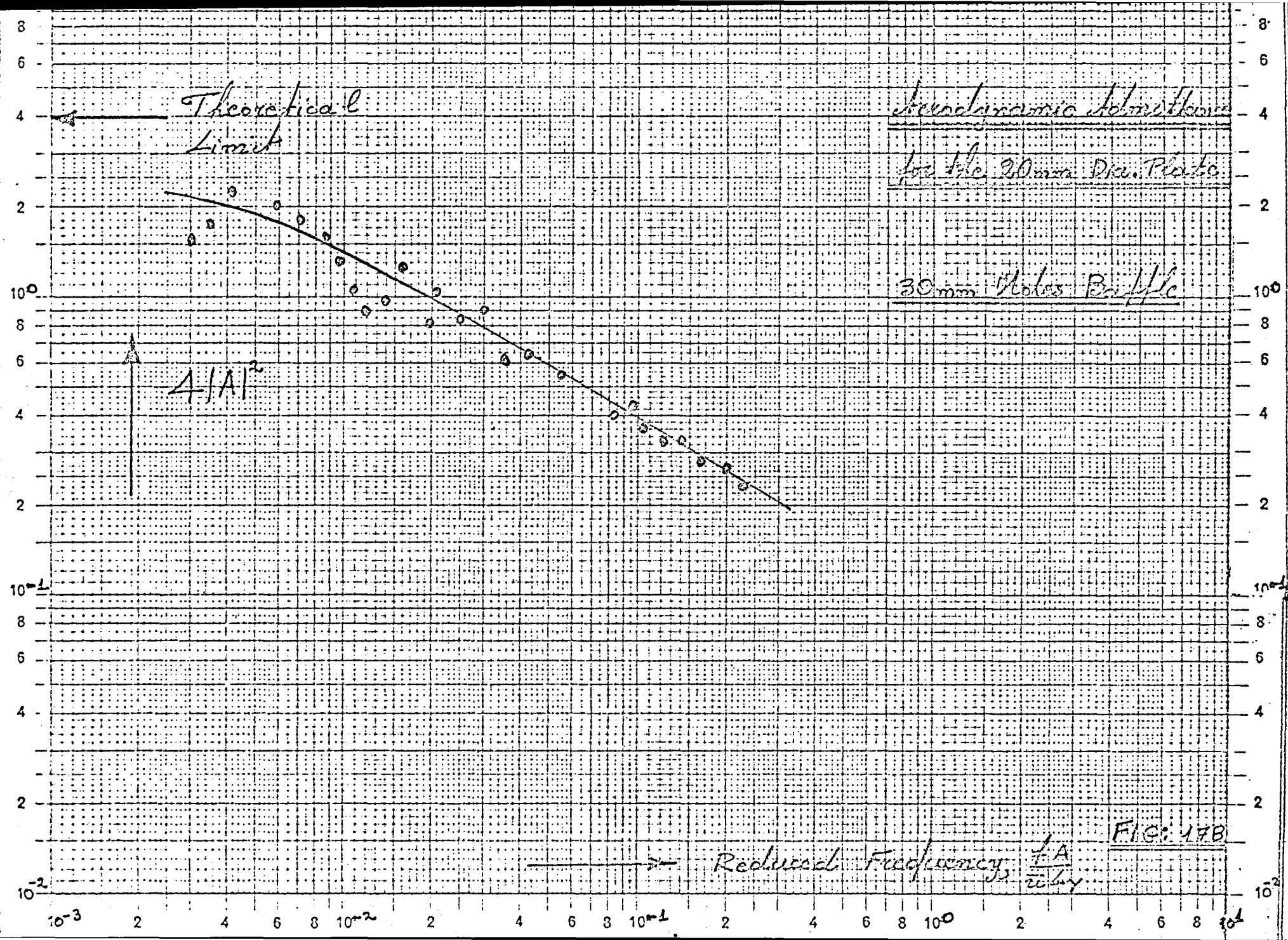


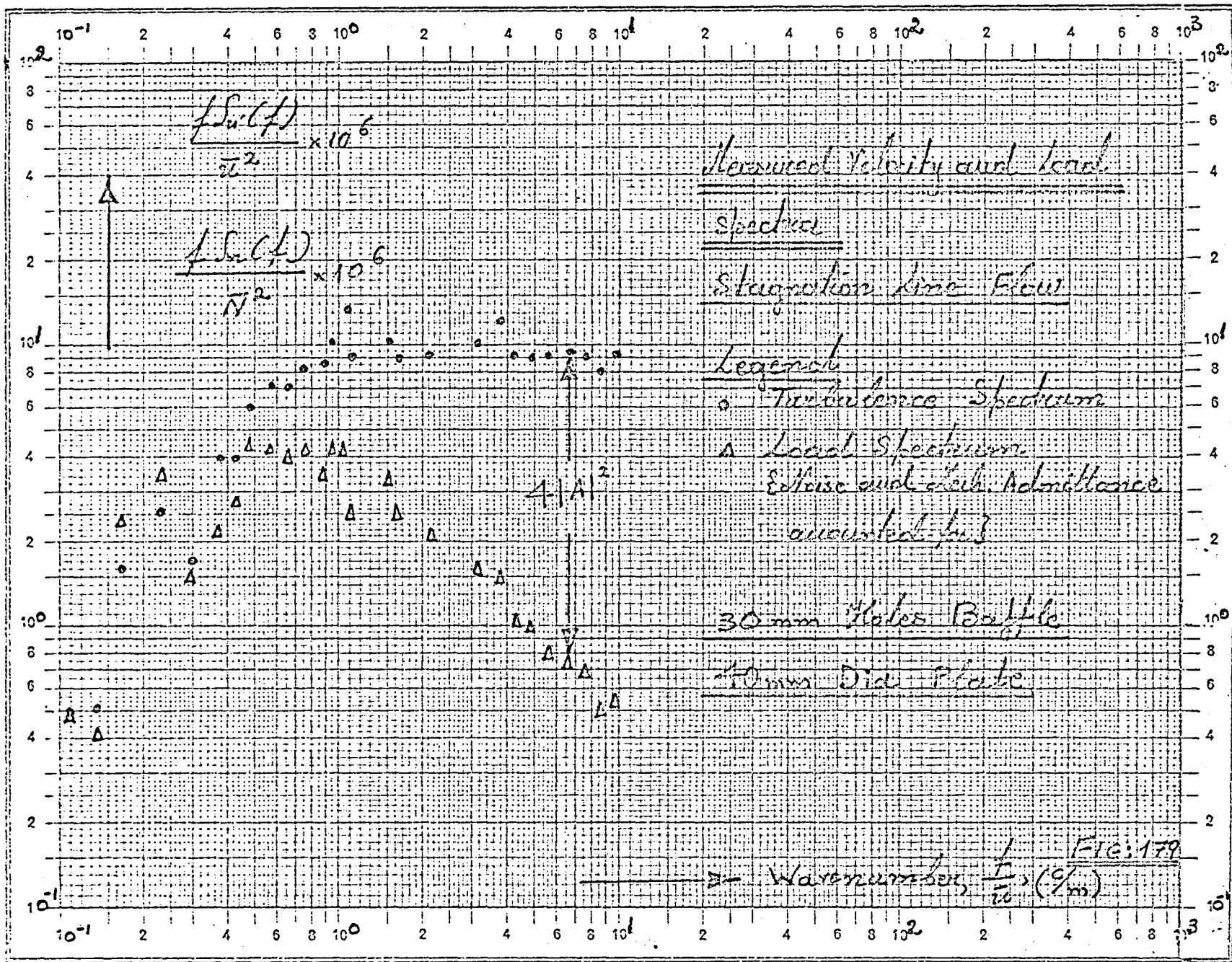


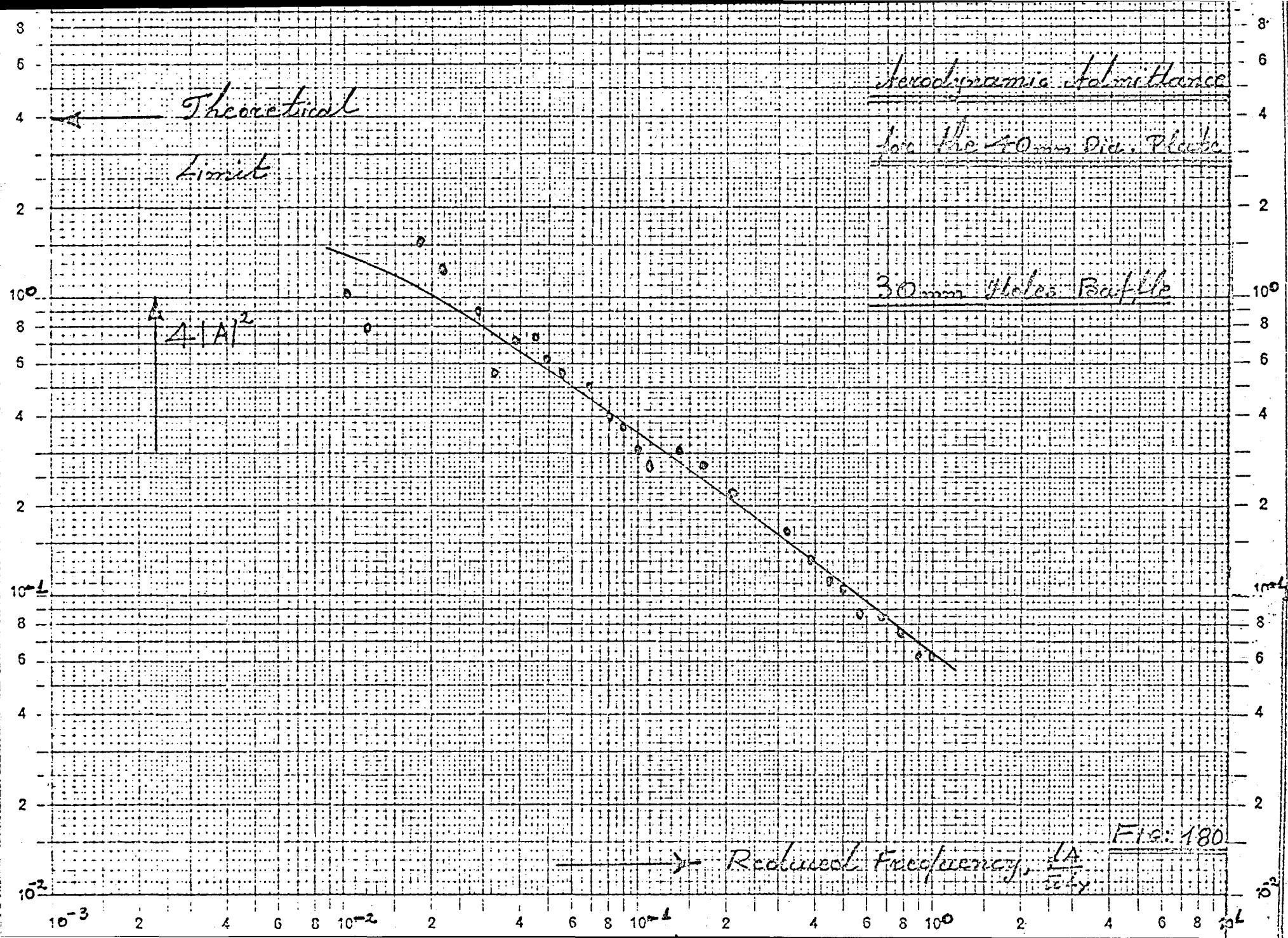


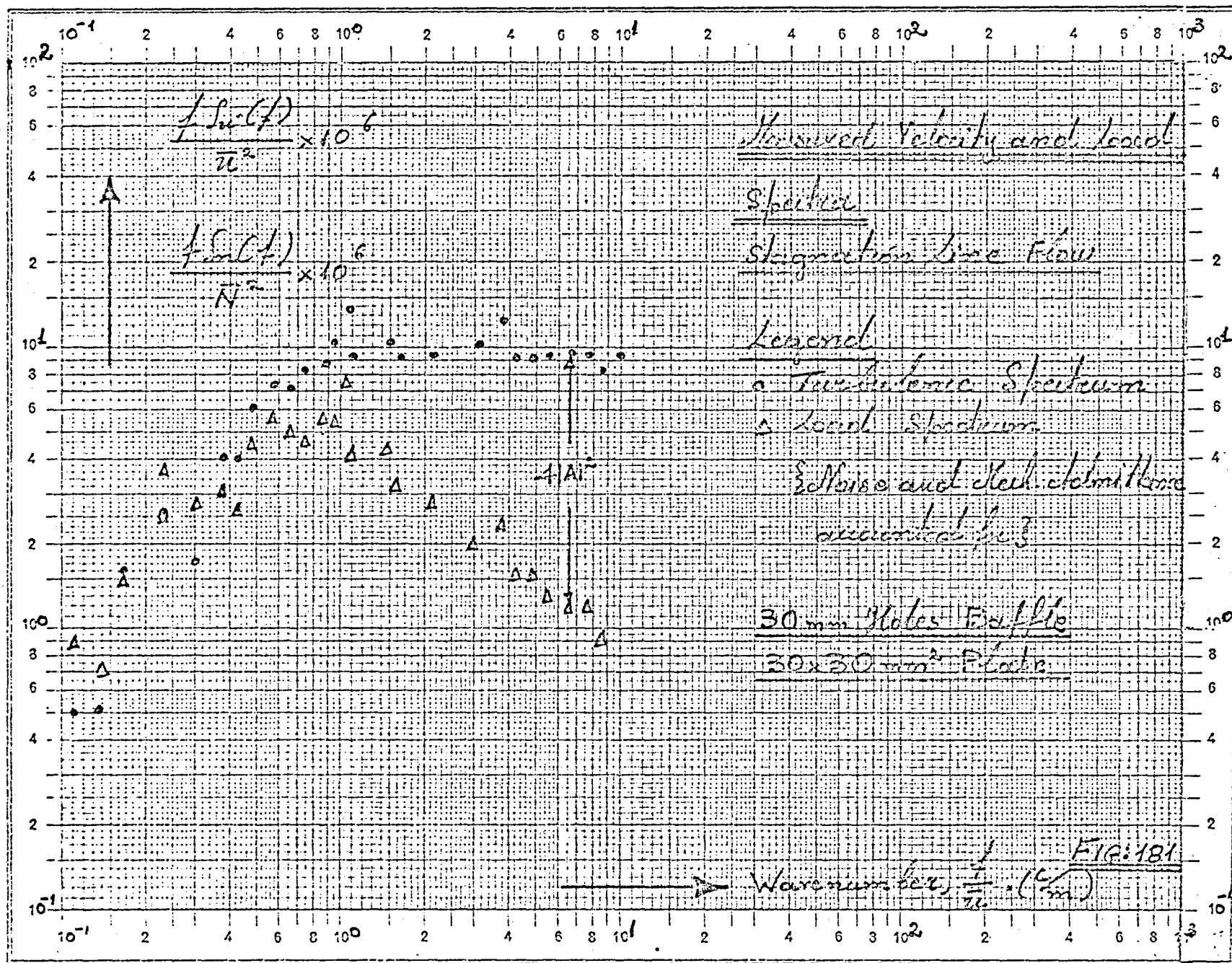


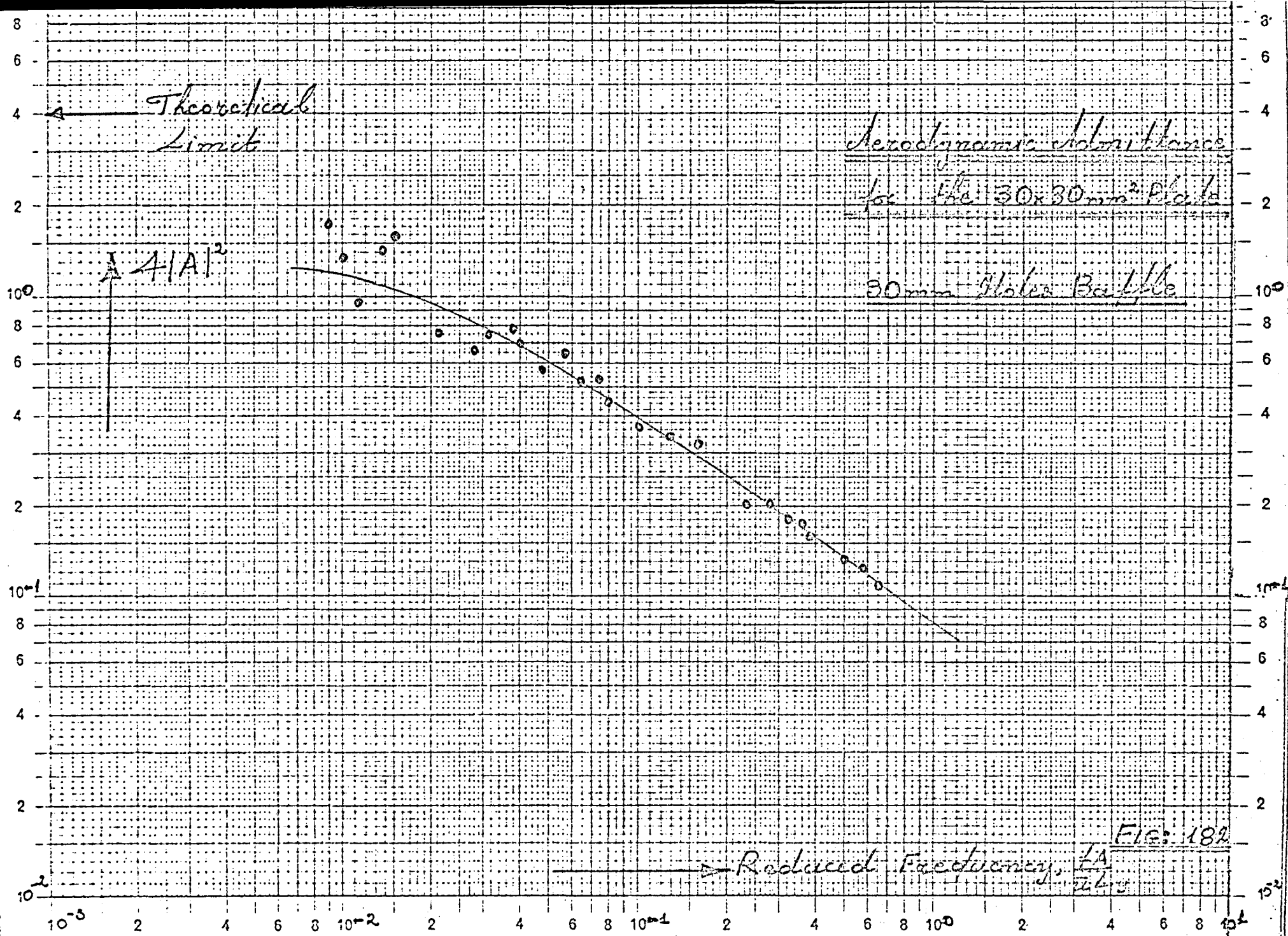


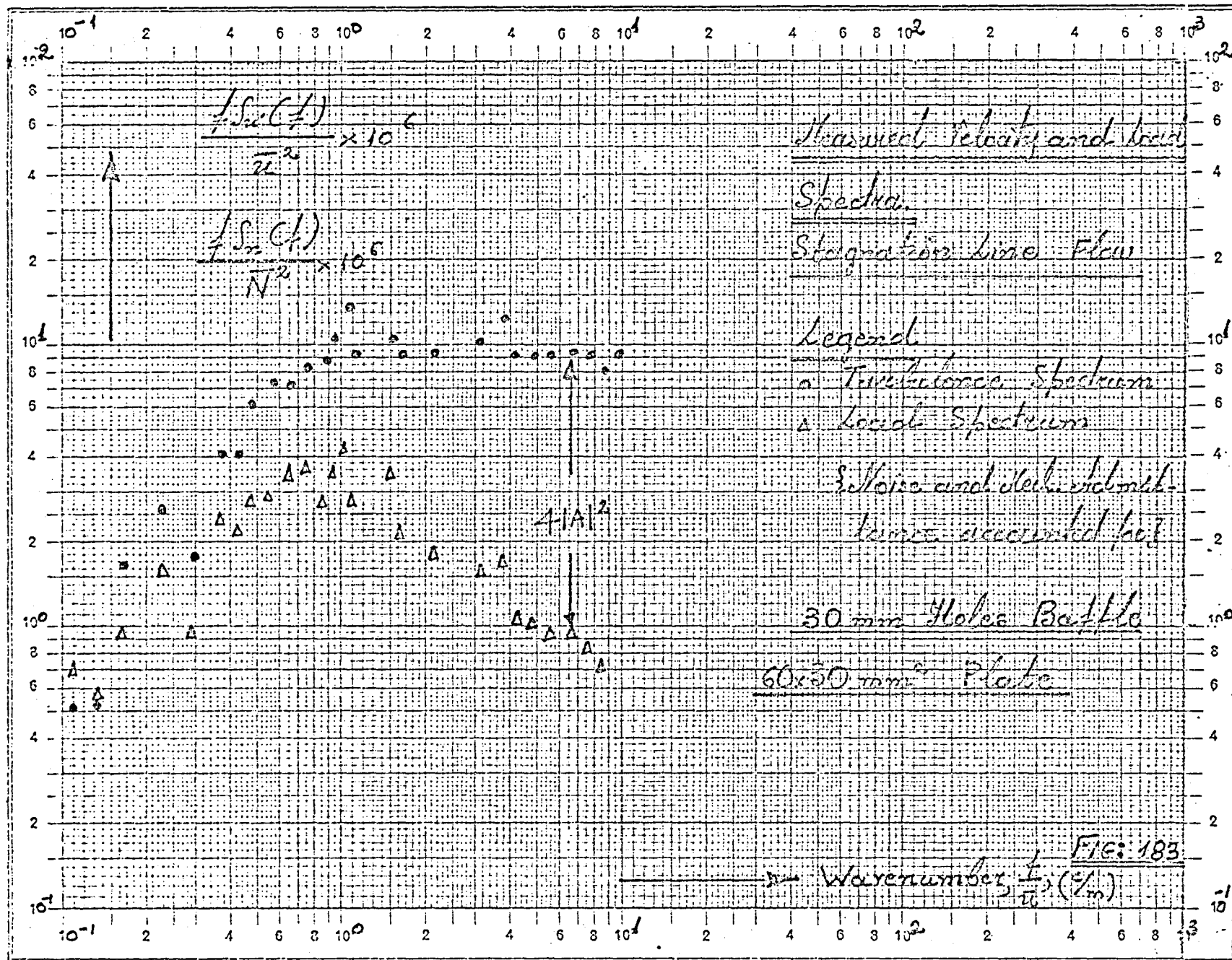


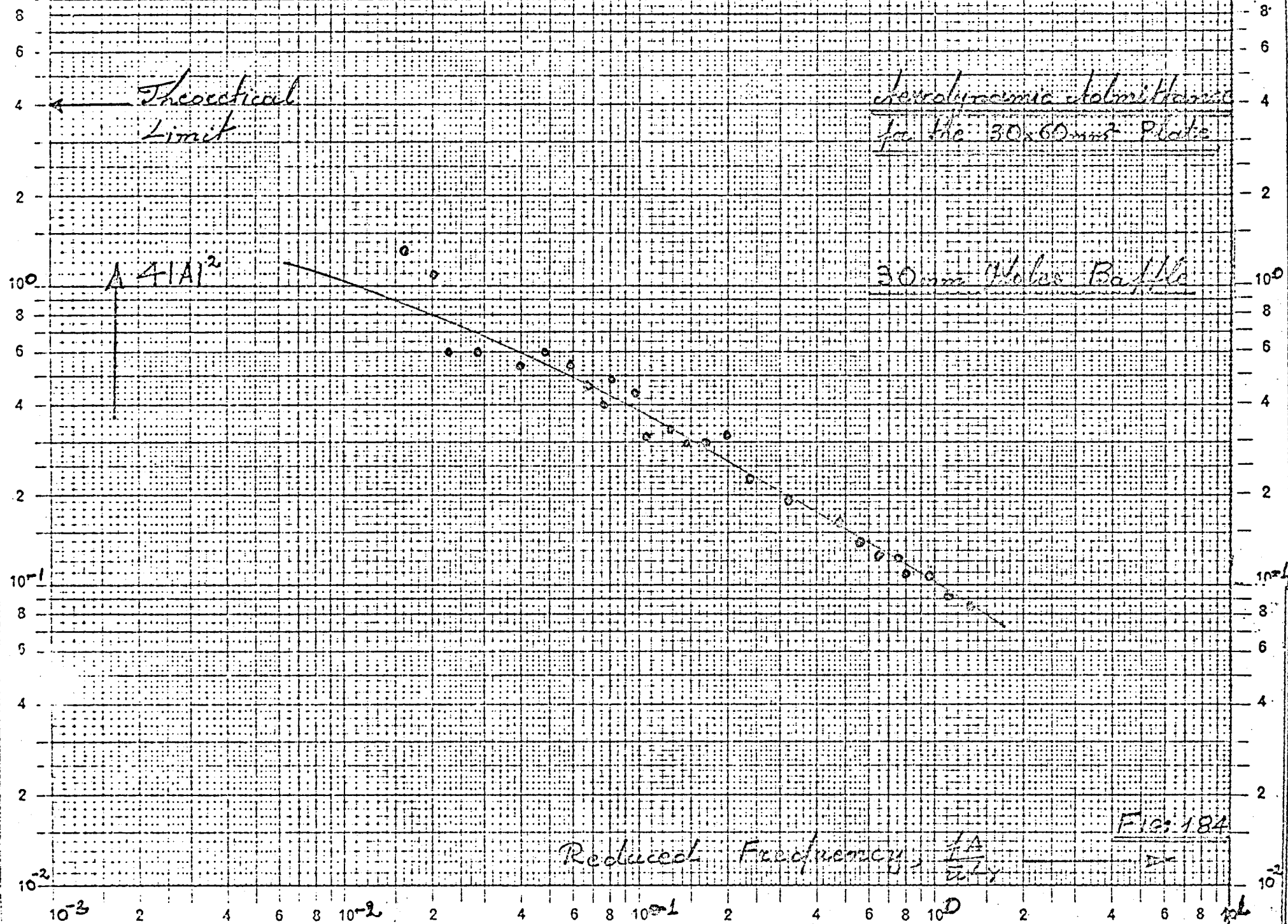


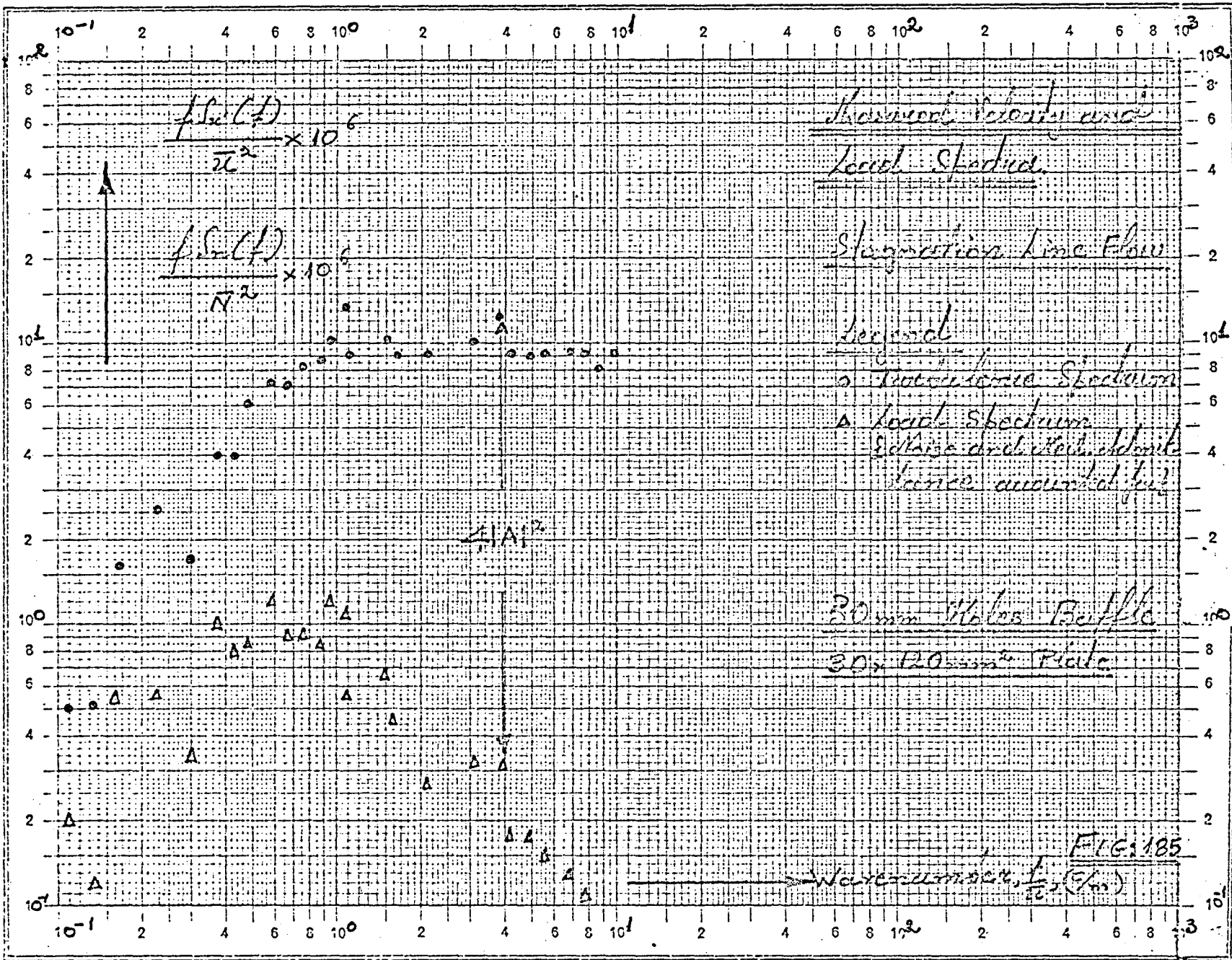












Theoretical

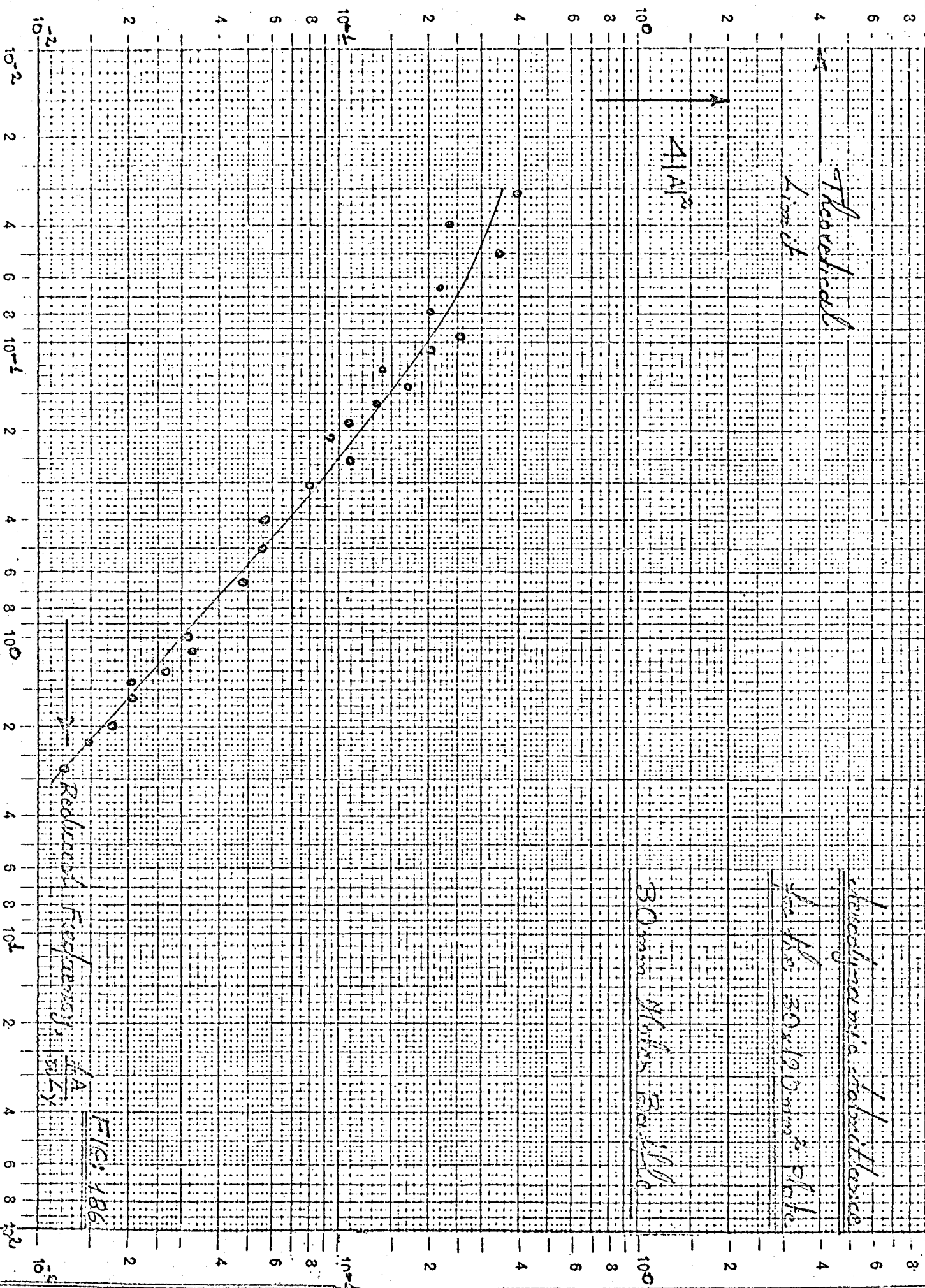
Limit

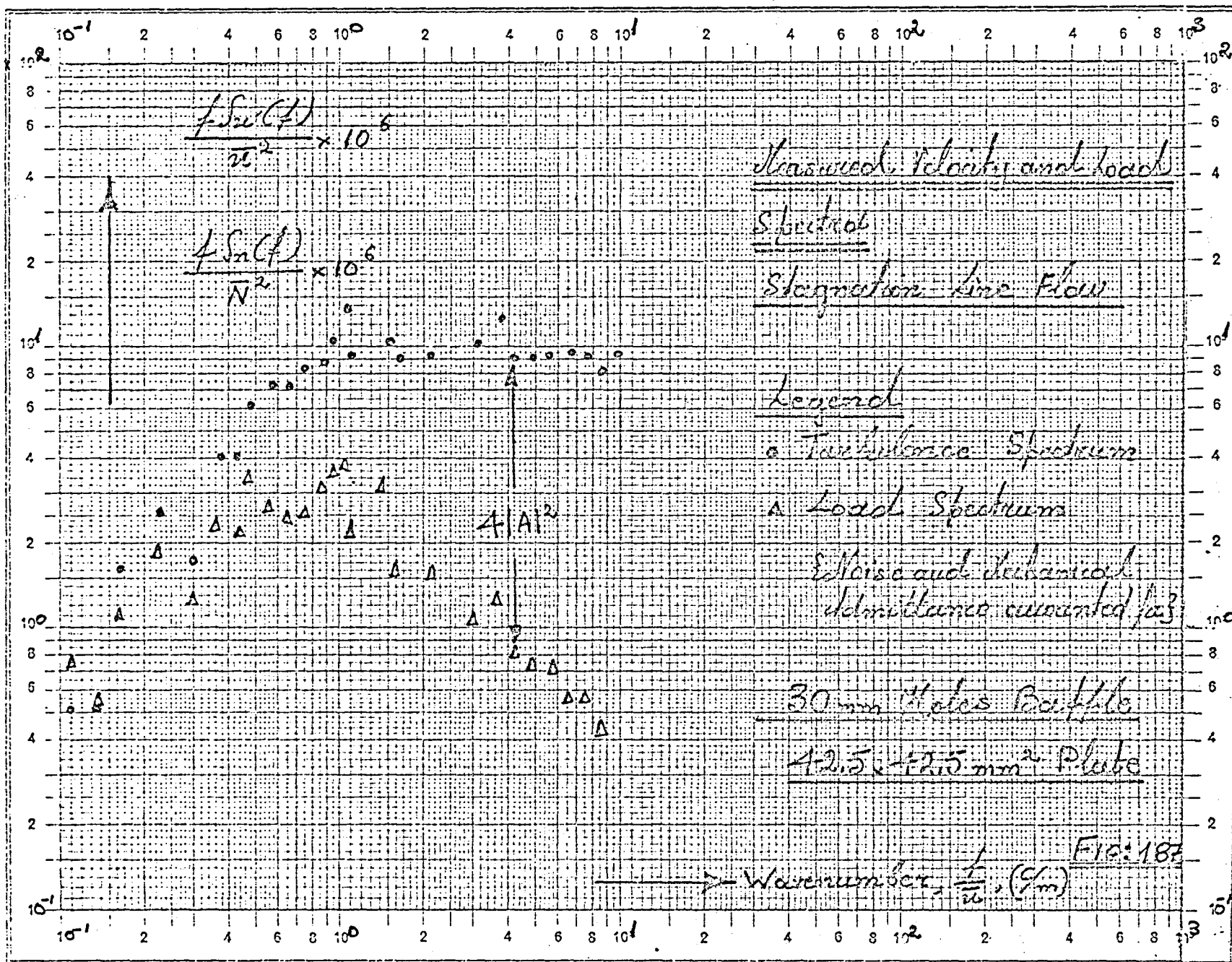
Chondromyia strobilifera

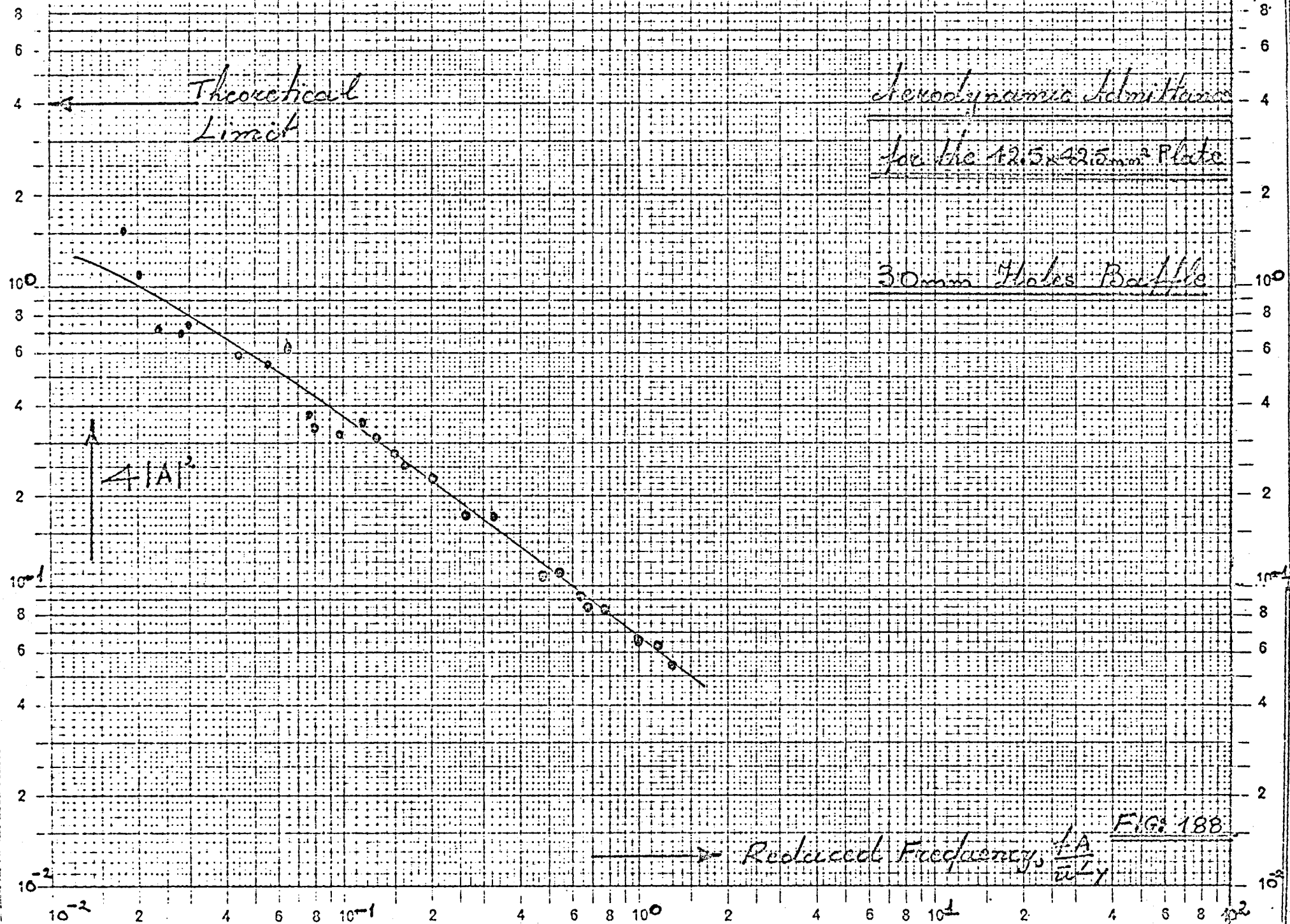
4000 20000 mm² plate

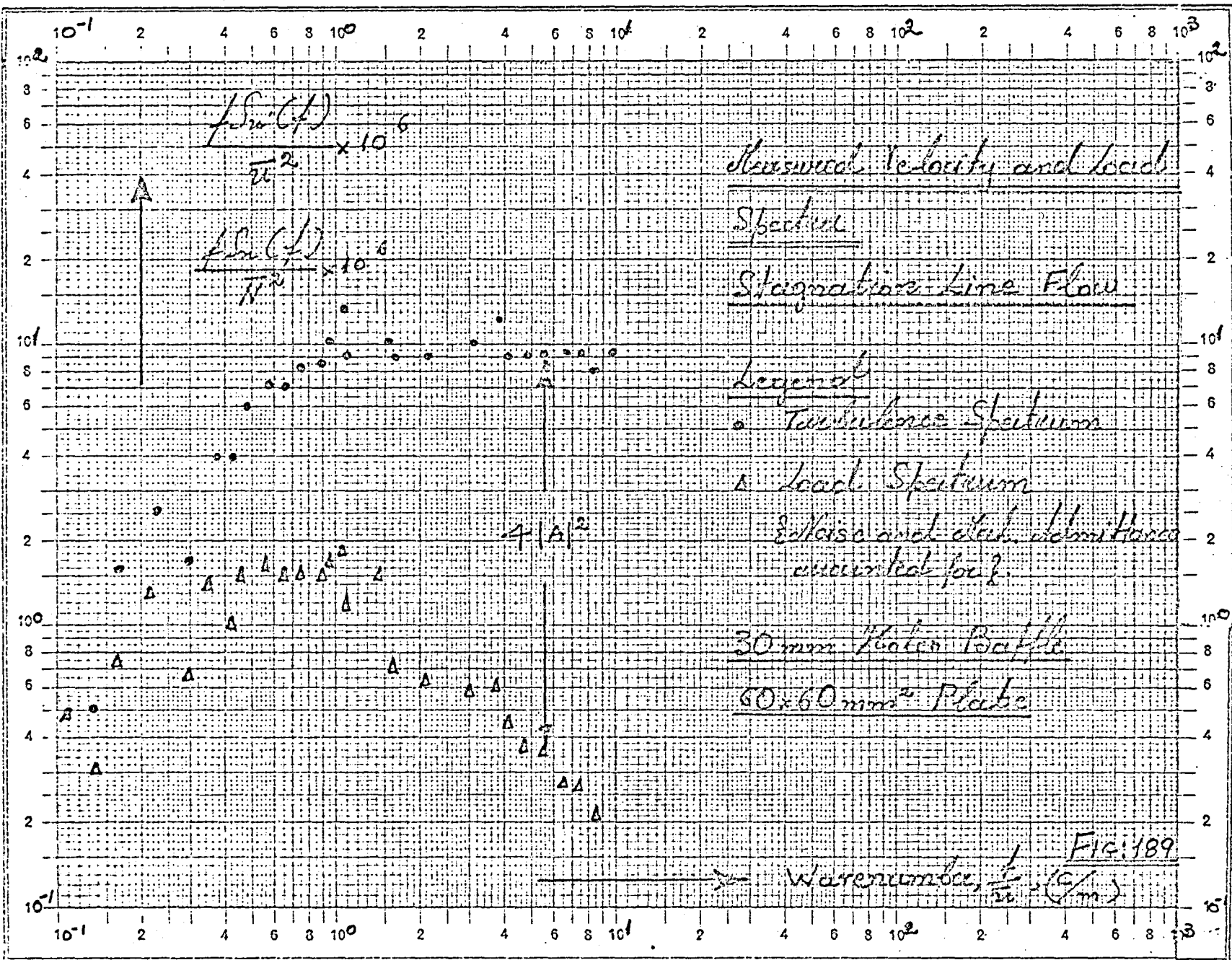
30 mm plates 3000

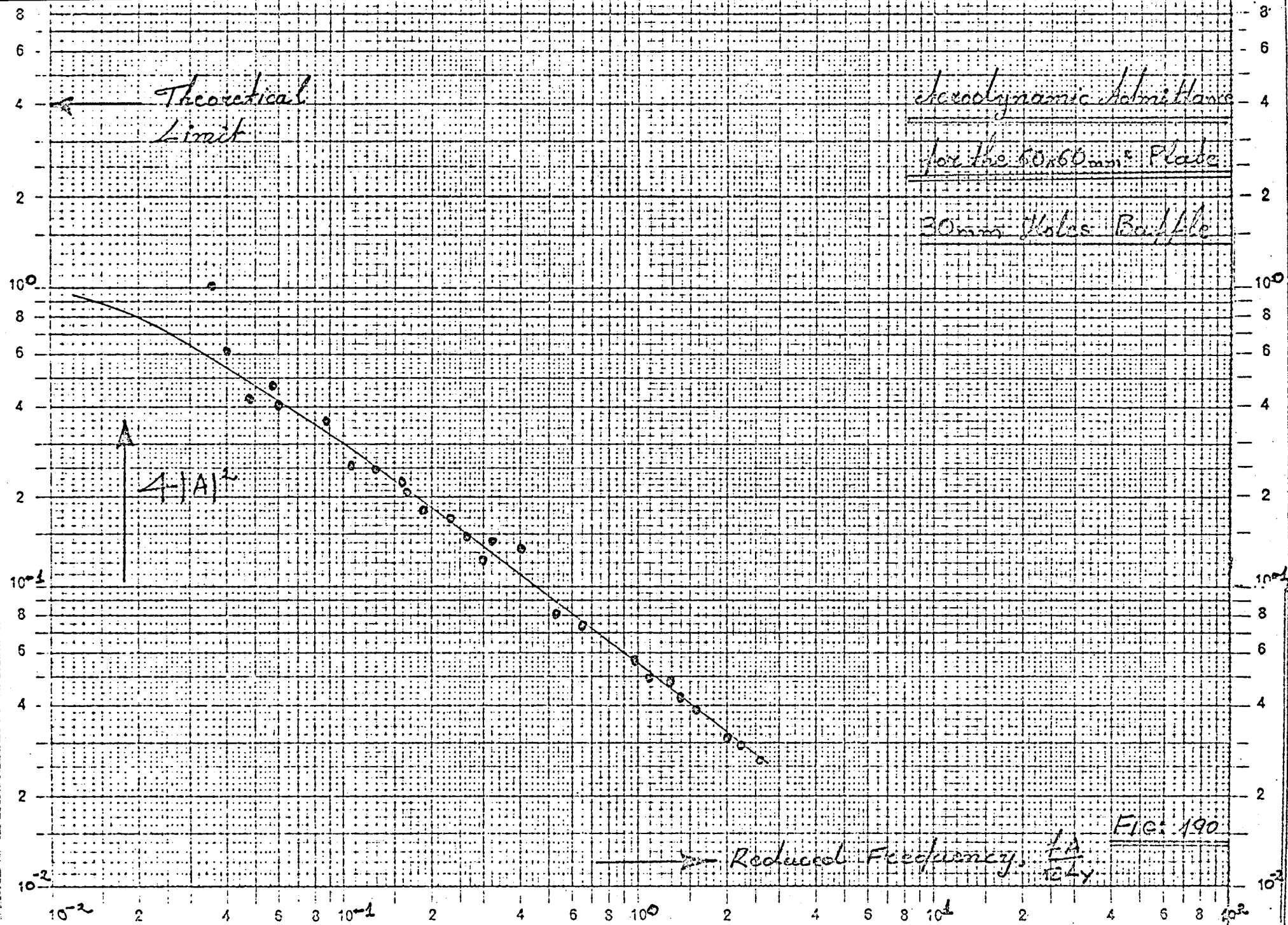
$41A^2$

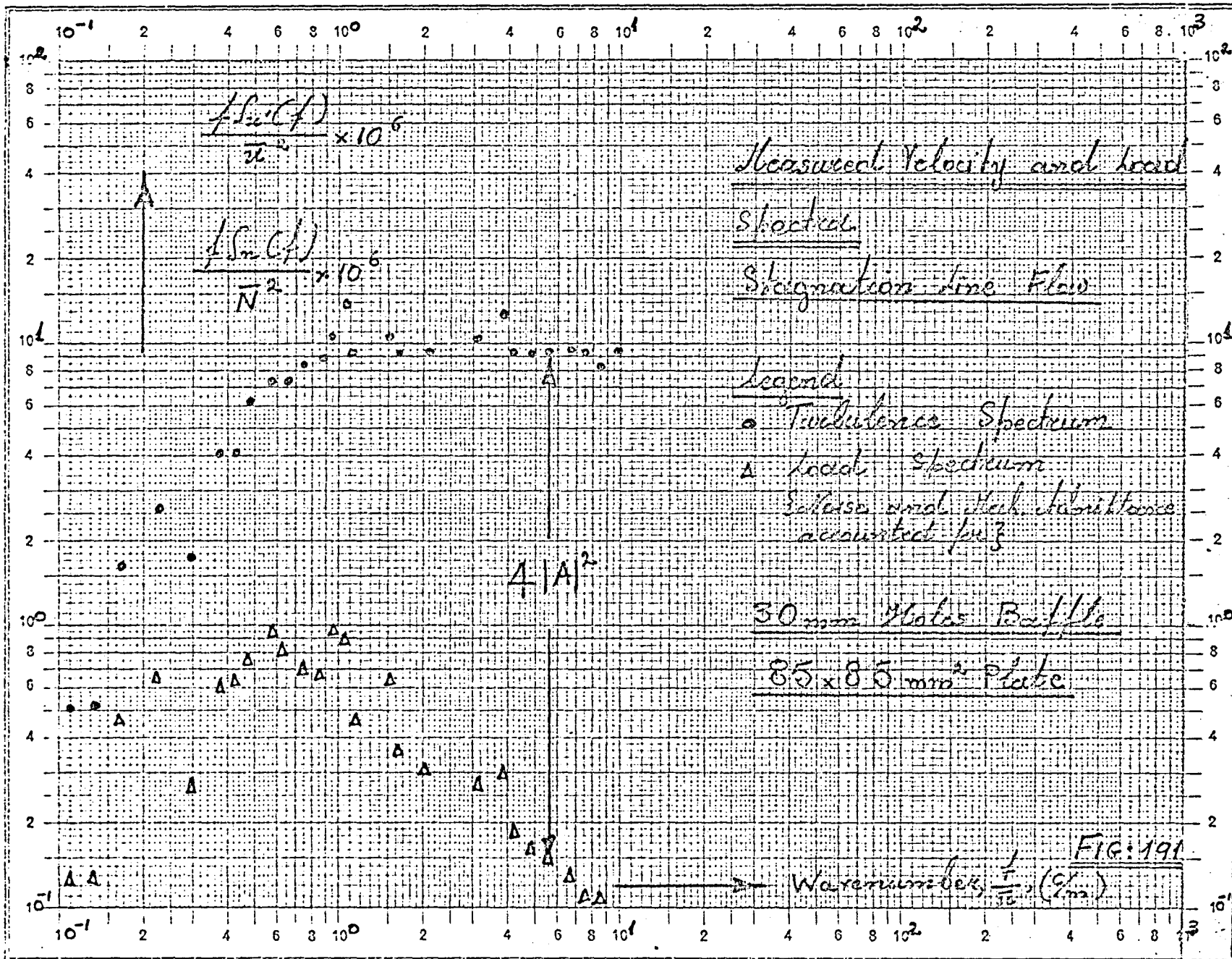












Theoretical

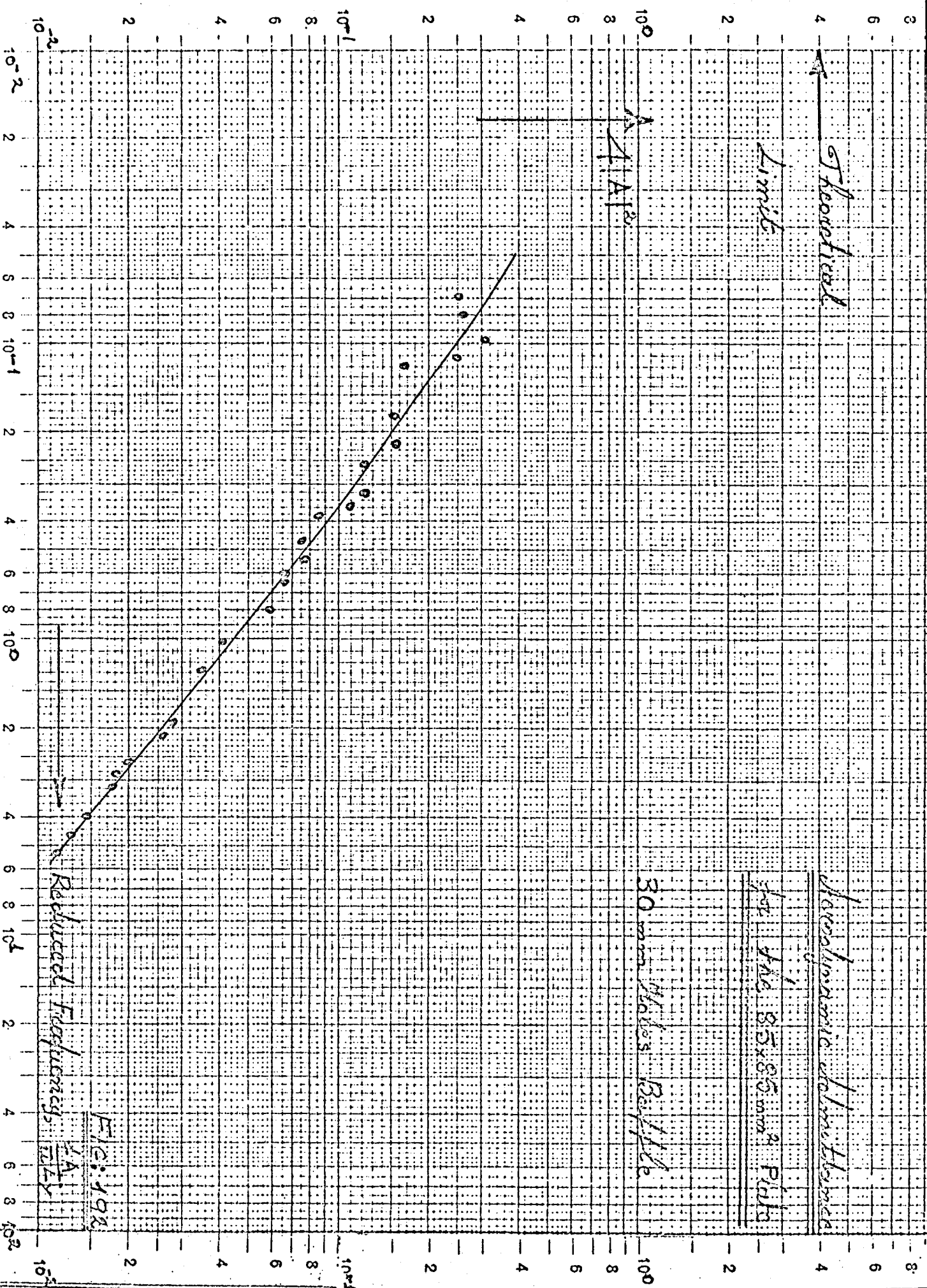
Limit

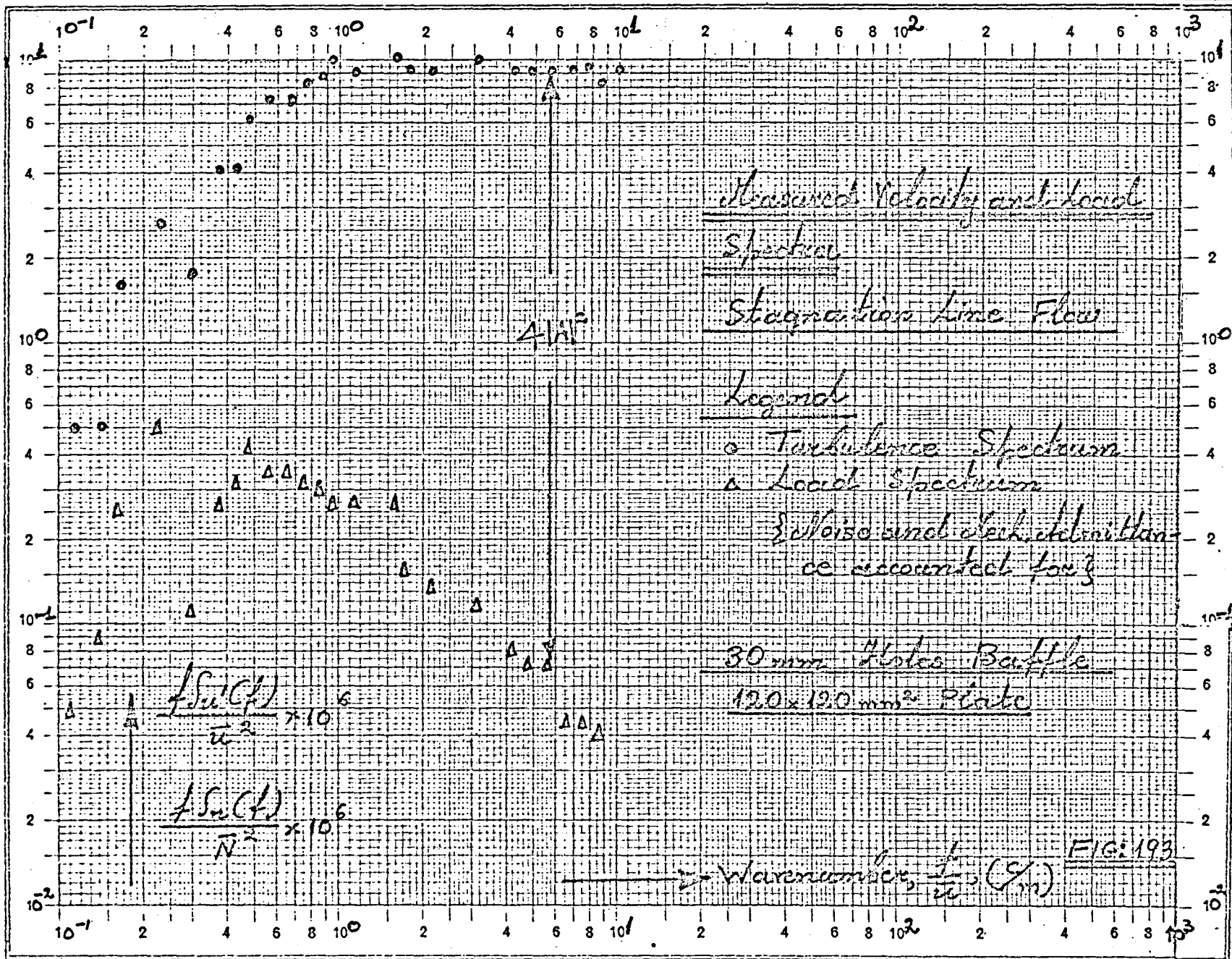
$A \propto A^{1/2}$

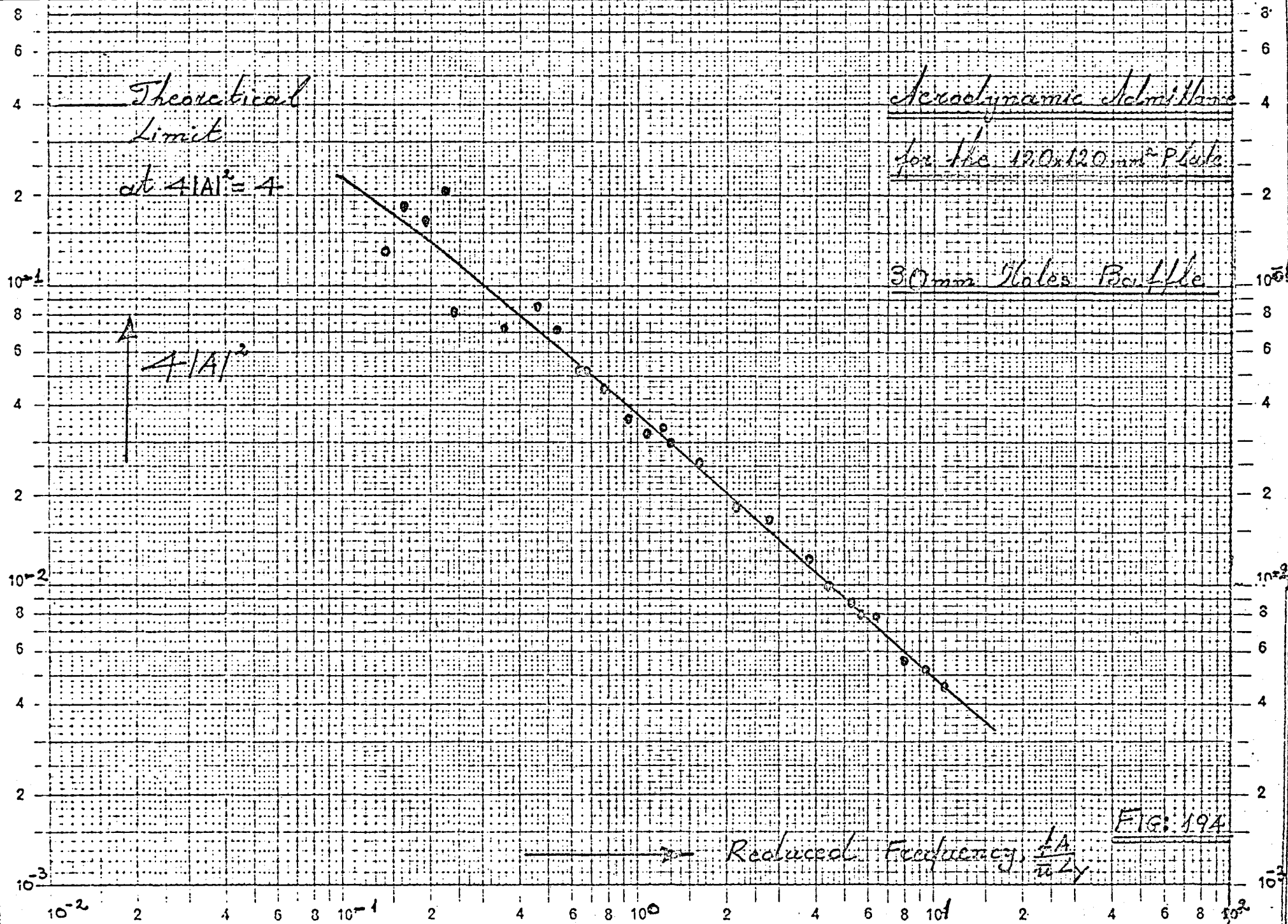
Barometric distance

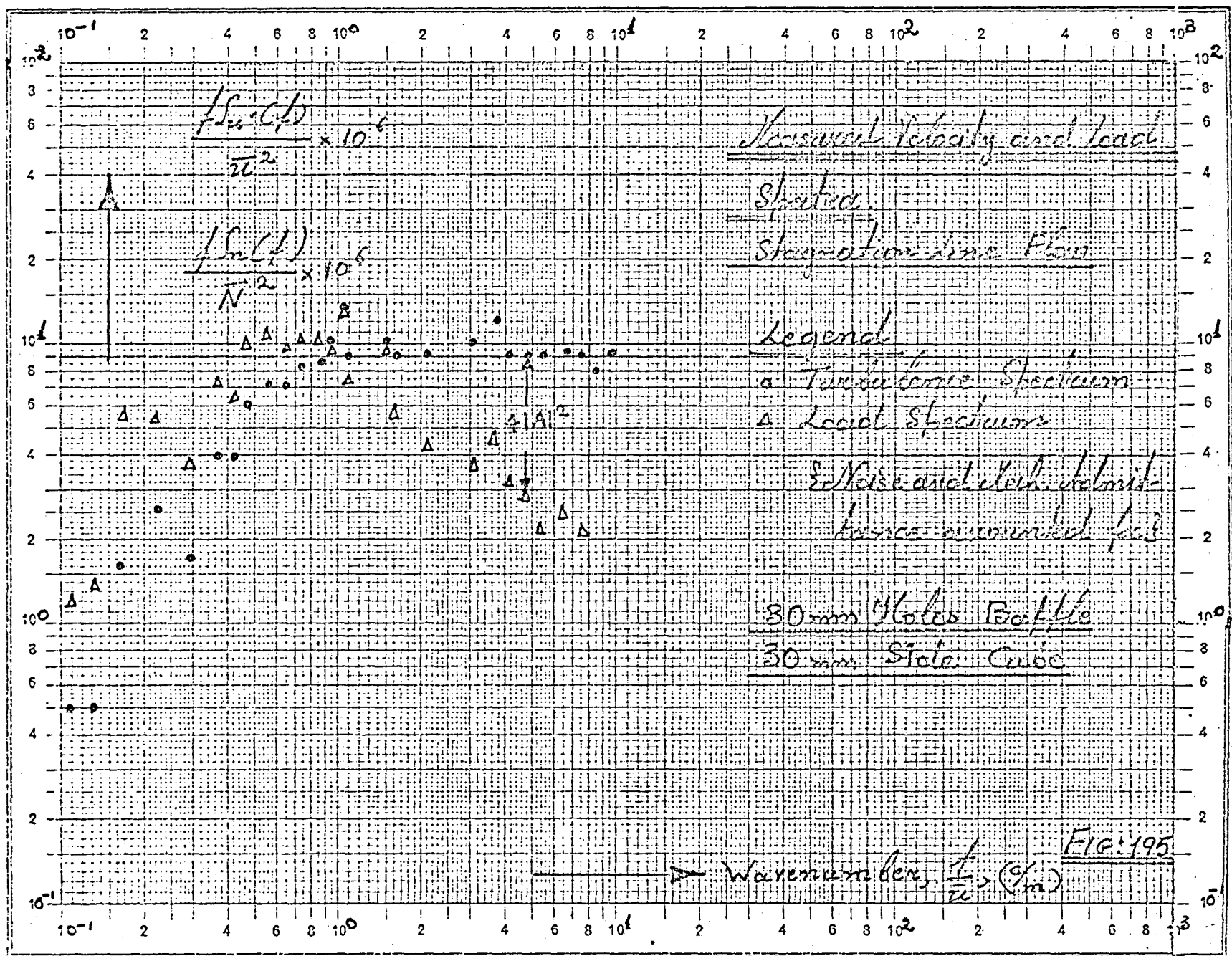
for the 85x85 mm² Pils

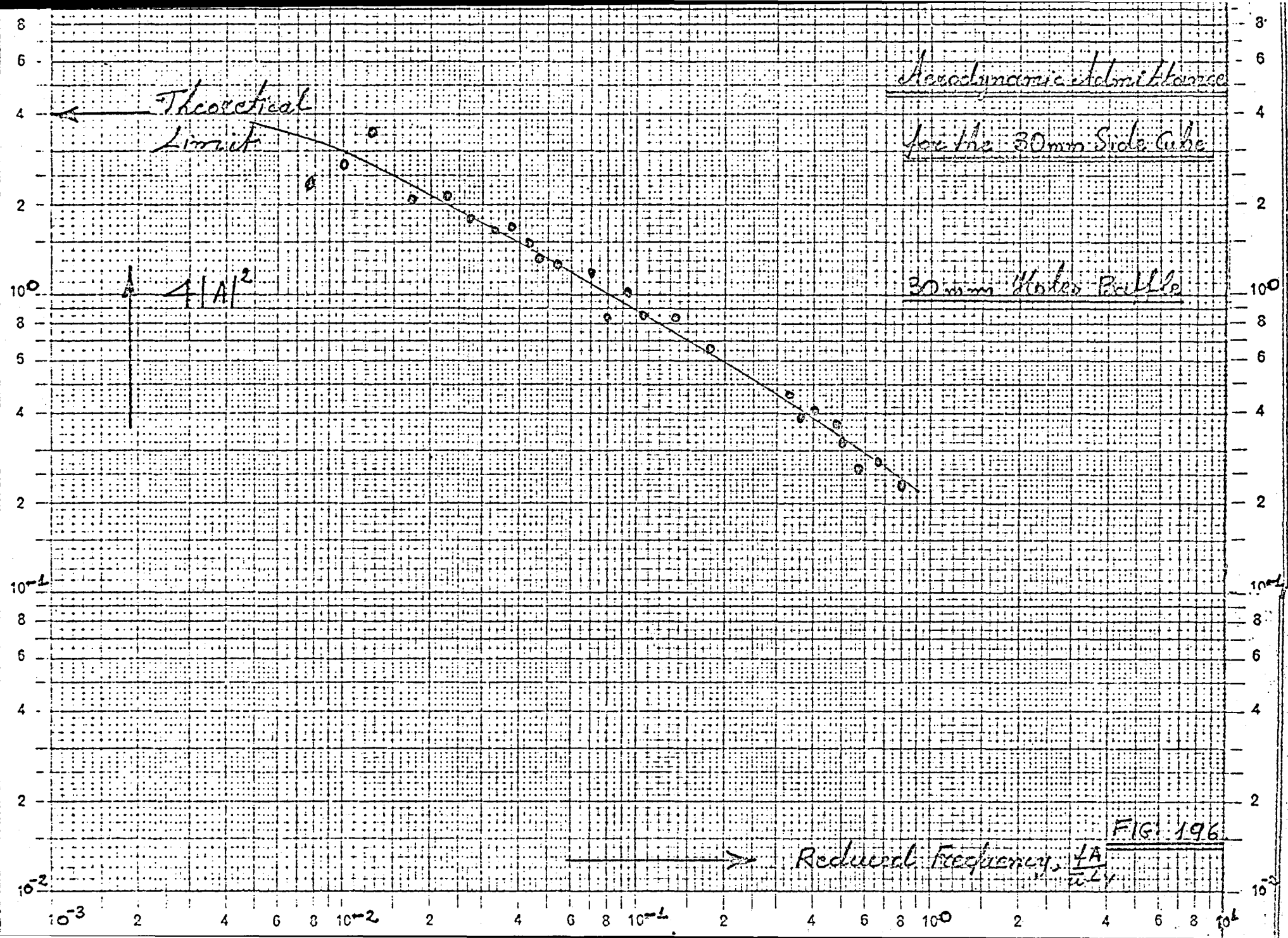
30 mm plates 130/116

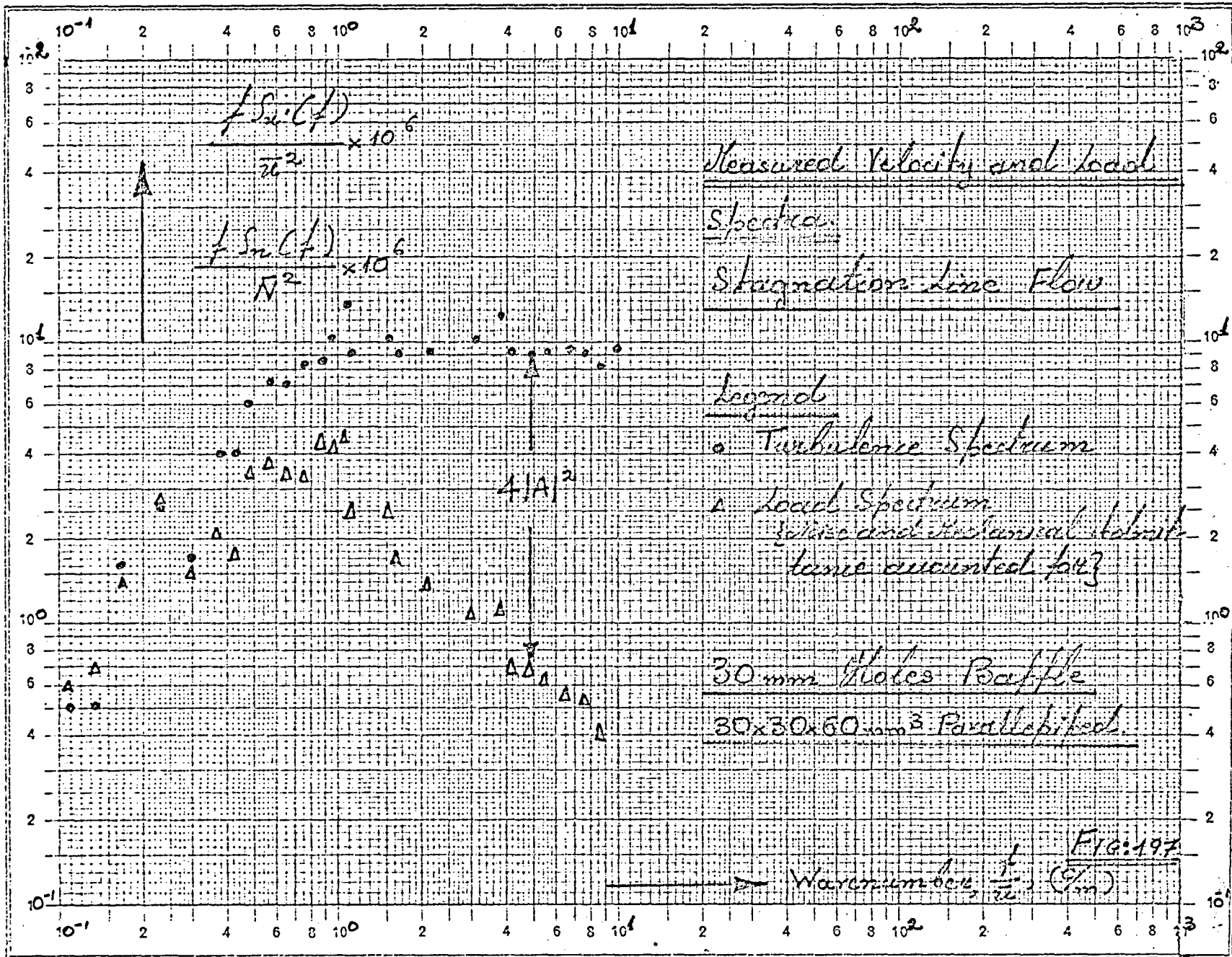












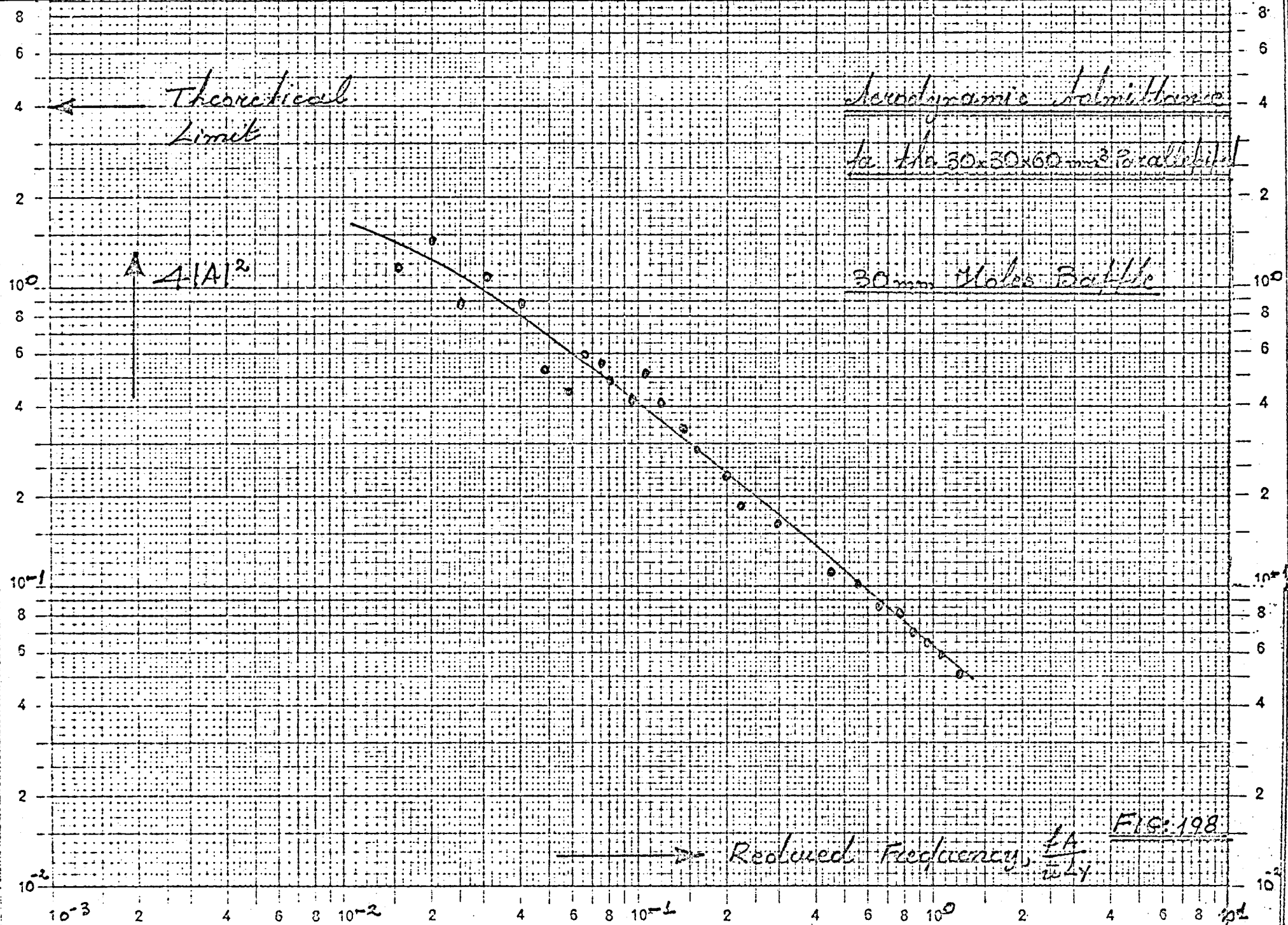
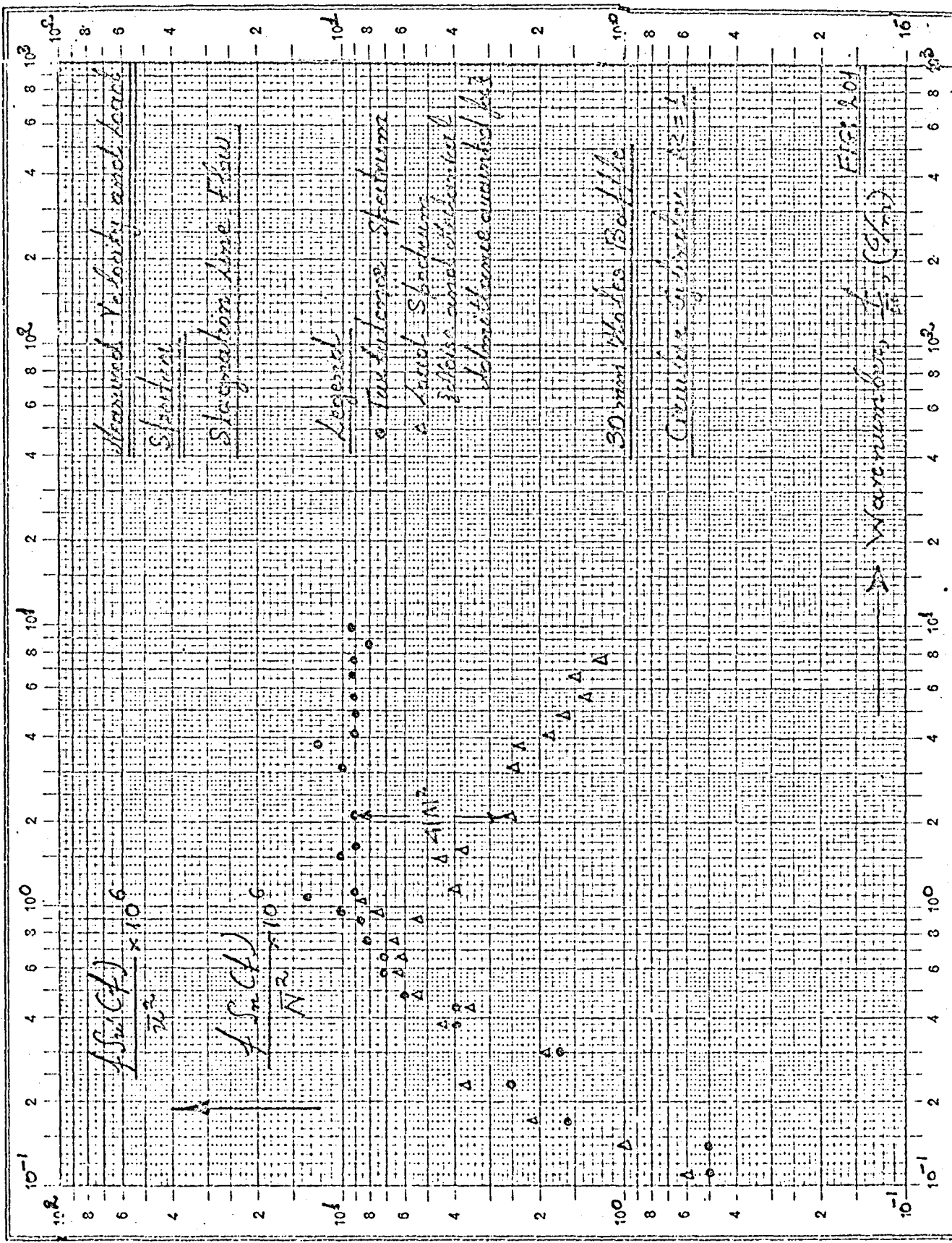
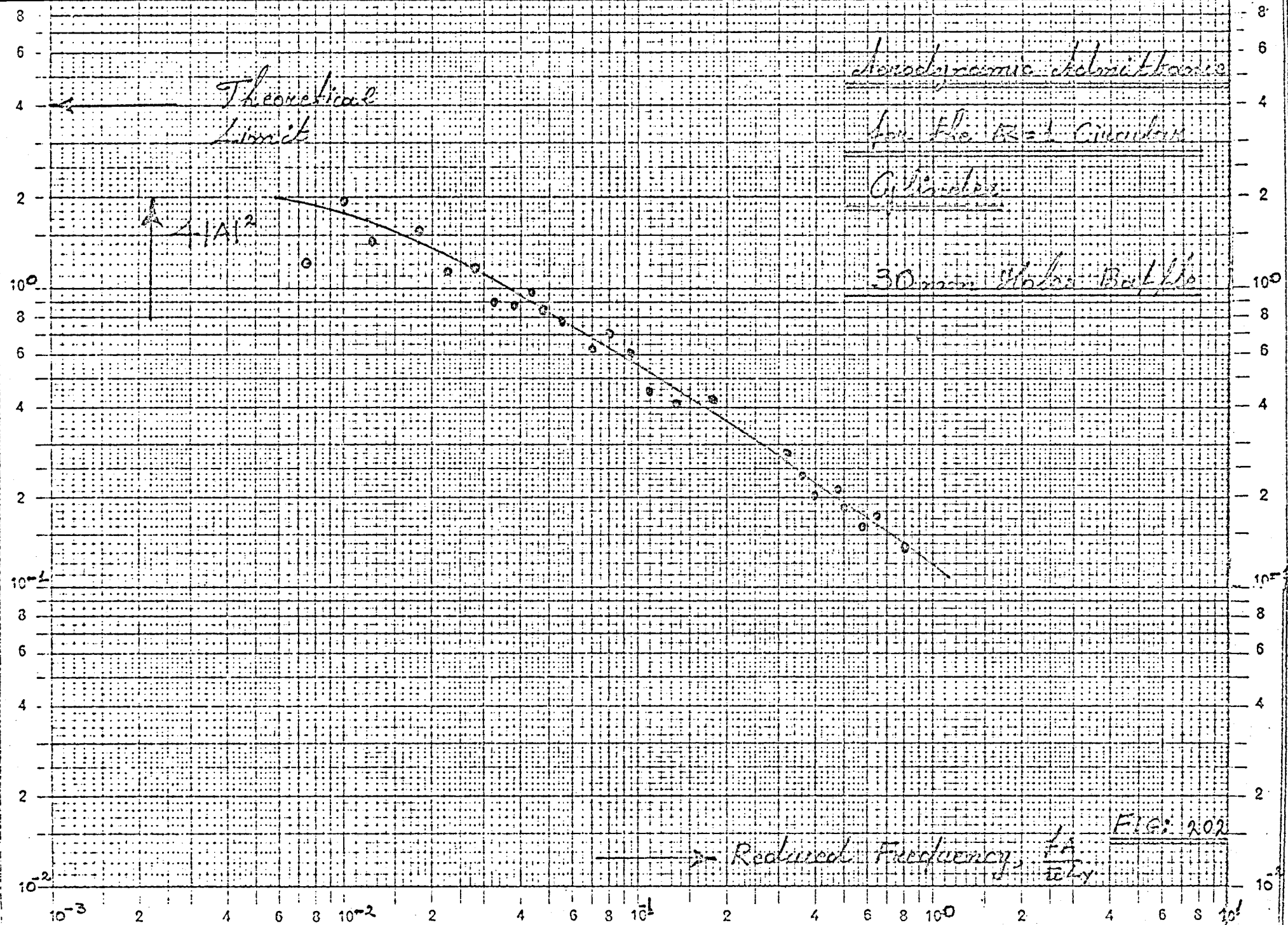


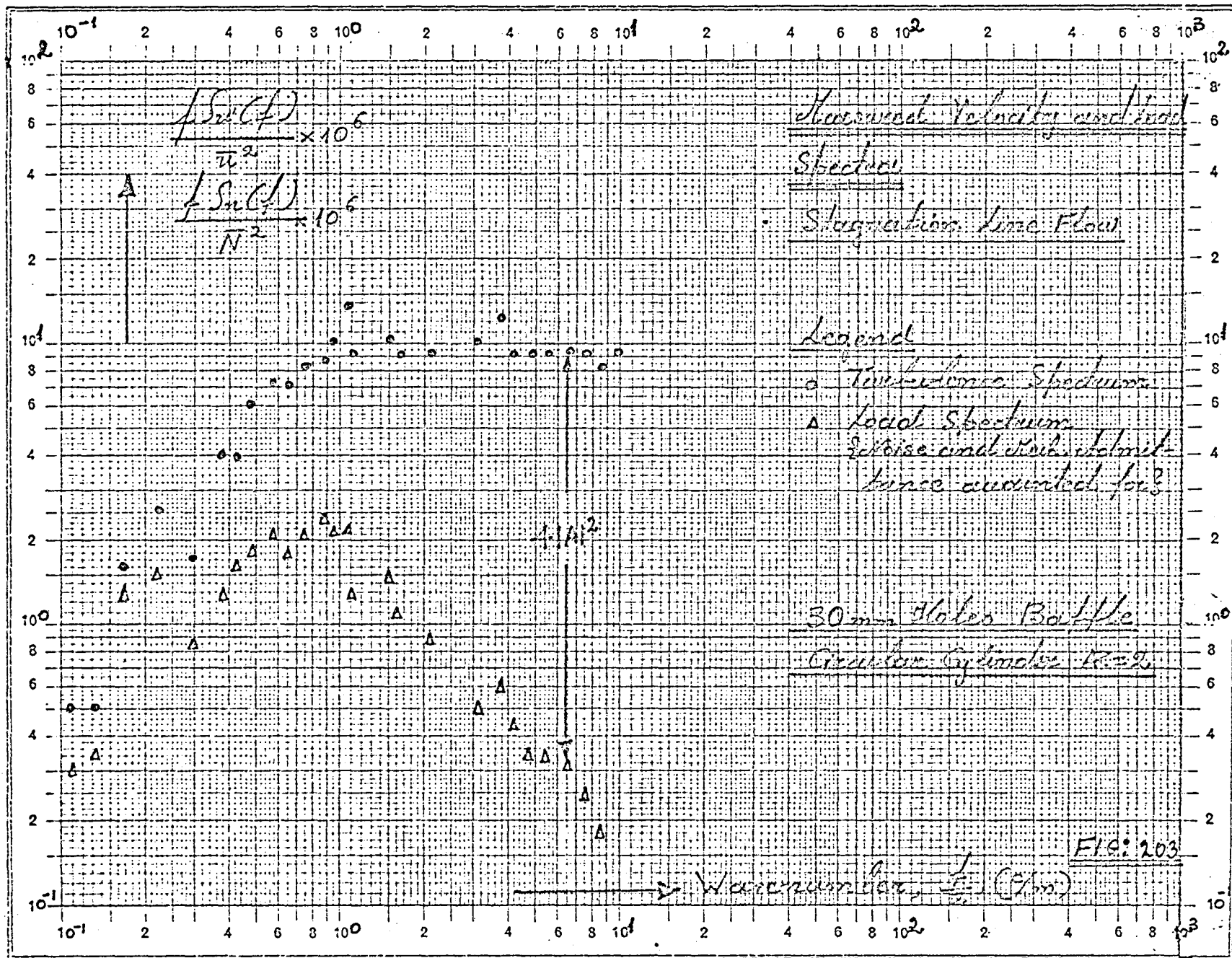




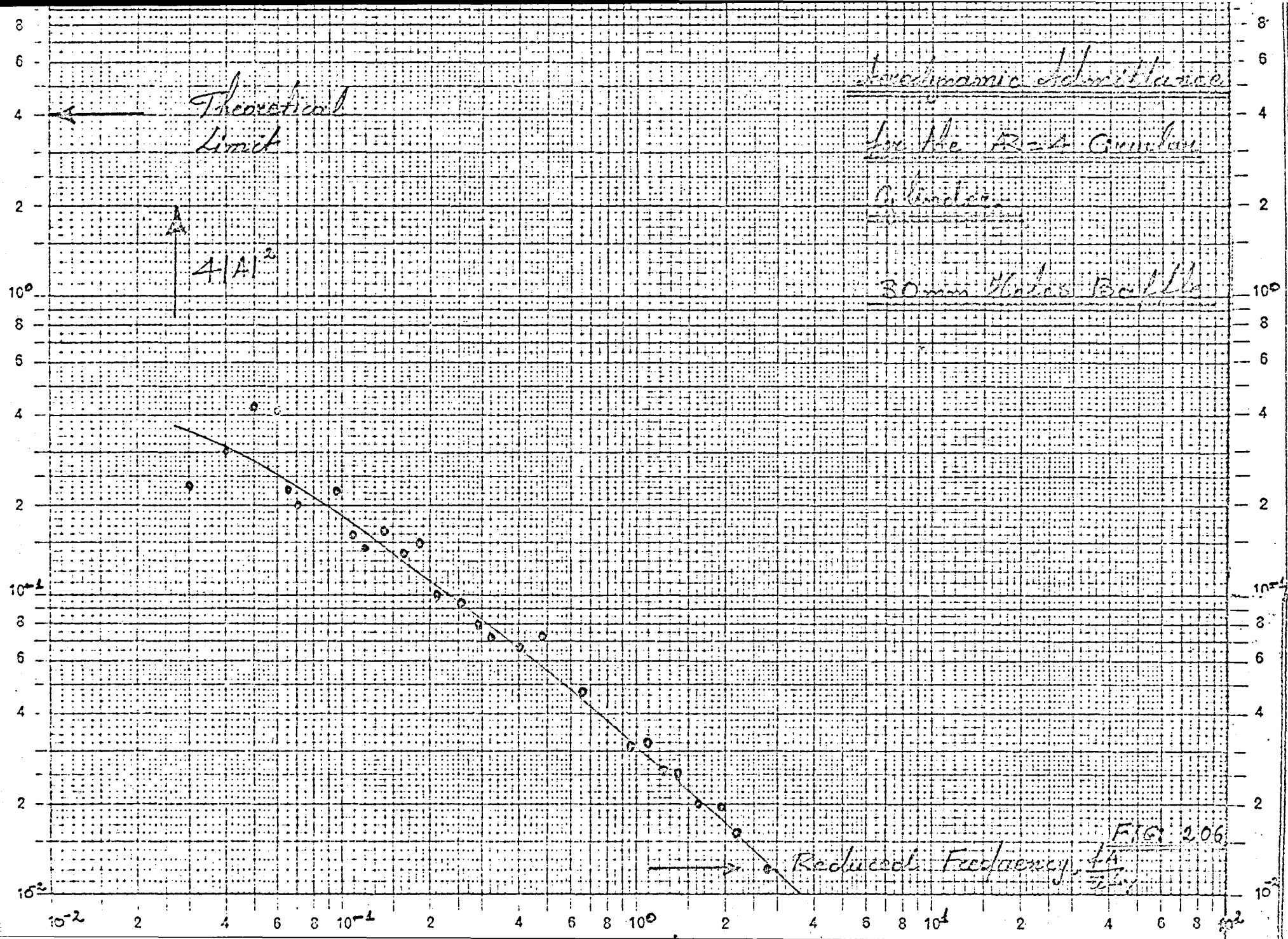
FIG. 2.00

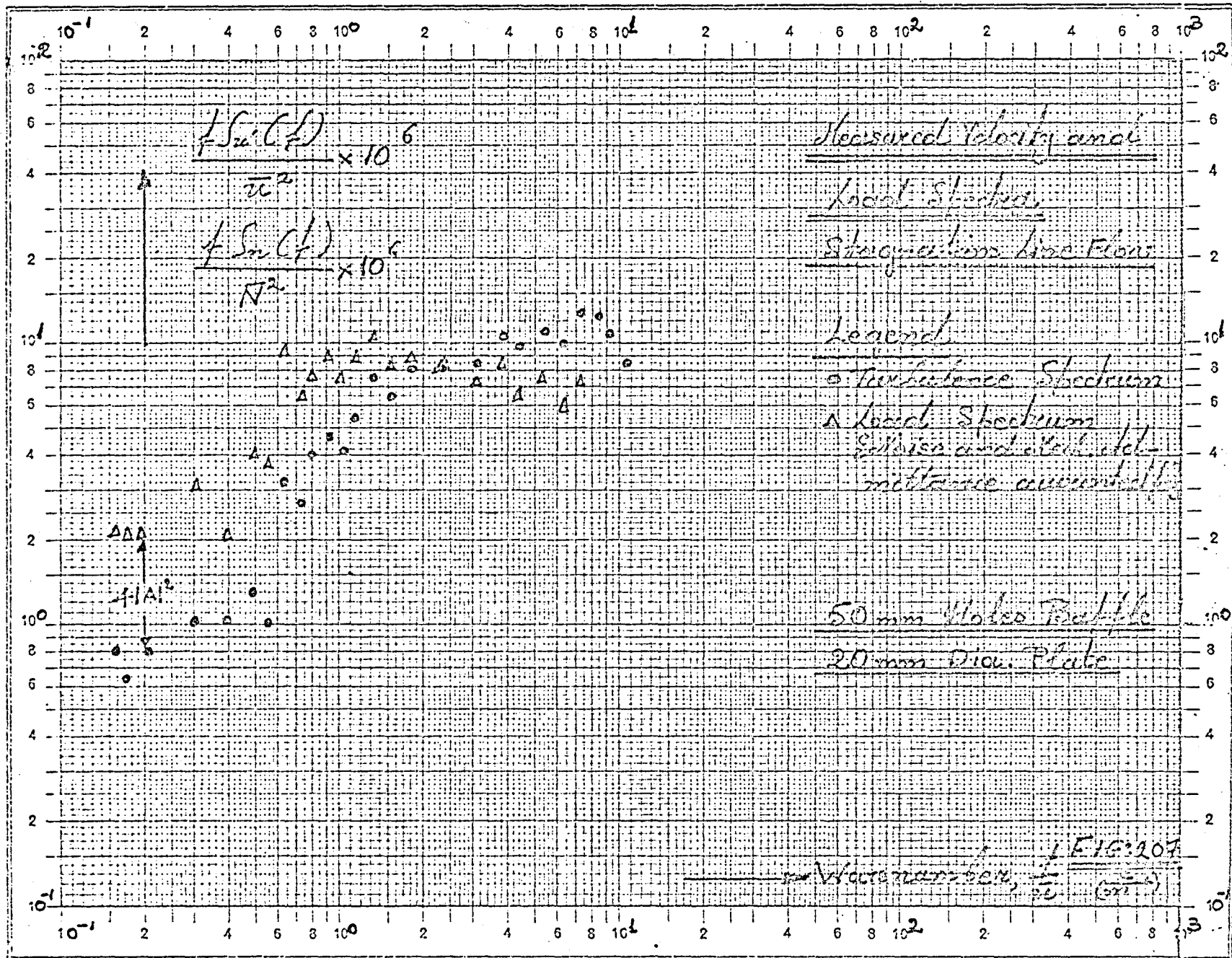


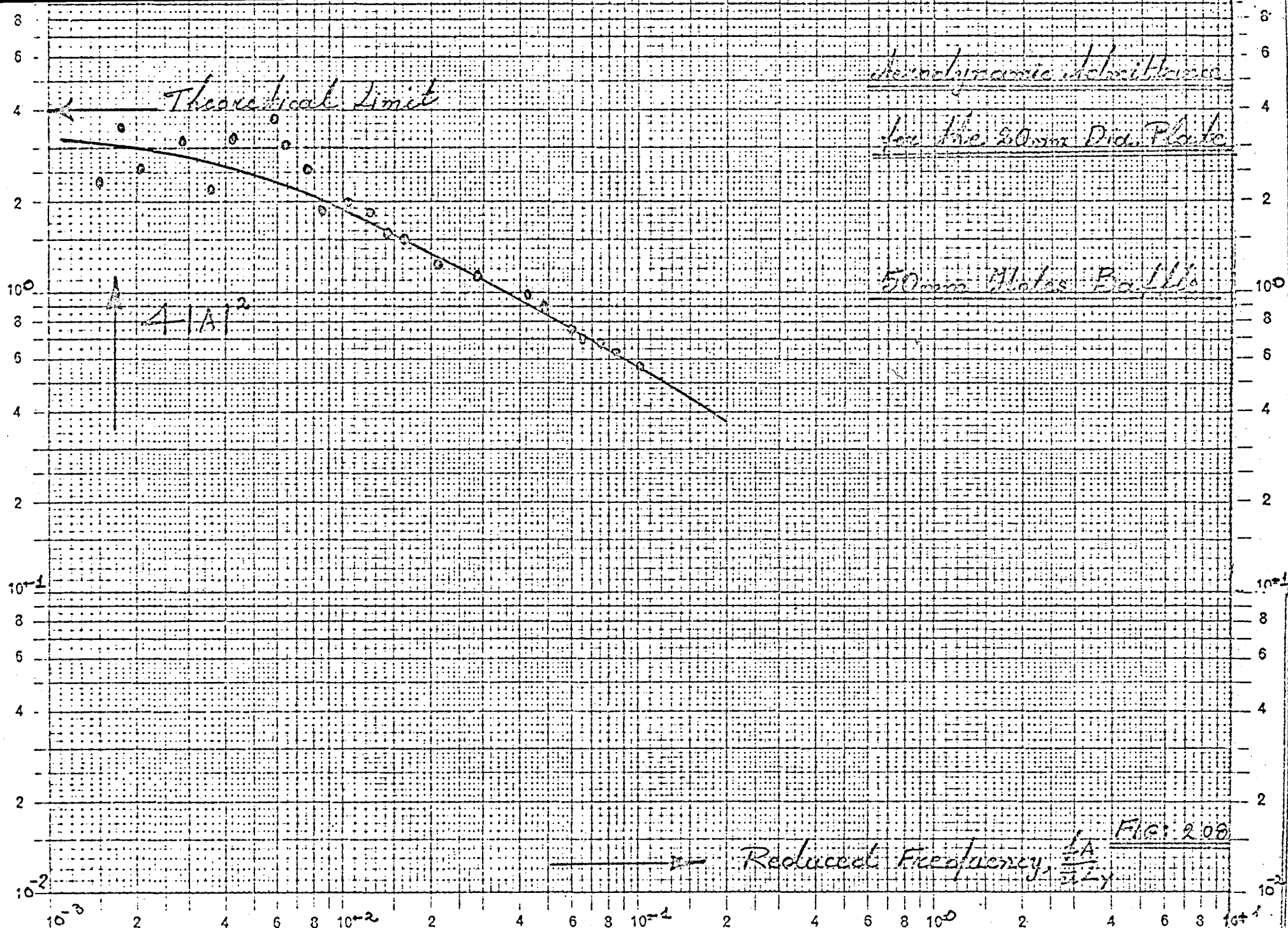


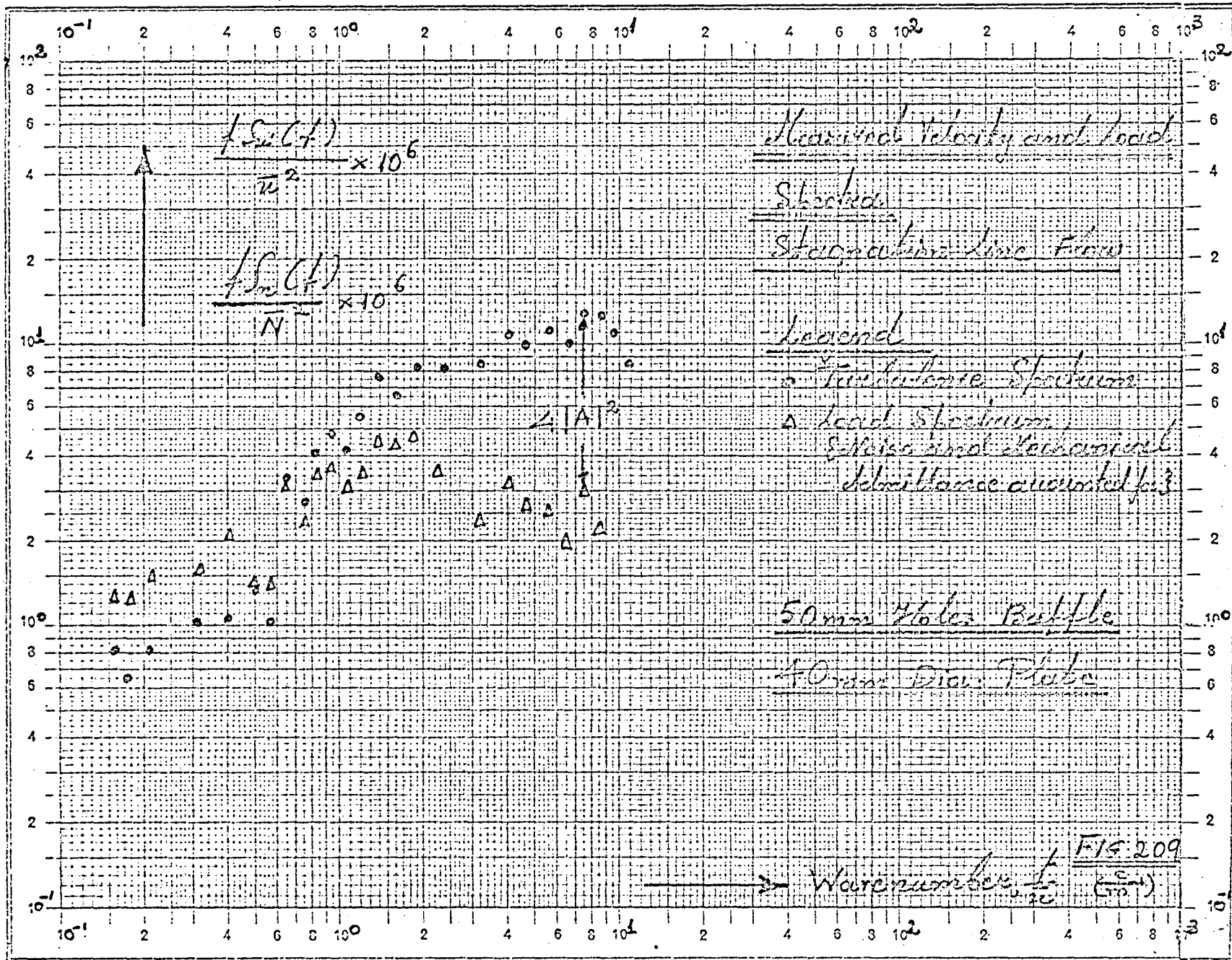


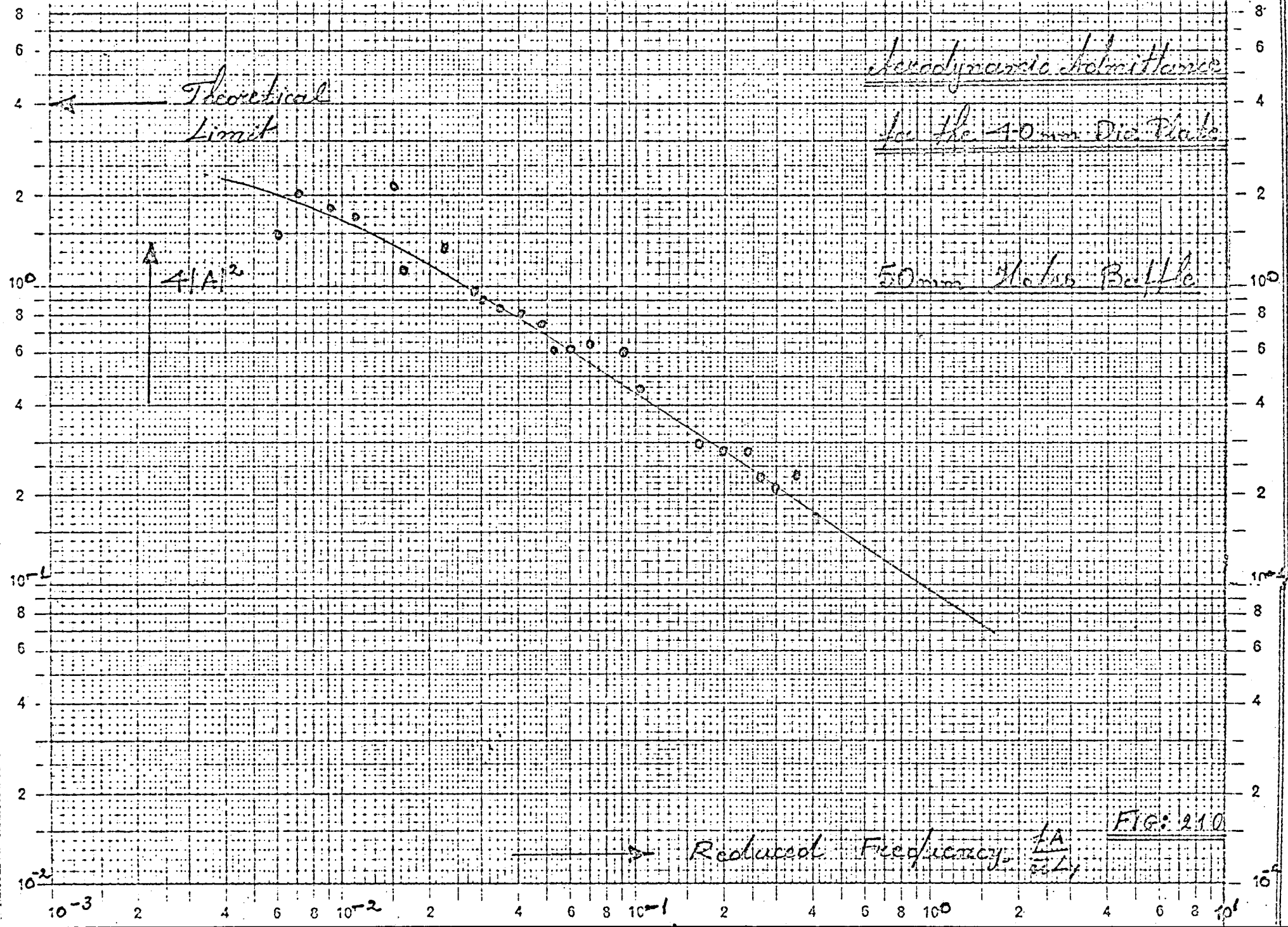


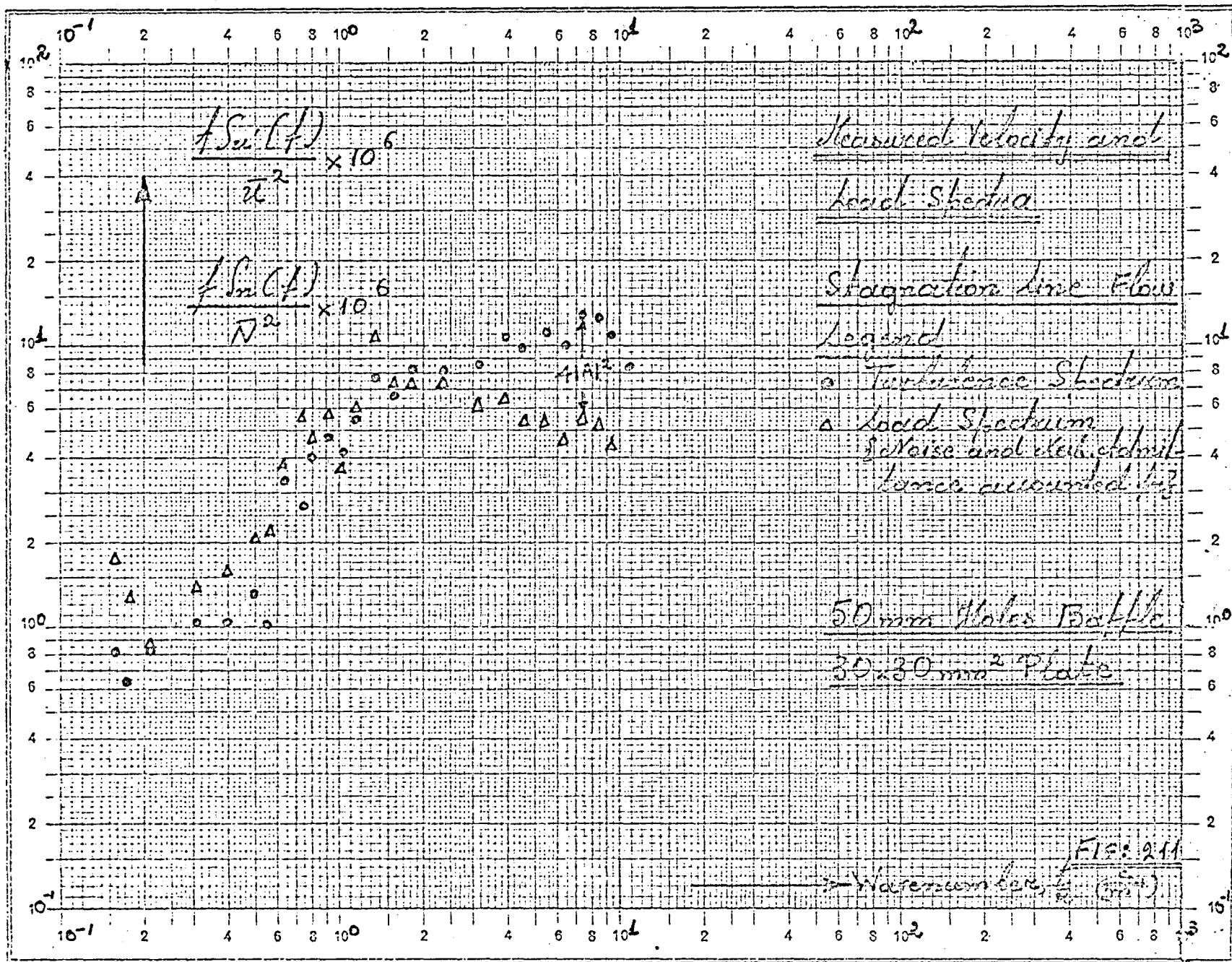


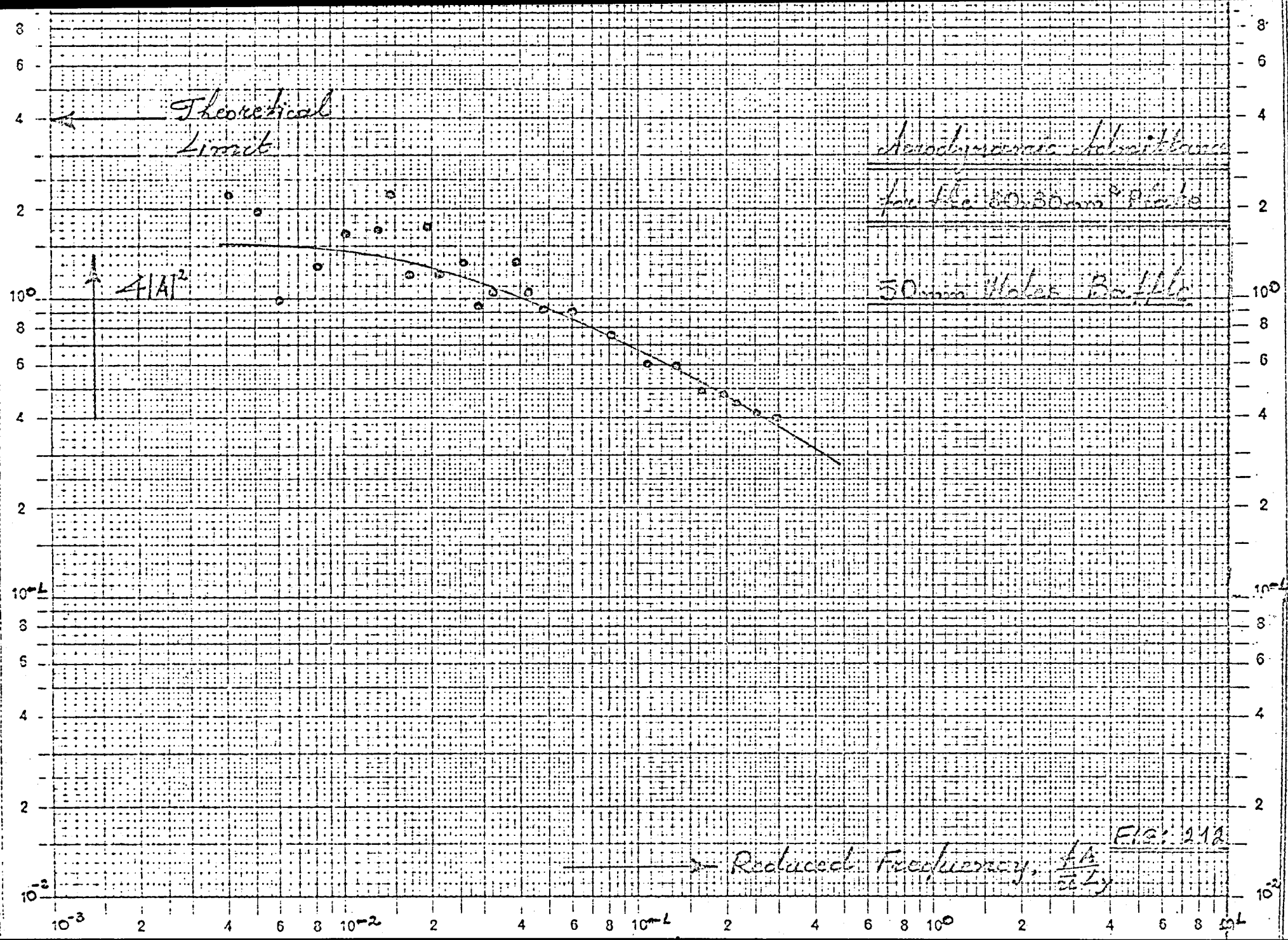


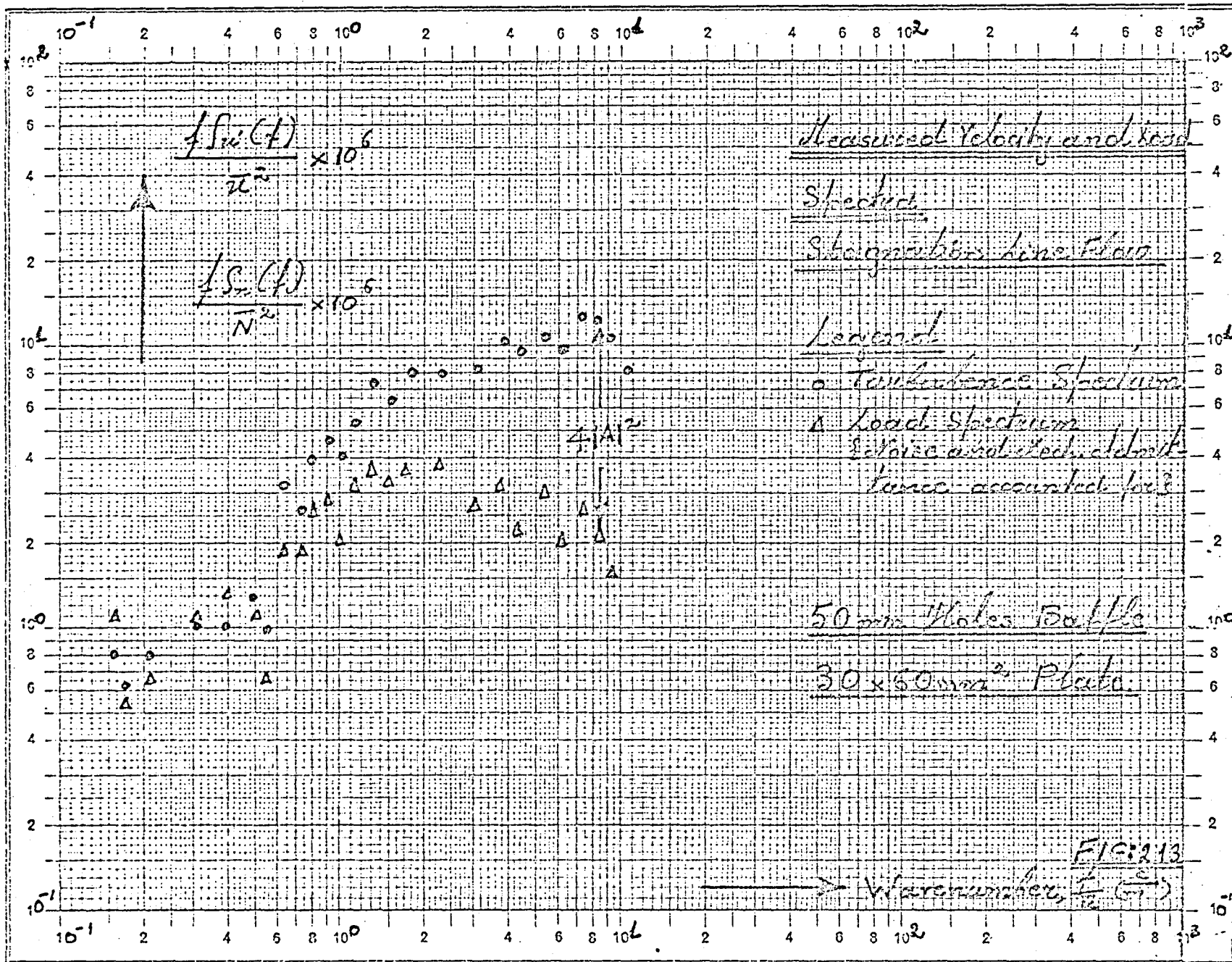


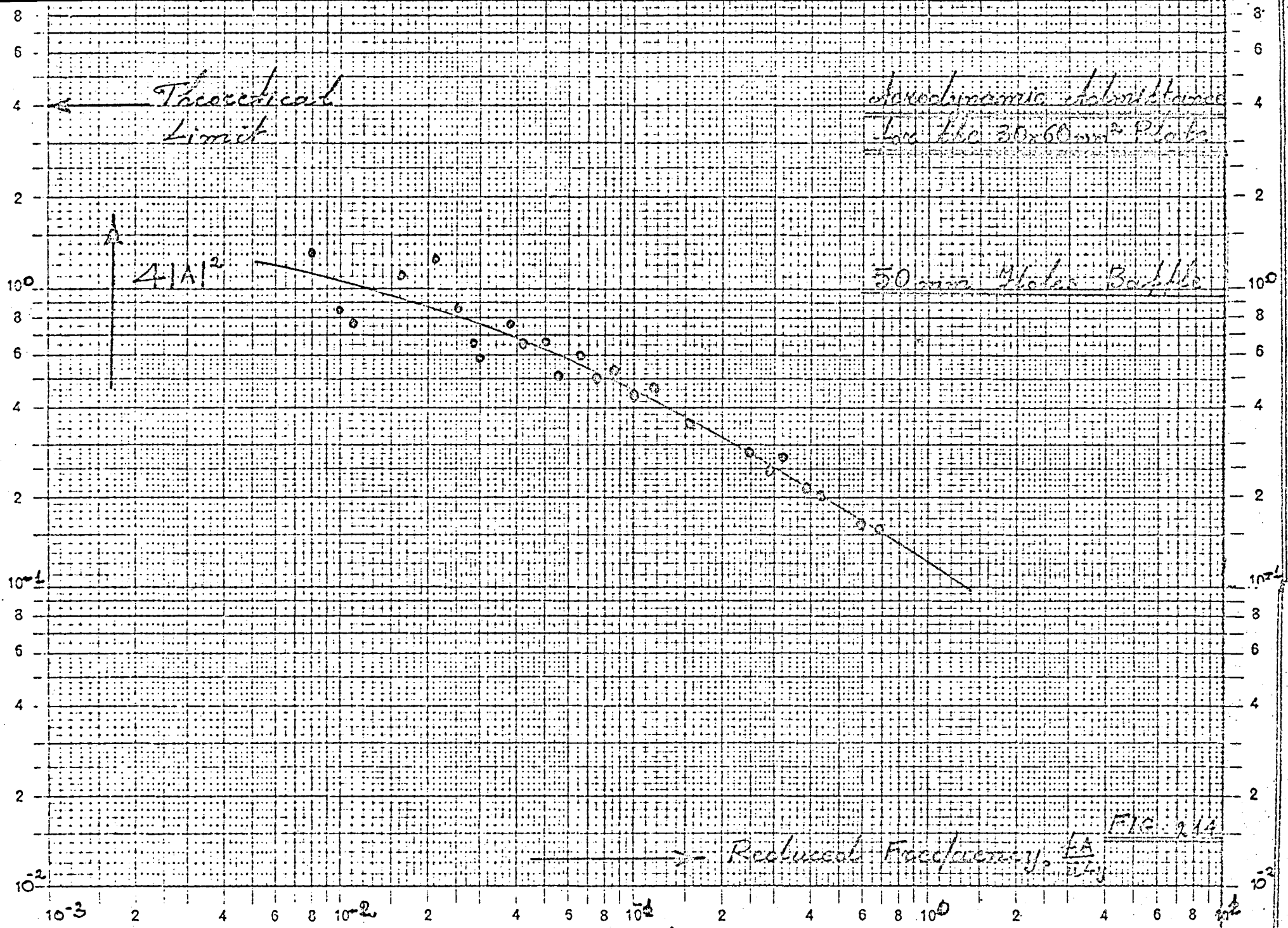


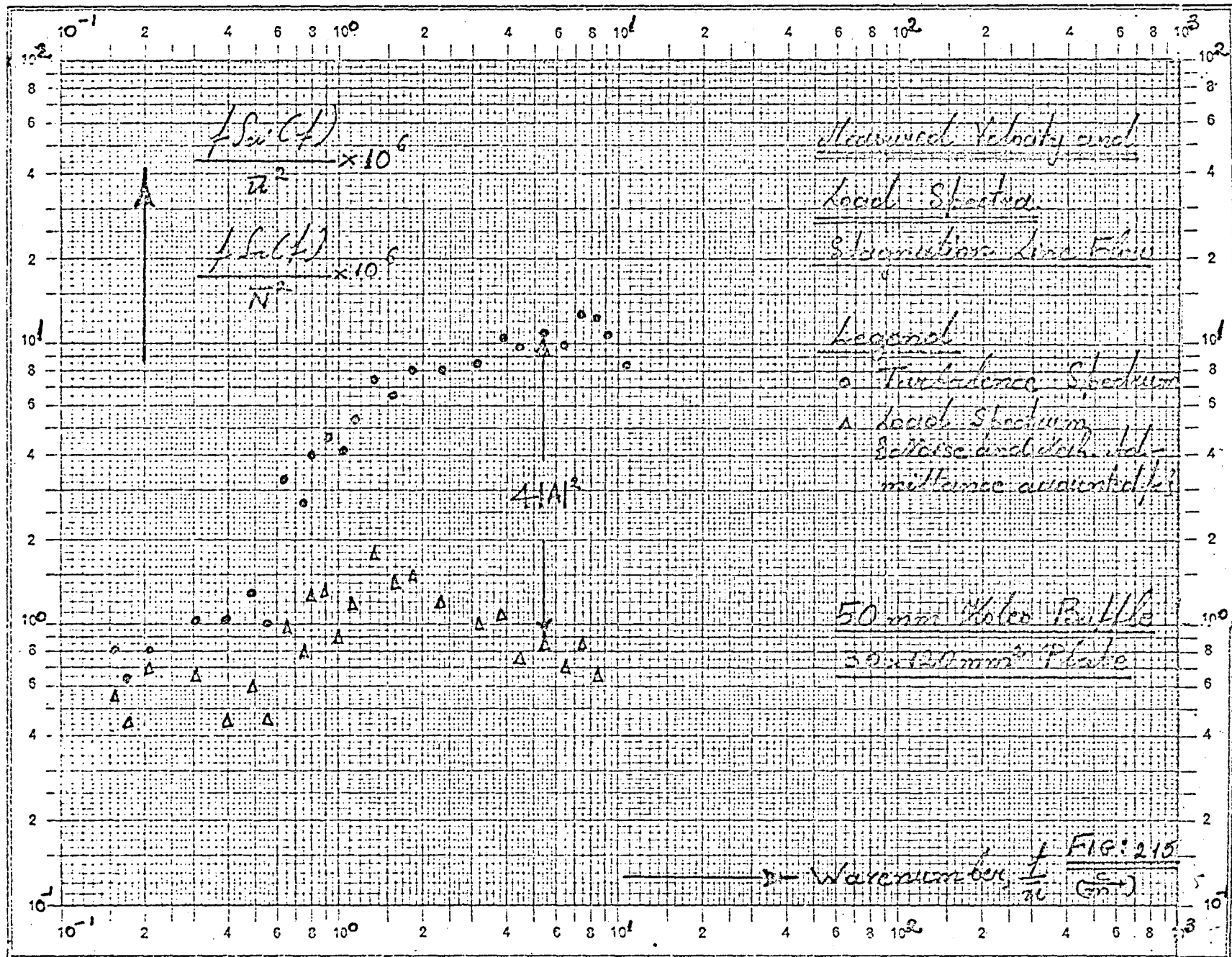


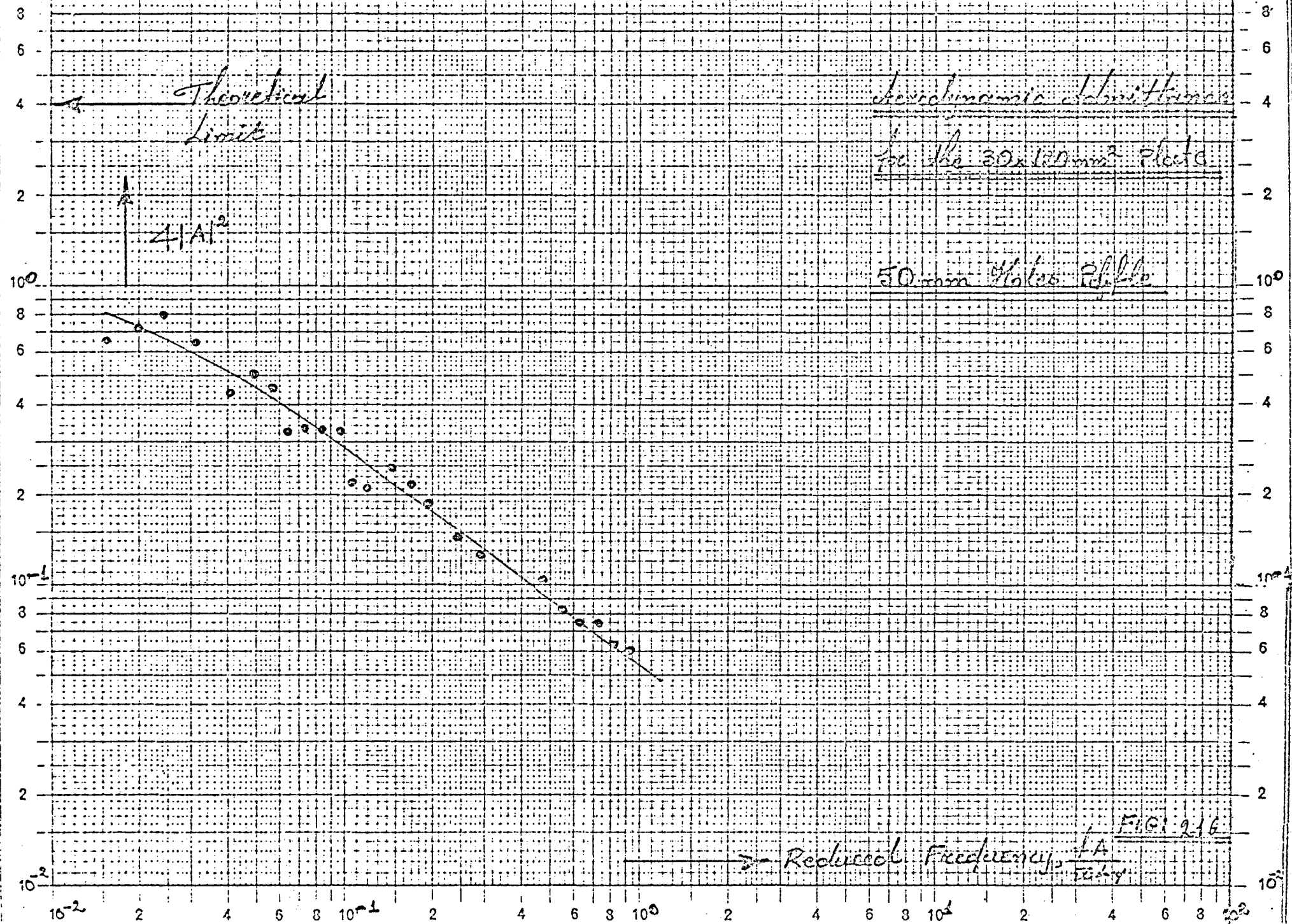


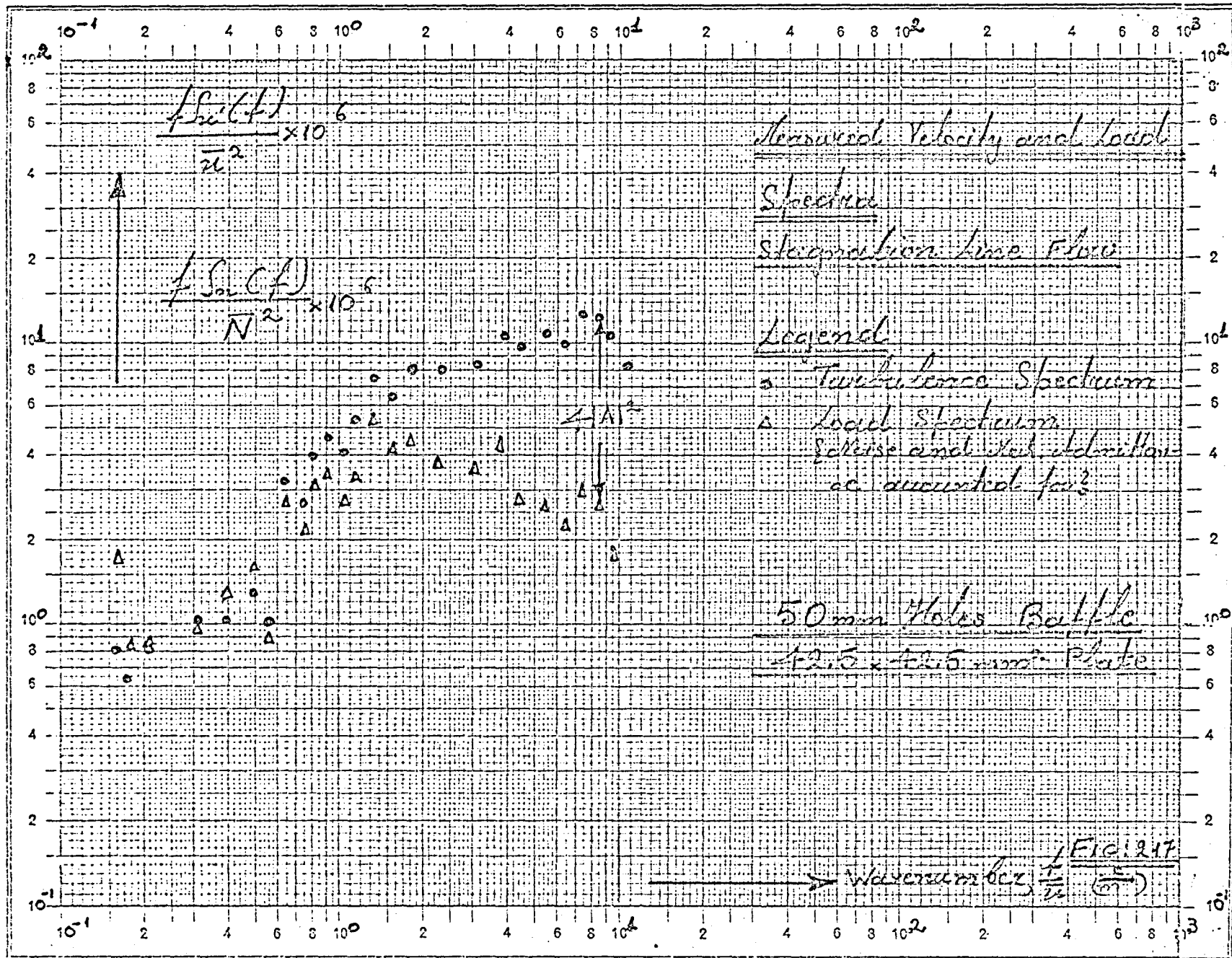


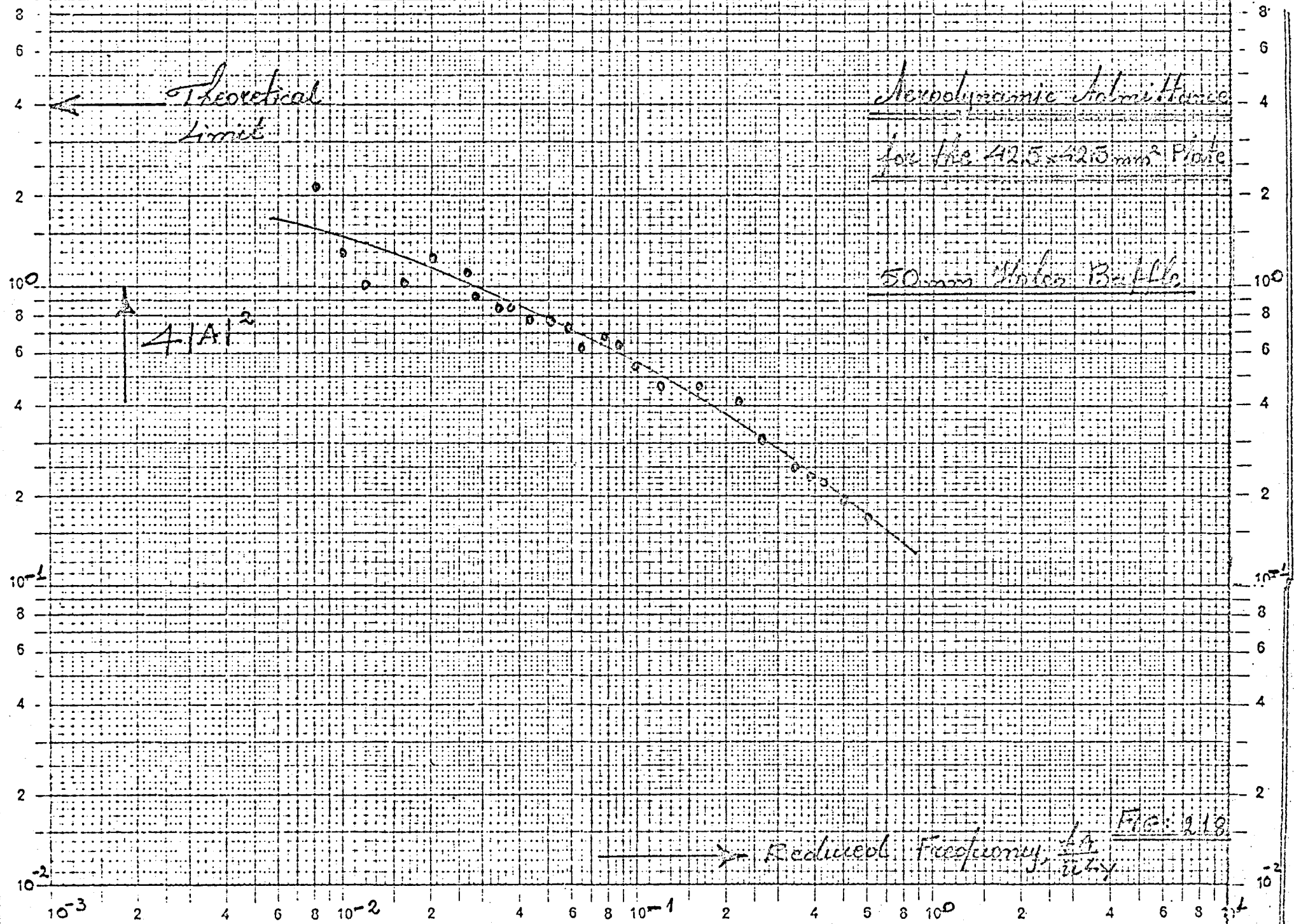


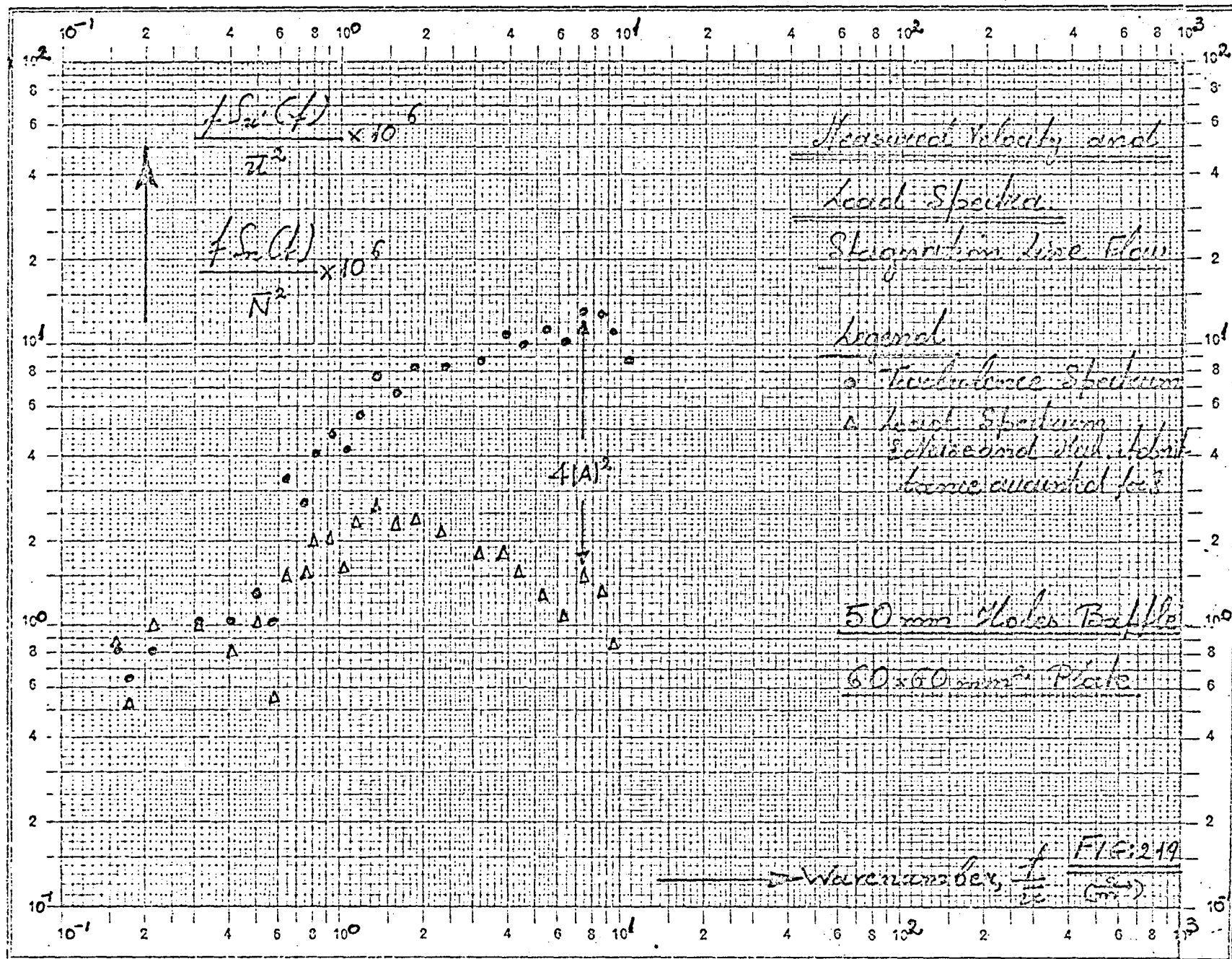


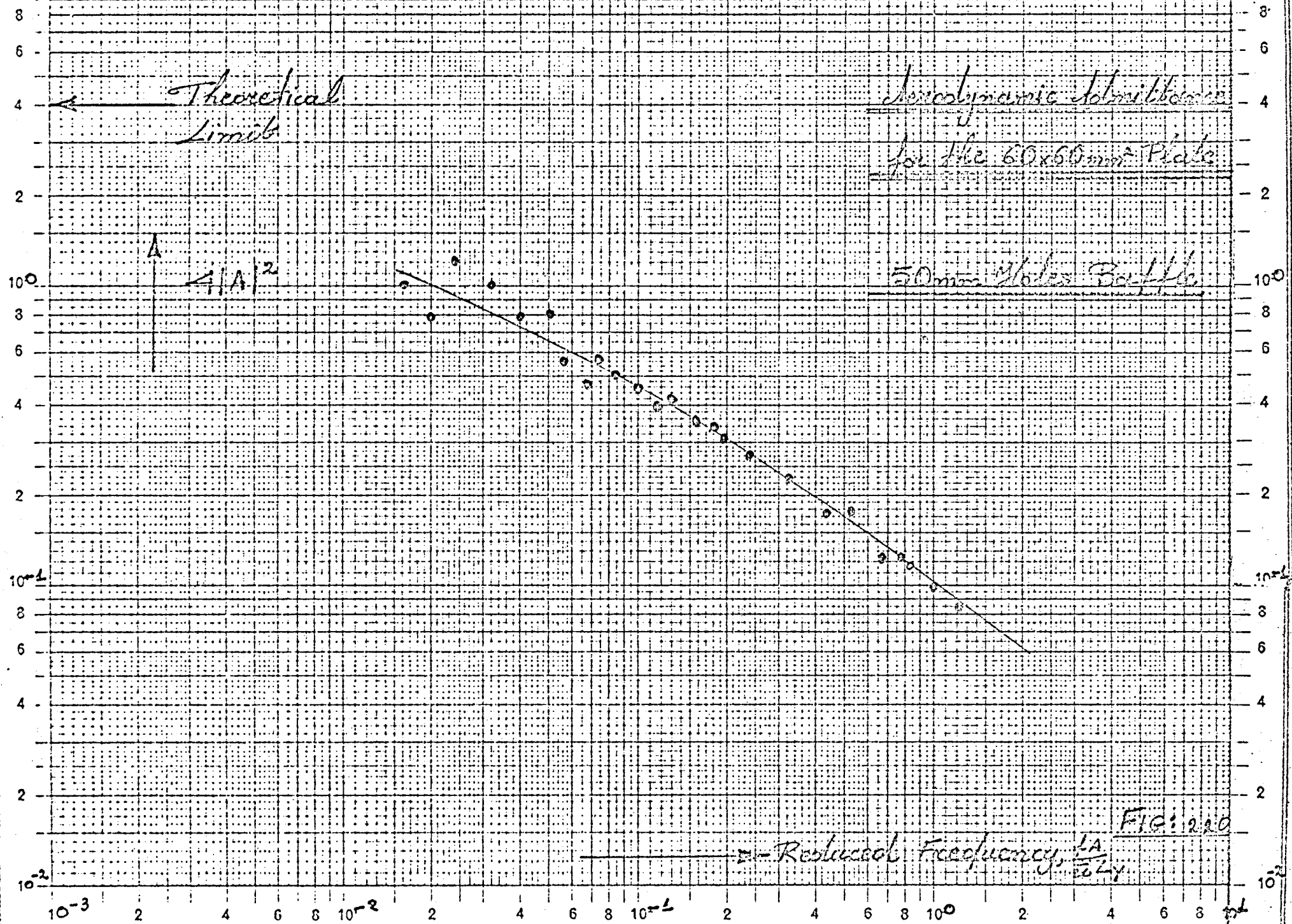


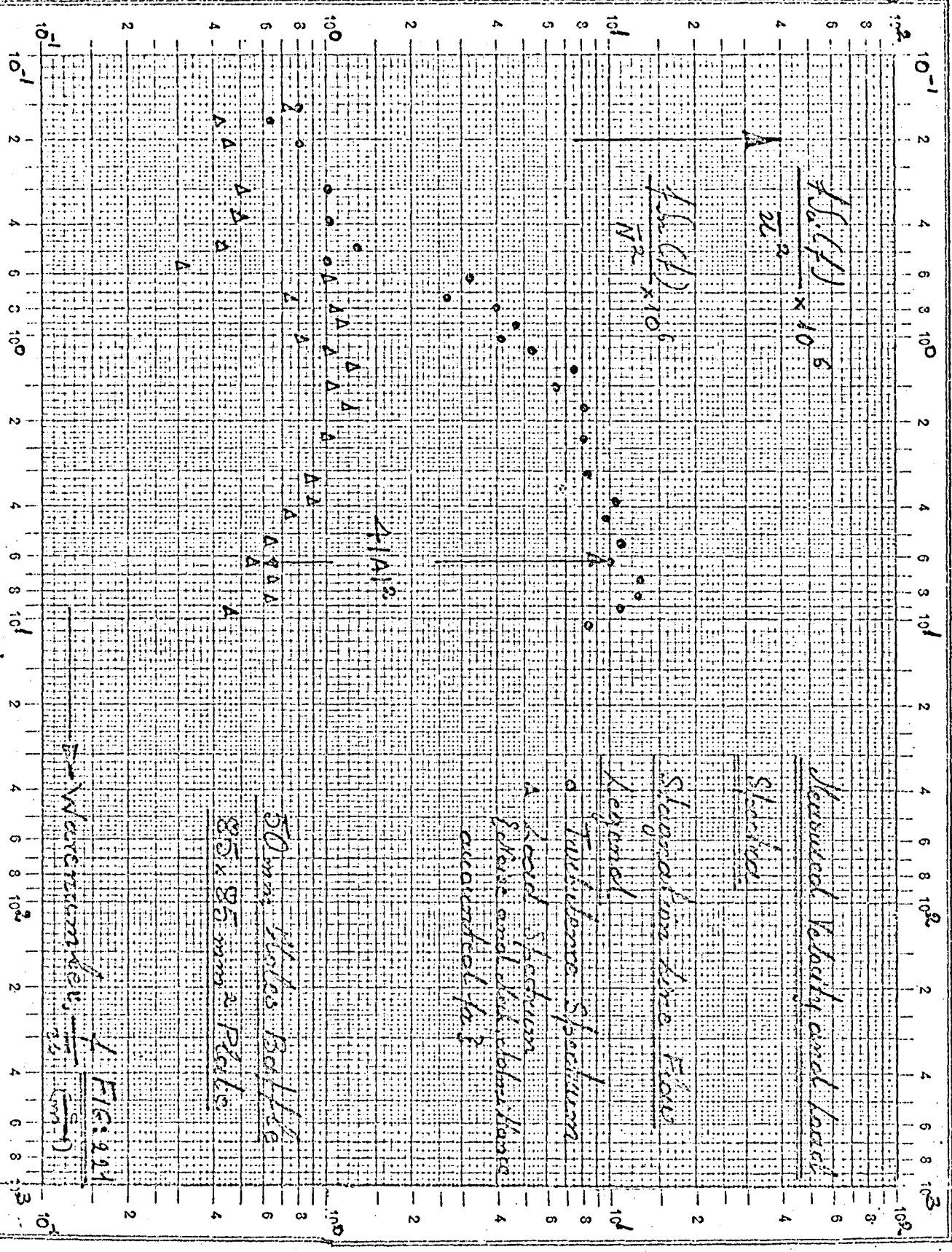




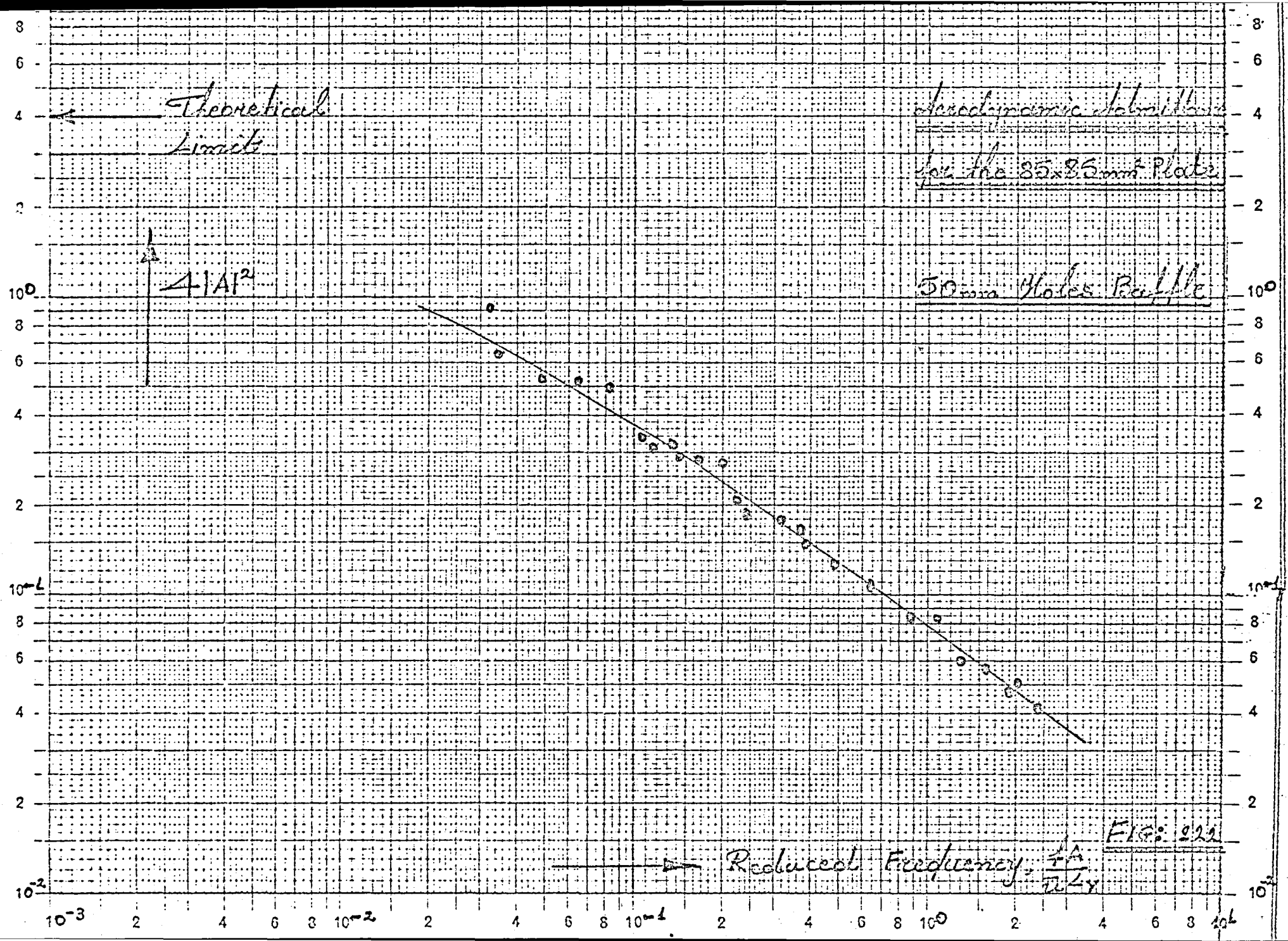


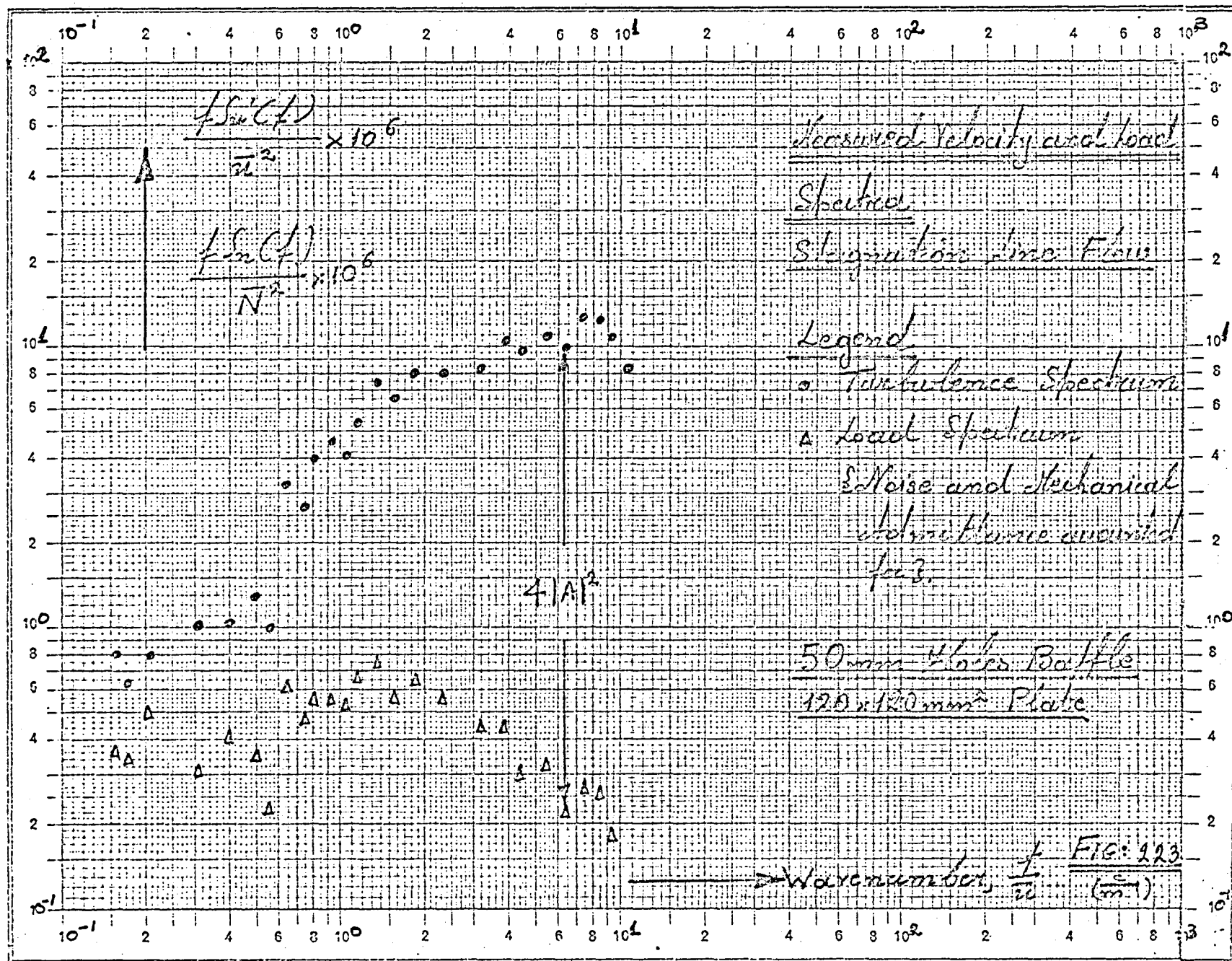


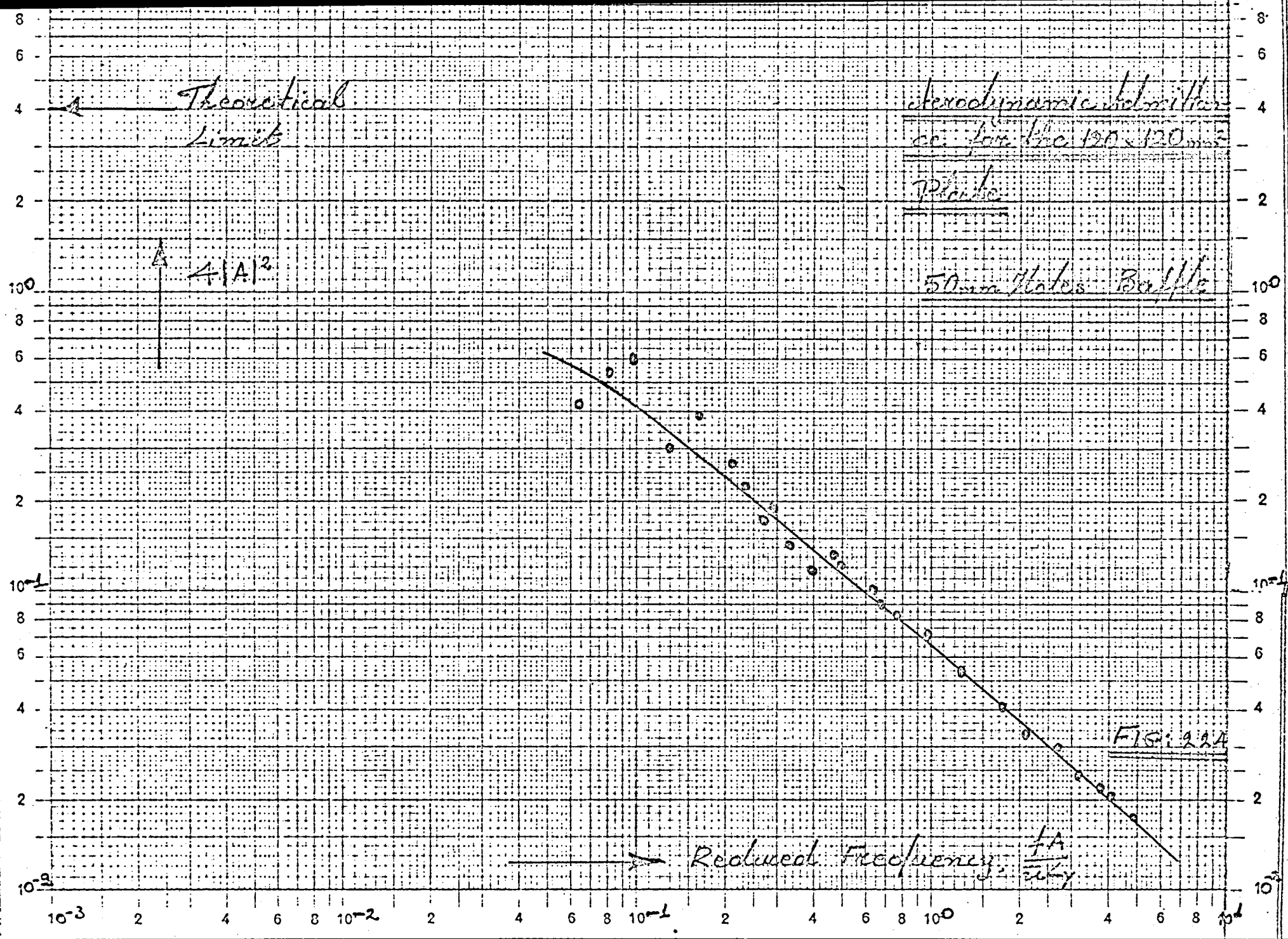


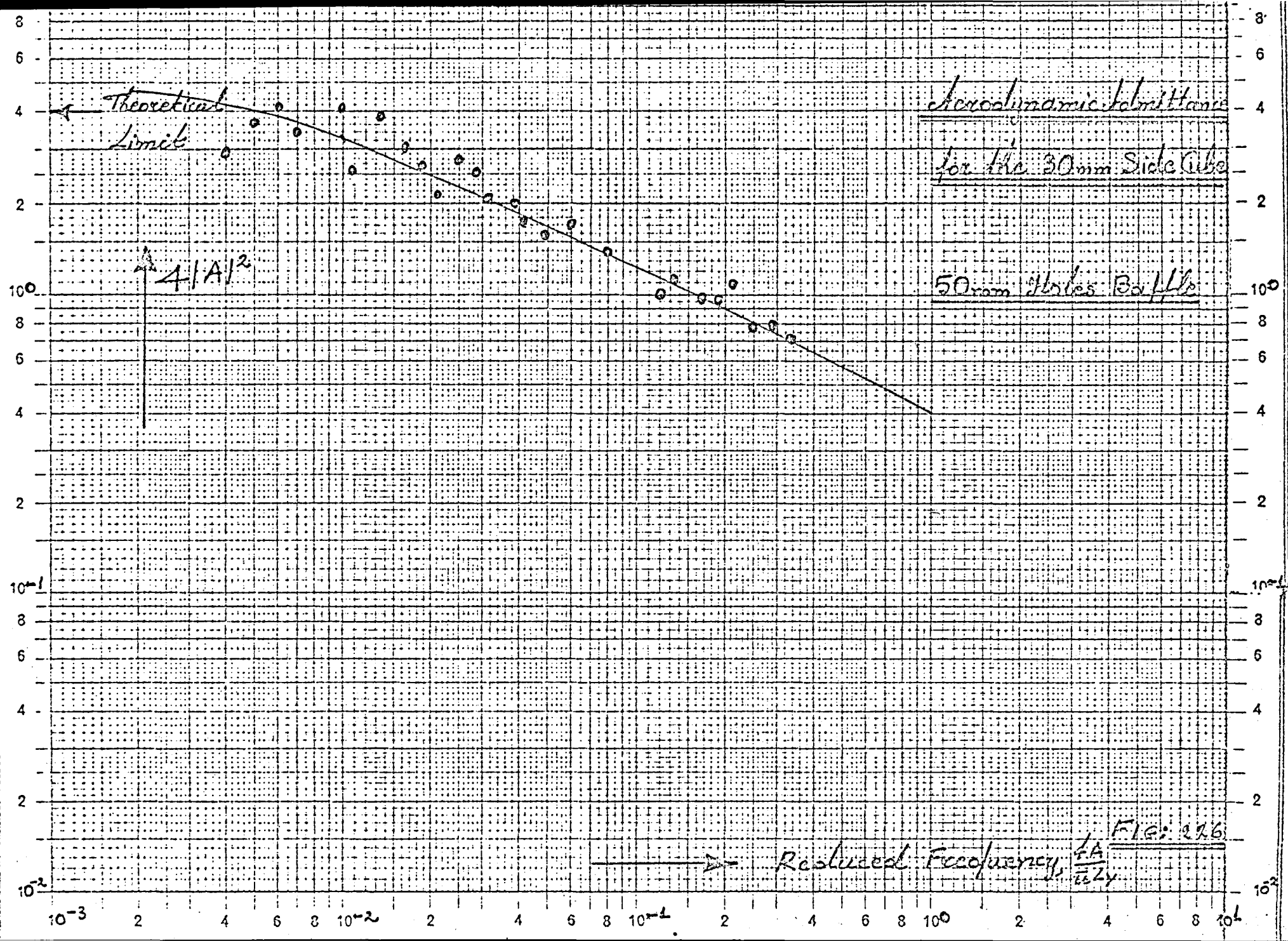


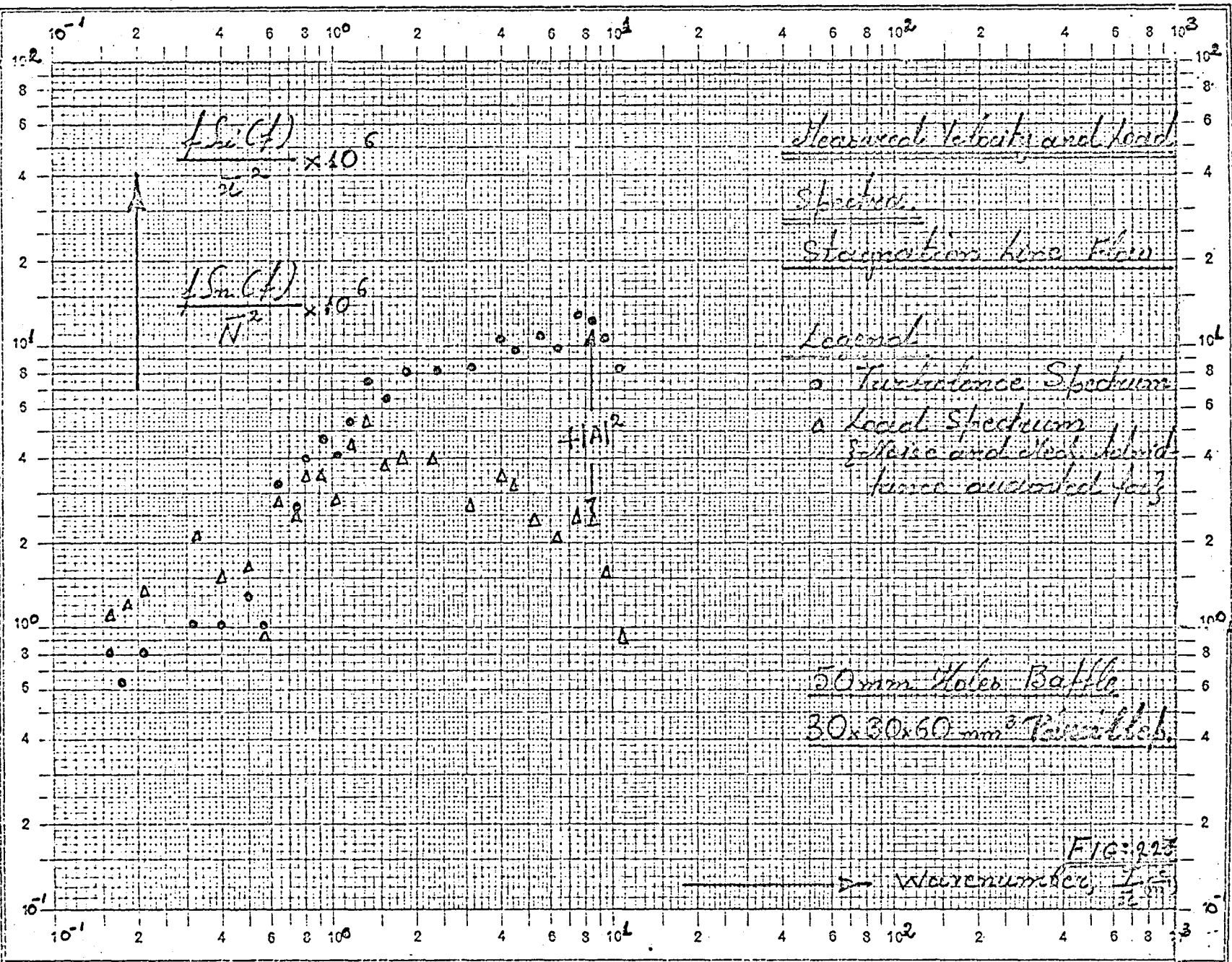
Teilung } 1-10000 u. 1-100000 Einheit } 50 mm
 Log.-r. Division

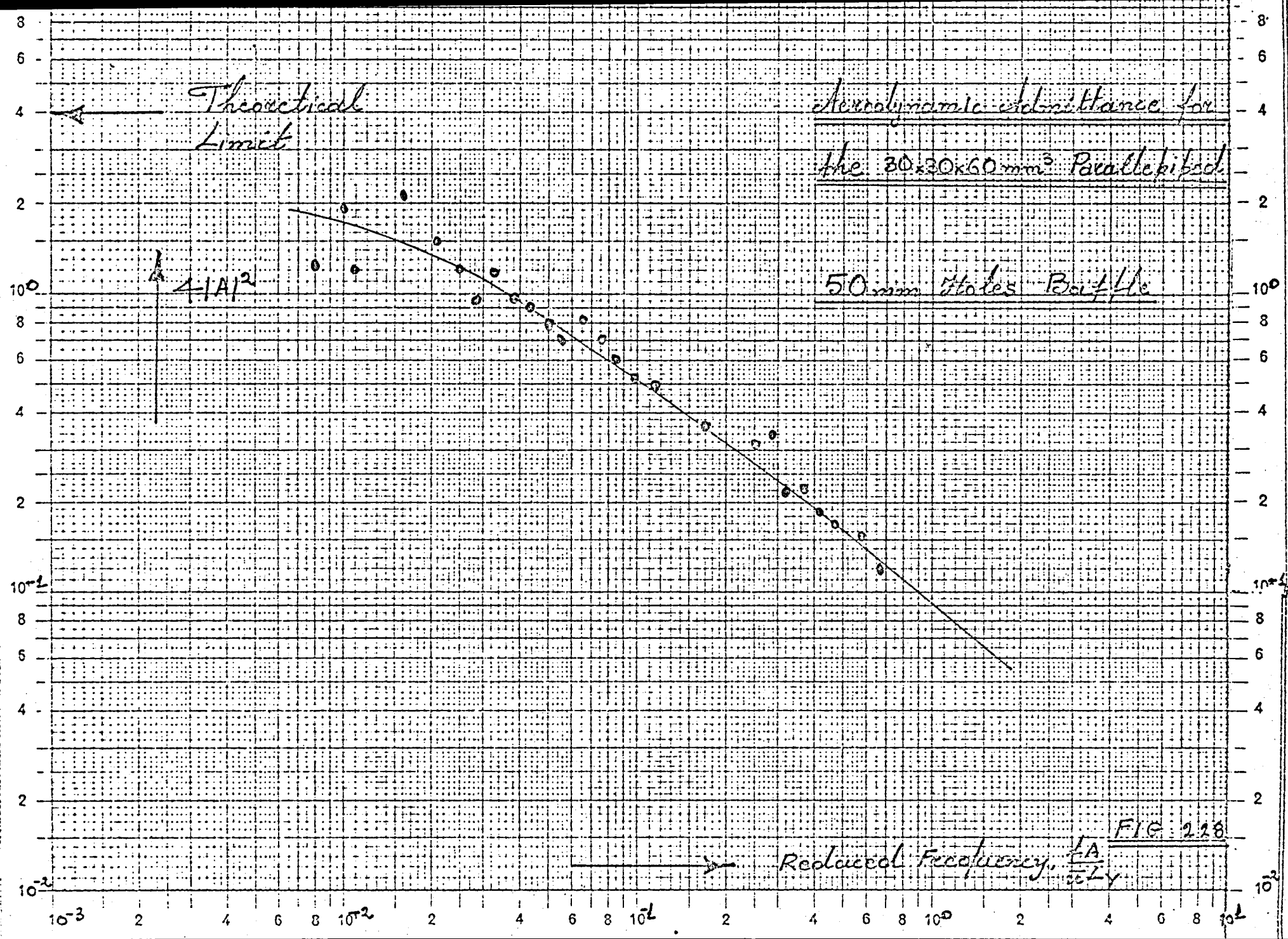


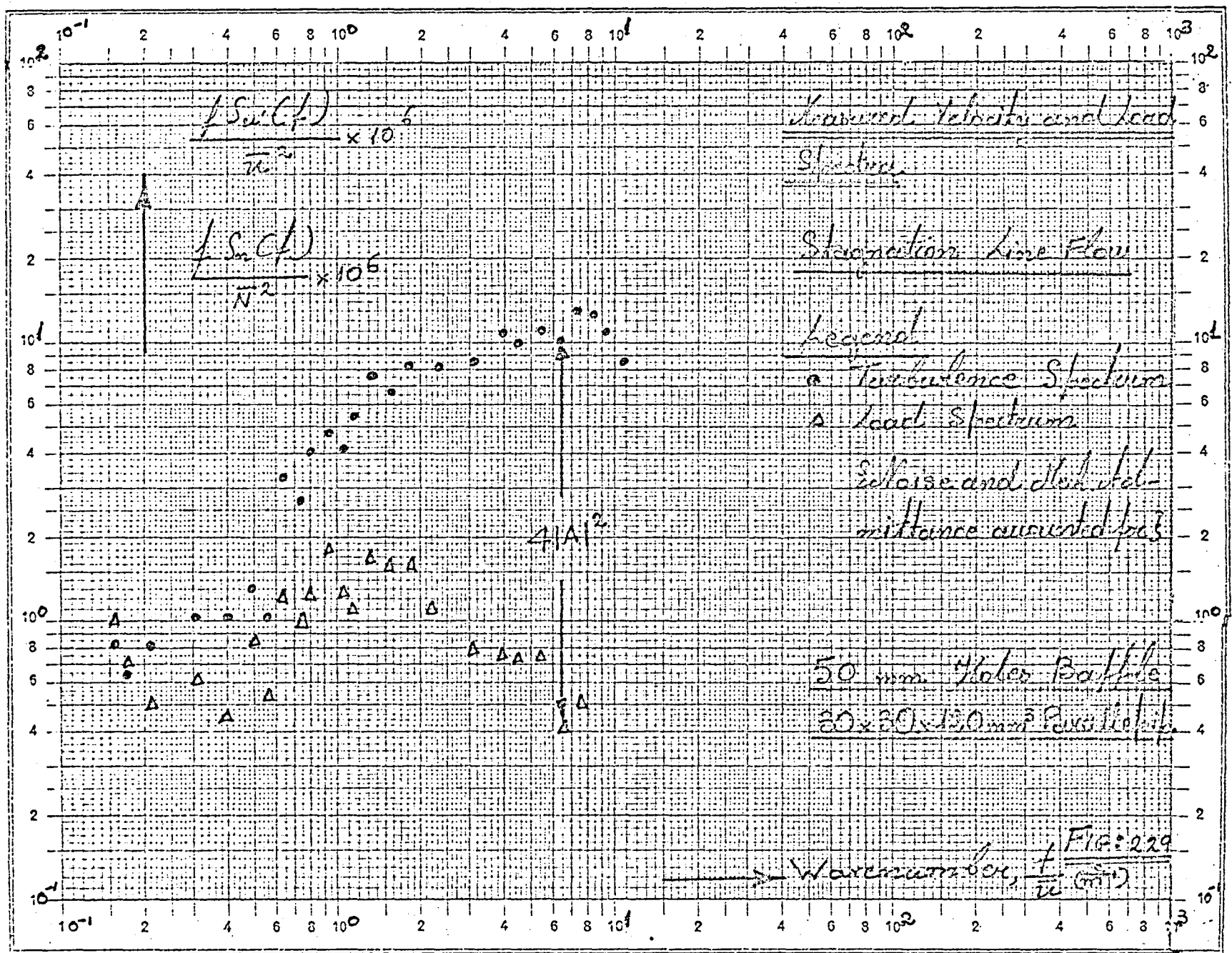


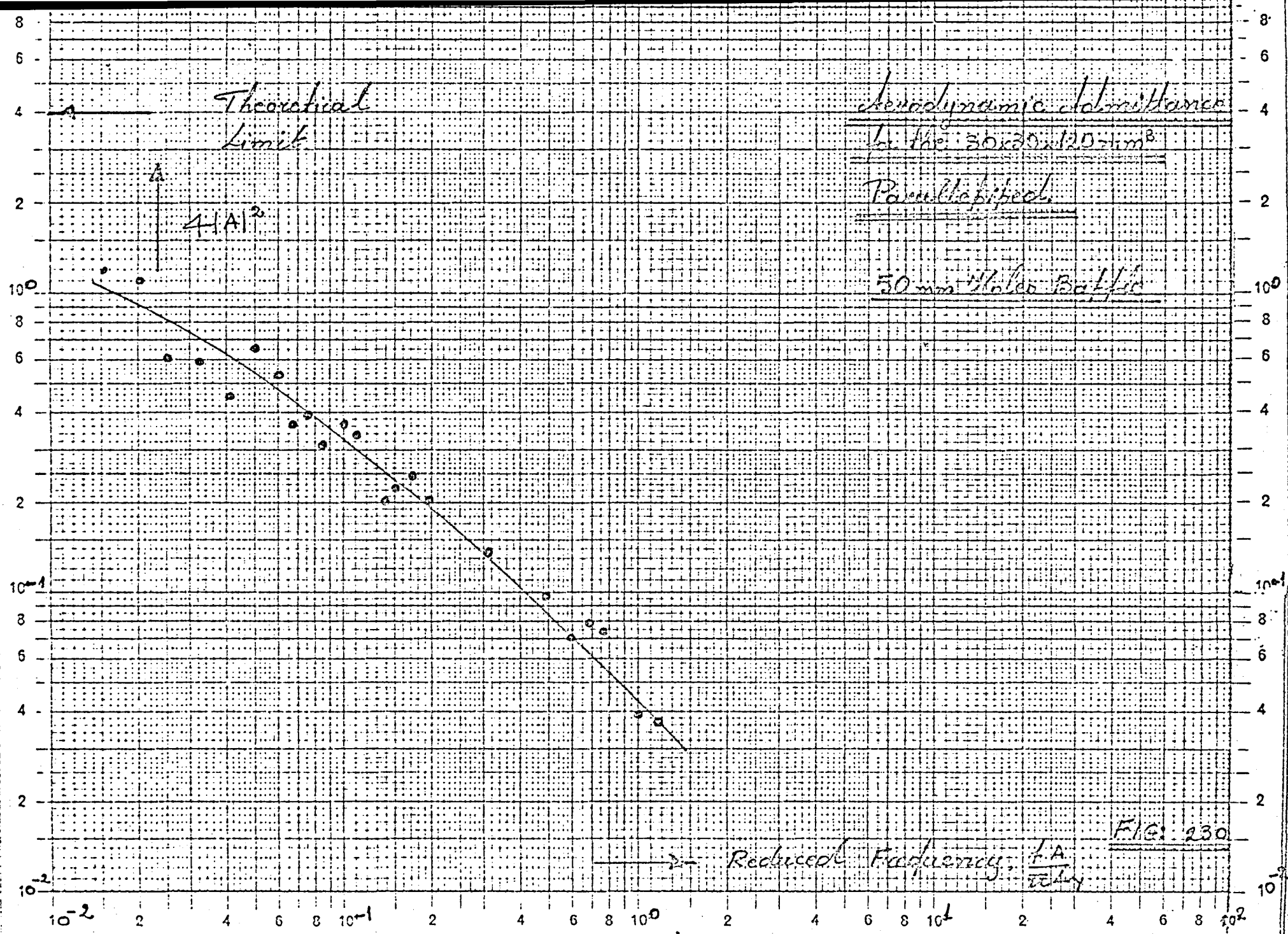


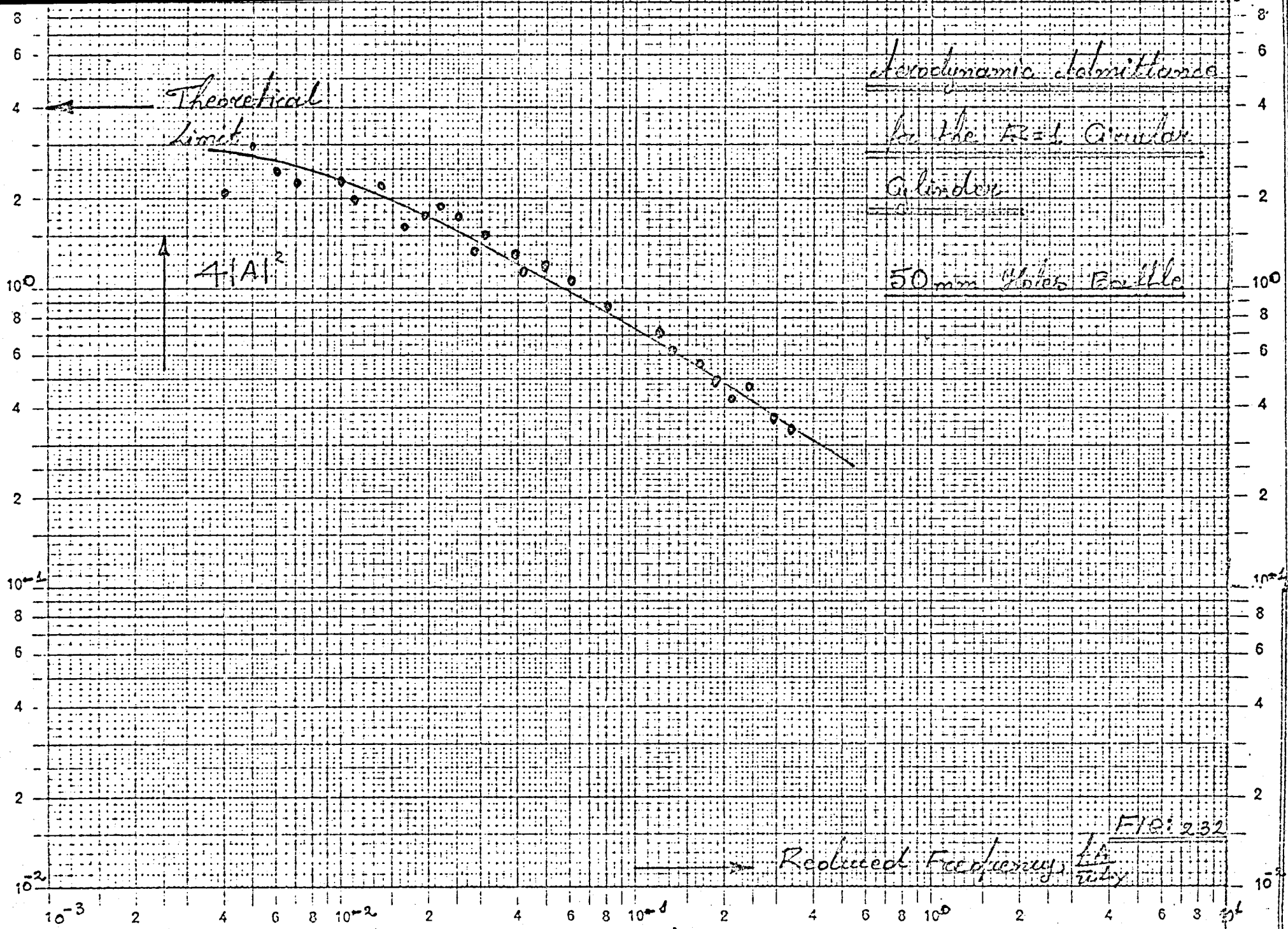


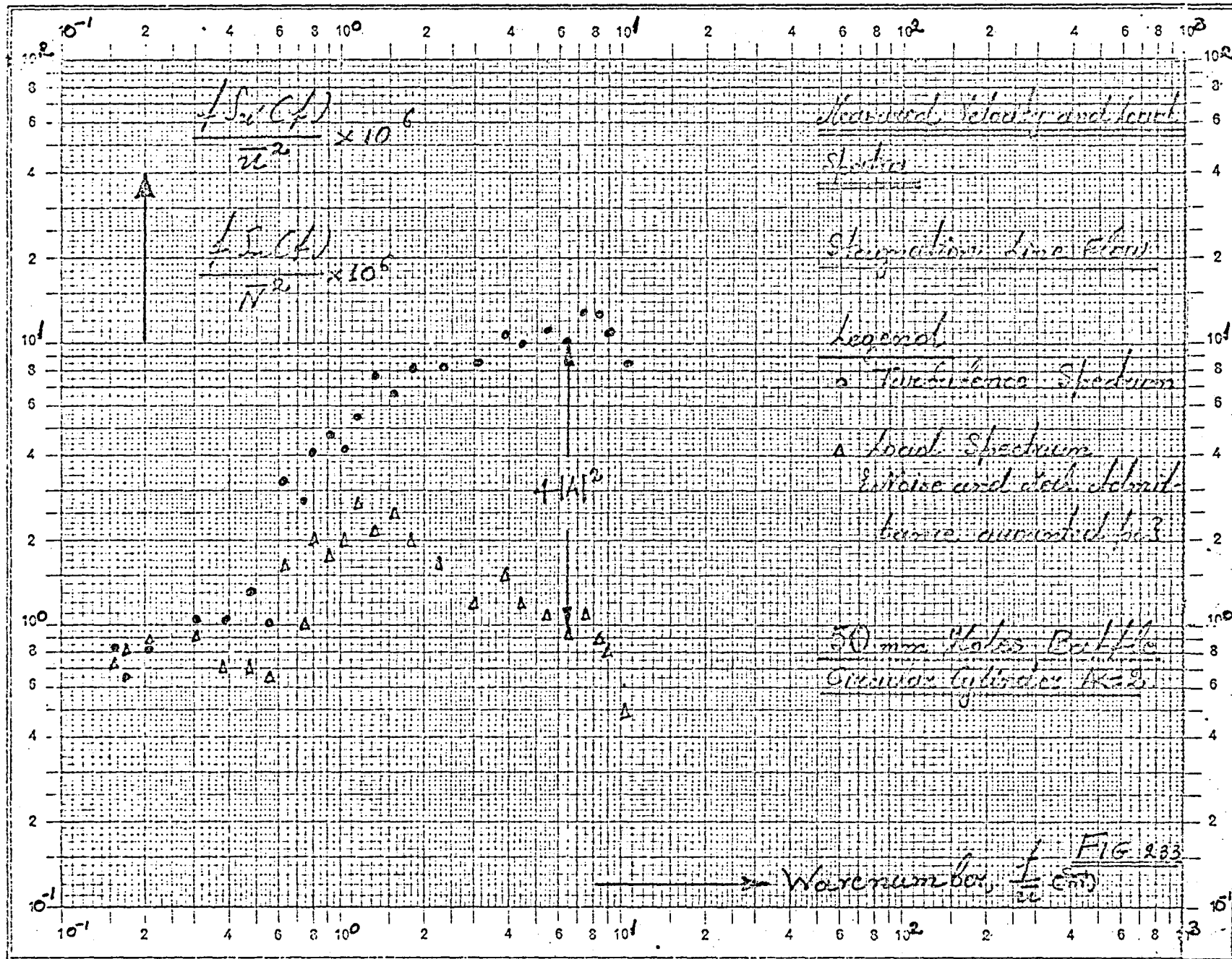




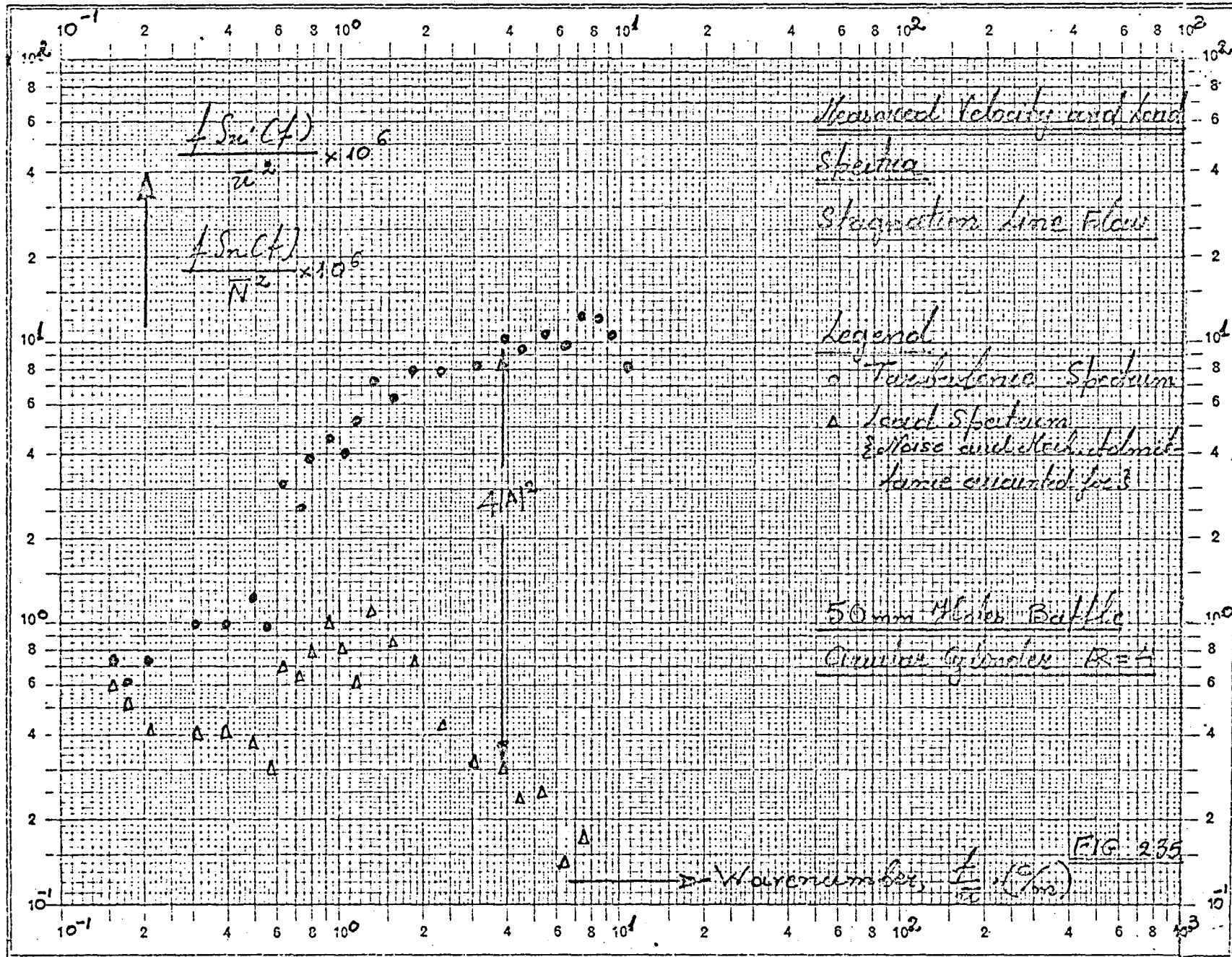




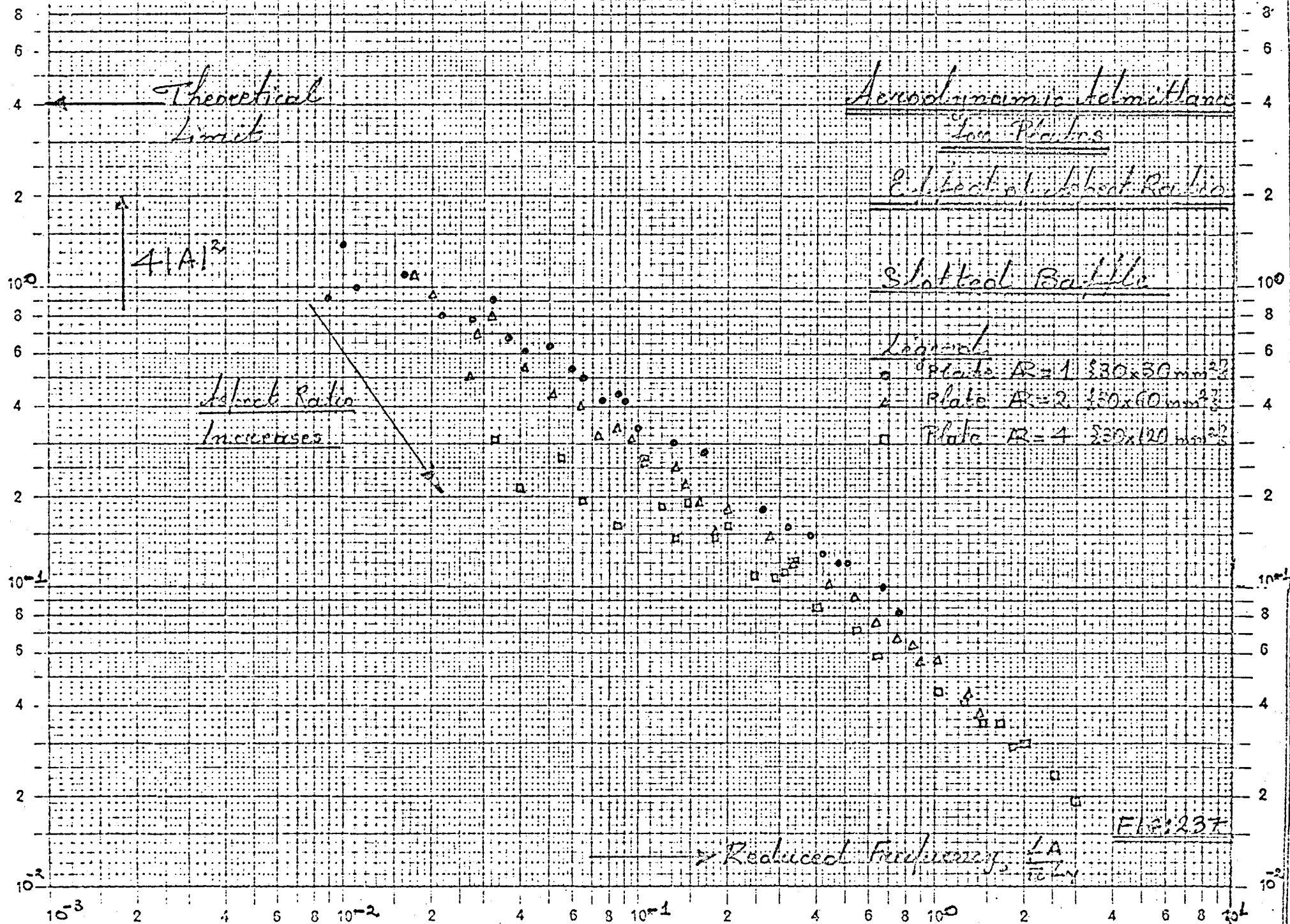


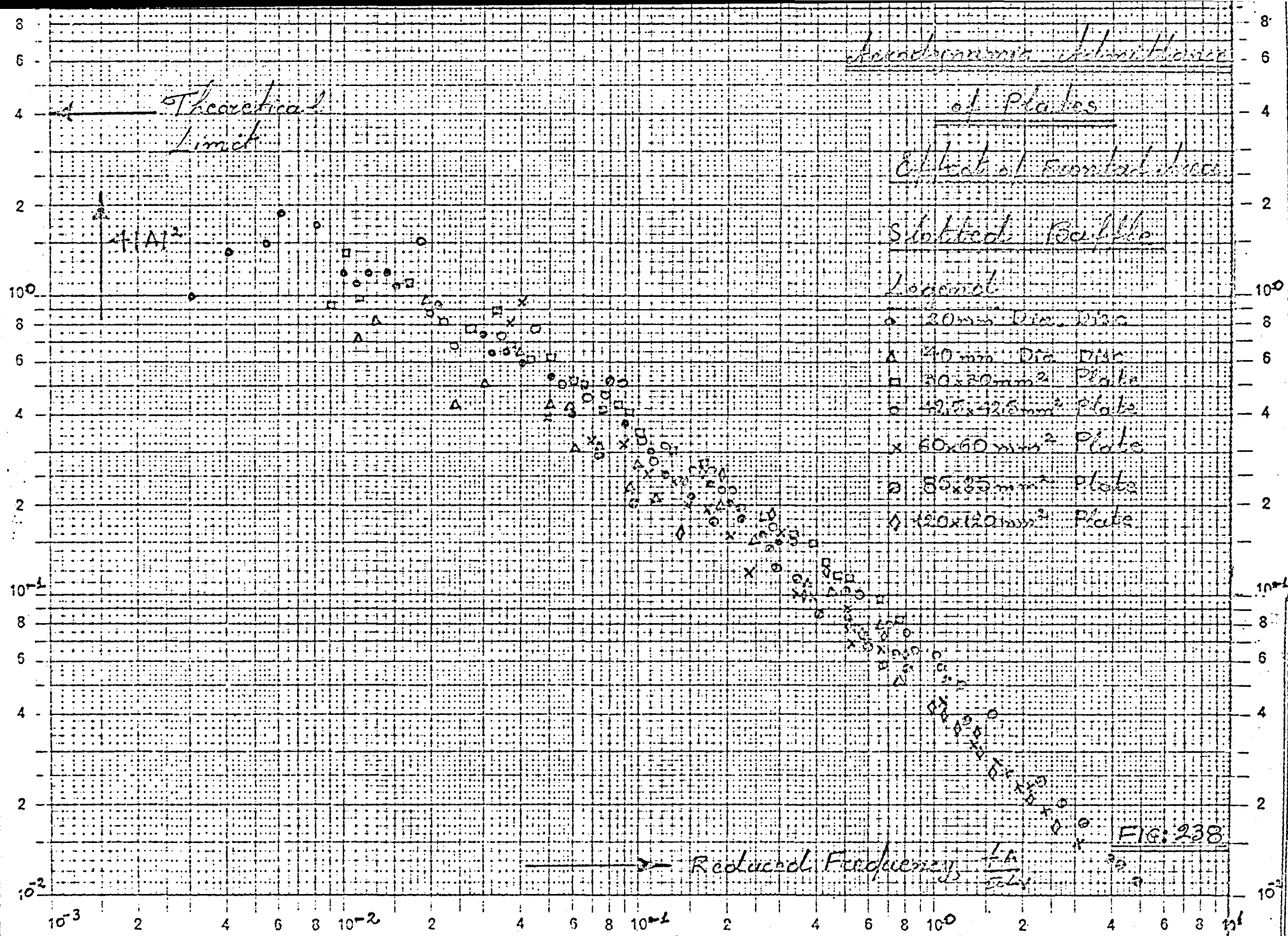


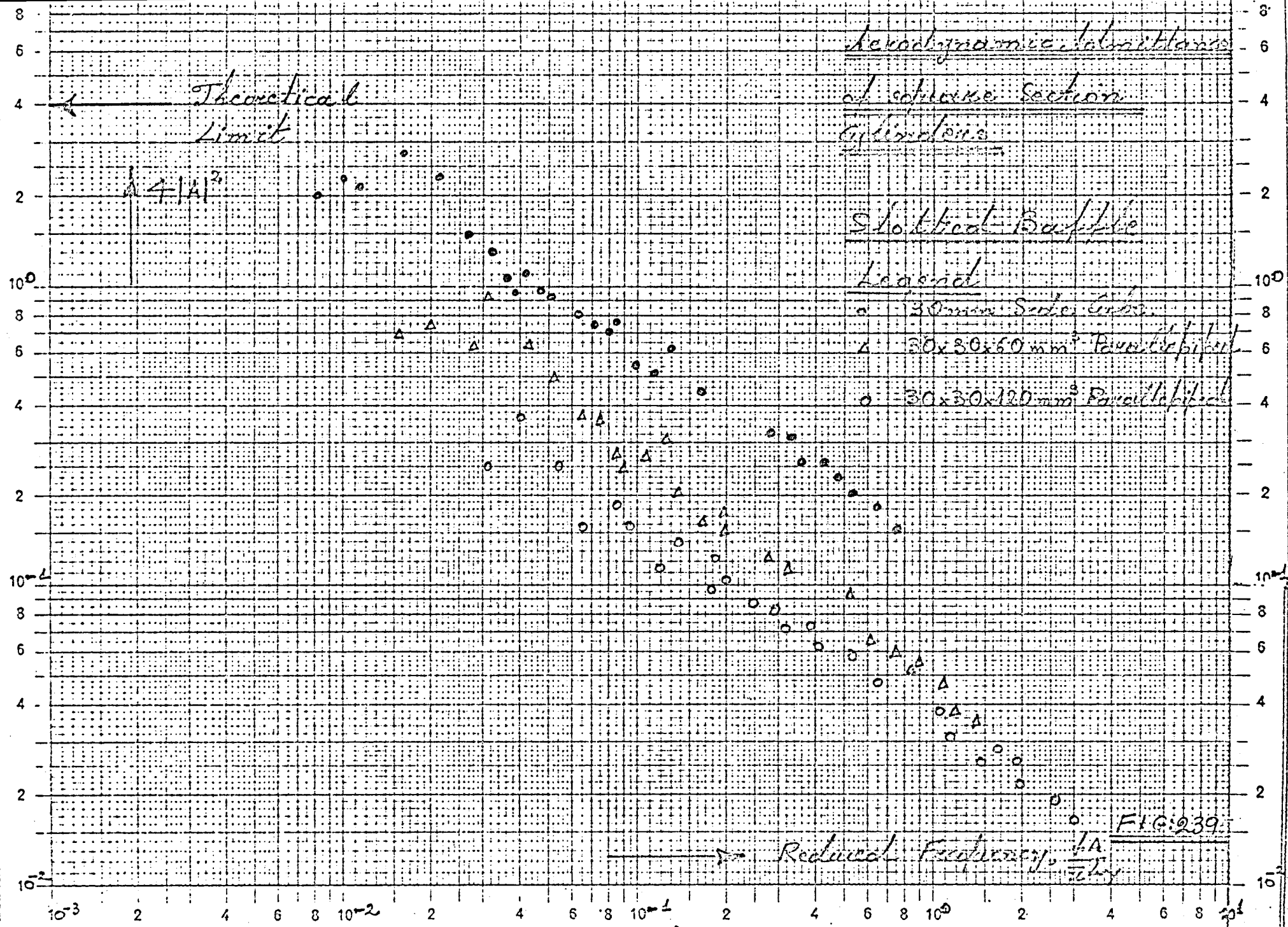


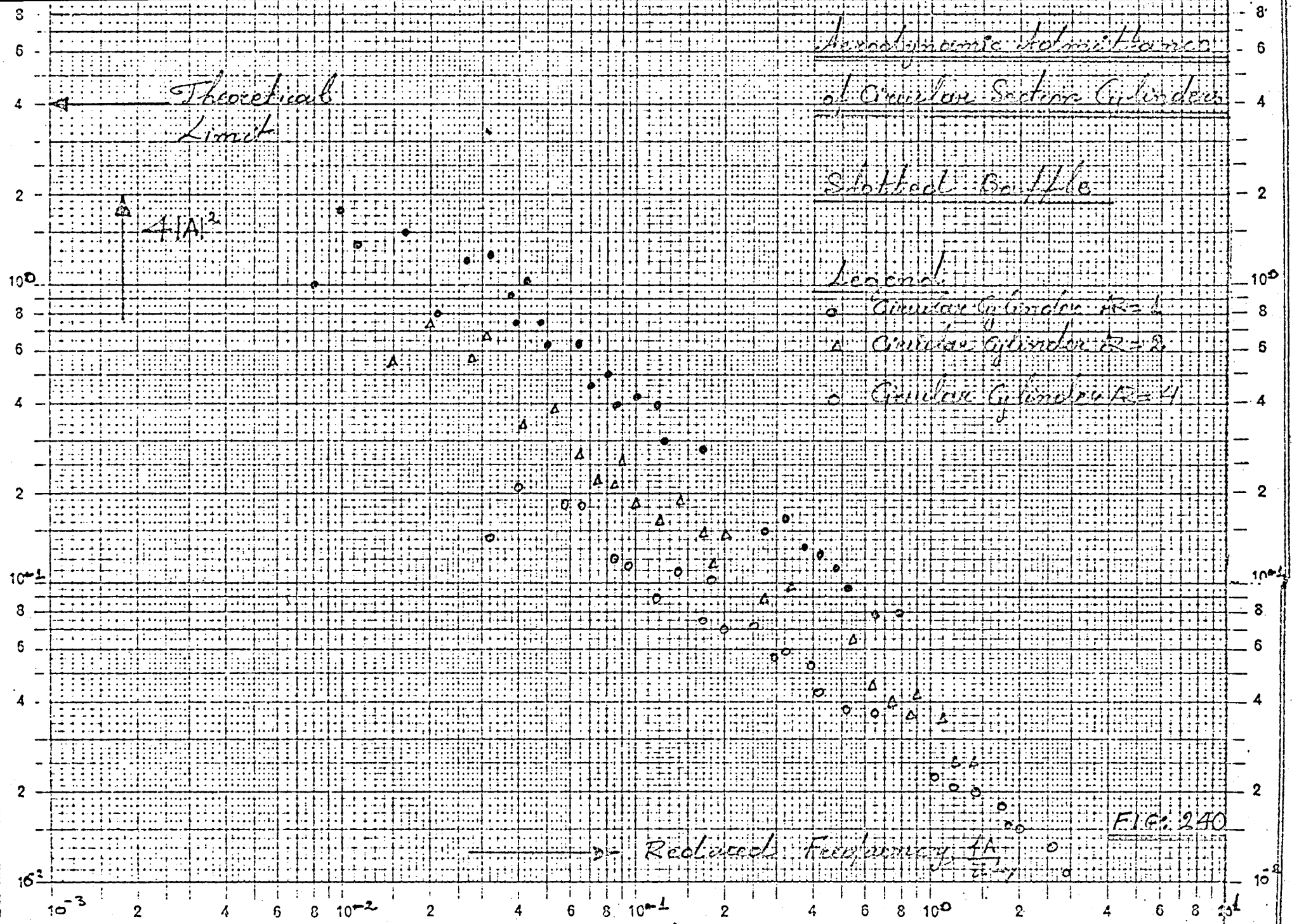


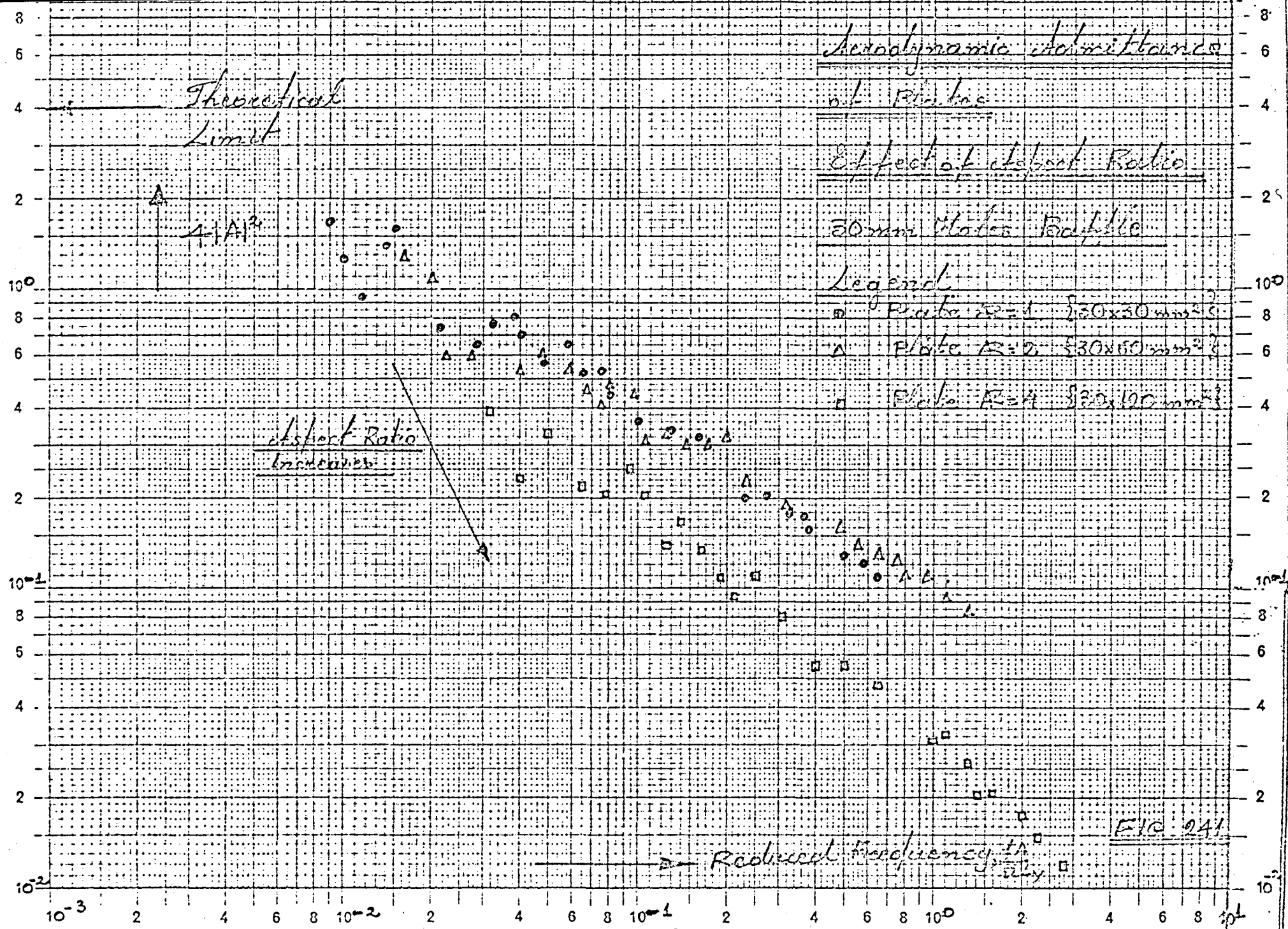


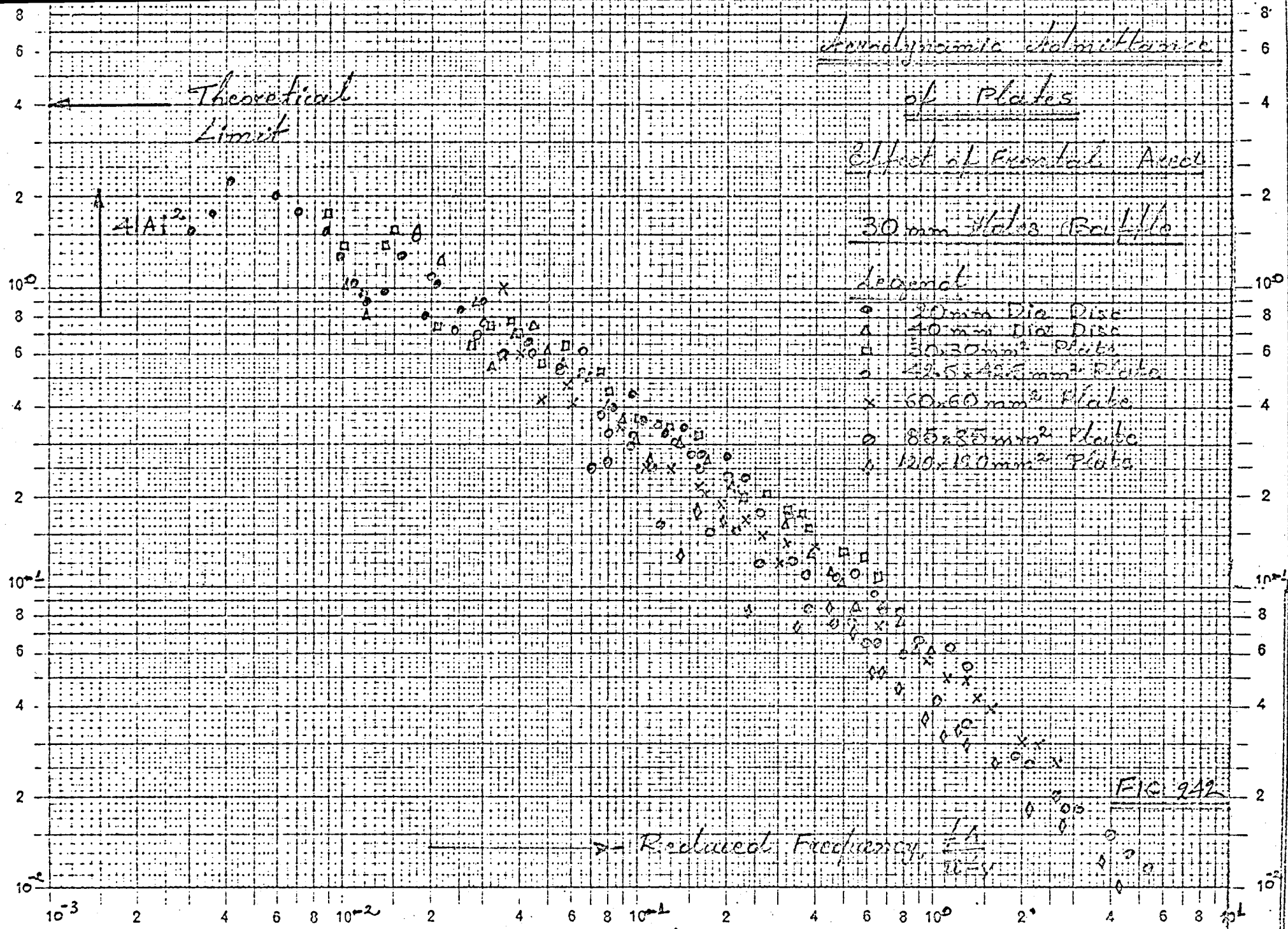


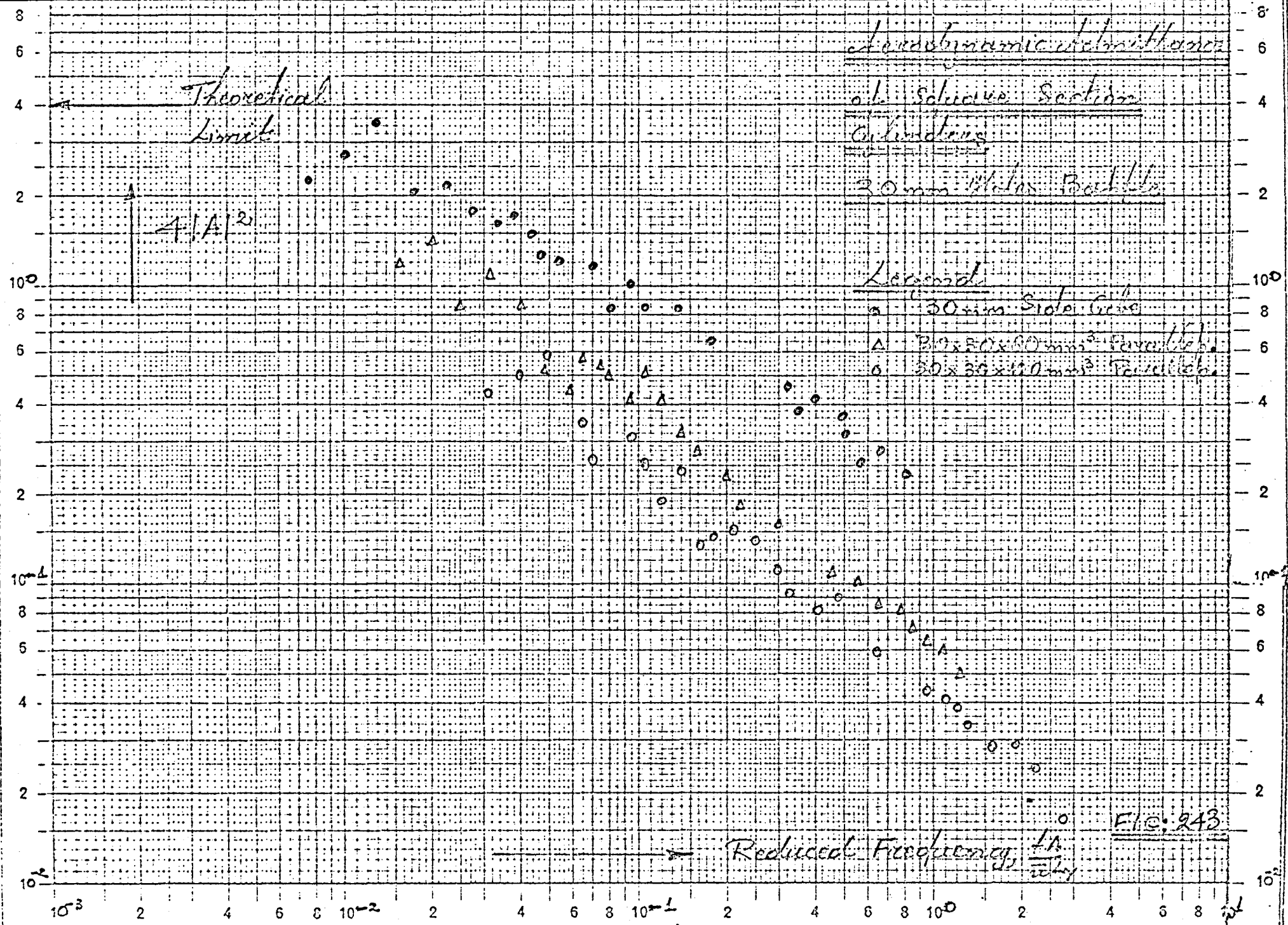












Theoretical
Limits

Aerodynamic Admittance
of Circular Section Cylinders

Blowing Glass Bottle

Legend

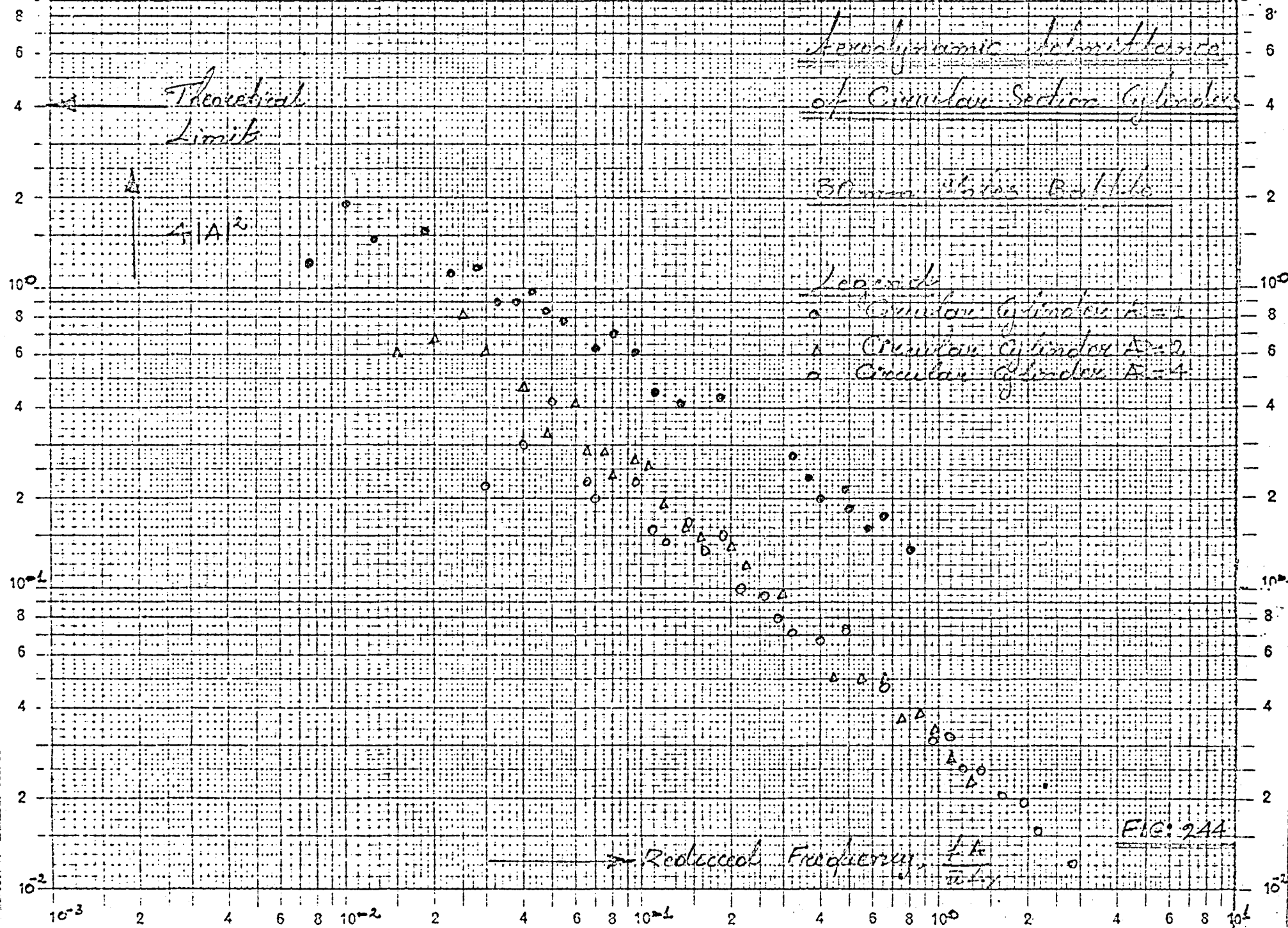
○ Circular Cylinder $A=1$

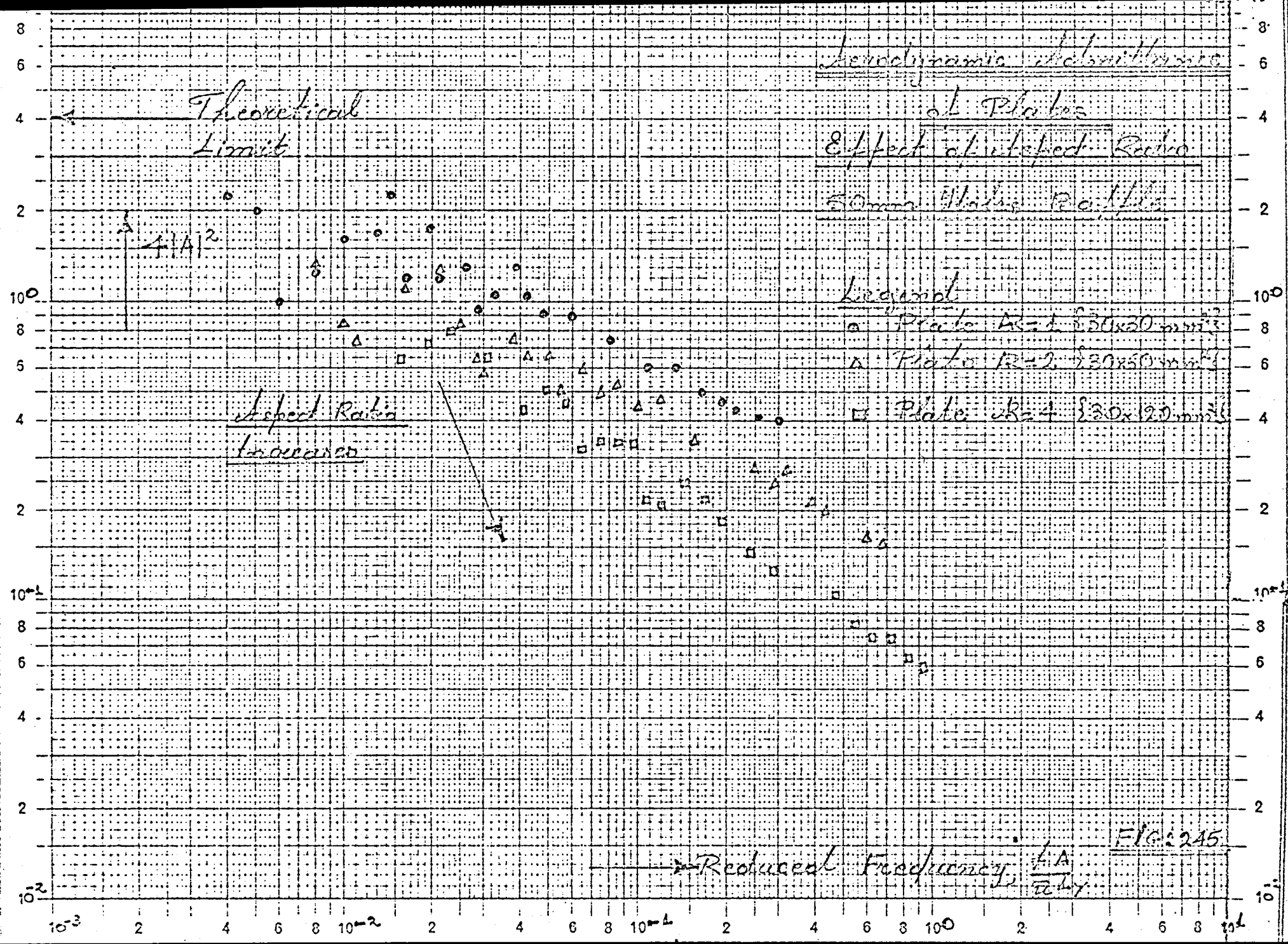
△ Circular Cylinder $A=2$

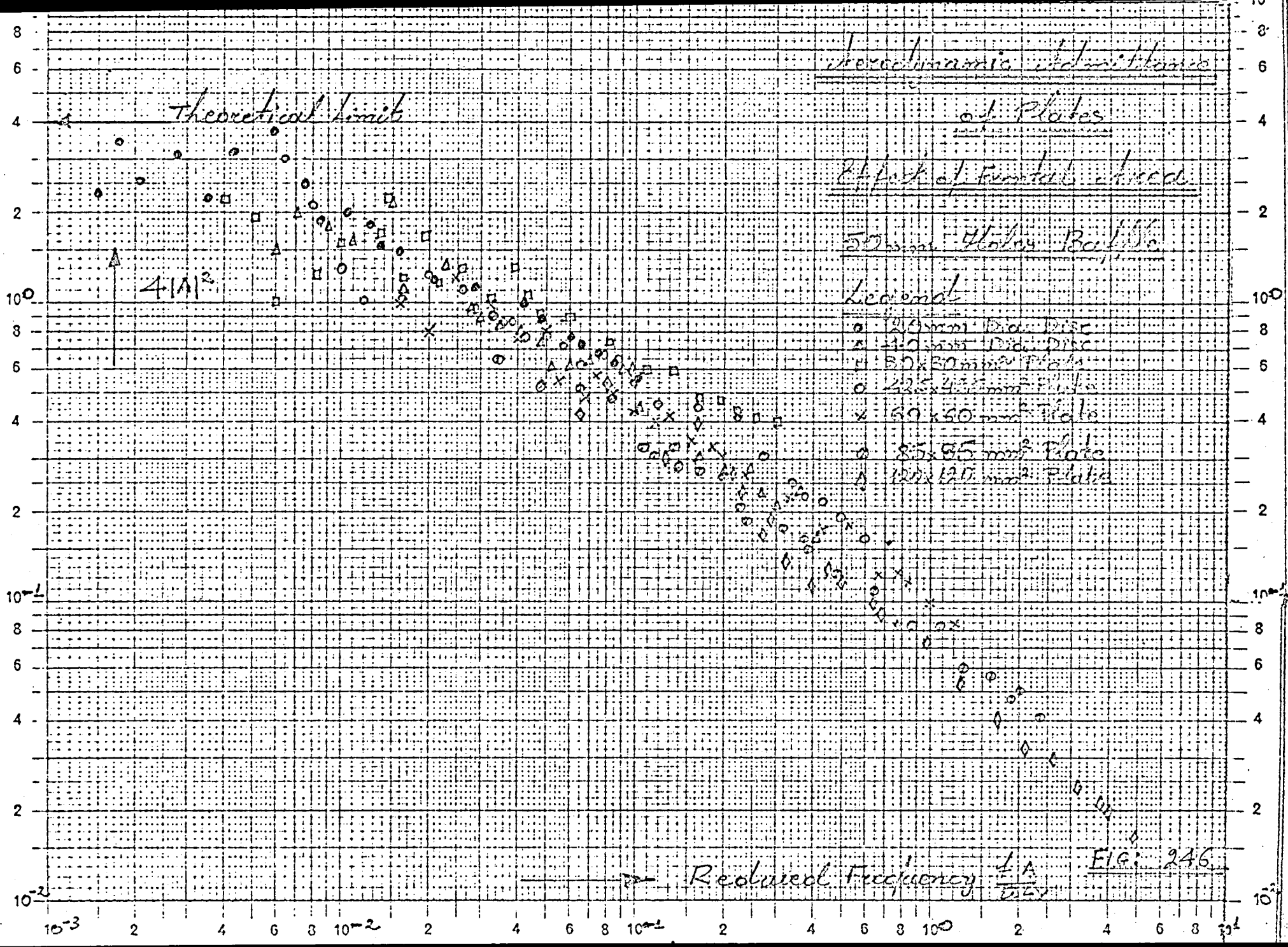
● Circular Cylinder $A=4$

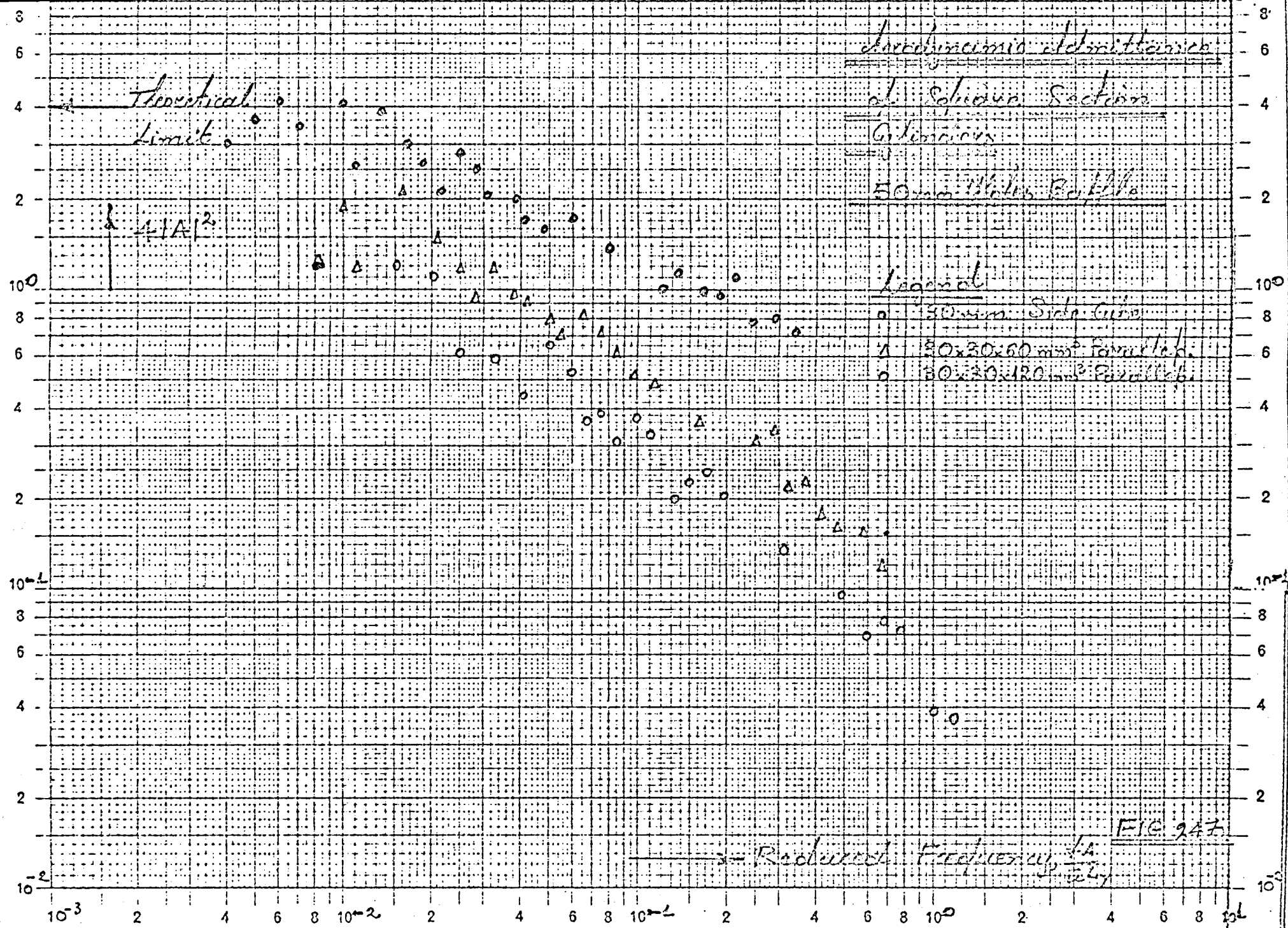
Reduction Frequency, $\frac{f}{\omega L}$

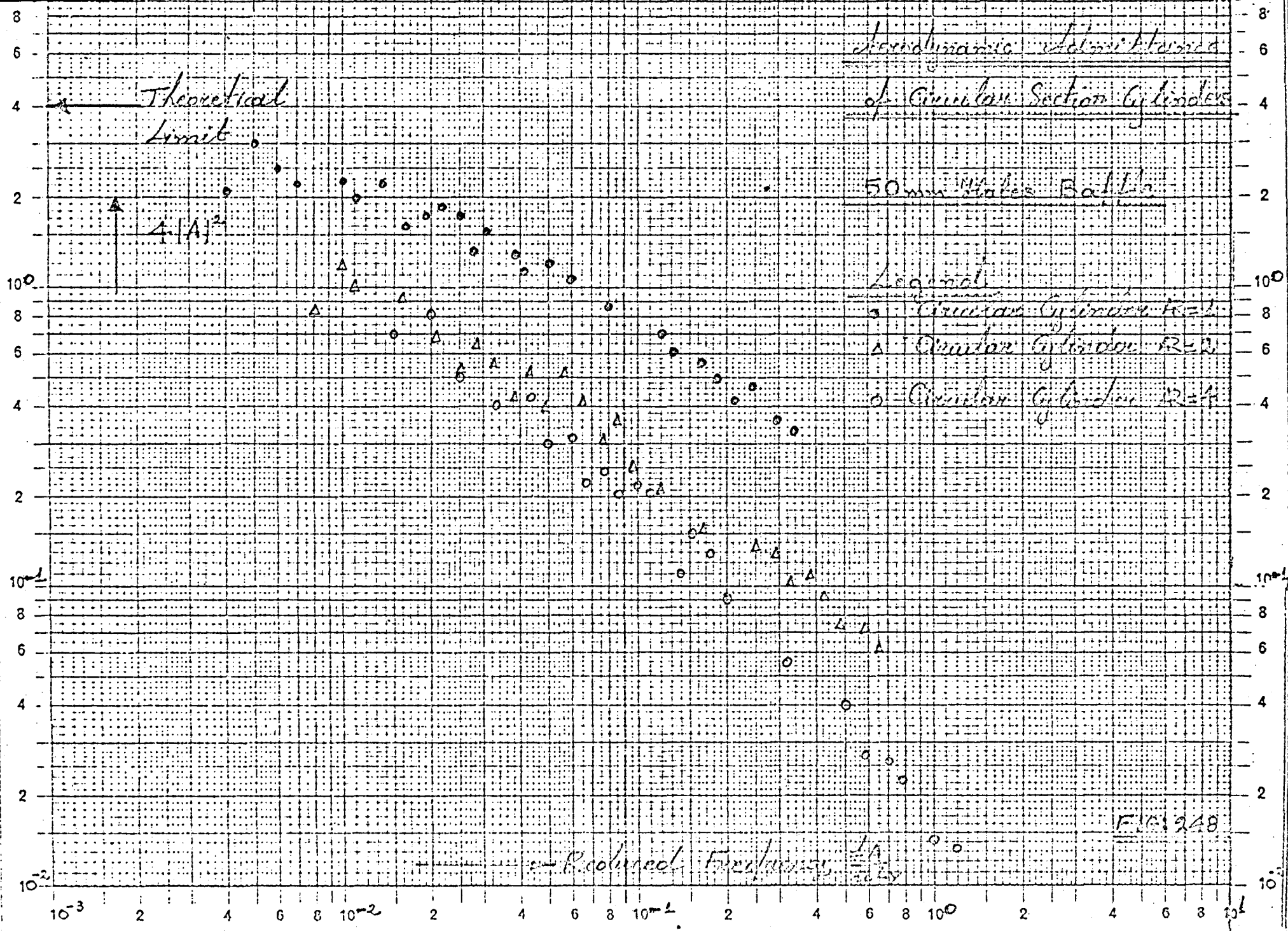
FIG. 24A

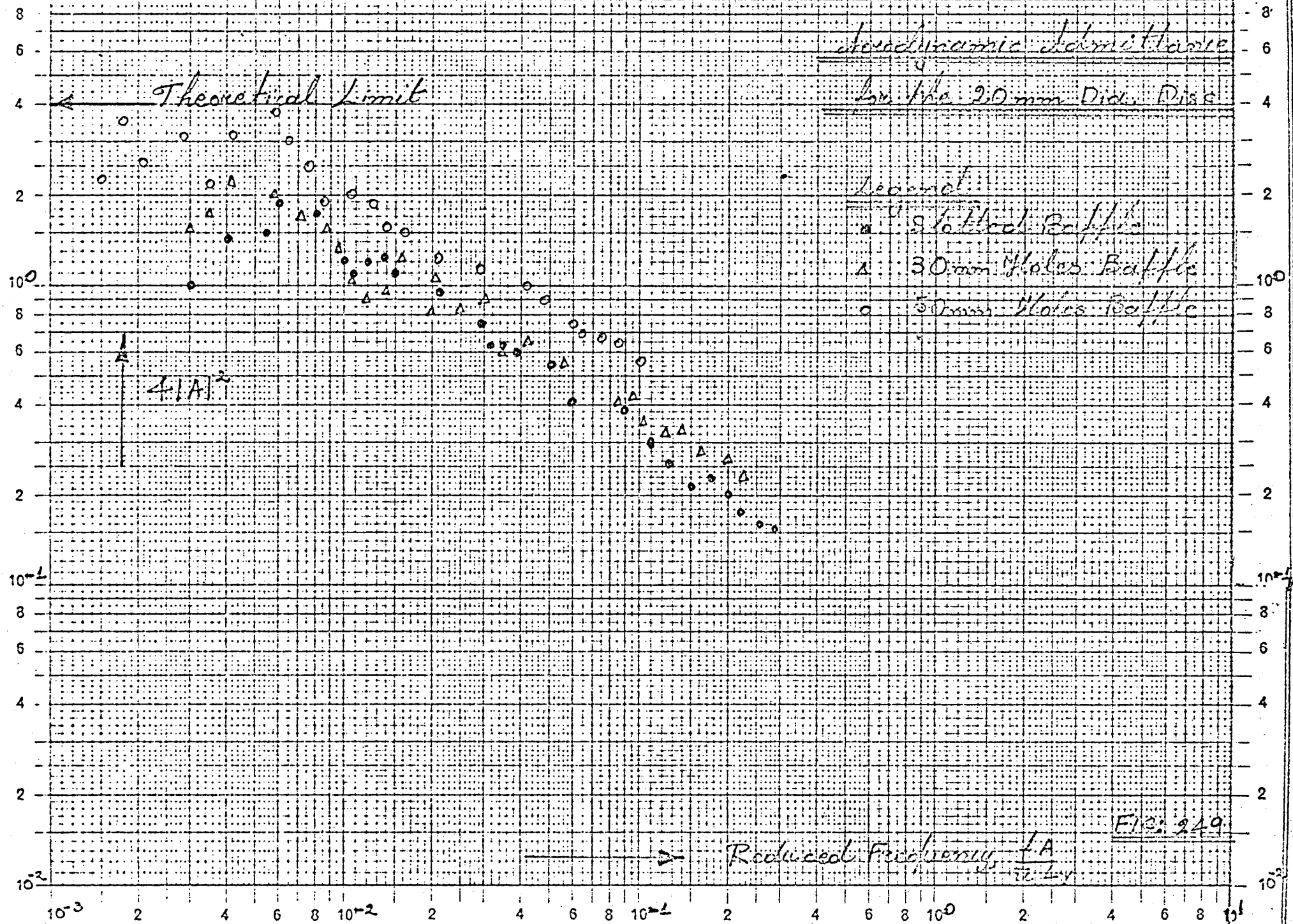


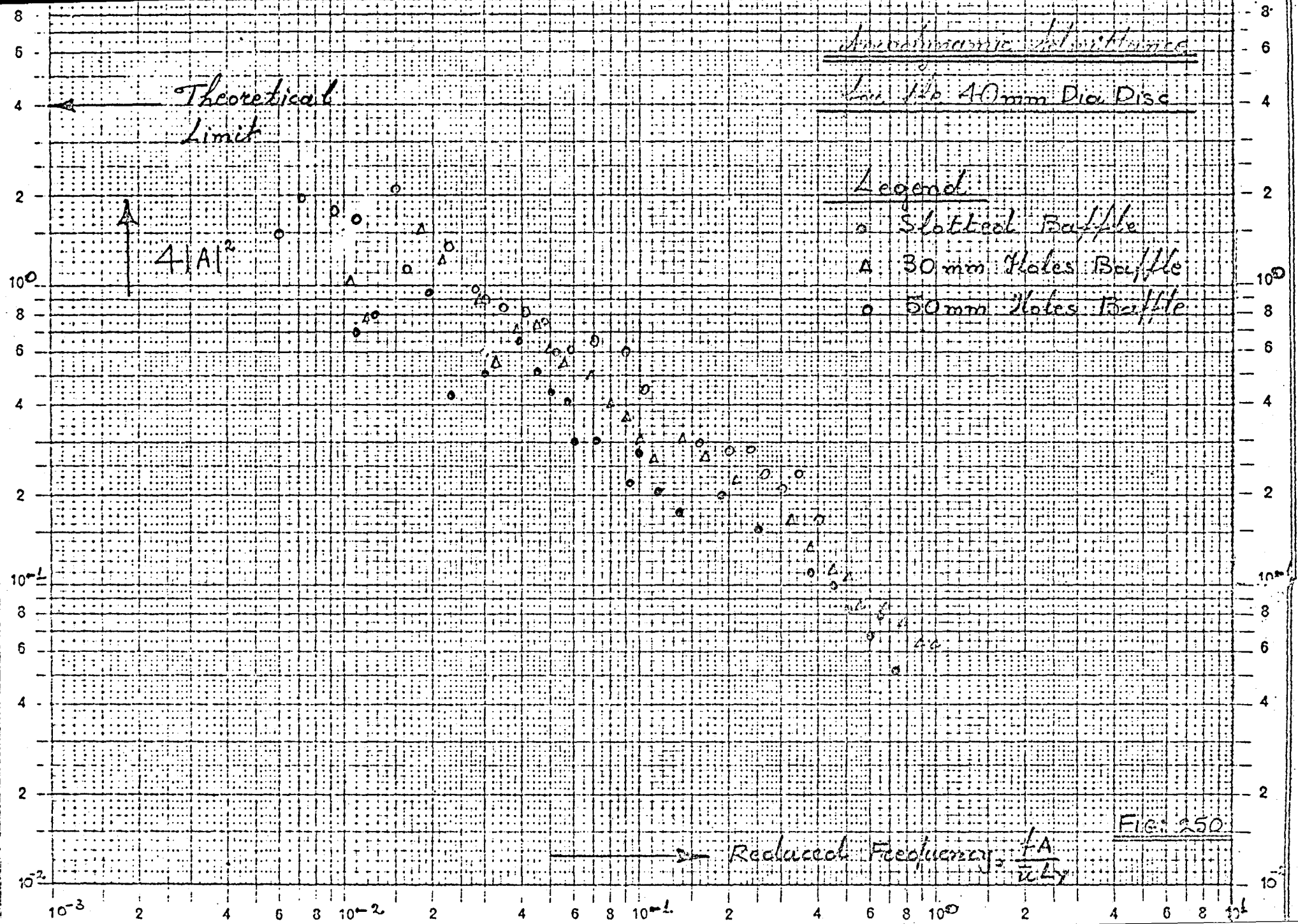












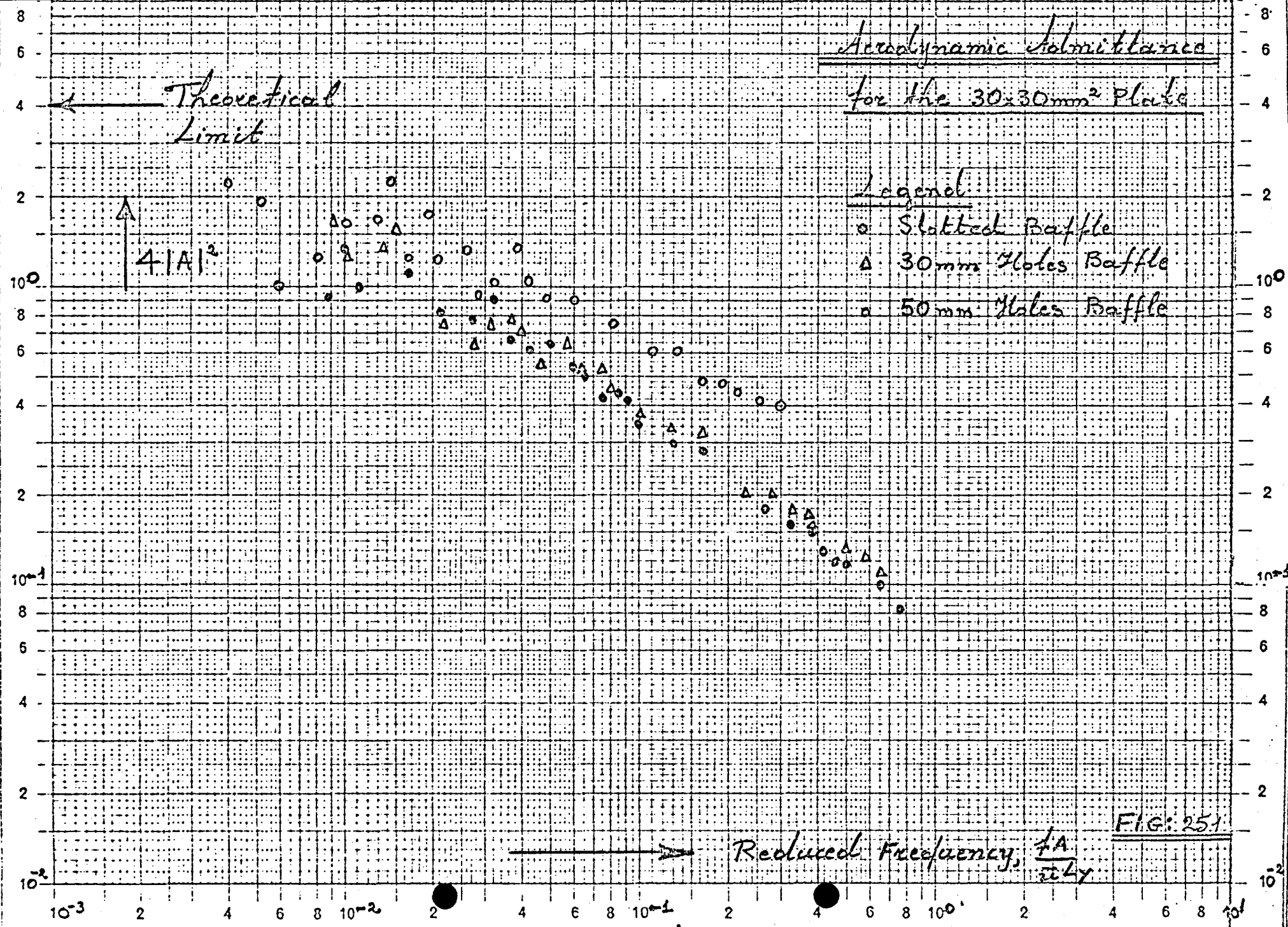


FIG: 25.1

Aerodynamic Admittance

for the 30x60mm² Plate

Theoretical Limit

Legend

• Slotted Baffle

Δ 30 mm Holes Baffle

○ 50 mm Holes Baffle

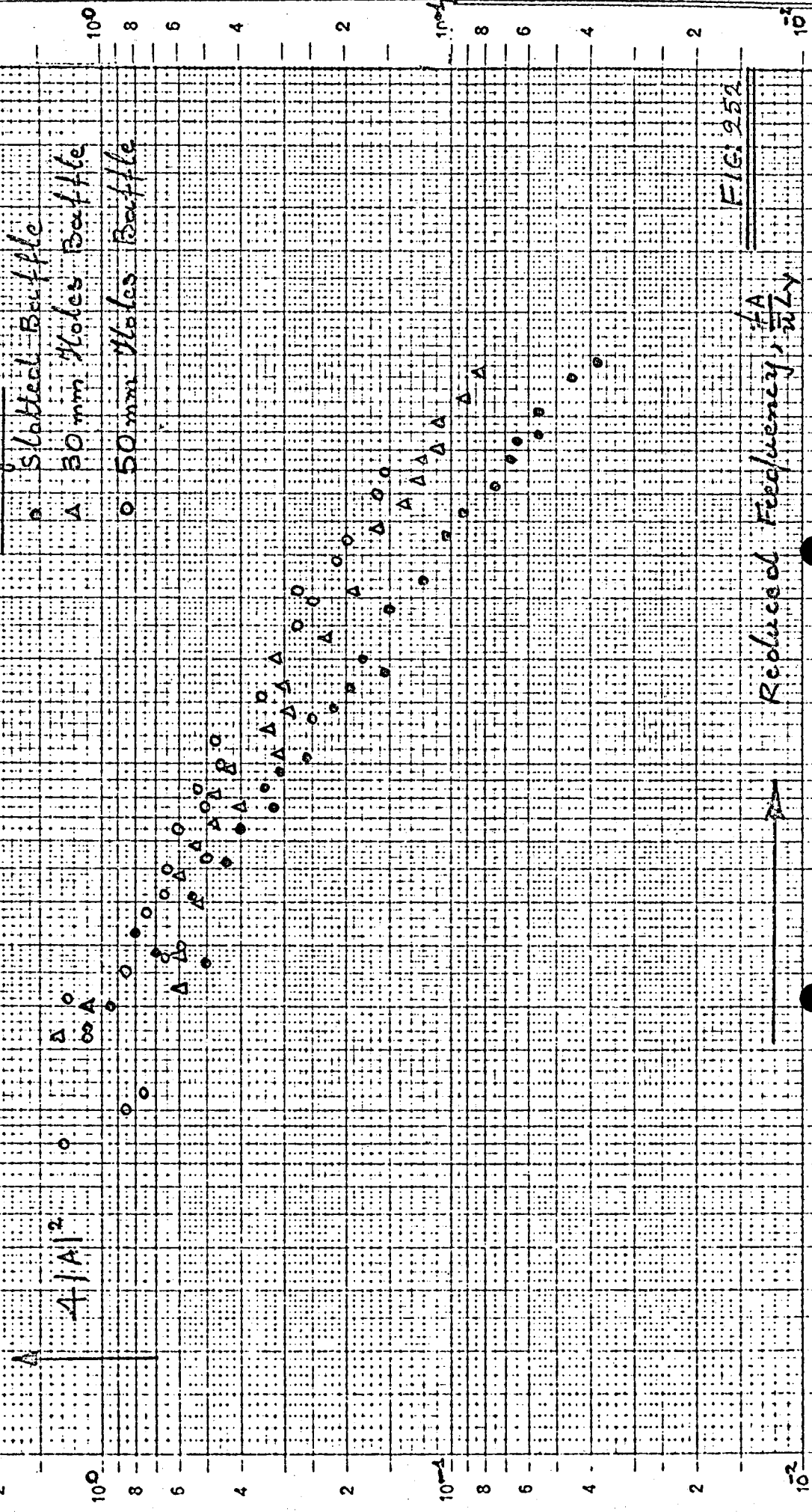
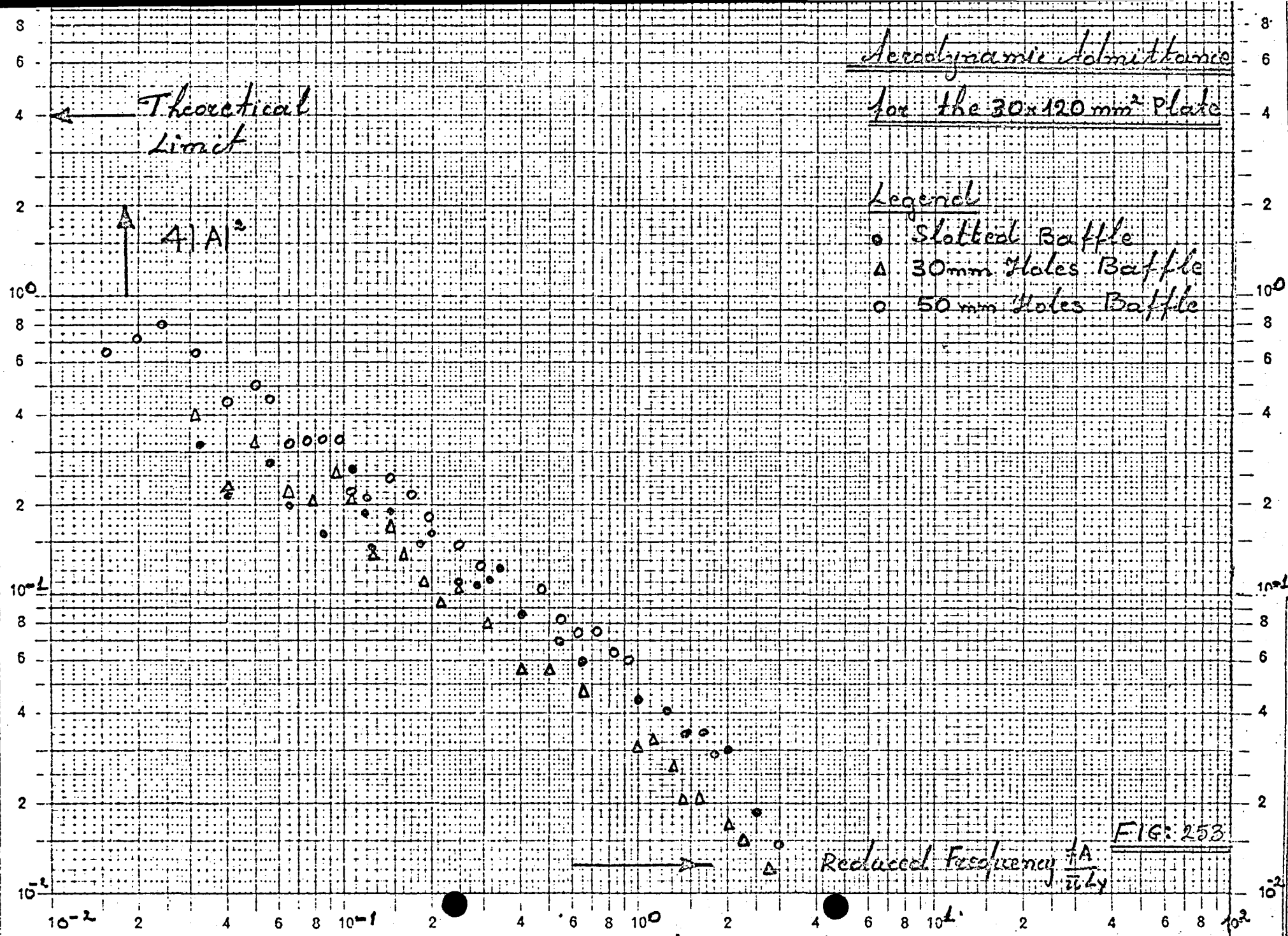
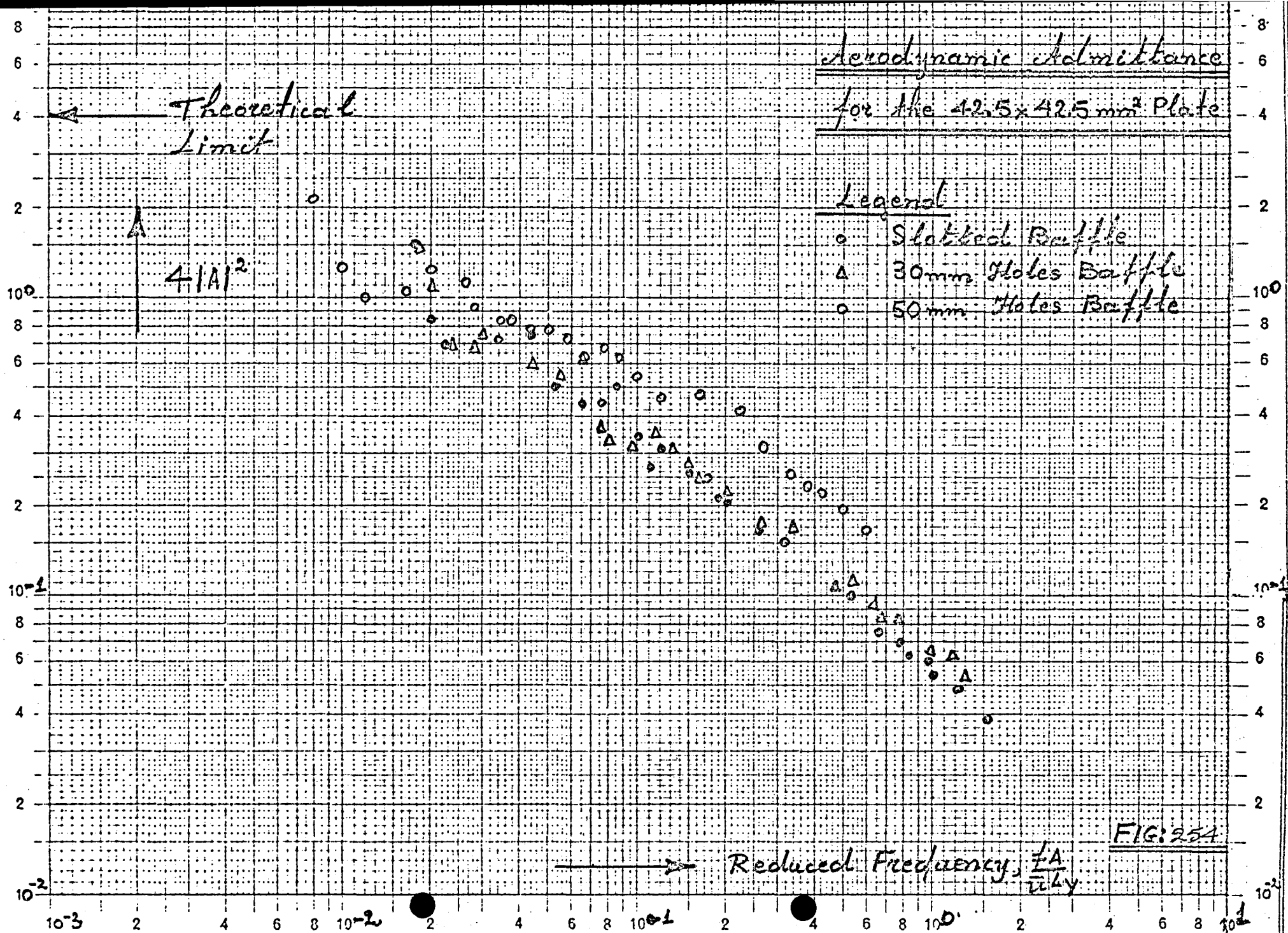
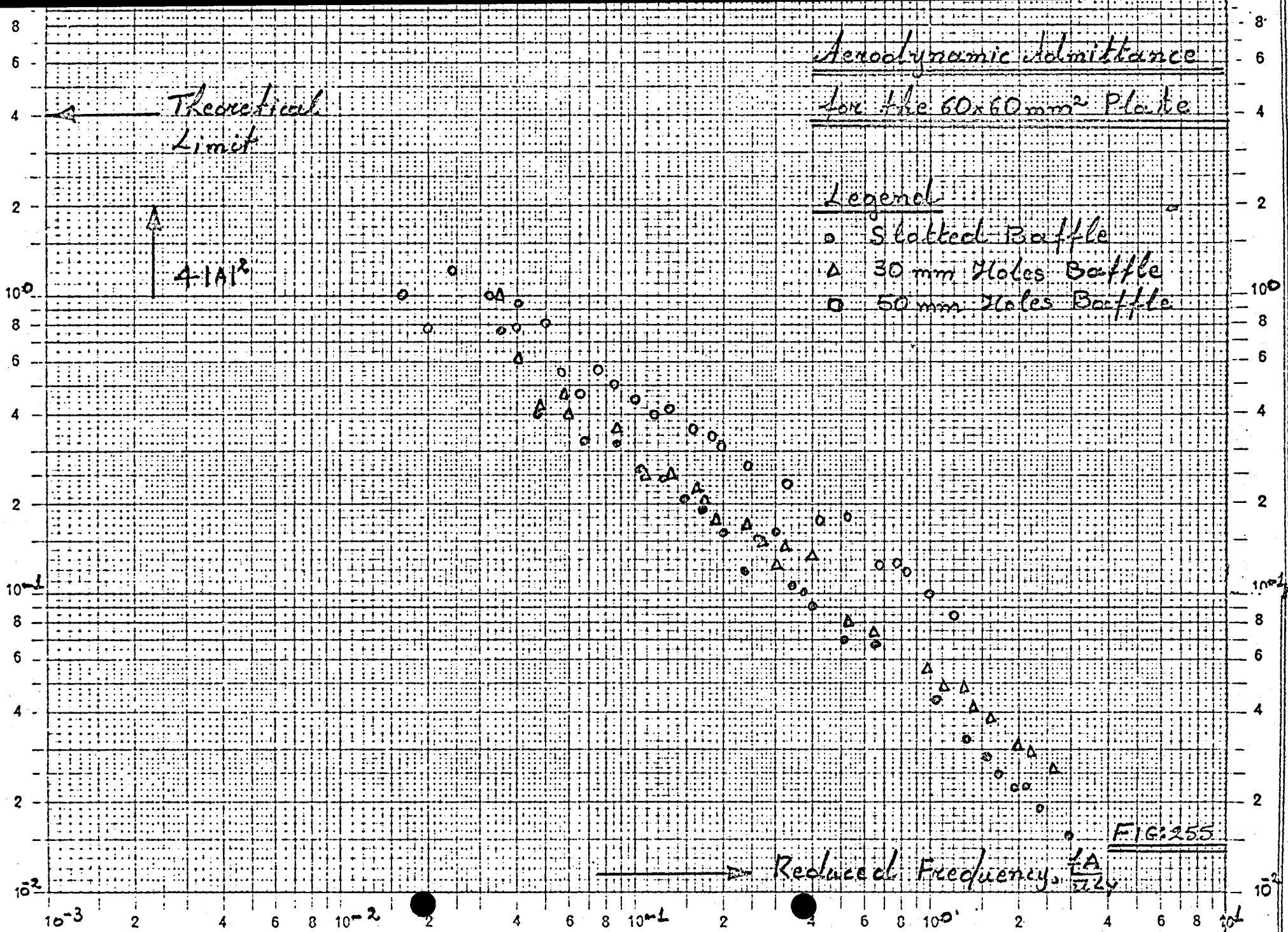
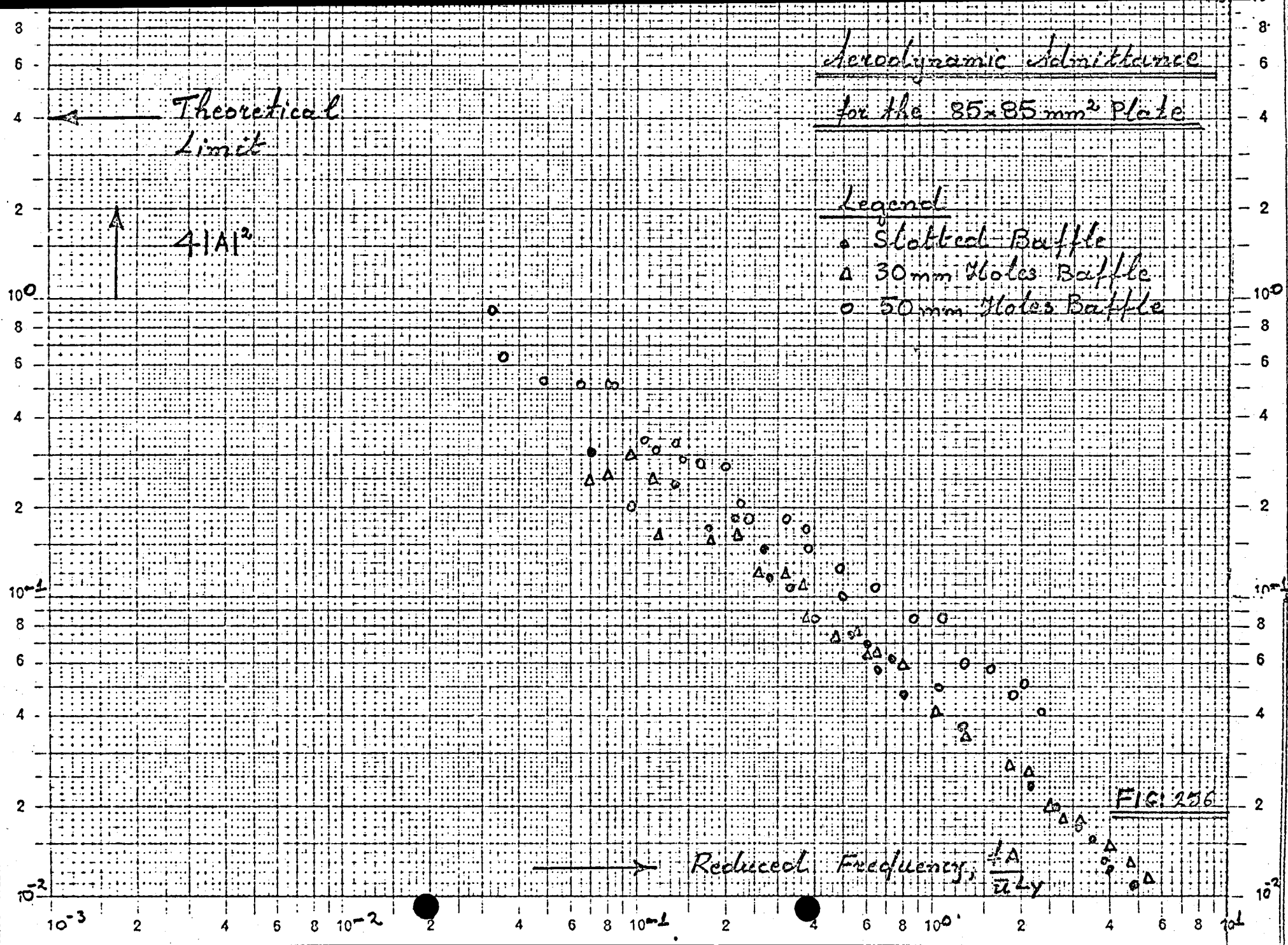


FIG. 252









Aerodynamic Admittance for the 120x120 mm² Plate

Legend

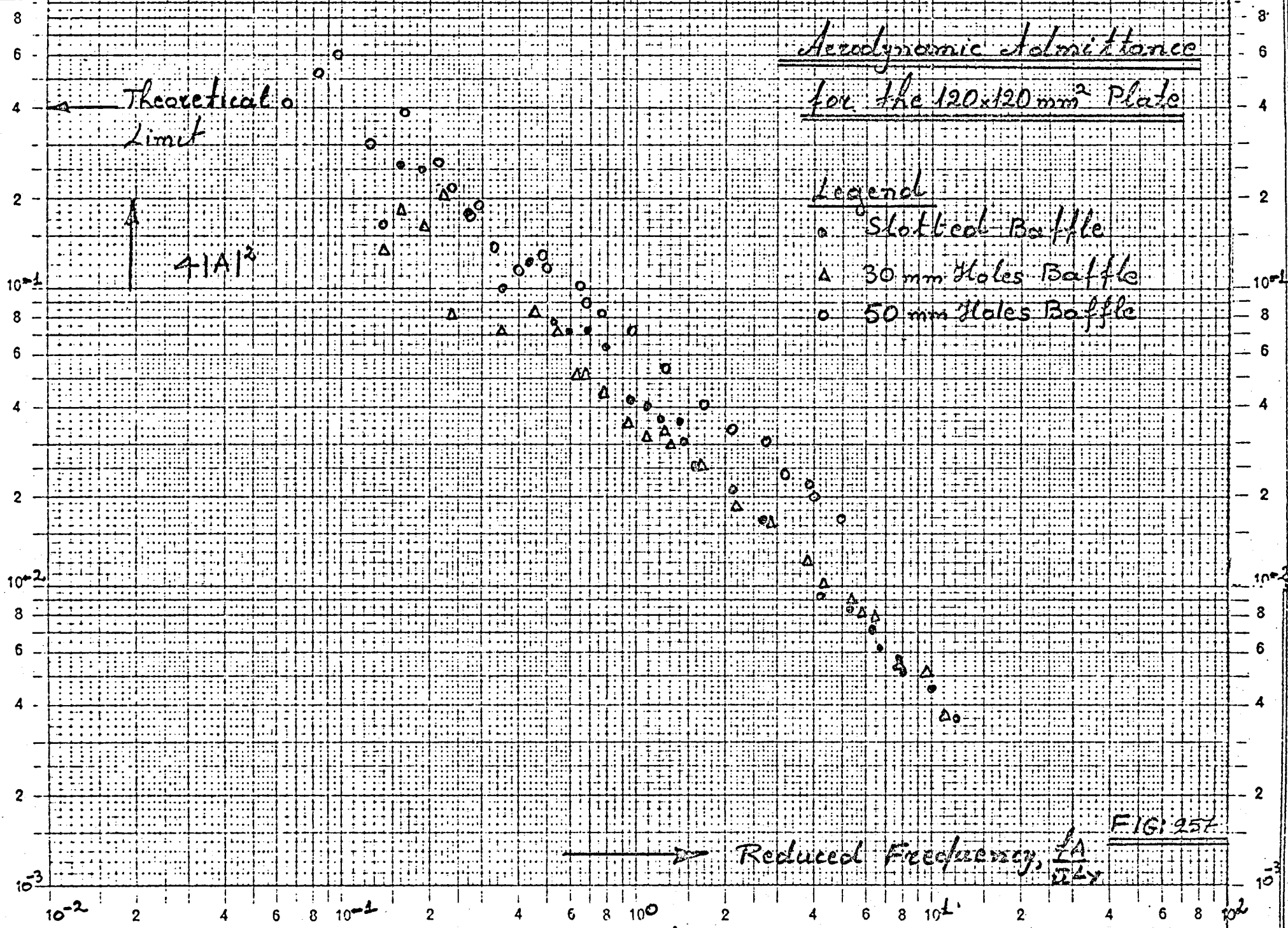
- Slotted Baffle
- △ 30 mm Holes Baffle
- 50 mm Holes Baffle

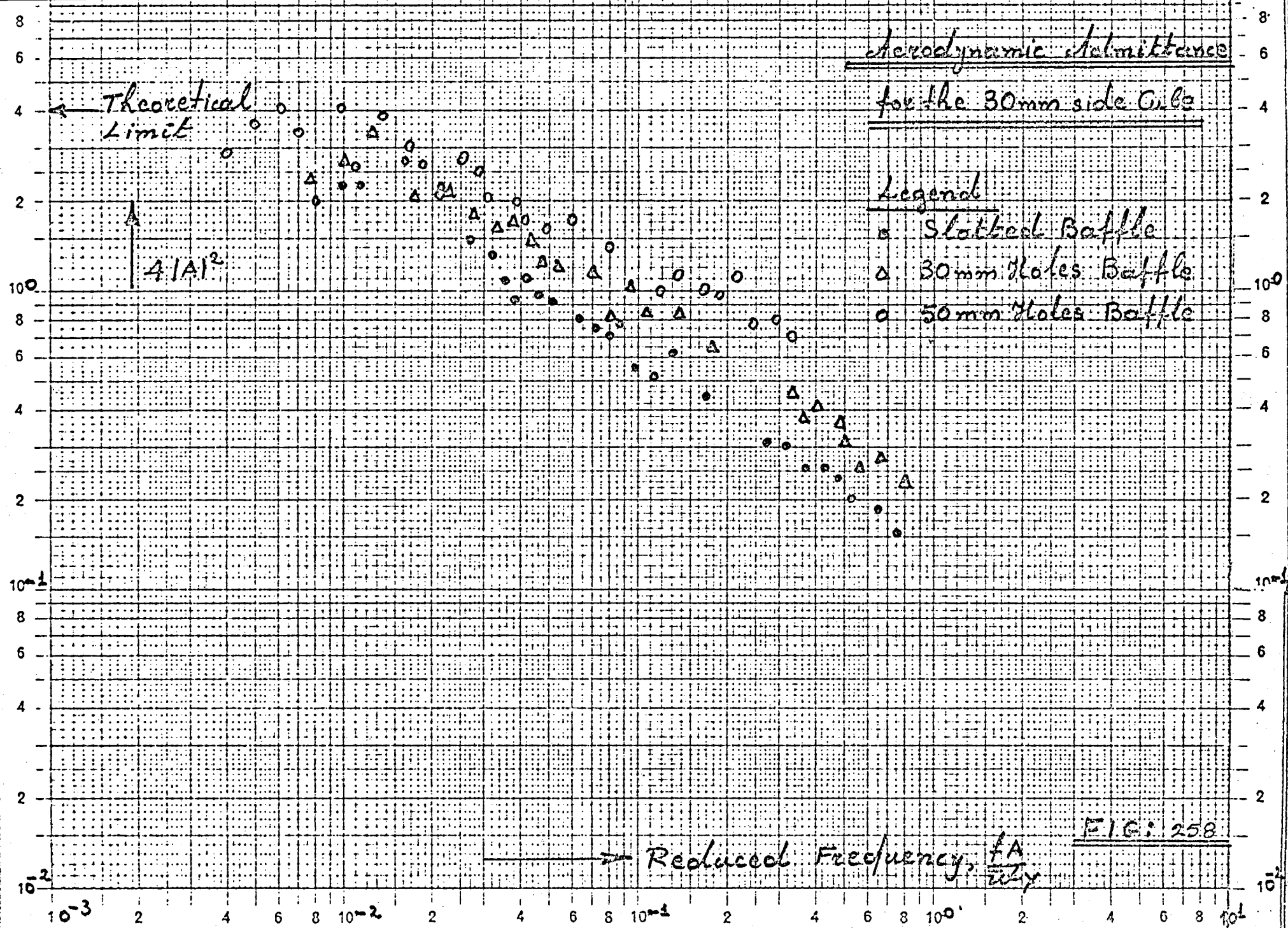
Theoretical Limit

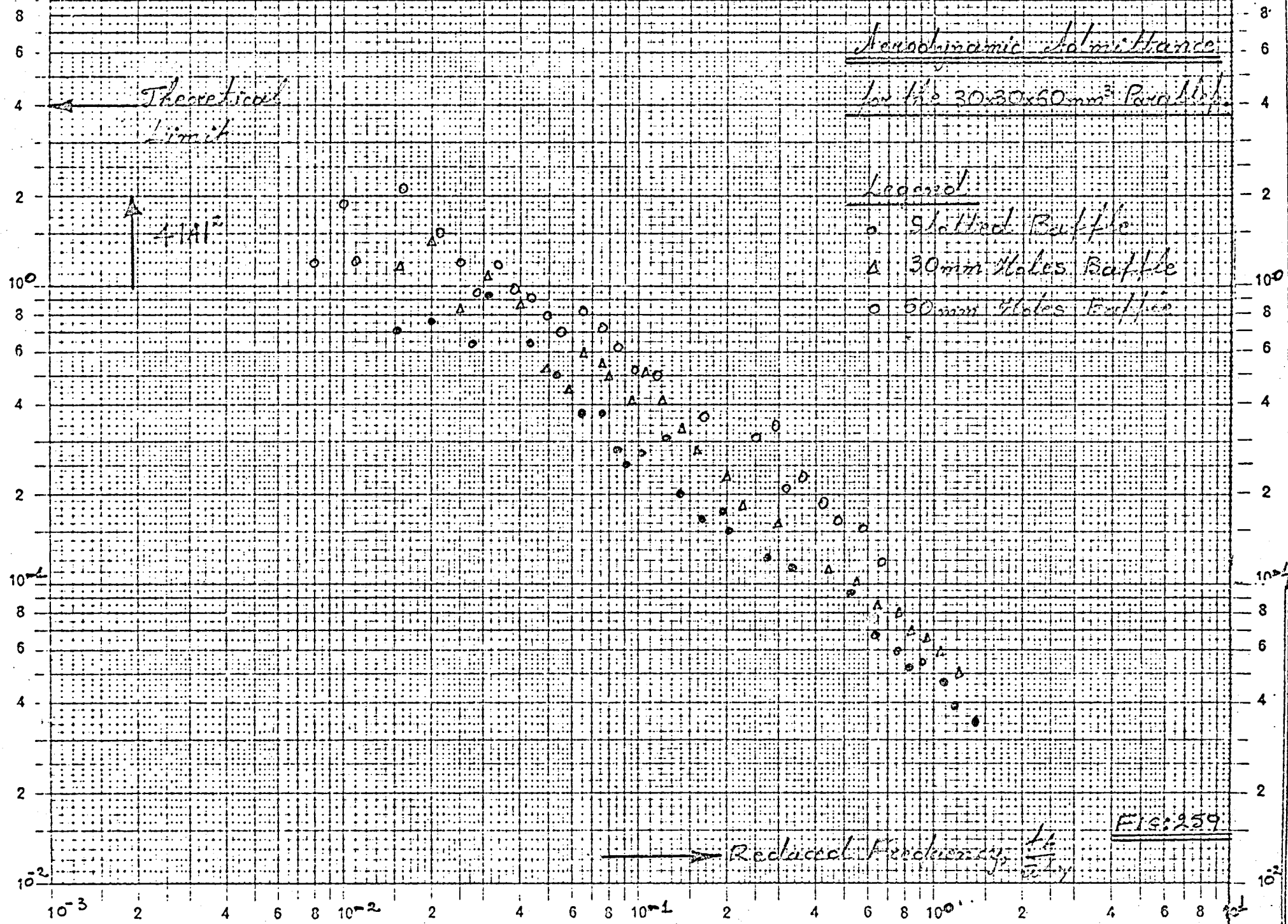
$$4|A|^2$$

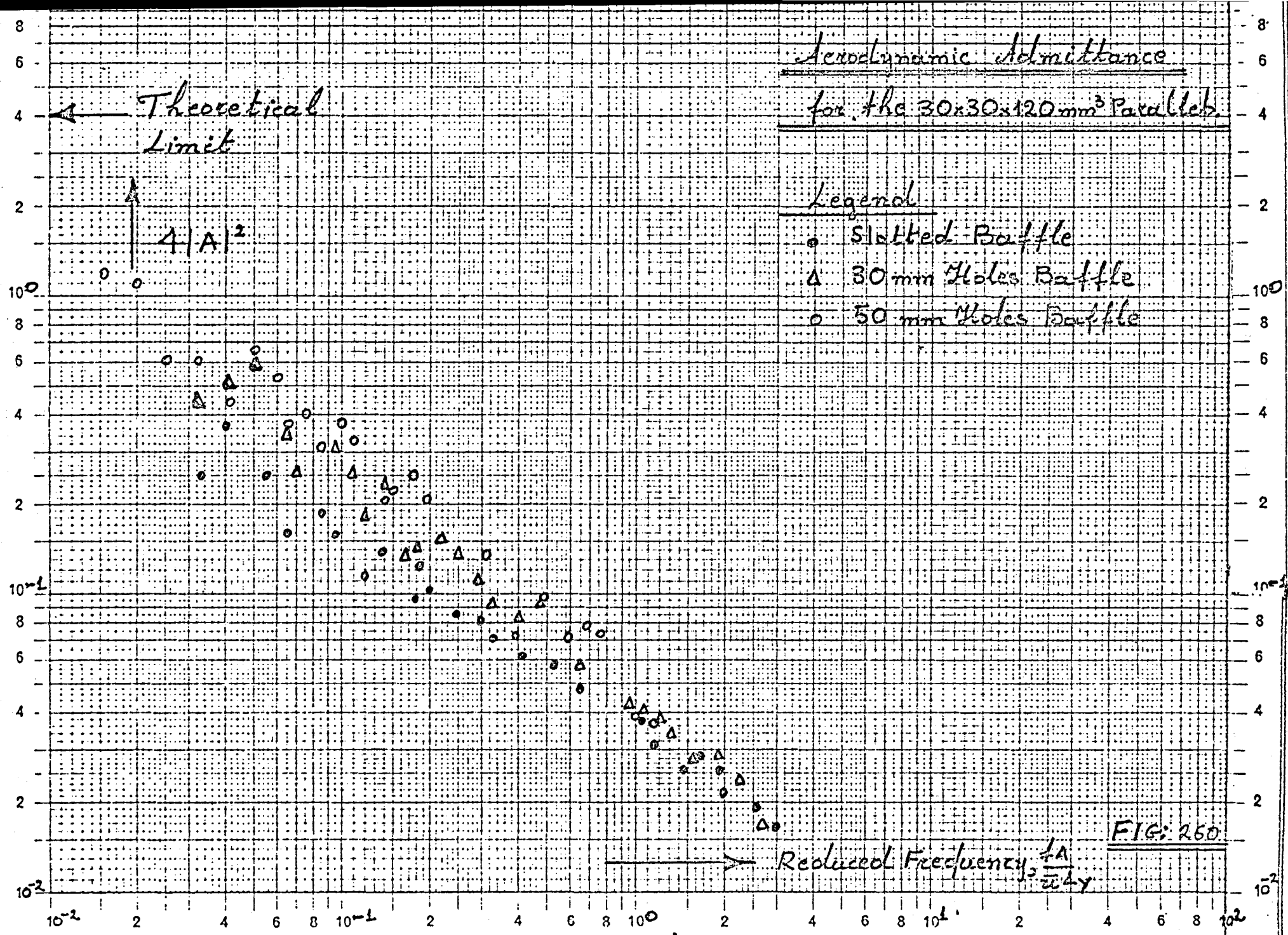
Reduced Frequency, $\frac{fA}{c}$

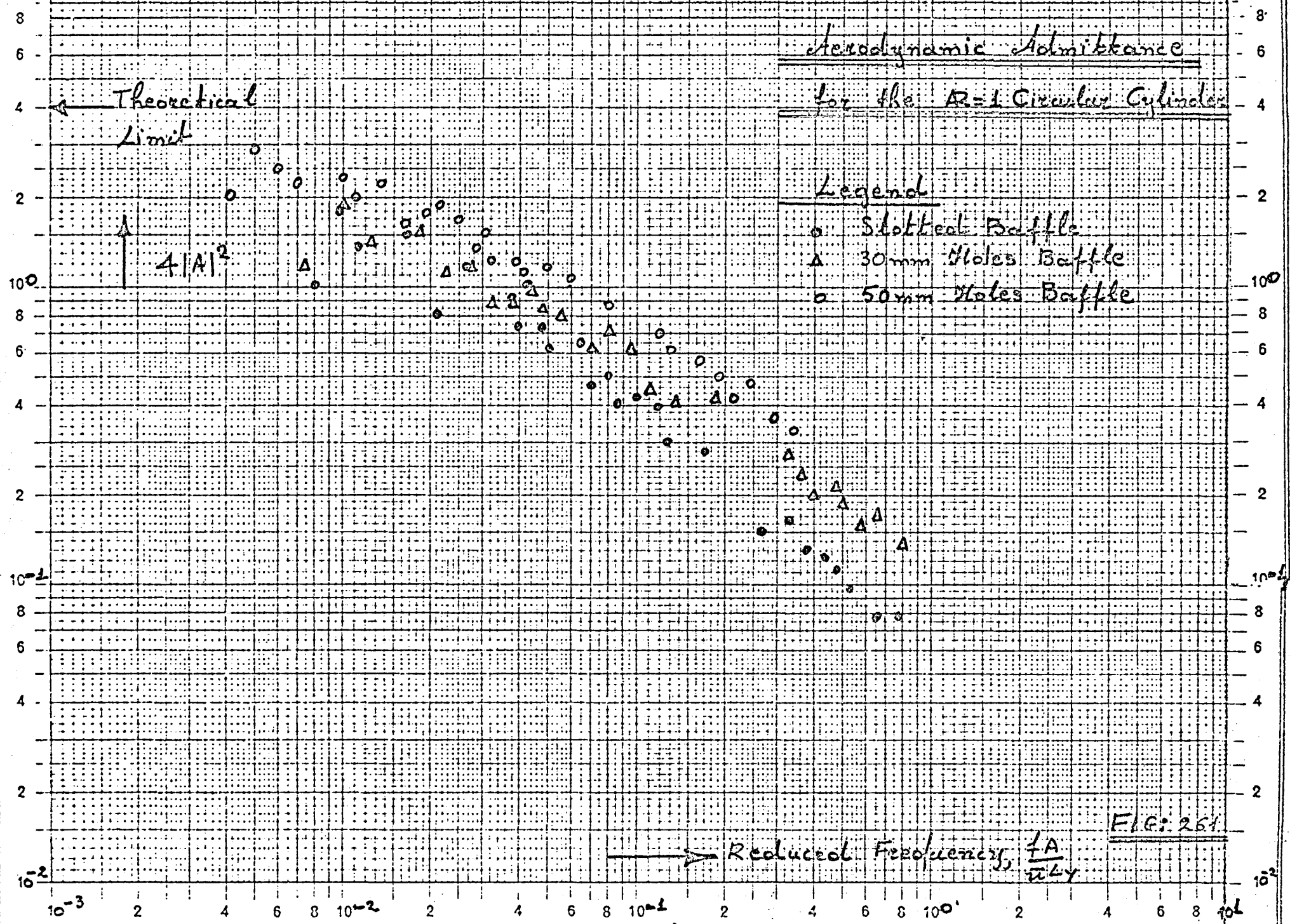
FIG: 257

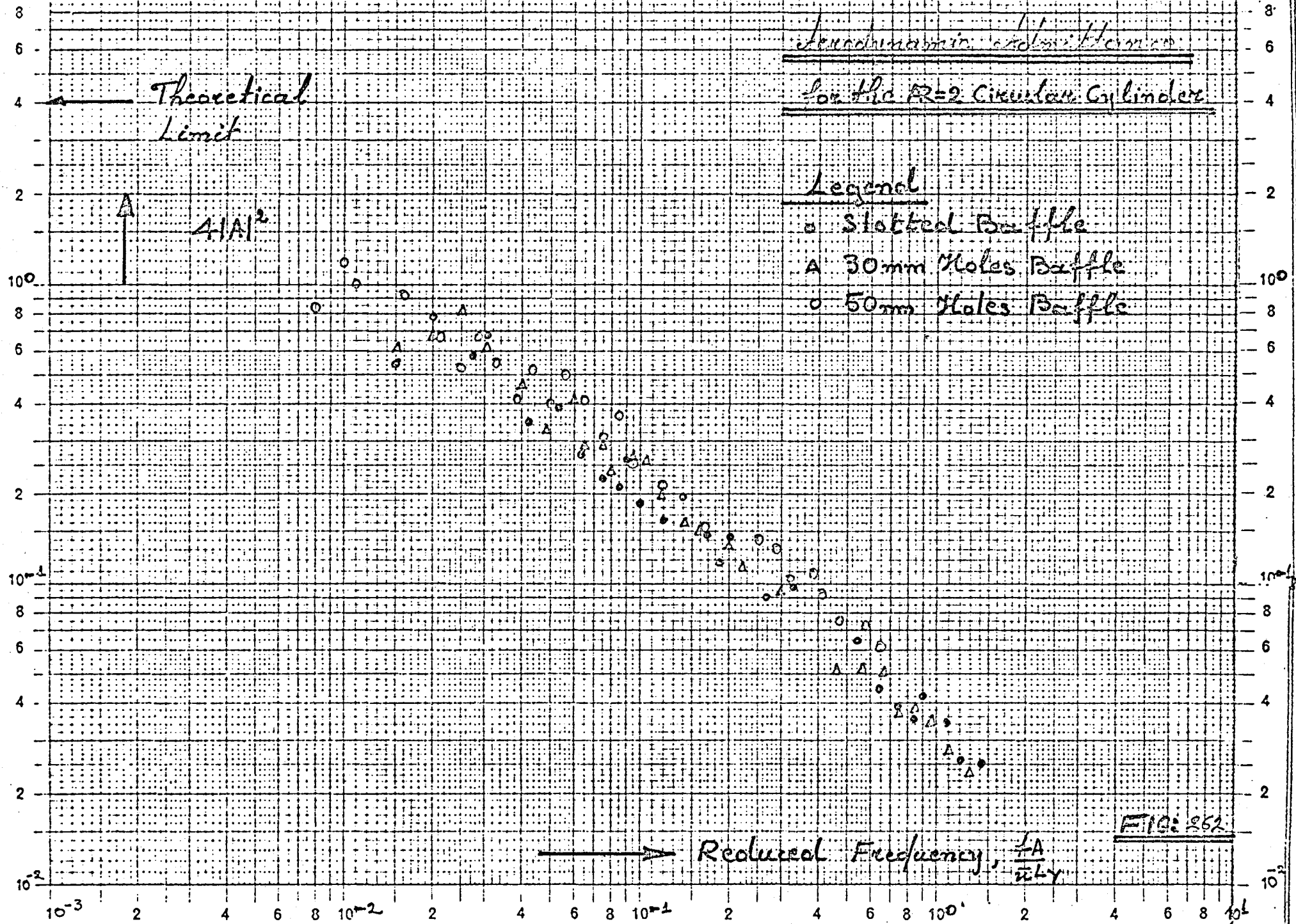












Theoretical
Limit

Aerodynamic Admittance

for the $R=4$ Circular Cylinder

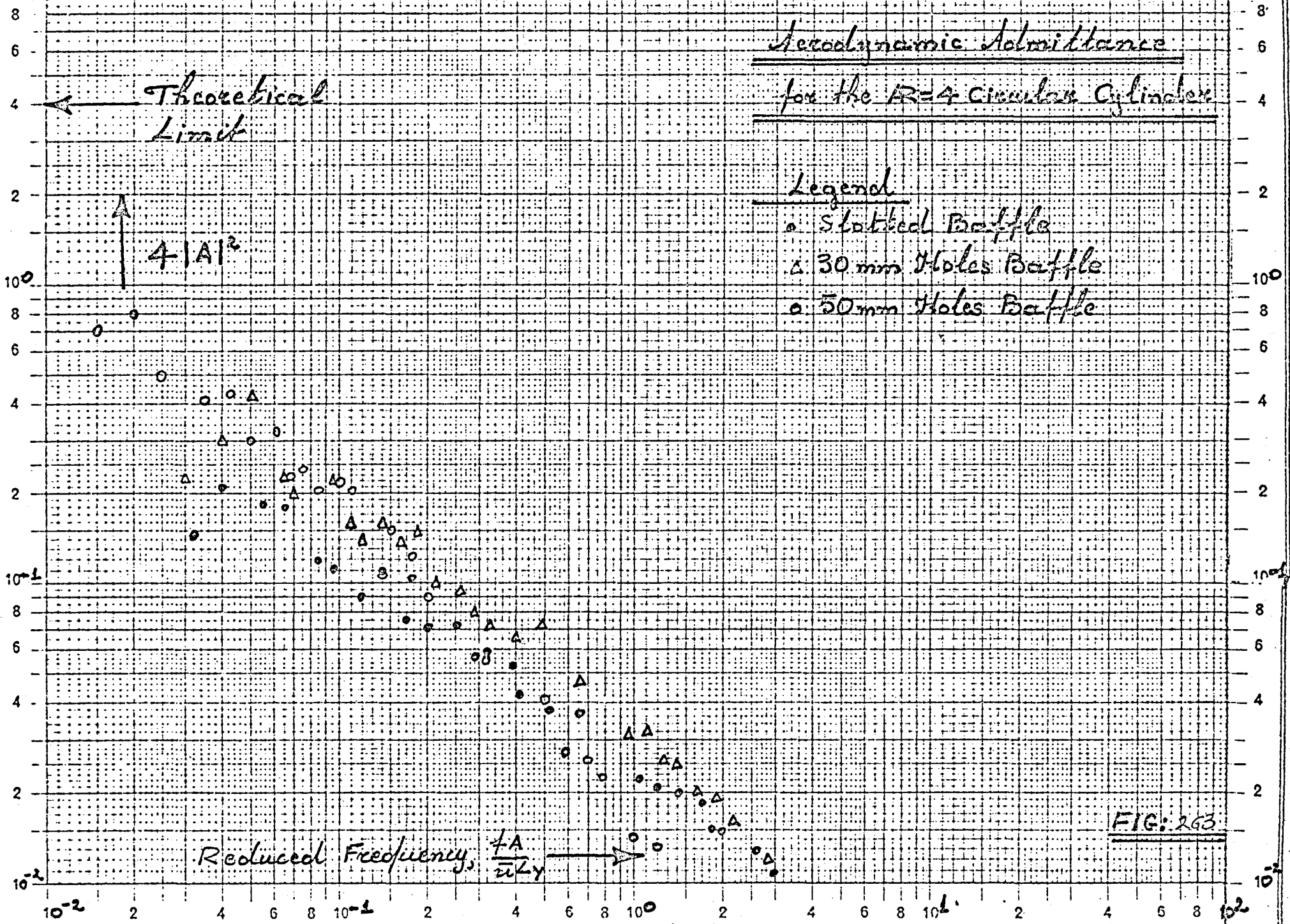
Legend

- Slotted Baffle
- △ 30 mm Holes Baffle
- 50 mm Holes Baffle

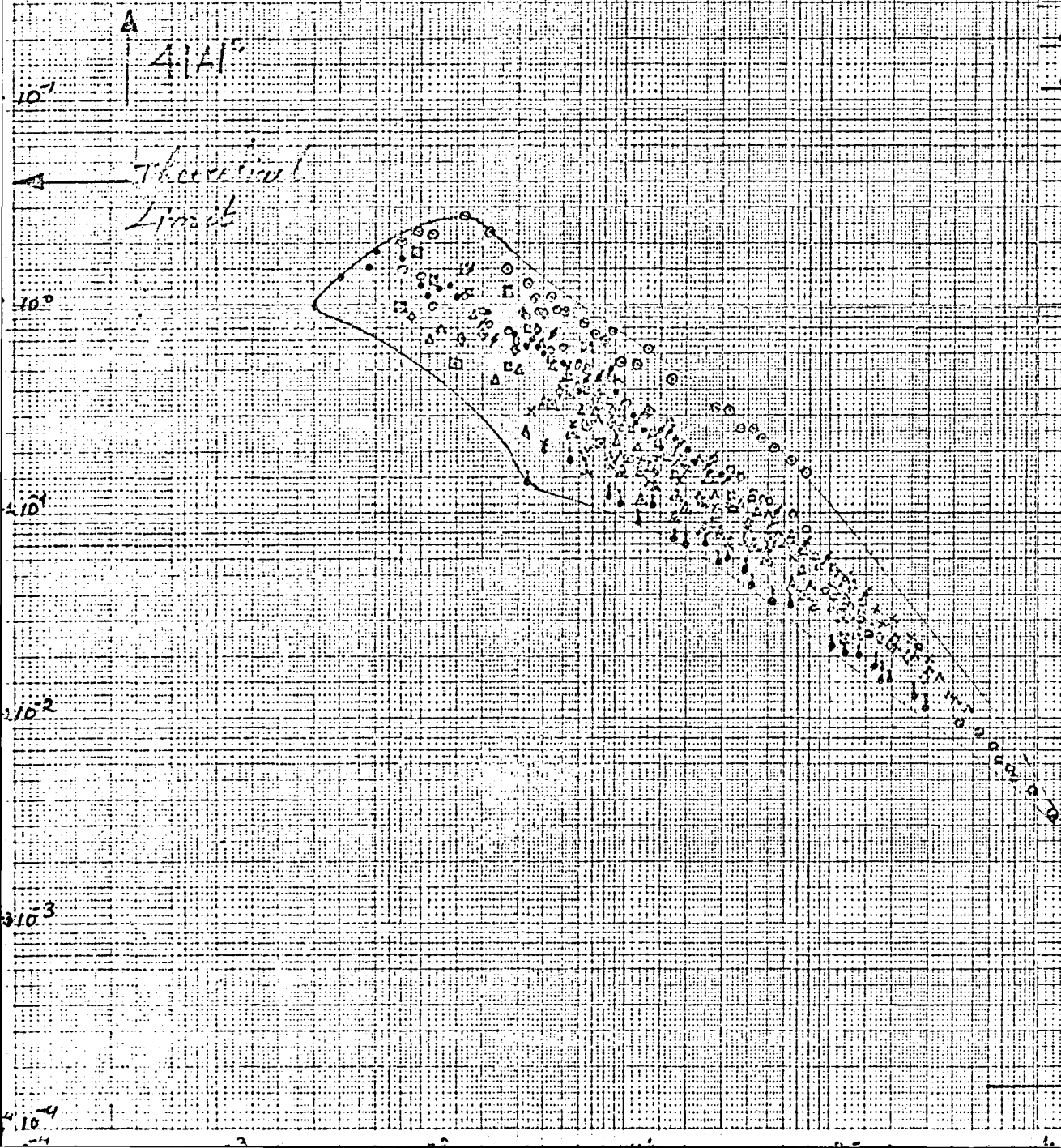
$$4|A|^2$$

Reduced Frequency, $\frac{fA}{u\lambda}$

FIG: 263



downward to distances and
different models when based
on the topographical field section
the initial section.

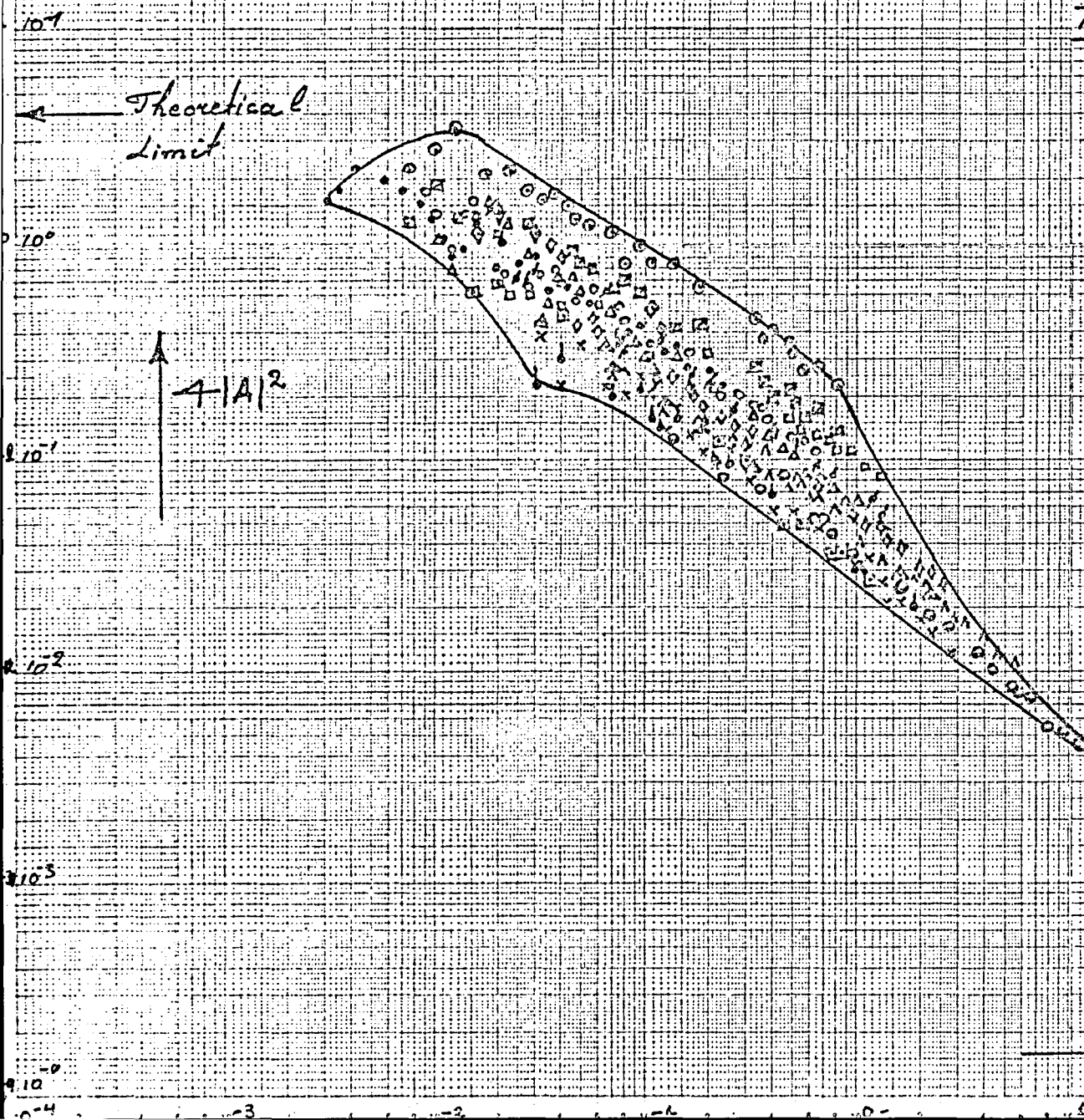


Leaves of

- | | | | |
|---|---------------------------|----------|---------|
| o | 10 mm Plate | Disc | 125 |
| A | 30 mm Plate | Disc | 125 |
| o | 30x50 mm ² | Plate | |
| A | 30x50 mm ² | Plate | |
| x | 30x110 mm ² | Plate | |
| ✓ | 42.5x42.5 mm ² | Plate | |
| o | 60x60 mm ² | Plate | |
| h | 85x85 mm ² | Plate | |
| o | 110x120 mm ² | Plate | |
| o | 30 mm | Stole | Cube |
| A | 30x30x30 mm ³ | Schwarz | Schwarz |
| A | 35x35x35 mm ³ | Schwarz | Schwarz |
| h | R=1 Circular | Cylinder | |
| h | R=2 Circular | Cylinder | |
| h | R=4 Circular | Cylinder | |

Reduced Frequency: $\frac{1}{2}$

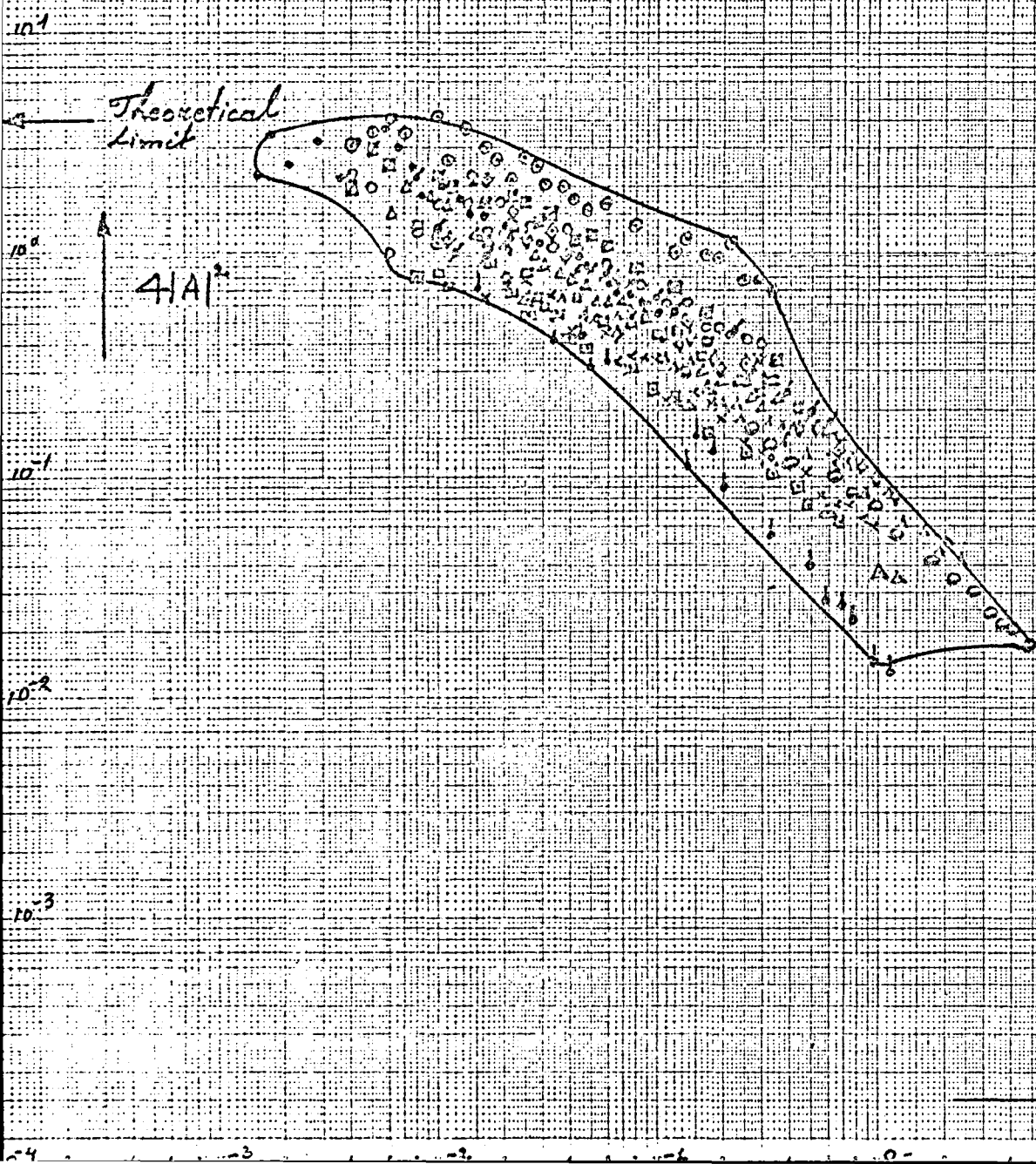
Aerodynamic Admittance for the Different Models when Placed in the Turbulent Field Produced by the 30mm Holes Baffle



Legend

- 20mm Dia. Disc
- △ 40mm Dia. Disc
- 30x30mm² Plate
- 30x60mm² Plate
- × 30x120mm² Plate
- ◇ 42.5x42.5mm² Plate
- ◊ 60x60mm² Plate
- ∧ 85x85mm² Plate
- 120x120mm² Plate
- 30mm Side Cube
- ◇ 30x30x60mm³ Square Section Cylinder
- △ 30x60x120mm³ Square Section Cylinder
- R=1 Circular Cylinder
- R=2 Circular Cylinder
- R=4 Circular Cylinder

Aerodynamic Admittance for the Different Models when Placed in the Turbulent Field Produced by the 50 mm Vortex Bench



Reduced Frequency, $\frac{fA}{uL}$

FIG. 200

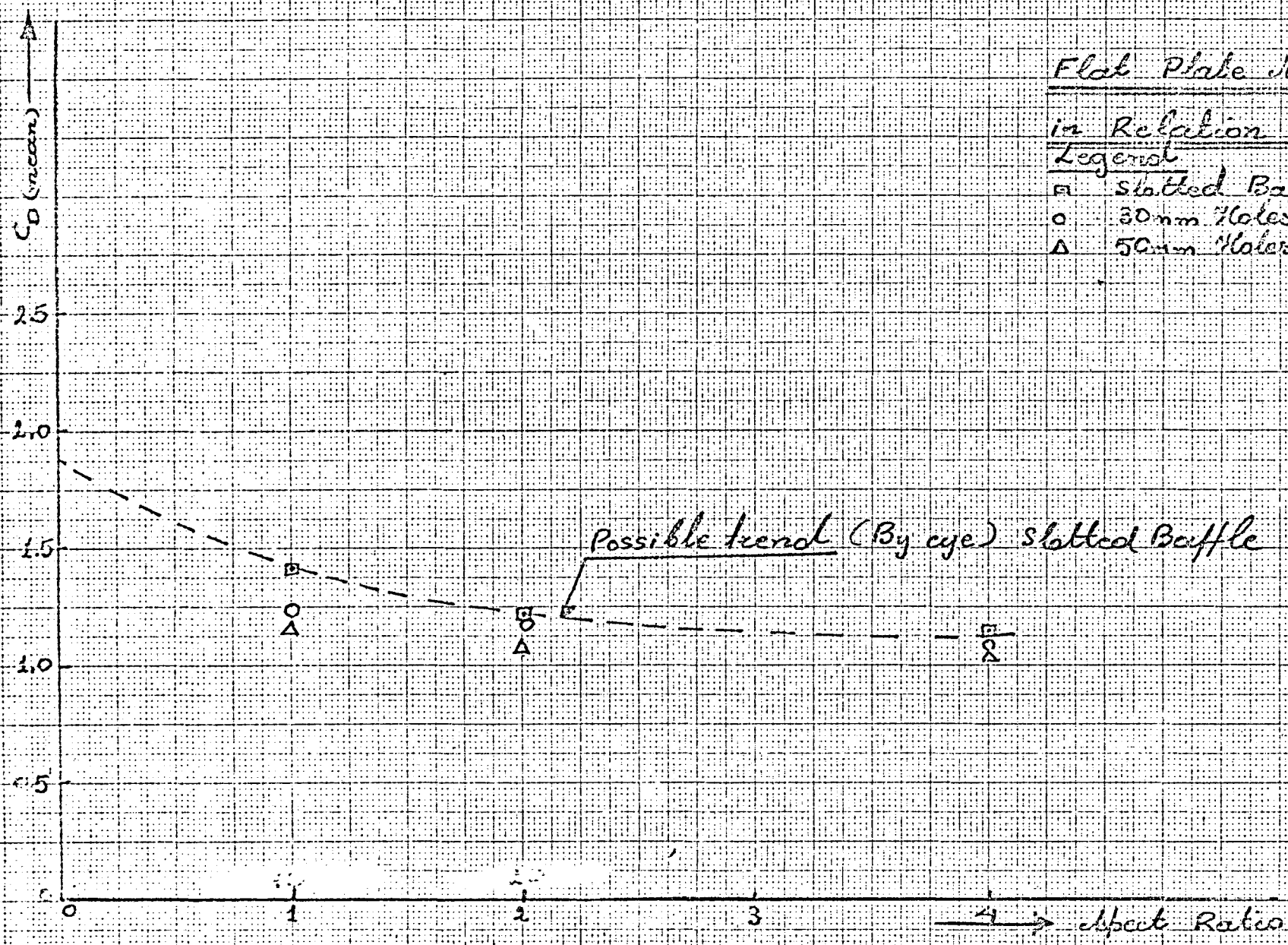
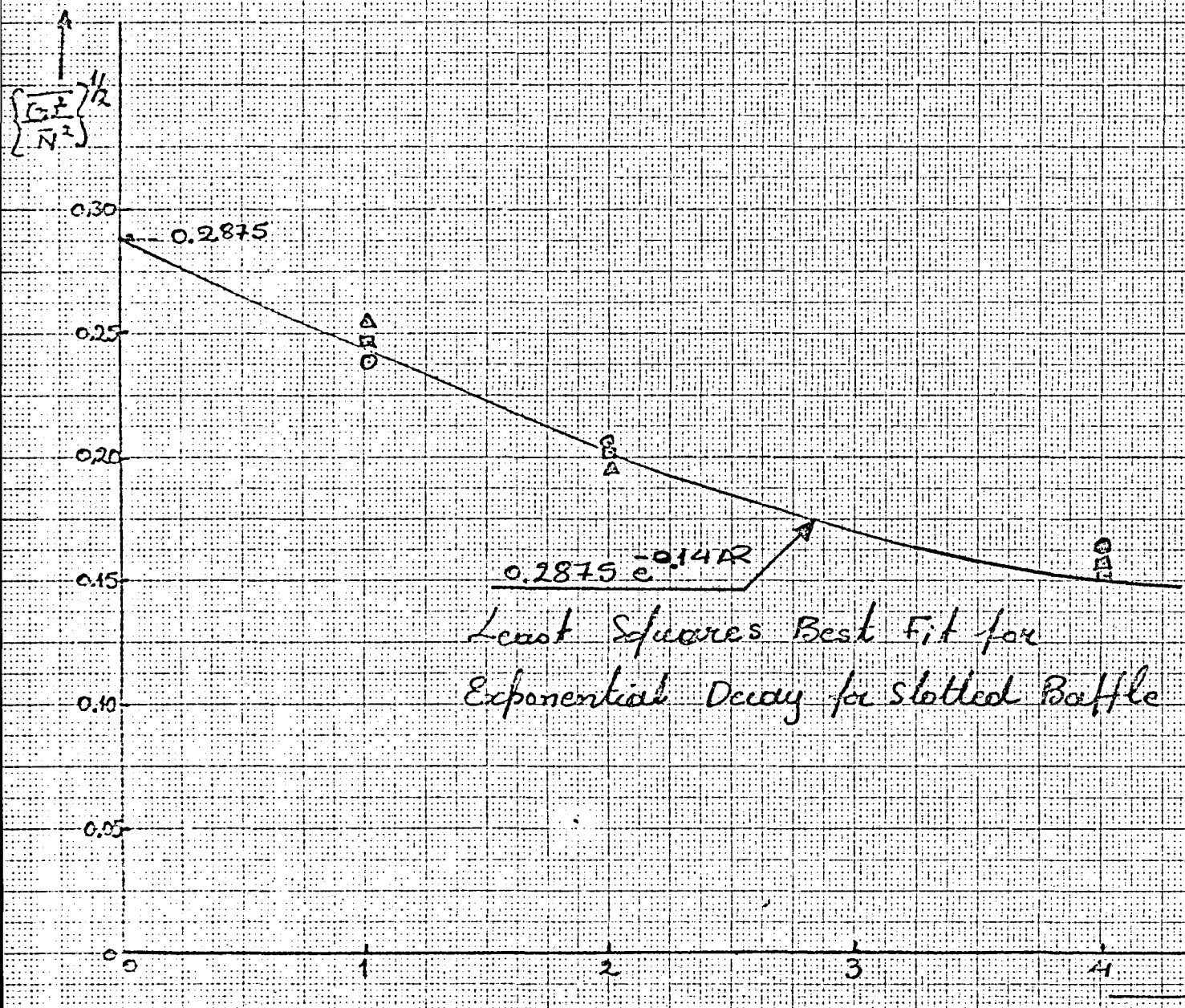


FIG: 267



Fluctuating Drag/Heave Drag of Flat Plates in Relation to R .

- Legend
- \square Slotted Baffle
 - \circ 30mm Slots Baffle
 - \triangle 50mm Slots Baffle

Least Squares Best Fit for
 Exponential Decay for Slotted Baffle

Flat Plate Mean Drag in Relation to Frontal Area

Legend

- Slatted Baffle
- 30mm Holes Baffle
- △ 50mm Holes Baffle

* → Refers to discs

(Frontal area of disc is not compared
to those of other plates)

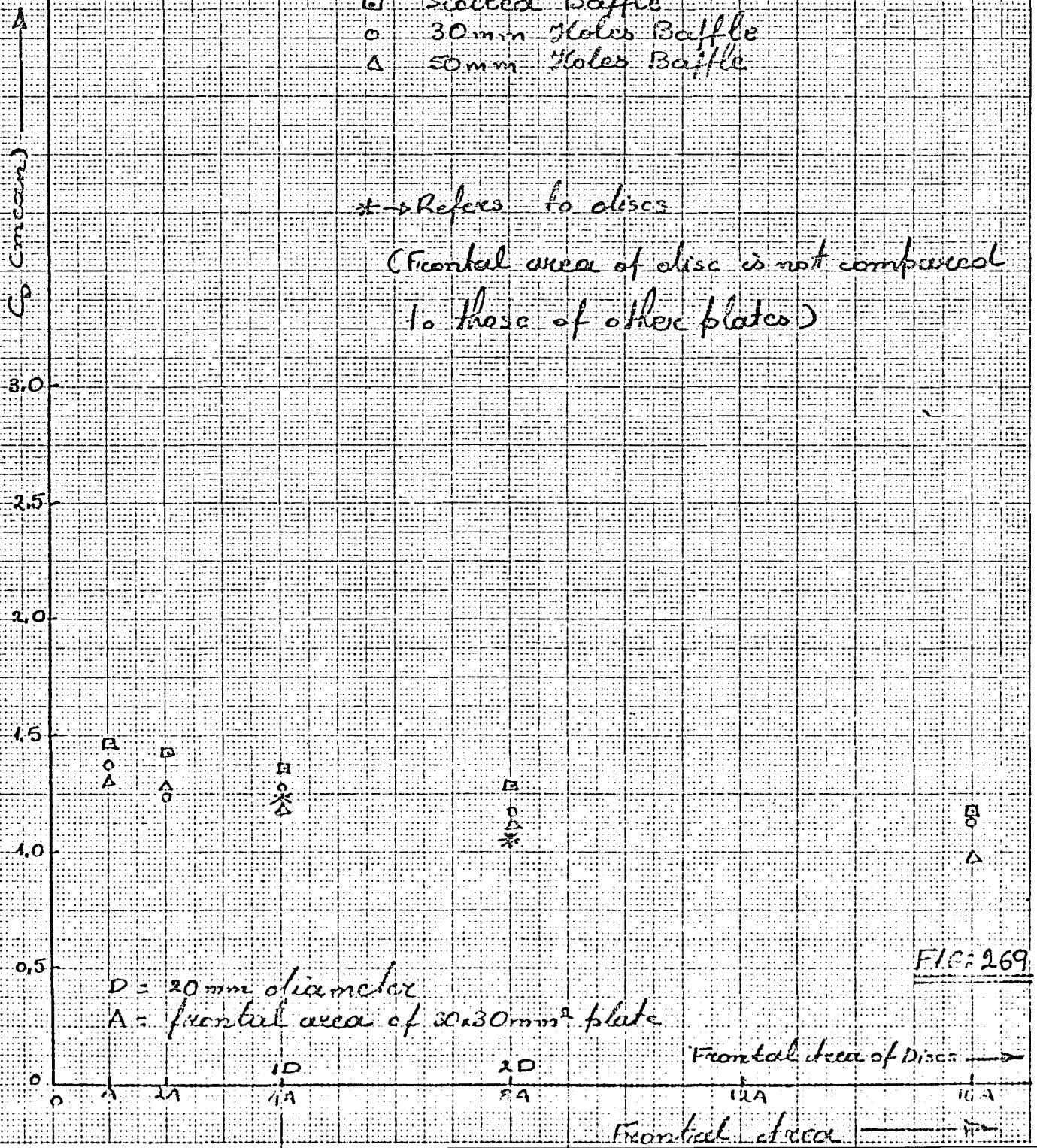


FIG: 269

Flat Plate "Fluctuating Drag / Steady Drag, in Relation to Frontal Area,

Legend

- Slotted Baffle
- 30 mm holes Baffle
- △ 50 mm holes Baffle

* → Refers to discs

(Frontal area of discs is not compared to those of other plates)

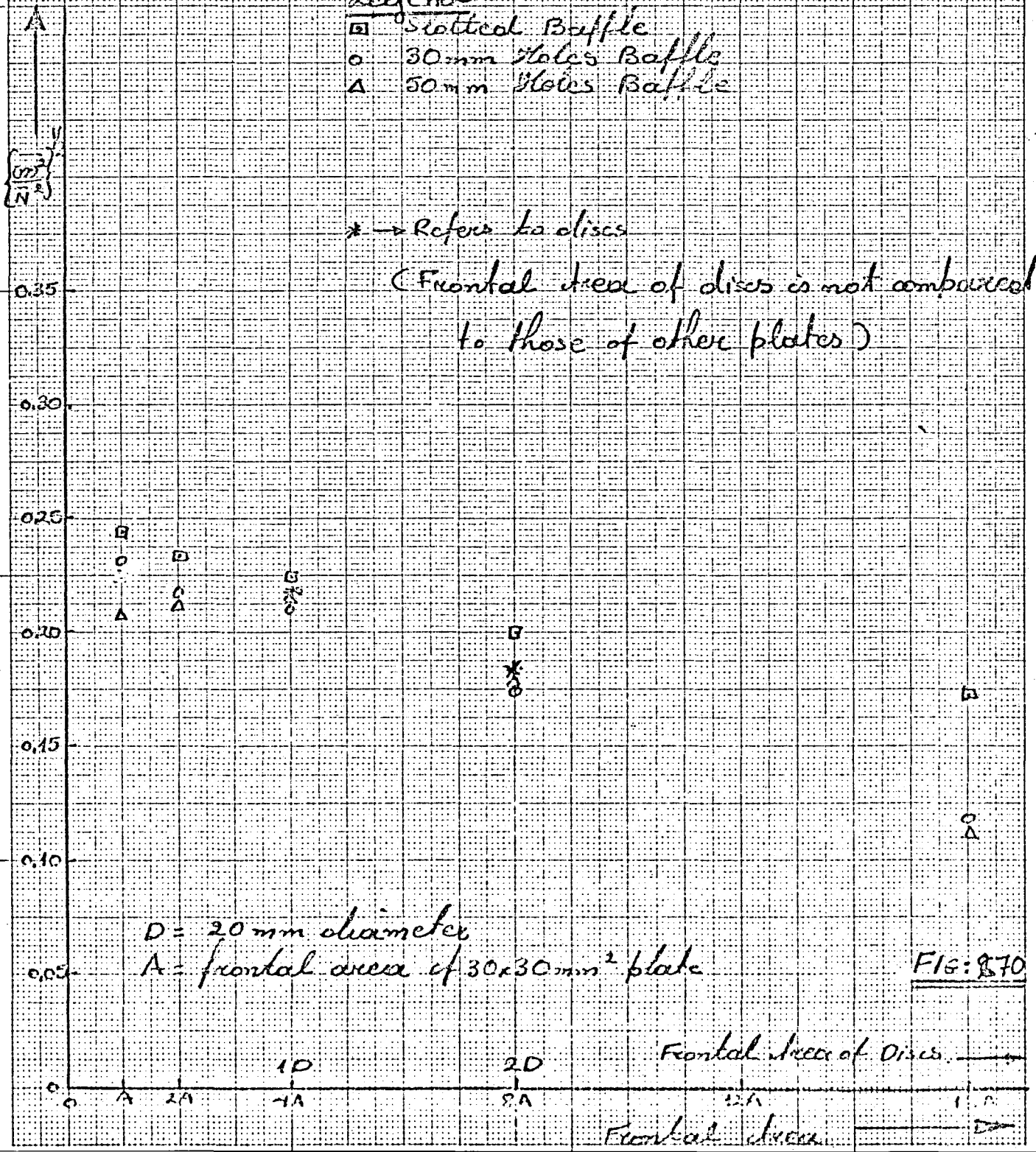


FIG: 870



FIG: 271

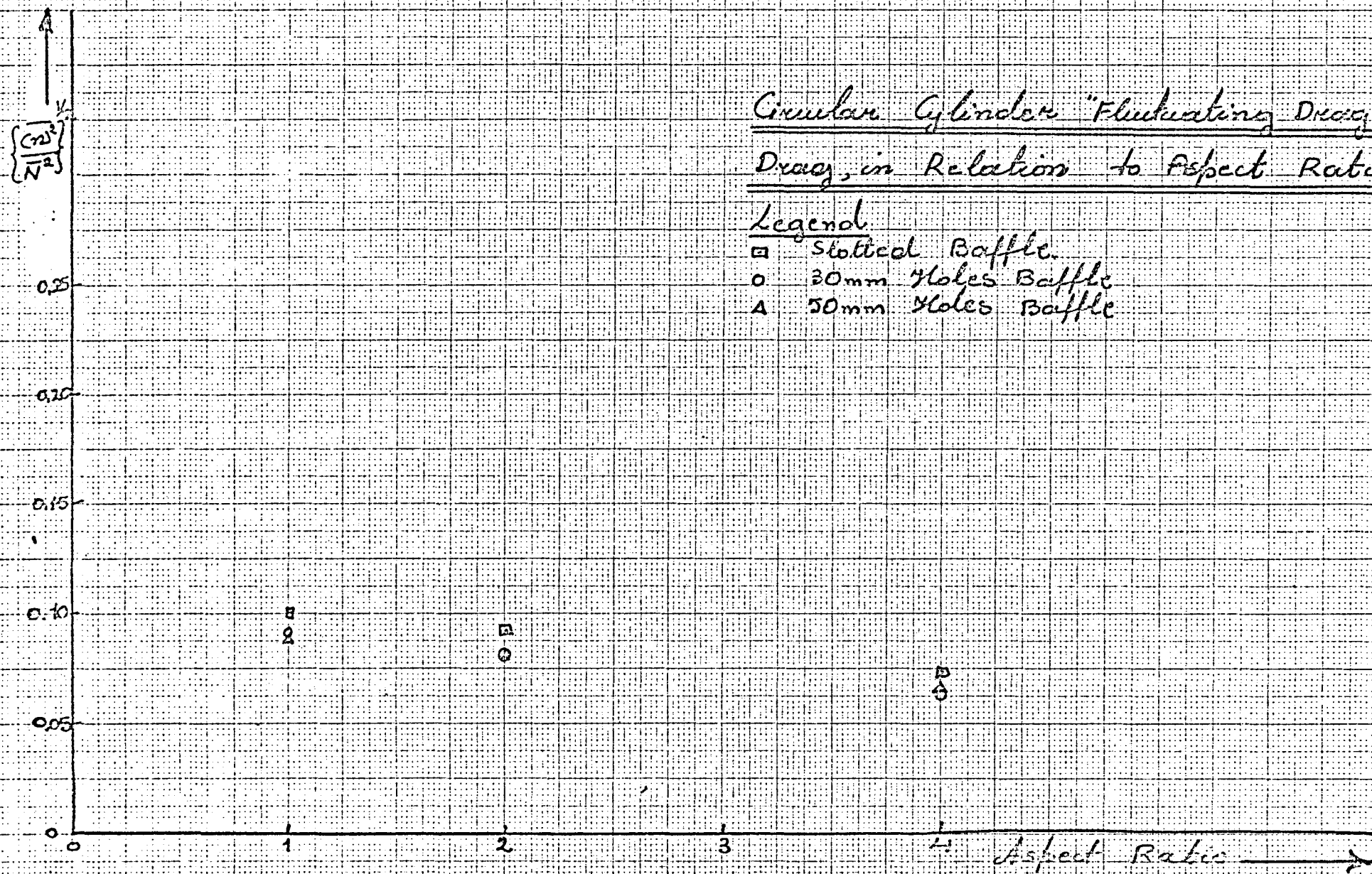
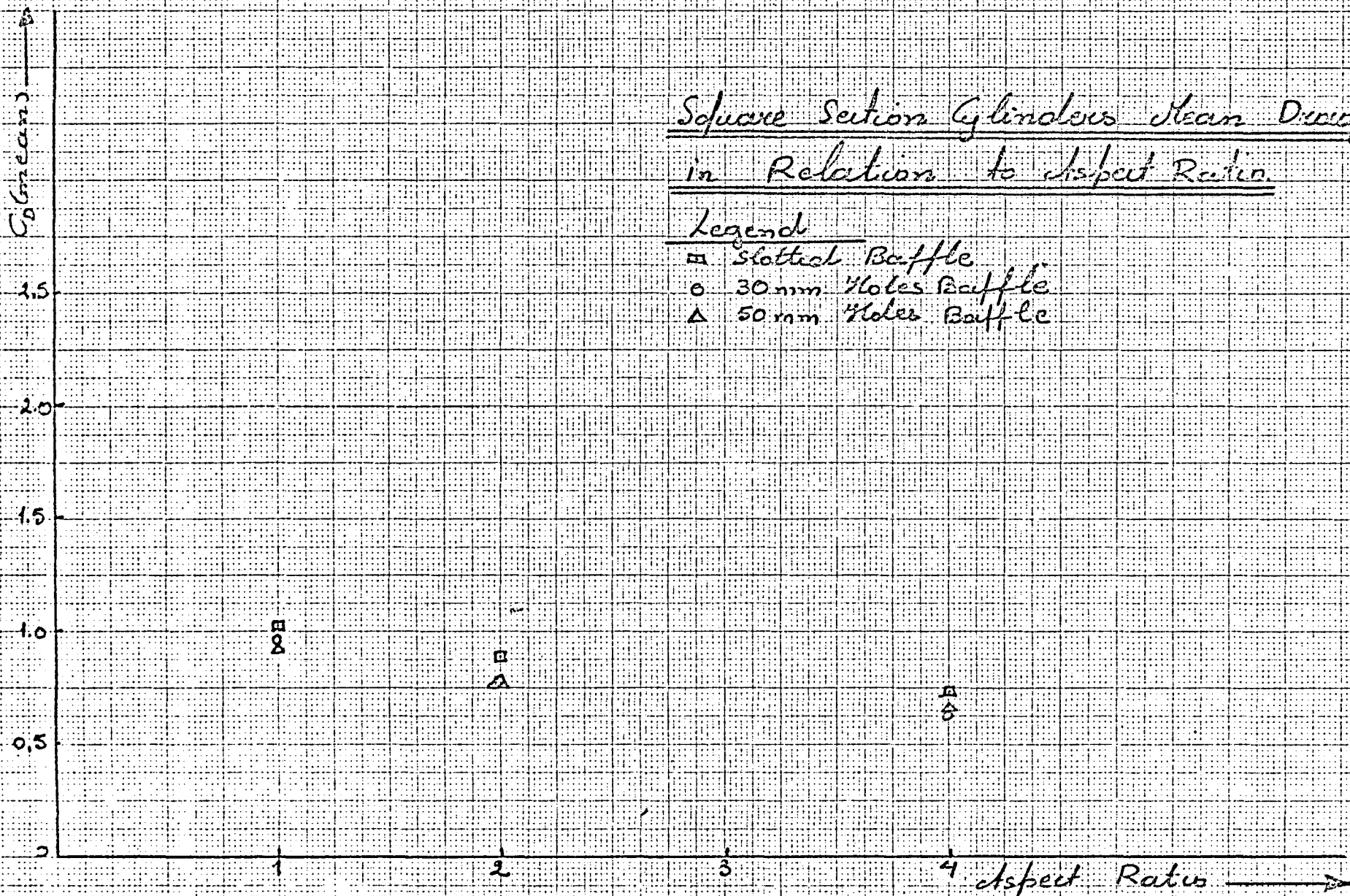


FIG. 272.

Square Section Cylinders Mean Drag
in Relation to Aspect Ratio.

Legend

- Slotted Baffle
- 30 mm Holes Baffle
- △ 50 mm Holes Baffle



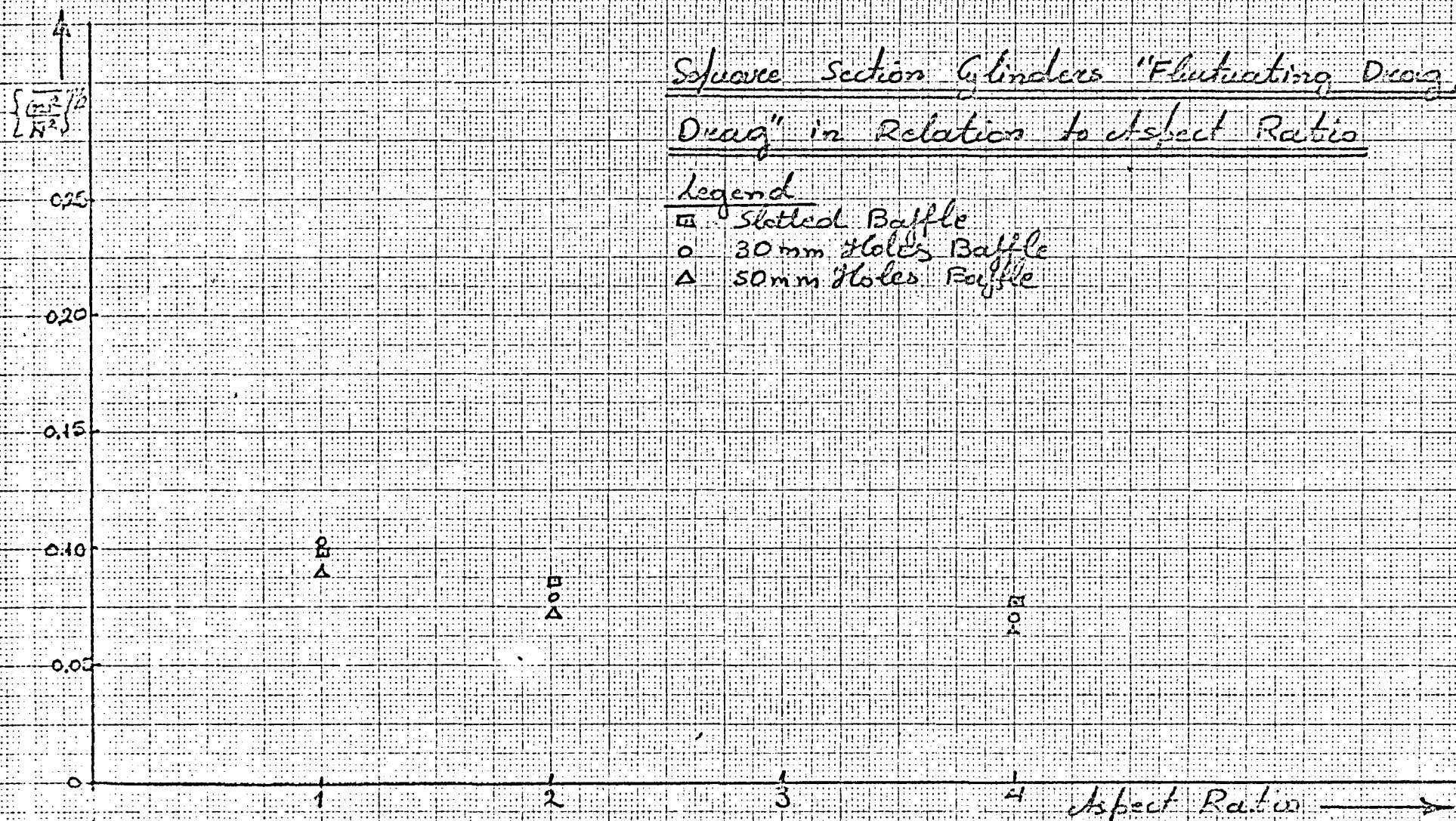
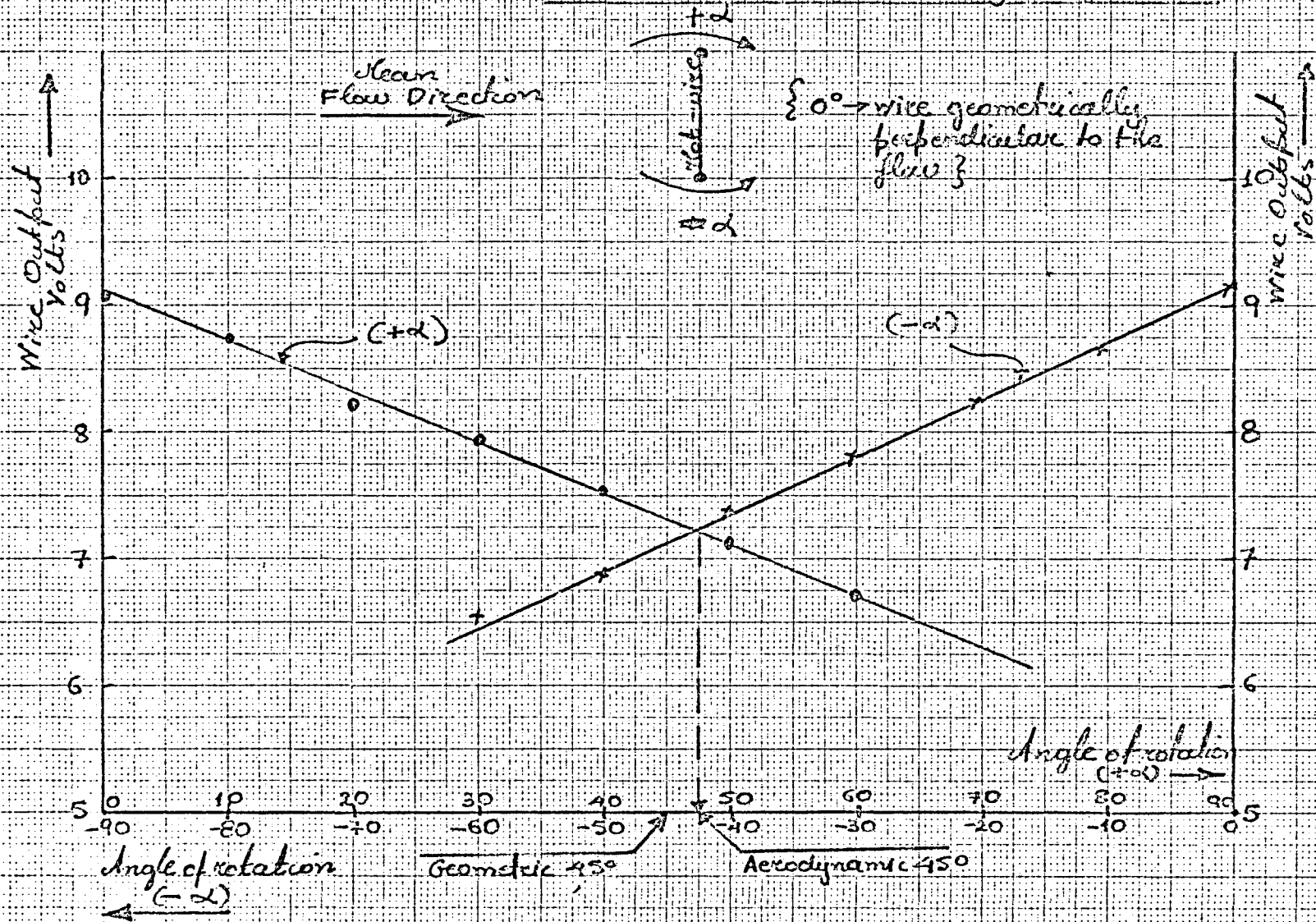
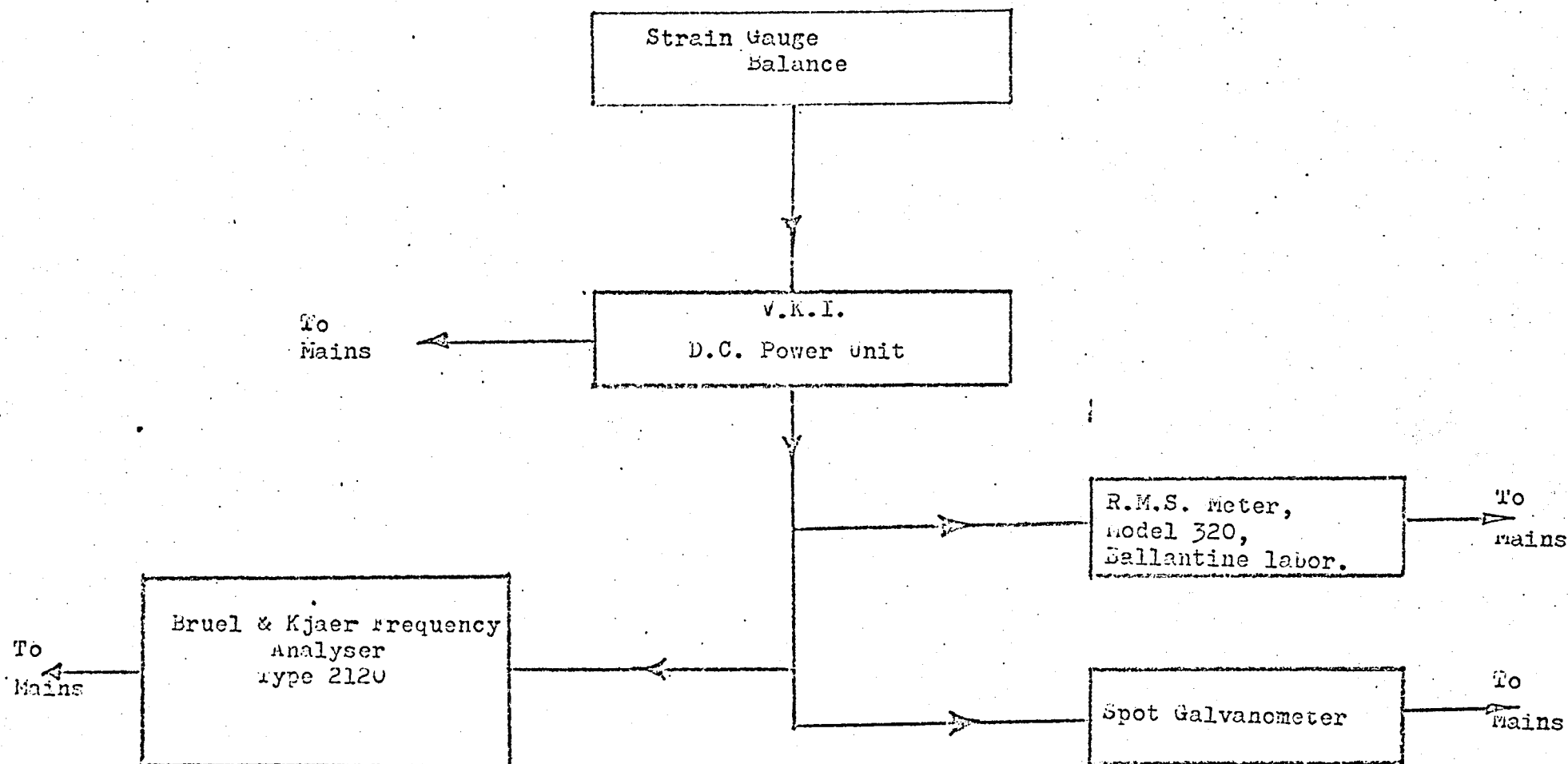


FIG. 274

Determination of the Mean Flow Direction Relative to the Rotating Hot-wire.





Block Diagram for the measurement of the Mean and Fluctuating Drag Forces.

FIG: 276

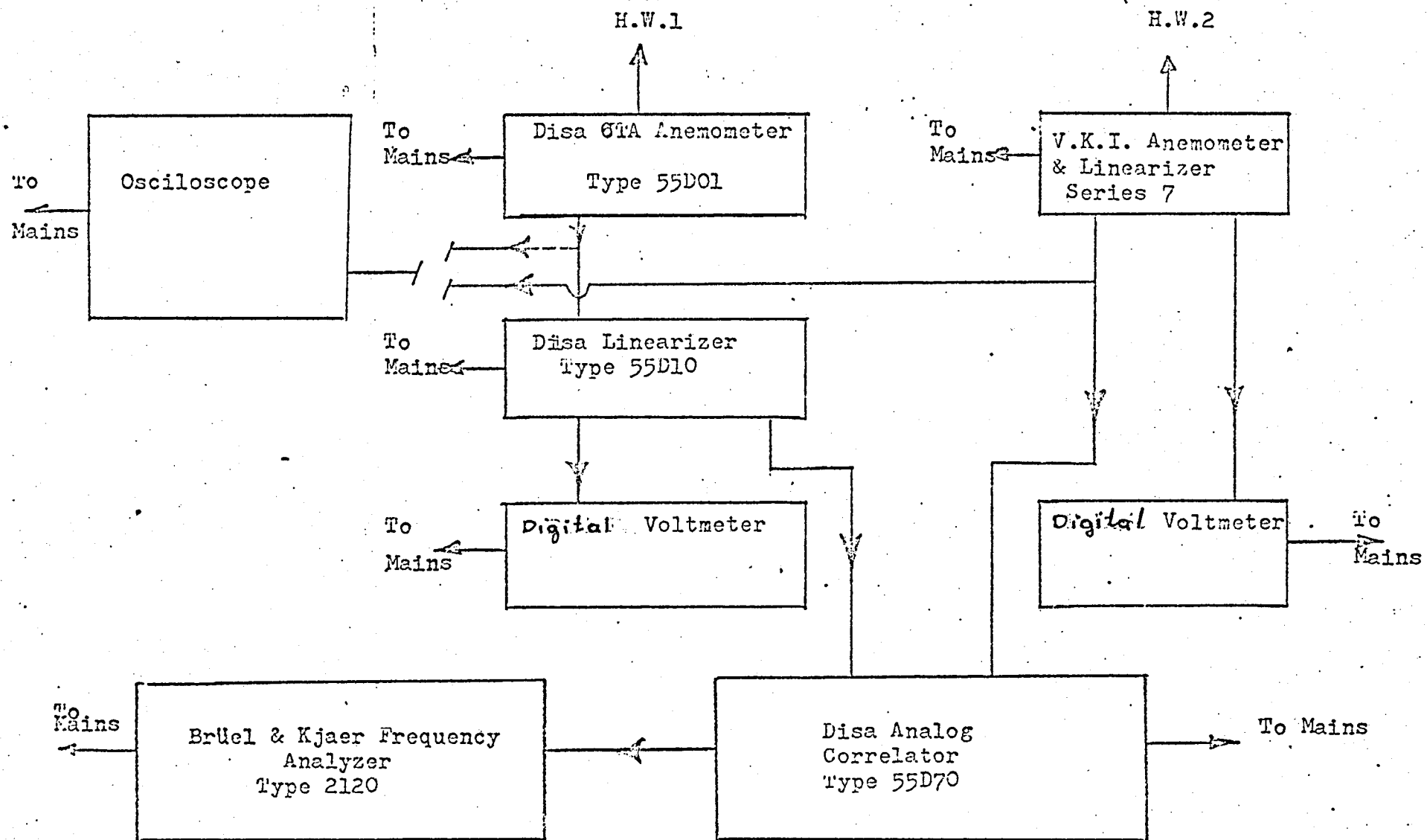


FIG: 278

Block Diagram for the Measurement of the Frequency-Dependent Correlation Coefficient $K_{11}(0, r_2, 0)$

Typical Probability Density Function Displayer

Calibration Circuit.

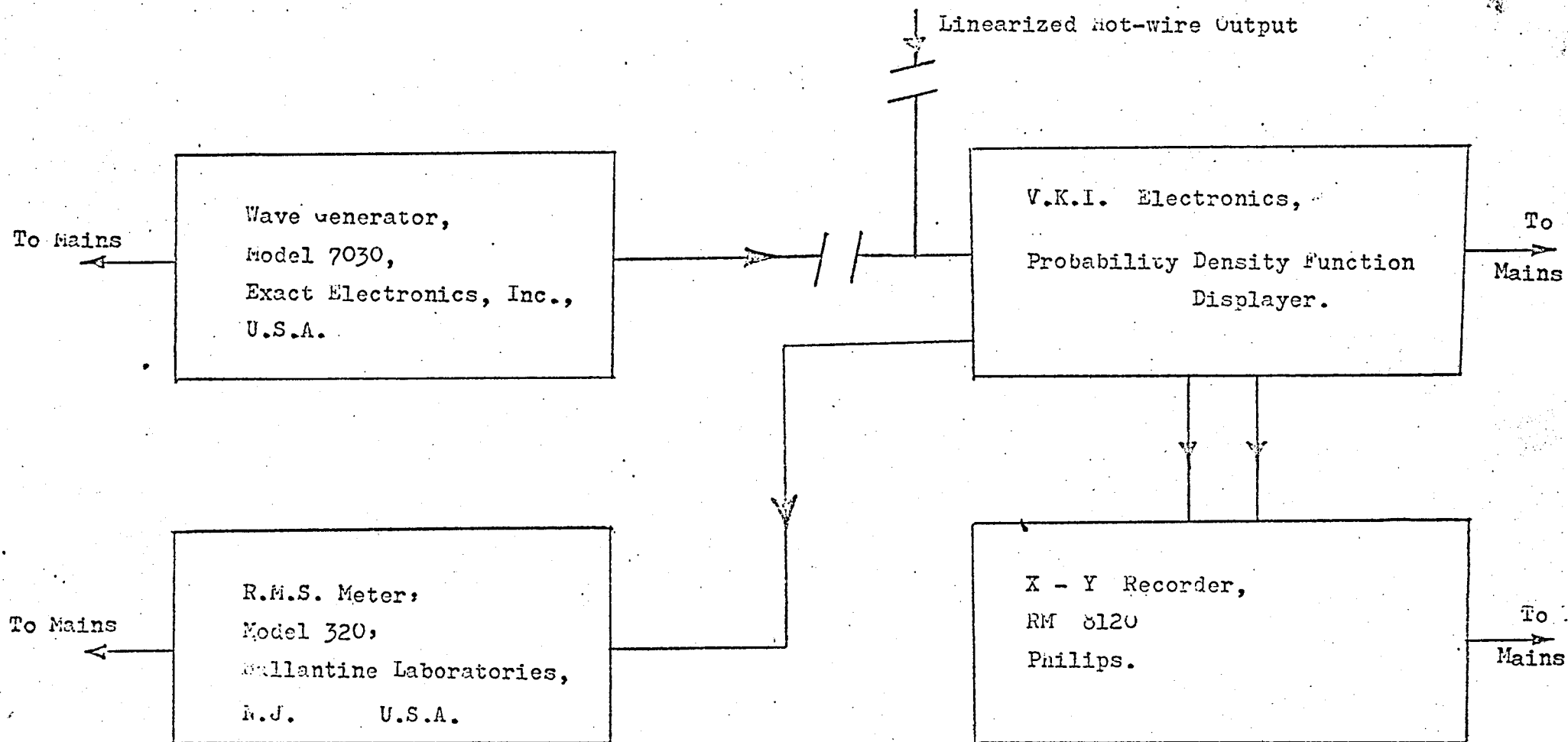
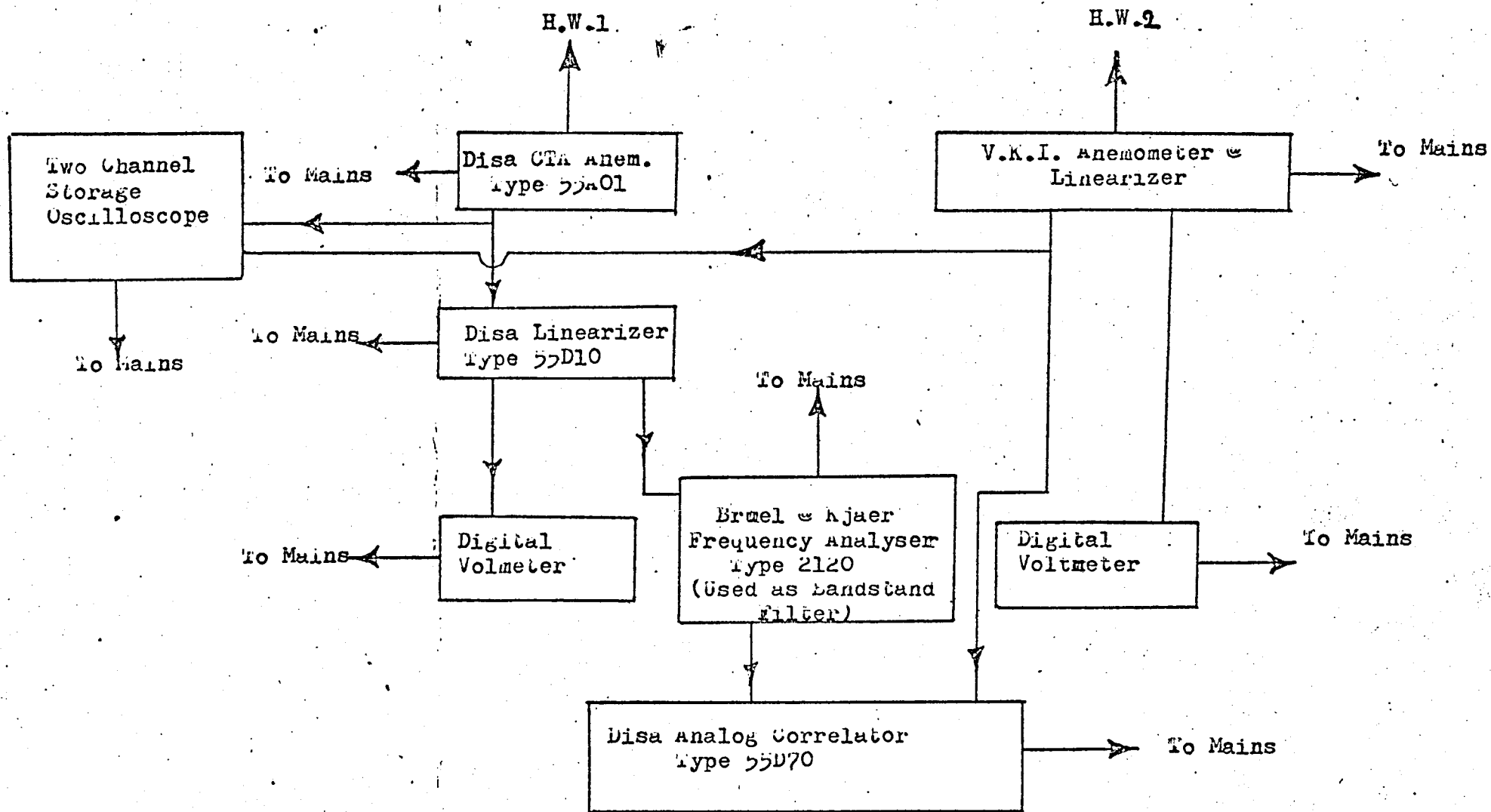
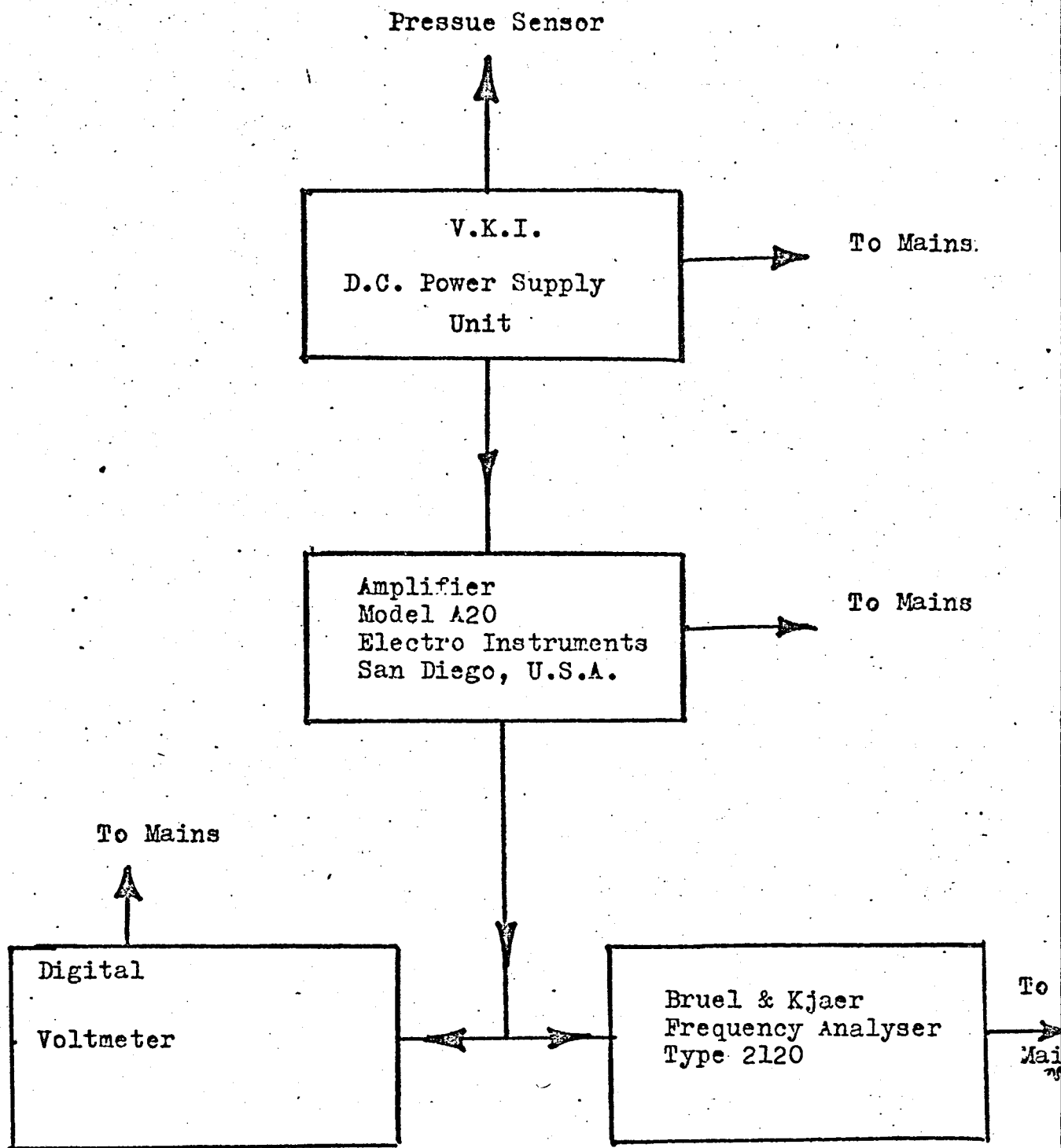


FIG: 279

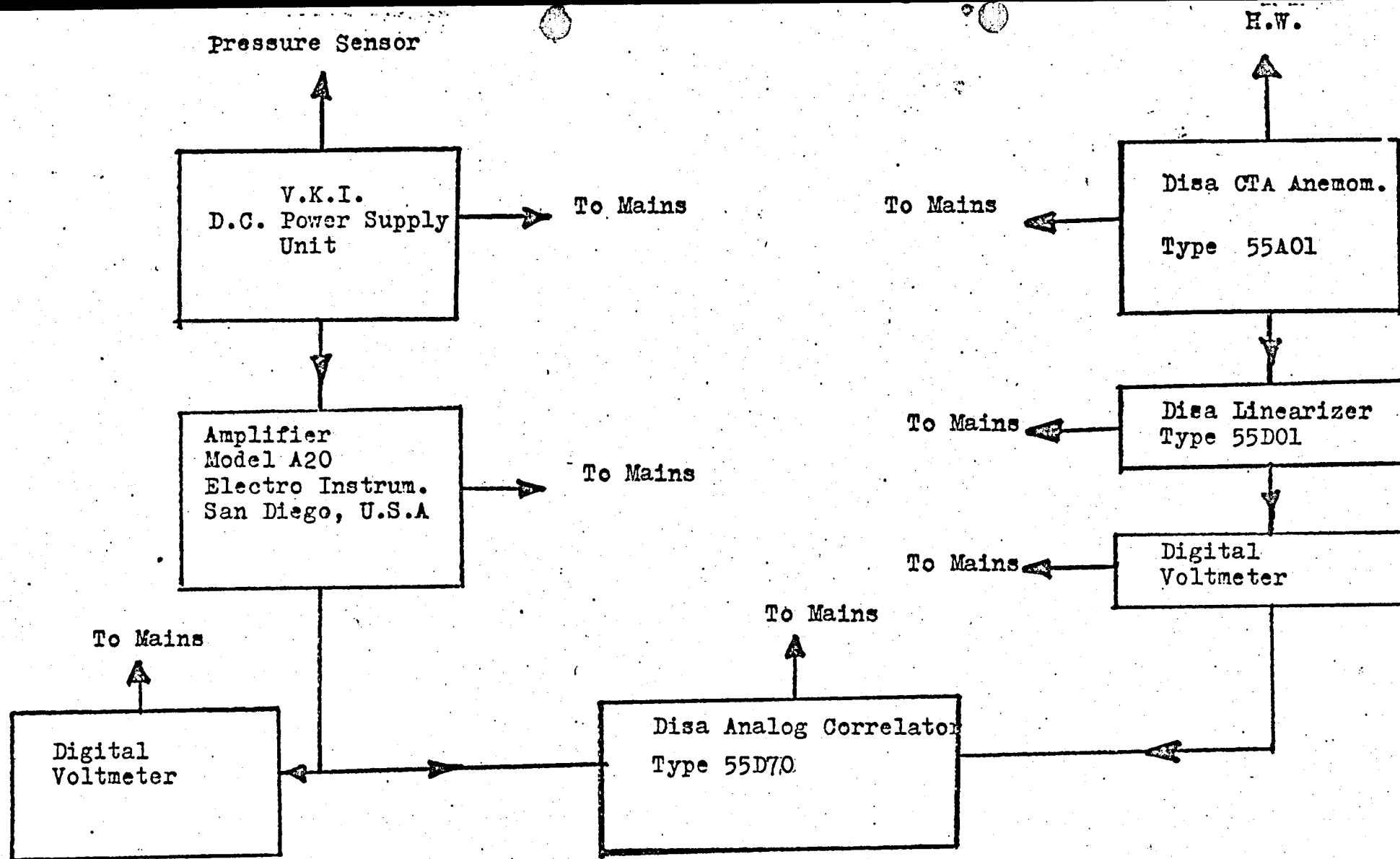


Block Diagram for the Measurement of the Lateral and Longitudinal Space Correlations of u' when the Model is Externally Oscillated.

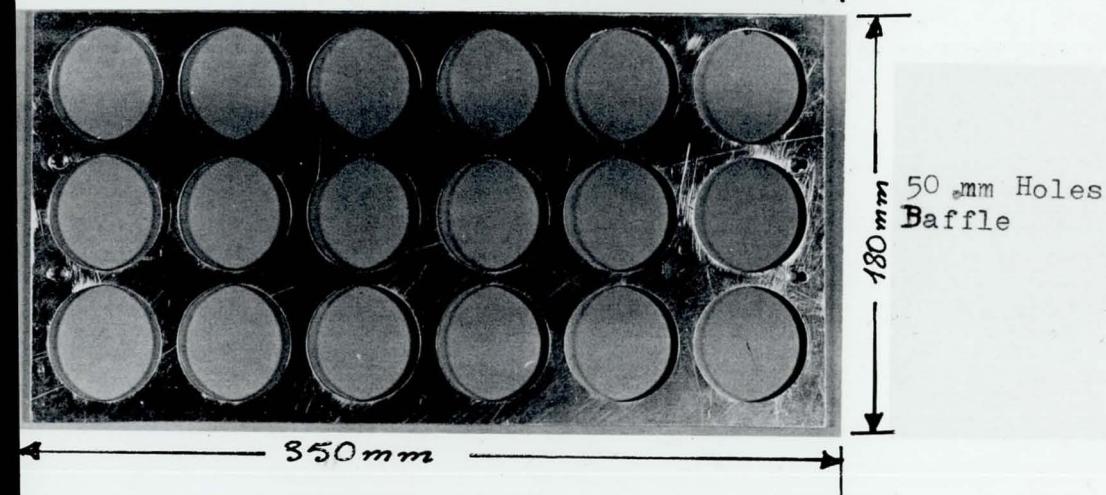
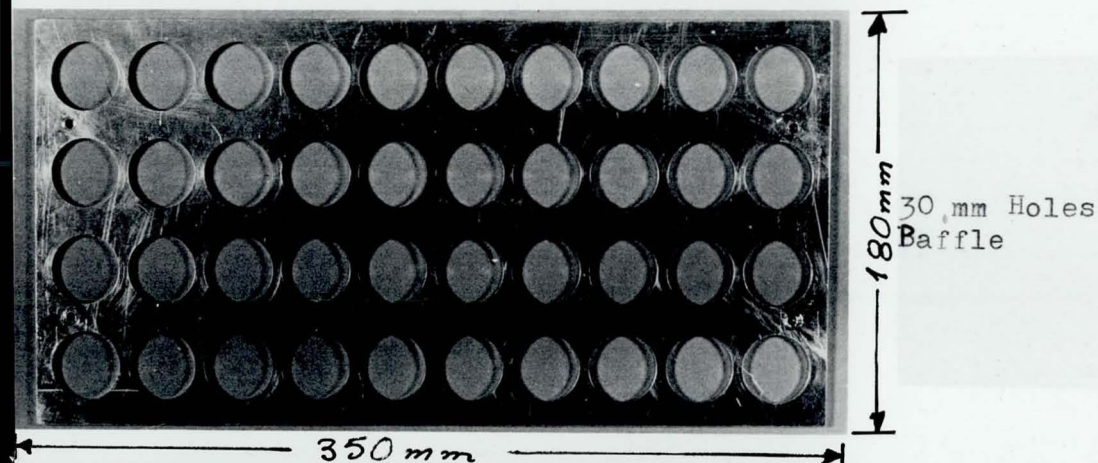
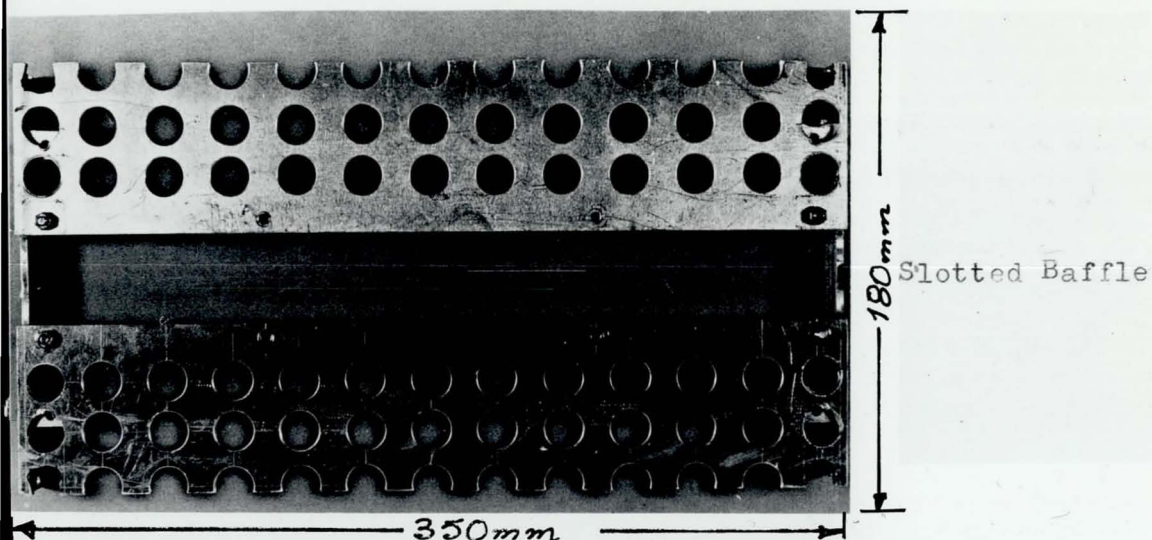


Block Diagram for the Measurement of the Pressure Spectrum.

FIG: 281

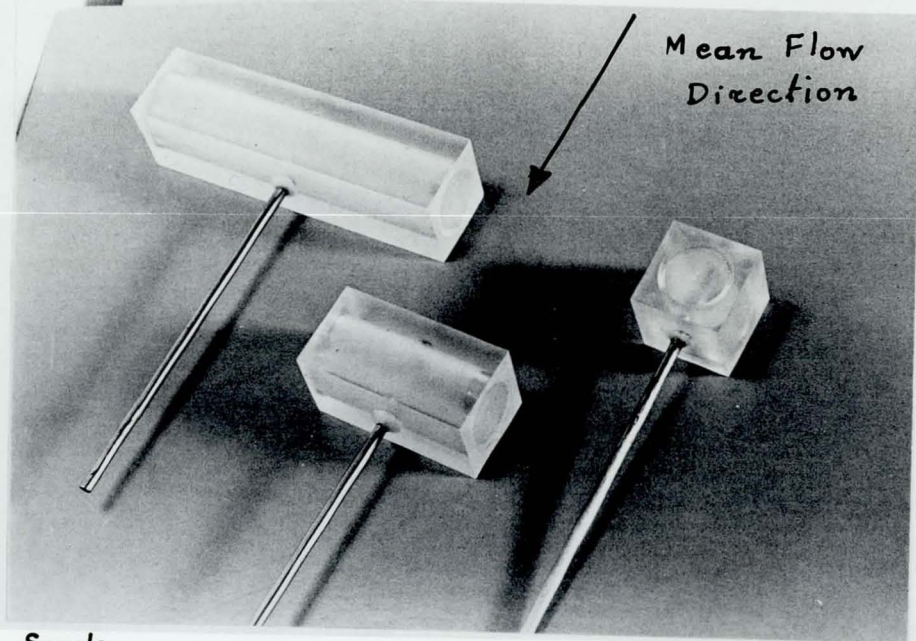


Block Diagram for the Measurement of the Pressure-
-Velocity Space Correlation.

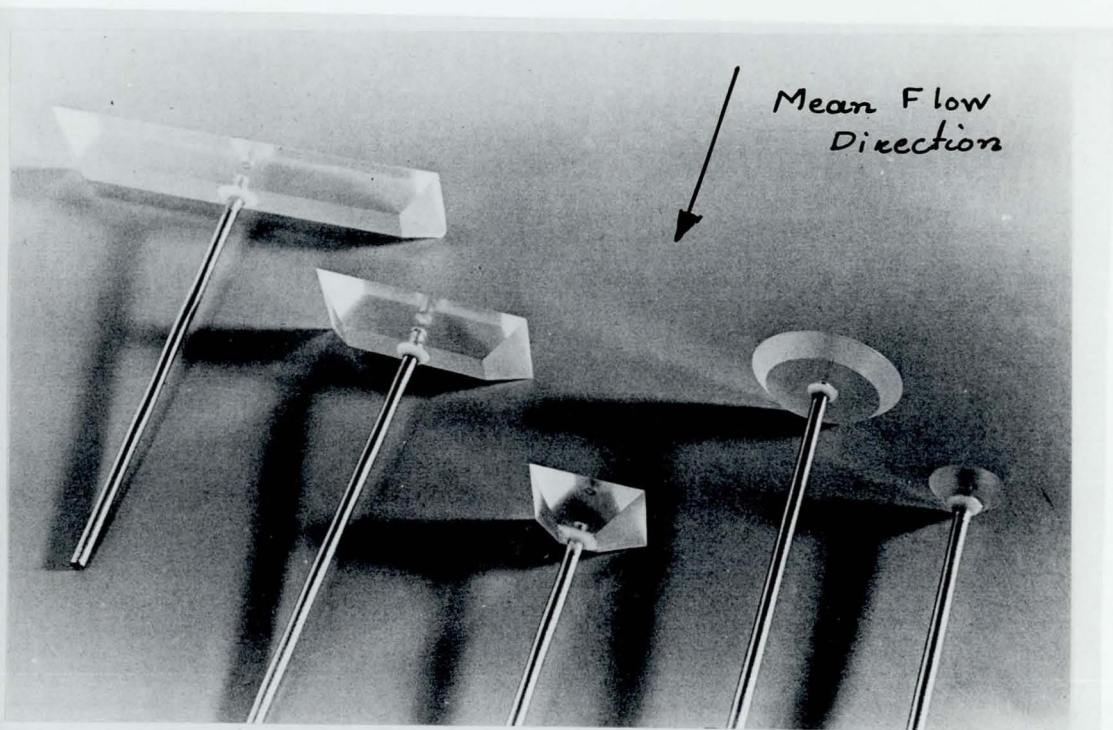


Baffles used for the generation of Turbulence

PL.I

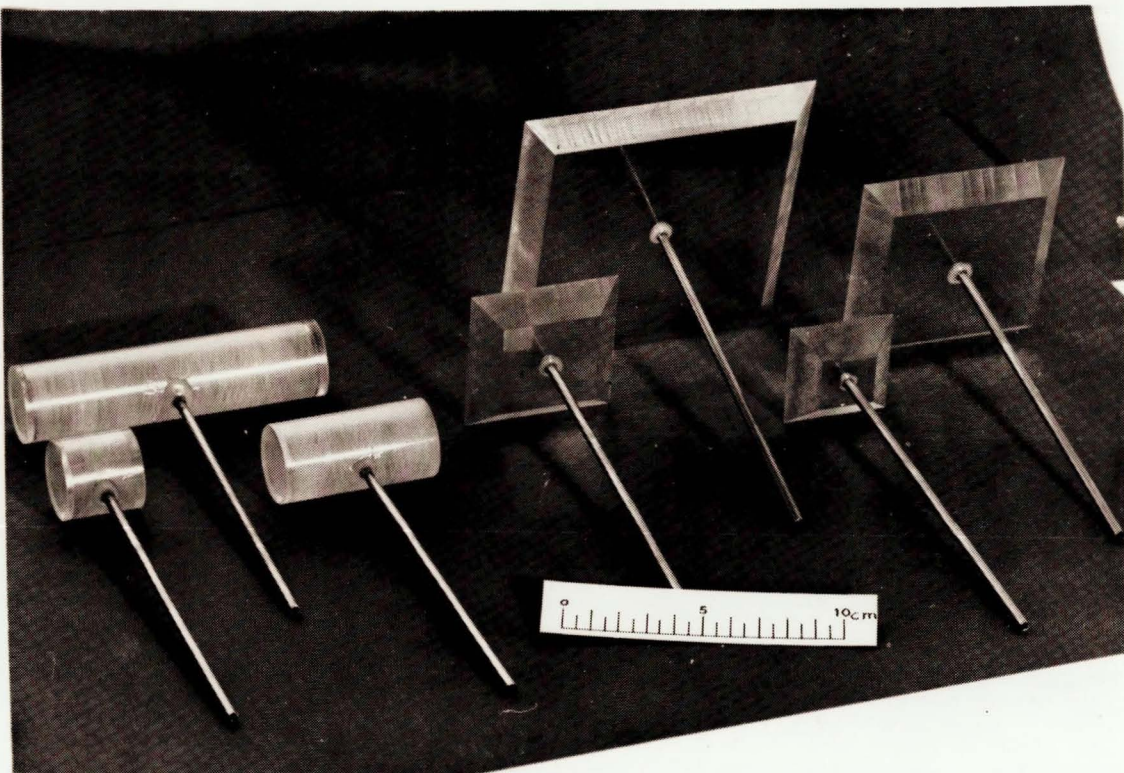


Scale
60 mm



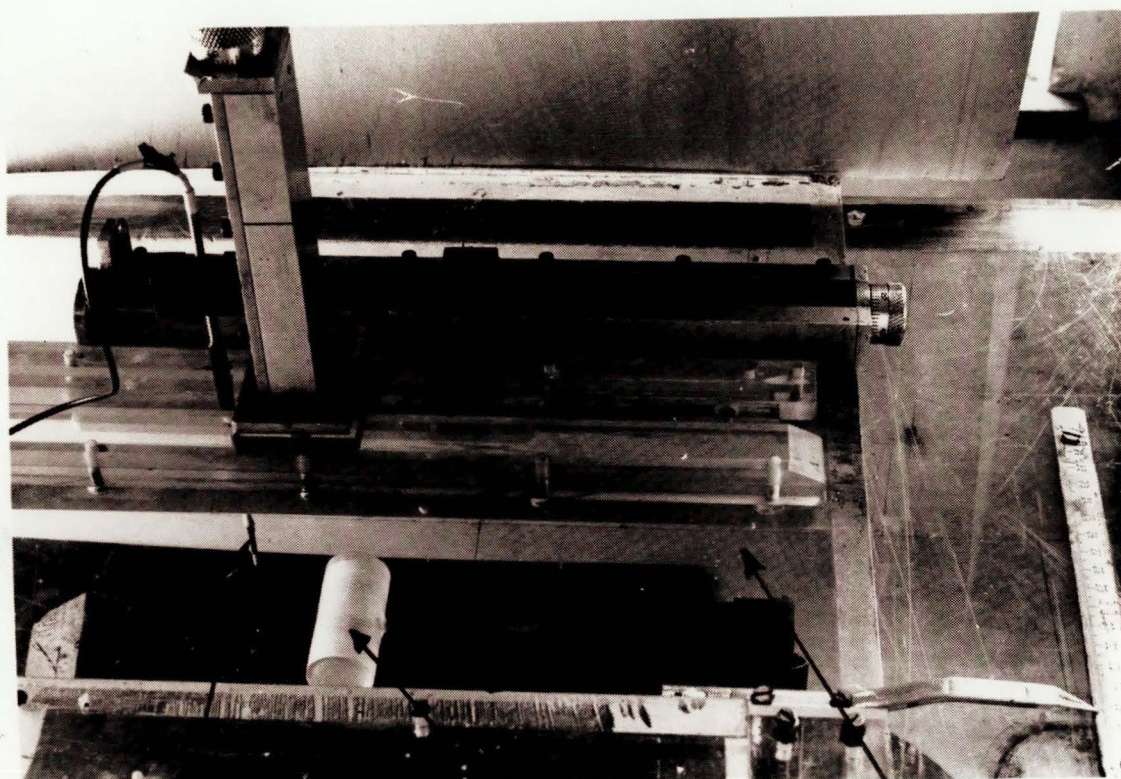
Models Tested

PL.II



MODELS TESTED

PL. III



HOT-WIRE PROBE

MODEL

THREE DEGREES OF FREEDOM
MECHANISM

EXPERIMENTAL SET-UP FOR THE DETERMINATION OF THE VARIATION
OF THE WAVENUMBER IN FRONT OF THE
MODELS

PL. IV

R.M.S. METER

WAVE
GENERATOR

LINEARIZER

PROBABILITY
DENSITY
FUNCTION
DISPLAYER

ANEMOMETER

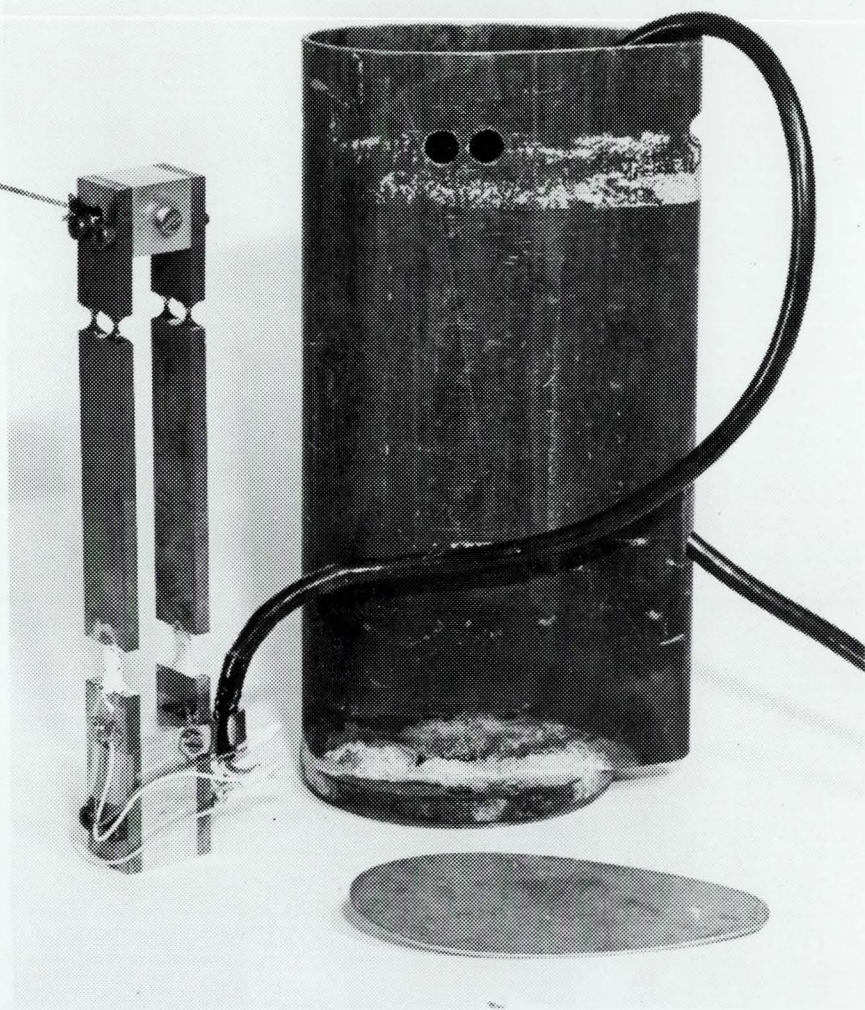
DIGITAL
VOLTMETER

X-Y RECORDER

Instrumentation used in the determination of
probability density function.

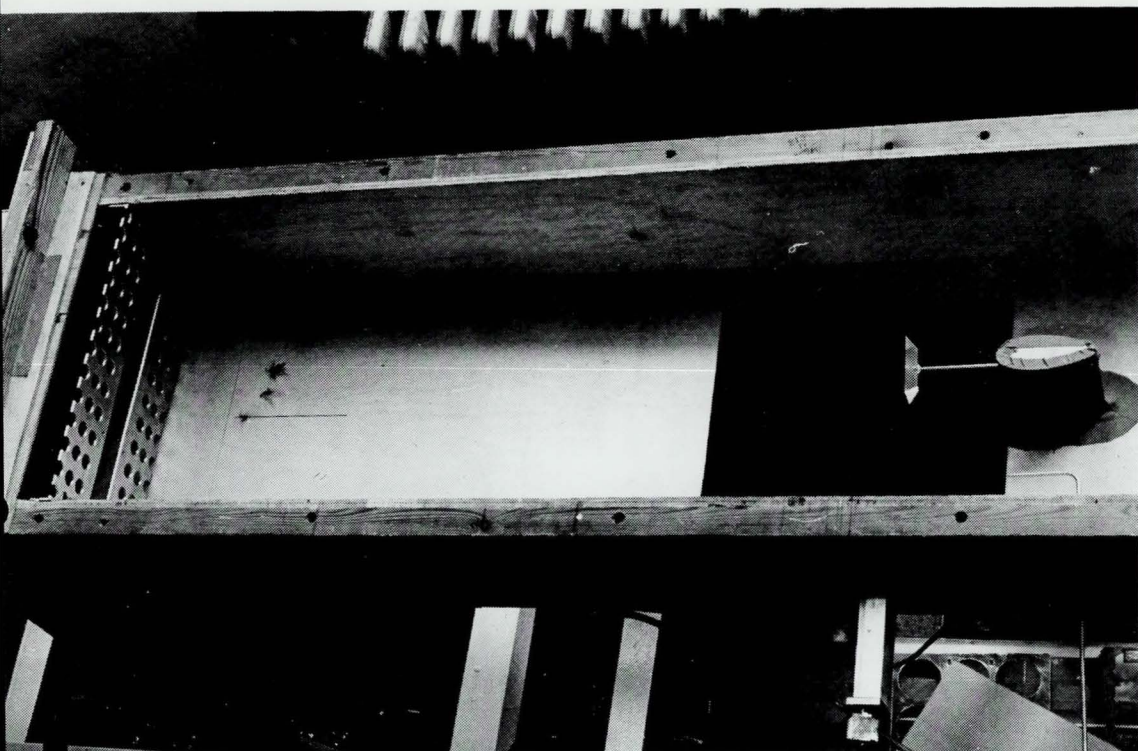
PL.V

MODEL
ATTACHMENT

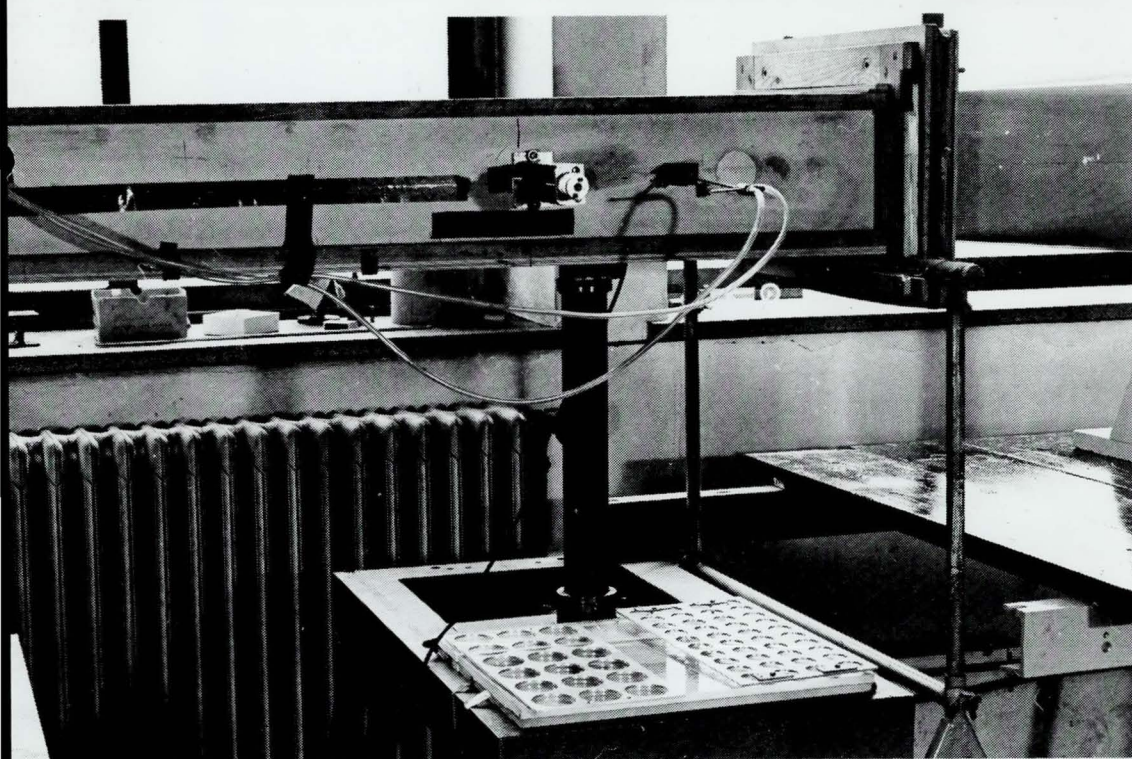


STRAIN GAUGE BALANCE AND SHIELD.

PL.VI

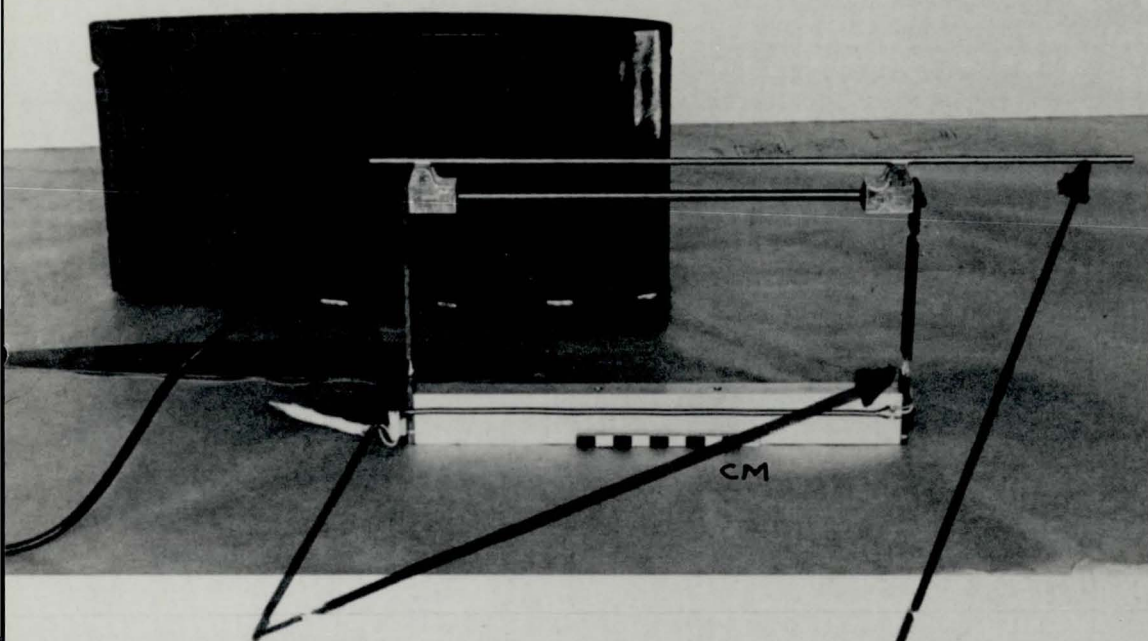


TURBULENCE BAFFLE, MODEL AND BALANCE ASSEMBLY : PLATE VII



BALANCE SUPPORT

PLATE VIII

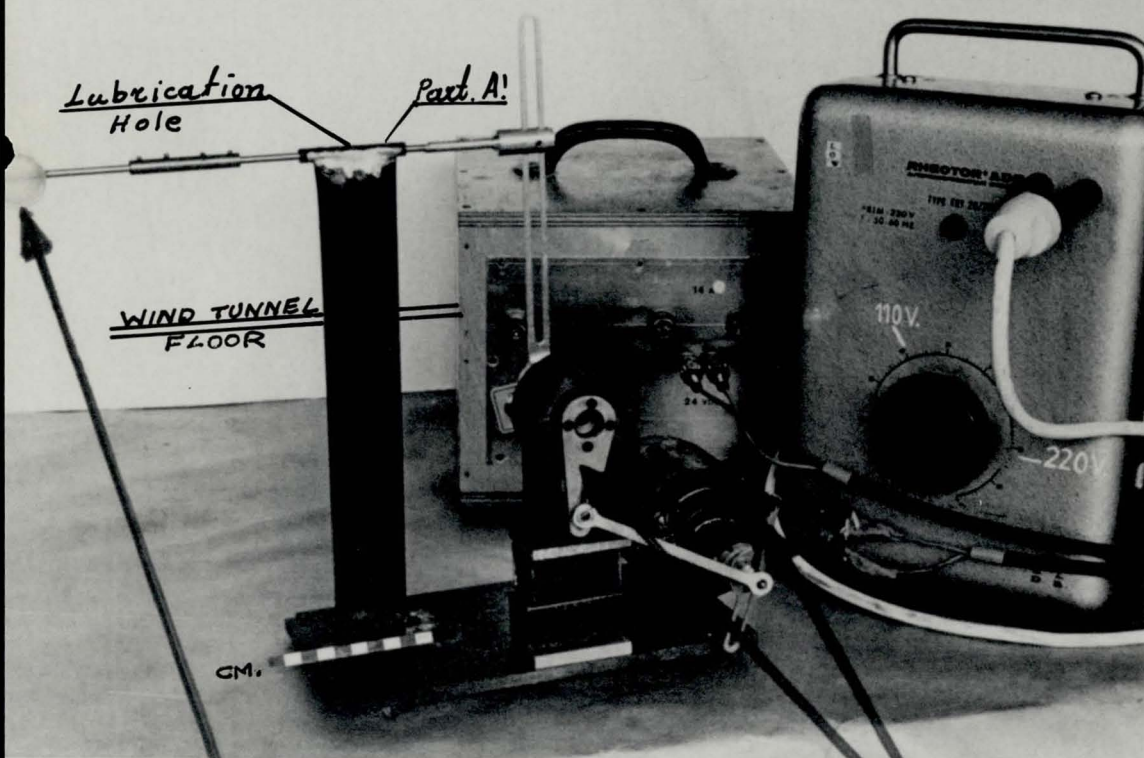


STRAIN GAUGES

MODEL ATTACHMENT

MODIFIED STRAIN GAUGE BALANCE

PL. IX



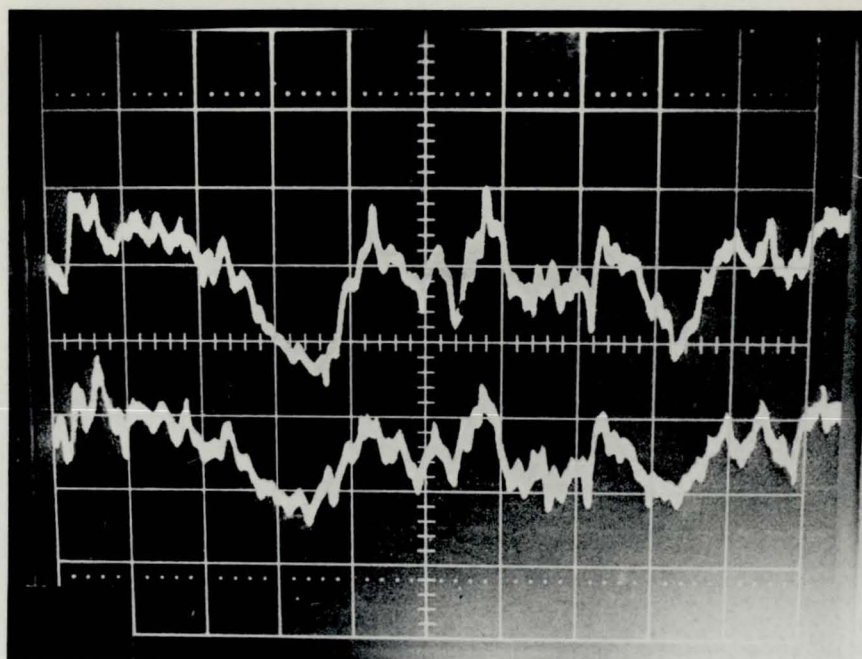
MODEL

AMPLITUDE ADJUSTERS

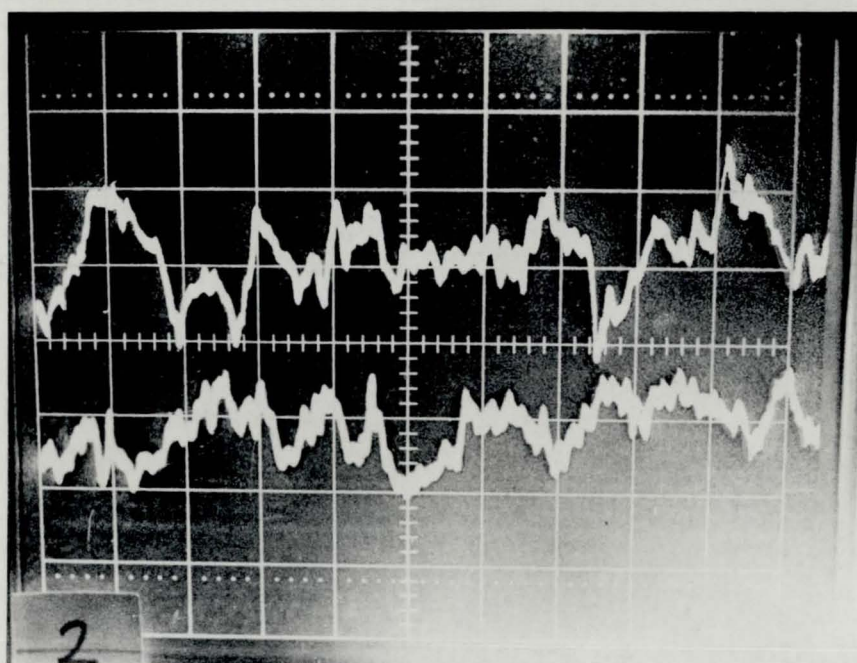
MECHANISM USED FOR THE EXTERNAL OSCILLATIONS
EXPERIMENTS

PL. X

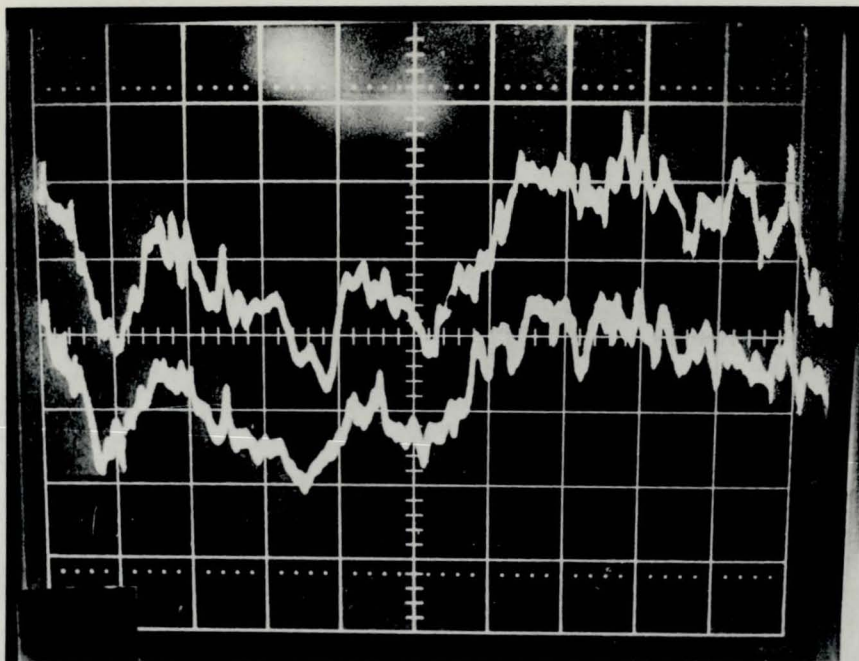
LATERAL SPACE CORRELATION



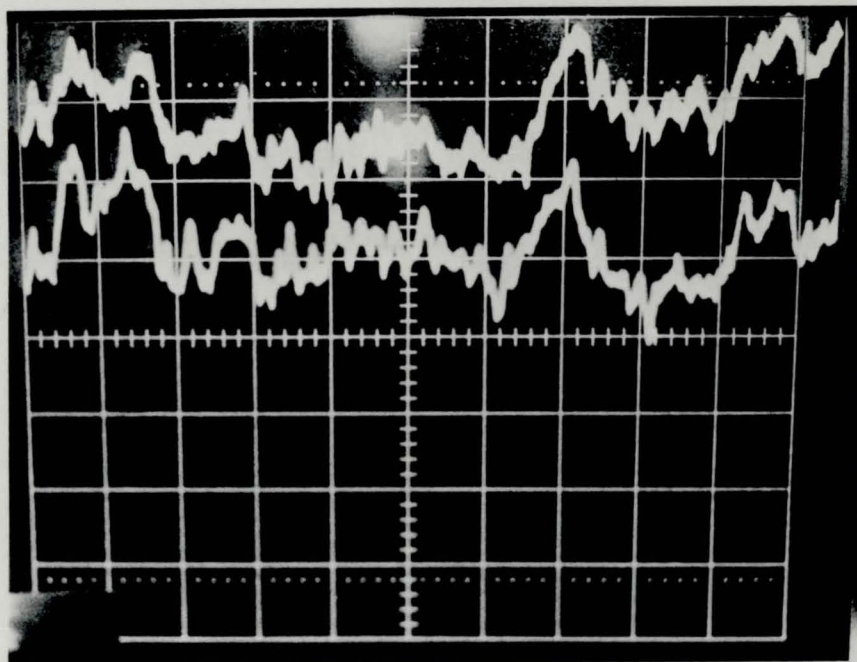
Slotted Baffle, Model Rigidly Held,
Plate $AR=2$, Wires Separation $dz=1mm$
H.W. at $x=-13.5mm$



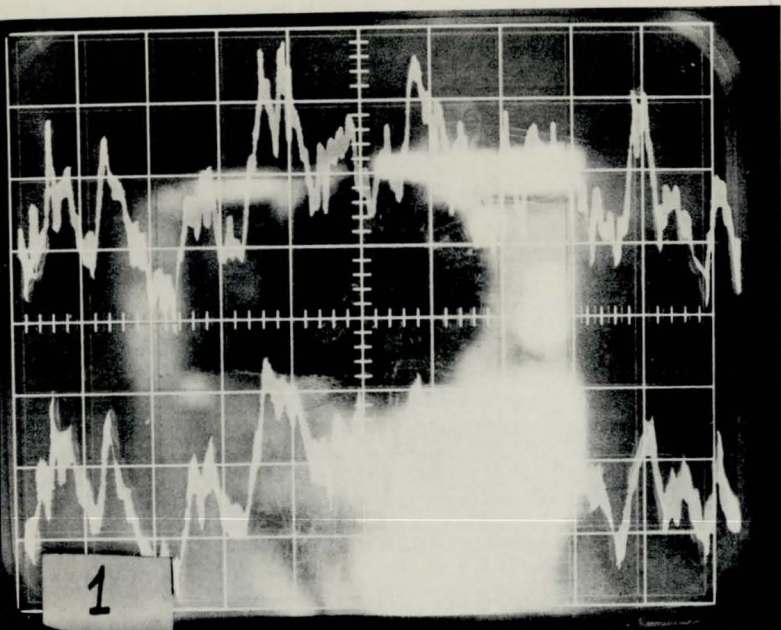
Slotted Baffle, Model Rigidly Held,
Plate $AR=2$, Wires Separation $dz=20mm$,
H.W. at $x=-13.5mm$



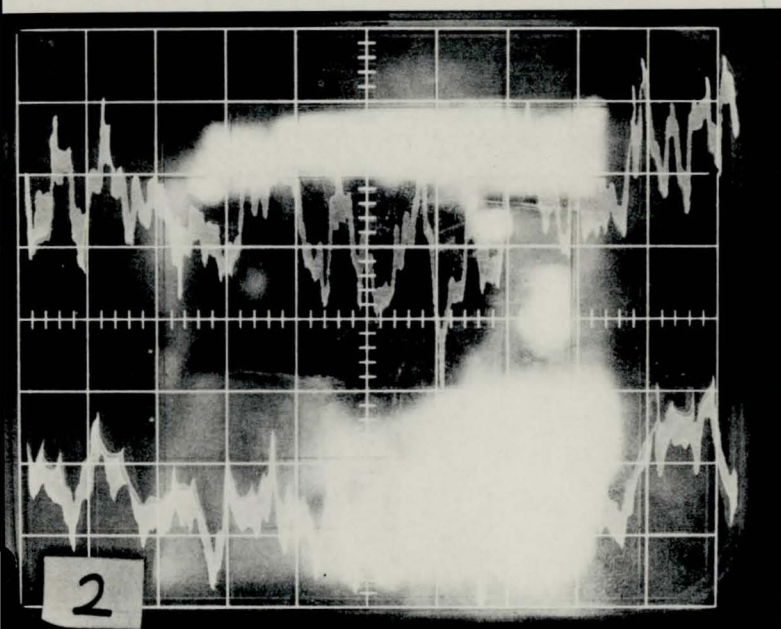
Slotted Baffle, Model Oscillating at 5.9Hz,
Amplitude = 3.5mm, Signal Unfiltered for Mean
Flow Oscillations, Plate AR=2, Wires Separation
 $dz=1\text{mm}$, Wires at $x=-13.5\text{mm}$



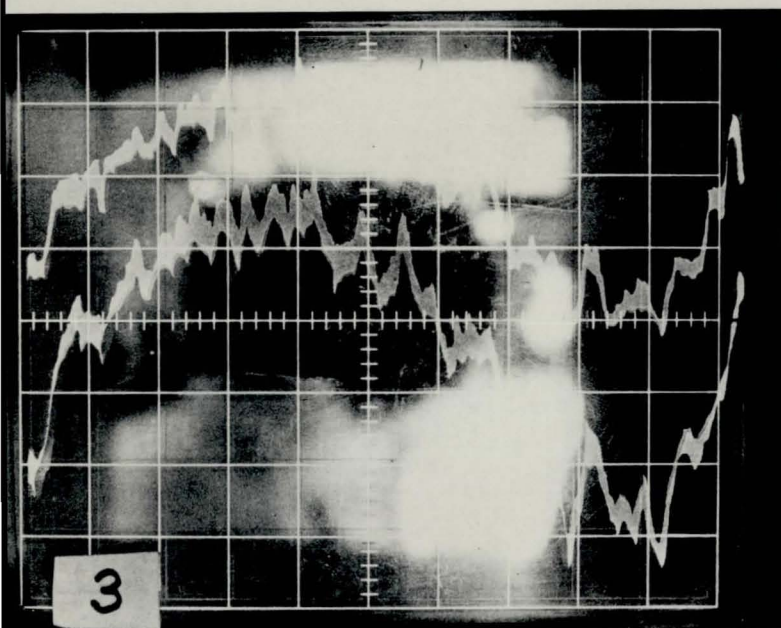
Slotted Baffle, Model Oscillating at 5.9Hz,
Amplitude = 3.5mm, Signal filtered for Mean
Flow Oscillations, Plate AR=2, Wires Separation
 $dz=1\text{mm}$, Wires at $x=-13.5\text{mm}$



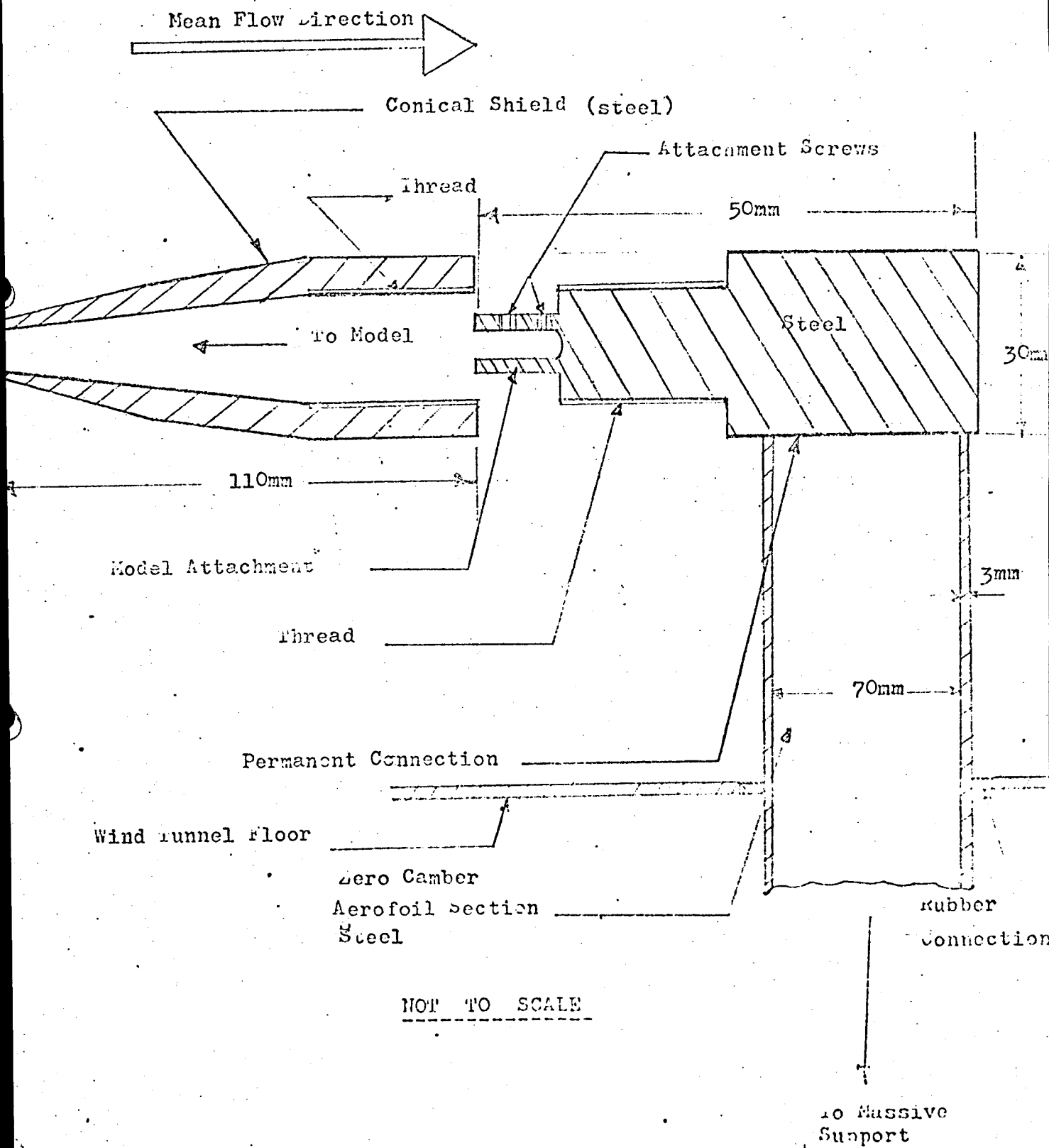
50 mm Holes Baffle,
Model Rigidly Held,
Circular Section
Cylinder : $AR = 2$,
Wires Separation: $dz = 1\text{mm}$,
H.W. at $x = -13.5\text{mm}$



50mm Holes Baffle,
Model Held Rigidly,
Circular Section
Cylinder : $AR = 2$,
Wires Separ. $dz = 15\text{mm}$,
H.W. at $x = -13.5\text{mm}$

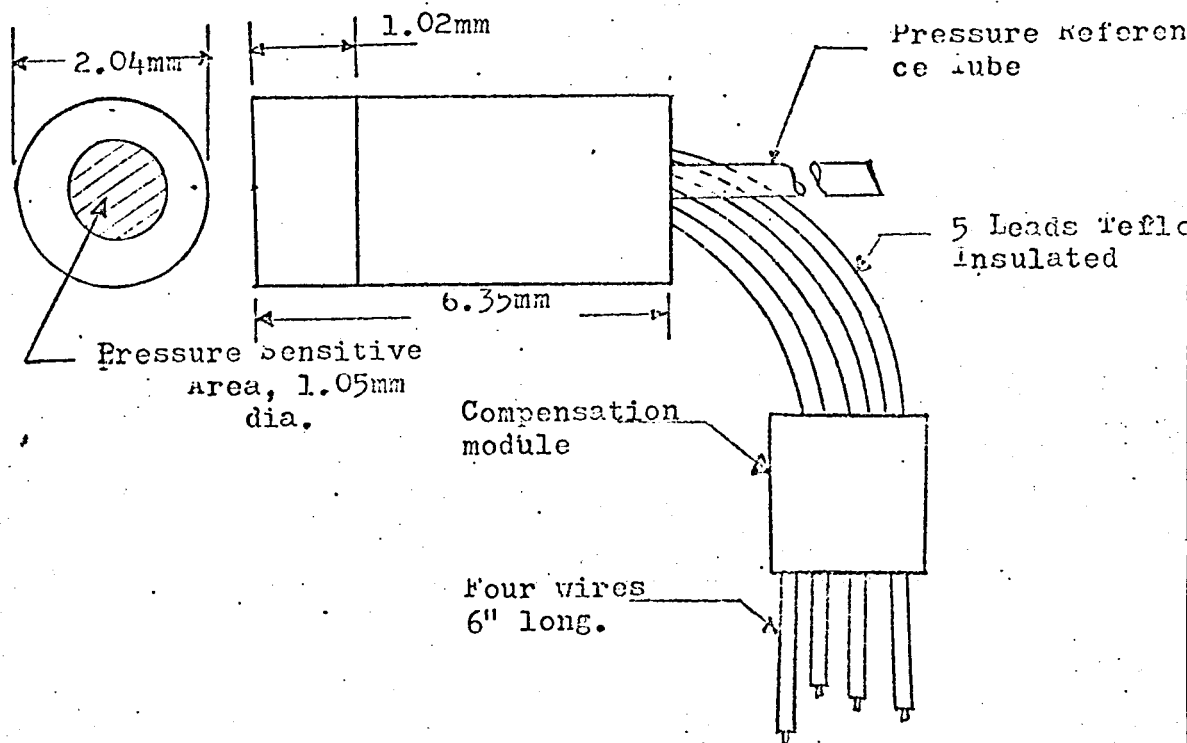


50 mm Holes Baffle,
Model Oscillating at
 6.1 Hz ,
Signal Unfiltered for
Mean Flow Oscillations,
Circular Section
Cylinder : $AR = 2$,
wires separation: $dz = 1\text{mm}$,
H.W. at $x = -13.5\text{mm}$



Attachment Mechanism for the Rigidly Held Model

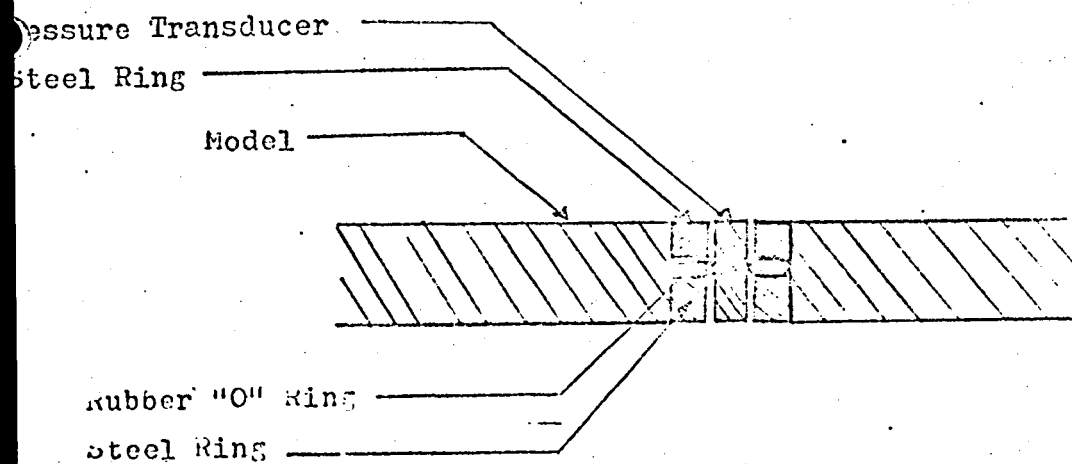
DIAGRAMS RELATED TO PRESSURE TRANSDUCER



NOT TO SCALE

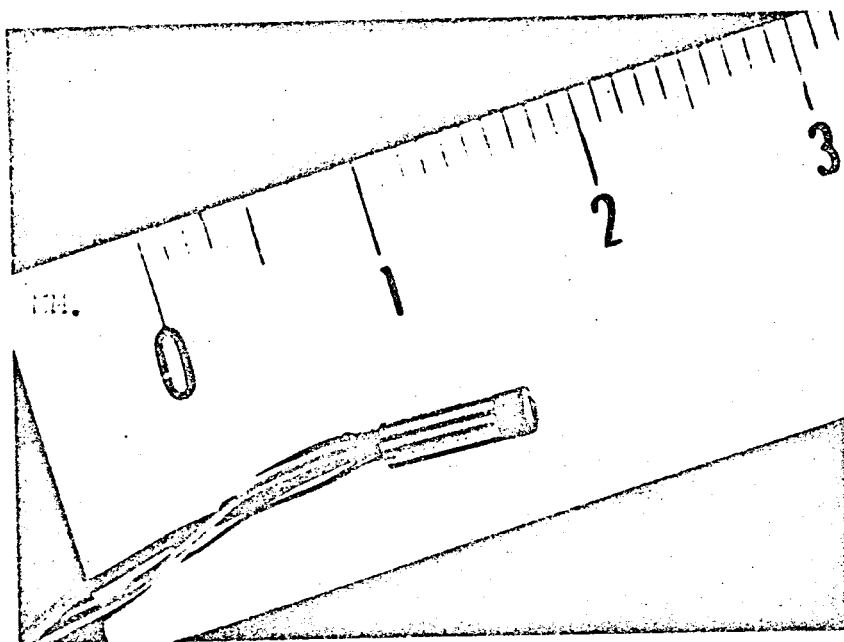
Schematic Presentation of the Pressure transducer

PL.XV



Mounting of Pressure transducer

PL.XVI



Pressure transducer used for the measurement
of the fluctuating Pressures on the face of
the AR = 2 Plate

PL.XVII: